

DETERMINATION OF MORPHOLOGICAL AND MOLECULAR ADAPTATIONS IN
VENTRAL TEGMENTAL AREA DOPAMINE NEURONS BY CHRONIC MORPHINE.

By

Sarah Emily Cooper

A DISSERTATION

Submitted to
Michigan State University
in partial fulfillment of the requirement
for the degree of

Neuroscience – Doctor of Philosophy

2018

ABSTRACT

DETERMINATION OF MORPHOLOGICAL AND MOLECULAR ADAPTATIONS IN VENTRAL TEGMENTAL AREA DOPAMINE NEURONS BY CHRONIC MORPHINE.

By

Sarah Emily Cooper

Opiate drugs are the leading treatment for severe or chronic pain in the USA despite their extremely addictive properties. Chronic opiate exposure induces unique neuroadaptations in the mesocorticolimbic system, particularly in ventral tegmental area (VTA) dopamine (DA) neurons. For example, opiates reduce VTA DA neuron soma size, a change correlated with increased DA activity and reward tolerance. Prevention of this morphological change is sufficient to rescue the morphine-induced changes to behavior, suggesting its direct involvement in addiction-related processes. To better understand the circuit-based consequences of morphine-induced neuroadaptations, we compared the morphology of VTA DA neurons that project to the nucleus accumbens (NAc) and medial prefrontal cortex (mPFC) in sham and morphine treated mice. Chronic morphine treatment significantly altered the soma size of NAc m.shell- and PFC-projecting VTA DA neurons, but conversely had no effect on NAc l.shell projecting VTA DA. While VTA DA structural and functional plasticity are central to morphine reward and addiction, the molecular responses driving these neuroadaptations remain elusive. To date, studies of drug-induced changes in VTA gene expression have been limited to the homogenization of the entire VTA, which includes GABAergic and dopaminergic (tyrosine hydroxylase (TH)-positive) neurons. While several candidate genes have been identified with this approach, it is unknown whether these changes occur specifically in

DA neurons and contribute to the structural neuroadaptations. To determine morphine-induced gene expression changes specifically in VTA DA neurons, we utilized Translating Ribosome Affinity Purification (TRAP). We crossed DA- (TH- or dopamine transporter (DAT)-Cre) driver lines with Rosa26 EGFP-L10a mice, thereby allowing for isolation of mRNA from VTA DA neurons. In both DA-specific lines (TH^{L10a-GFP} and DAT^{L10a-GFP}), we found significant enrichment of DA-specific markers and depletion of GABAergic markers in DA-specific IP fractions compared to input controls, consistent with successful purification. We then completed RNA sequencing on samples from DAT^{L10a-GFP} as an unbiased approach to identify changes that occur specifically in VTA DA cells. Using differential gene expression (DEG) analysis, we first identified 4,499 significantly enriched/depleted genes in sham-treated VTA DA-specific IP compared to sham-input (VTA DA transcriptome). In the following DEG analyses, we identified 410 significant morphine regulated genes in whole VTA input, and 393 significant morphine regulated genes in VTA DA-specific IP. We then validated select candidate genes in separate DAT^{L10a-GFP} TRAP samples using RT-PCR. Overall, the results of this dissertation identified projection-specificity of morphine-induced changes in VTA DA neuron morphology and identified morphine-induced gene expression changes specifically in VTA DA neurons. These findings are critical in driving our understanding of morphine-induced adaptations in specific VTA DA circuits as well as to identify novel mechanisms that underlie opiate-induced neuroadaptations in the VTA in order to develop innovative targets for improved therapeutics.

To my family and husband Ryan Simmons for their unconditional support and love.

ACKNOWLEDGMENTS

I would like to first thank my advisor, Michelle Mazei-Robison, for her remarkable mentorship throughout the years. I consider myself very lucky to have joined her lab, in 2014, to begin an immensely exciting and productive graduate school experience. I am forever grateful for the time she took for hands-on training in experimental procedures, editing, and experiment planning. I feel that I would not be the scientist I am today without her thoughtful guidance, and hope that in the future, my students look to me as I look up to her. I am grateful that she let me take the initiative on ideas and entrusted me to develop and troubleshoot my project as it progressed. I would also like to thank my other committee members, Dr. Robison, Dr. Leininger, and Dr. Wang for their thoughtful insight on my project over the years, as well as the multitude of shared resources and collaborations; which were stemmed from our meetings.

I'd also like to thank all members of the Mazei-Robison and Robison labs, which have formed such a lively and collaborative research team that will doubtlessly see success in their own hard work. These fellow collaborators are not only a team, but what I call my "lab family". It has been a pleasure to work with my fellow graduate students Marie Doyle, Amber Garrison, Claire Manning, Liz Williams, and Hallie Lynch, and postdoc's Dr. Andrew Eagle and Dr. Vedrana Bali. Their continued support, friendship, and shared enthusiasm for research and brainstorming are what made such an incredible and enjoyable 5 years. While I focus on the science, as is in my nature, I am forever grateful for the personal support and friendships we have developed through the years; through the shared celebrations and at times commiserating over the

burdens of graduate school. I would also like to thank Ken Moon for his impeccable management of the labs and maintaining a positive working environment despite many variables. You were truly an honor to work side by side and I am forever grateful for your assistance in mouse colony maintenance for my large and time-consuming experiments.

I would like to acknowledge the assistance we received through several collaborations and cores for their contribution to this work. Firstly, I'd like to thank NIDA Drug Supply for supplying sham and morphine pellets used throughout my dissertation research. Additionally, I'd like to thank Melinda Frame and MSU's microscopy core for her assistance and training with confocal imaging and for allowing me after-hours and weekend access to the instruments for my large data analysis. I would also like to acknowledge the assistance received from MSU's mass spectrometry core for their assistance in experiment design and personal training for use of the LC/MS/MS instruments. In regards to experiments outlined in Chapter 2, I'd first like to acknowledge the genomics core at University of Maryland for the final sample preparation and RNAsequencing. As well as the collaborations formed with Dr. Elizabeth Heller lab and Dr. Qiwen Hu for their assistance in the bioinformatic processing of the RNAsequencing data. Receipt of the initial RNAseq results was truly one of my best Christmas presents. I appreciate the assistance and collaboration with Dr. Joesph Beatty and Dr. Lee Cox for their assistance with piloting projection specific dendritic morphology and electrophysiology experiments and I hope to continue collaborating towards this project.

All research presented here were graciously funded through several NIH NIDA grants and Fellowship sources. Firstly, the research was funded primarily through Dr. Mazei-Robison's MSU start-up funding, NIDA RO3 (DA037426), NIDA, RO1 (DA039895). Additionally, I consider myself extremely lucky to have the opportunity to obtain the NIDA F31 individual personal fellowship award (DA042502) for the final year and a half of my studies.

TABLE OF CONTENTS

LIST OF TABLES	xi
LIST OF FIGURES.....	xii
KEY TO ABBREVIATIONS	xiv
Chapter 1. Introduction.....	1
1.1. The United States Opioid Epidemic	1
1.2. Substance Use Disorder (SUD): Dependence, Tolerance, and Abuse....	6
1.3. Opioid Receptors and Pharmacology.....	9
1.4. Mesocorticolimbic Reward Circuitry	14
1.4.1. Ventral Tegmental Area (VTA)	14
1.4.2. Dorsal Striatum (dStr) and Nucleus Accumbens (NAc).....	17
1.4.3. Primary Sources of Glutamatergic Input: PFC, BLA and Hipp	20
1.4.4. Regulation of VTA DA Neuronal Activity	21
1.5. VTA DA Neuron Heterogeneity and Function	22
1.5.1. Cytoarchitecture of the VTA.....	22
1.5.2. VTA Neuron Cellular Properties and Projections.....	27
1.6. Opioid Reward Circuitry.....	30
1.6.1. DA-independent Mechanisms of Opioid Reward	31
1.6.2. DA- and MOR-dependent Mechanisms of Opioid Reward	33
1.6.3. Opioid-induced VTA GABA Signaling.....	34
1.6.4. Chronic Opioid-induced Structural Plasticity.....	36
1.6.5. Molecular Mediators of Opioid-induced VTA DA Structural Plasticity	37
1.7. Hypothesis and Specific Aims	39
REFERENCES.....	42
Chapter 2. Determination of Circuit-specific Morphological Adaptations in Ventral Tegmental Area Dopamine Neurons by Chronic Morphine.....	63
2.1. Introduction.....	63
2.2. Materials and Methods	65
2.2.1. Animals and Stereotaxic Surgery.....	65
2.2.2. Morphine Treatment	67
2.2.3. Immunohistochemistry (IHC).....	68
2.2.4. Microscope Image Acquisition	69
2.2.5. Statistical Analysis	71
2.3. Results.....	71

2.3.1. Characterization of Basal Soma Size of VTA DA Projection Neurons	71
2.3.2. Morphine-induced Changes in Soma Size are Projection-specific	74
2.3.3. Projection-specific Protein Expression Patterns in DA Neurons	77
2.3.4. Viral-mediated Visualization of VTA DA Dendritic Spine Morphology	80
2.4. Discussion	84
REFERENCES.....	90
Chapter 3. Chronic Morphine-induced Transcriptome of VTA DA Neurons	97
3.1. Introduction.....	97
3.2. Materials and Methods	99
3.2.1. Animals.....	99
3.2.2. Morphine Treatment	100
3.2.3. Immunohistochemistry (IHC) and Microscope Image Acquisition	100
3.2.4. Translating Ribosome Affinity Purification (TRAP)	101
3.2.5. RT-PCR Analysis.....	102
3.2.6. RNA Sequencing (RNAseq)	104
3.2.7. Statistical Analyses	104
3.3. Results.....	105
3.3.1. Determination of DA-specific Expression of L10a-GFP	105
3.3.2. Validation of TRAP Enrichment of DA Markers.....	109
3.3.3. RNA Sequencing of VTA from DAT ^{L10a-GFP} Following Sham and Morphine Treatment	112
3.3.3.1. Determination of VTA DA Transcriptome (Sham Input vs. Sham IP).....	113
3.3.3.2. Global Changes in VTA Gene Expression (Sham Input vs. Morphine Input).....	118
3.3.3.3. Morphine-induced Transcriptome in VTA DA Neurons (Sham IP vs. Morphine IP).....	120
3.3.4. Validation of Morphine-Induced Changes in Gene Expression in VTA DA IP	124
3.4. Discussion	129
APPENDICES.....	138
Appendix A. L10a-GFP Expression Patterns Across Prefrontal Cortex and Nucleus Accumbens	139
Appendix B. Significant Enriched and Depleted Genes in VTA DA neurons: Sham Input vs. Sham IP	142
Appendix C. Significant Morphine-regulated Genes in Whole VTA: Sham Input vs. Morphine Input.....	149
Appendix D. Significant Morphine-regulated Genes in VTA DA neurons: Sham IP vs. Morphine IP	156
REFERENCES.....	163

Chapter 4. Conclusions and Future Directions	171
4.1. Summary of Dissertation	171
4.2. Chronic Morphine-induced Soma Size Change is Projection-specific	172
4.3. Determine NAc I.shell-projecting VTA DA Morphological Response to Chronic Morphine.....	174
4.4. Determine Projection-specific Chronic Opioid-induced Activity	176
4.5. Determine Basal and Opioid-induced VTA DA Dendritic Morphology	178
4.6. Viral-Mediated Visualization of VTA DA Dendritic Morphology.....	180
4.7. Projection-specific Labeling of VTA DA Neurons for Dendritic Morphology and Electrophysiological Studies.....	181
4.8. Identification of Novel VTA DA Chronic Morphine-induced Molecular Changes	183
4.9. Validation of DA-specific Morphine-induced Genes.....	186
4.10. Determine Cell-specificity of Morphine-regulated Genes Identified in Whole VTA Input.....	187
4.11. Validation of Behavioral Relevance of Projection-specific Chronic Opioid-induced Plasticity.....	189
4.12. Conclusion.....	191
REFERENCES.....	193

LIST OF TABLES

Table 1. Comparison Between DSM-IV and DSM-5 Diagnostic Criteria: Substance Abuse, Dependence, and Substance Use Disorder (SUD).	8
Table 2. Opioid Receptor Knockout Effects on Reward-related Behavior.	11
Table 3. Electrophysiological Properties Across DA Projection Target.....	29
Table 4. Experimental Primer Sequences.	103
Table 5. Statistical Values of 2-way ANOVA DAT^{L10a-GFP} Cell-specific Markers... ..	110
Table 6. Statistical Values of 2-way ANOVA TH^{L10a-GFP} Cell-specific Markers.....	111
Table 7. Significant Morphine-regulated Genes in RNAseq DA-IP.....	124
Table 8. RT-PCR of Candidate Genes (Normalized to Sham Input).	125
Table 9. Results of 2-way ANOVA of Up-regulated Genes.	126
Table 10. Results of 2-way ANOVA of Down-regulated Genes.	126
Table 11. Combined RT-PCR Validation of Candidate Genes, Multiple t-tests. ...	129
Table 12. Top 100 Significantly Enriched Genes in Sham VTA DA Neurons.	143
Table 13. Top 100 Significantly Depleted Genes in Sham VTA DA Neurons.	146
Table 14. Top 100 Significant Morphine Up-regulated Genes in VTA Input.	150
Table 15. Top 100 Significant Morphine Down-regulated Genes in VTA Input. ...	153
Table 16. Top 100 Significant Morphine Up-regulated Genes in VTA DA Neurons.	157
Table 17. Top 100 Significant Morphine Down-regulated Genes in VTA DA neurons.....	160

LIST OF FIGURES

Figure 1. 3 Waves of the Rise in Opioid Overdose Deaths.....	2
Figure 2. Mesocorticolimbic Reward Circuitry.	15
Figure 3. Anterior VTA Anatomy.	24
Figure 4. Posterior VTA Anatomy.	25
Figure 5. Basal Soma Size Characterization of NAc-projecting VTA DA Neurons.	73
Figure 6. Chronic Morphine Effects on VTA DA Soma Size Differ Based on Projection Target.....	75
Figure 7. Protein Markers Differentiate SNc DA Neurons that Project to the dStr, but not VTA DA Neurons that Project to the NAc m.shell vs. core.....	79
Figure 8. AAV5-DIO-eYFP Expression in VTA Fill Soma but Have Variable Expression Across Dendrites.	81
Figure 9. HSV-GFP Expression in VTA Fill Cell Soma but Have Variable Expression Across Dendrites.	82
Figure 10. AAV2-DIO-ChR2-eYFP Expression in VTA DA Neurons Increase Dendritic Spine Resolution.	83
Figure 11. Dopamine-specific Expression of L10a-GFP in the VTA.....	106
Figure 12. Comparison of GFP Expression Across VTA Nuclei in TH^{L10a-GFP} and DAT^{L10a-GFP} Mice.....	107
Figure 13. RT-PCR of Cell-specific Marker Expression in DAT^{L10a-GFP} Input and IP.	110
Figure 14. RT-PCR of Cell-specific Marker Expression in TH^{L10a-GFP} Input and IP.....	111
Figure 15. Cre-driver Differences in DAergic and GABAergic Marker Enrichment and Depletion.	112
Figure 16. Volcano Plot of Differential Gene Expression Analysis of Sham Input vs. Sham IP.	114
Figure 17. Distribution of Significantly Enriched and Depleted Genes in Sham IP.	115

Figure 18. Significant Enrichment of DA Markers and Depletion of Non-DA Markers in Sham IP.	116
Figure 19. Top 25 Enriched Genes in Sham VTA DA-IP.....	117
Figure 20. Volcano Plot of Differential Gene Expression Analysis of Sham Input vs. Morphine Input.	118
Figure 21. Top 25 Significant Morphine-regulated Genes in RNAseq of VTA Inputs.	119
Figure 22. Volcano Plot of Differential Gene Expression Analysis of Sham IP vs. Morphine IP.....	120
Figure 23. Top 25 Significant Morphine-regulated Genes in RNAseq of VTA DA IP.	121
Figure 24. Identification of Highly Distinct Morphine-regulated Genes in Whole VTA Input Compared to DA-specific IP.	122
Figure 25. RT-PCR of Sgk1 Gene Expression in Input and IP of Sham- and Morphine-treated DAT^{L10a-GFP}	123
Figure 26. Combined RT-PCR Validation of Chronic Morphine-induced Genes in DAT^{L10a-GFP} Input and IP.	128
Figure 27. Comparison of GFP Expression Across PFC and NAc in TH^{L10a-GFP} and DAT^{L10a-GFP} Mice.....	140
Figure 28. VTA DA Dendritic Spine Morphology of Projection-specific Microinjected VTA DA Neuron.	182

KEY TO ABBREVIATIONS

AAV adeno-associated virus

Acta2 actin, alpha 2, smooth muscle, aorta

aif1 allograft inflammatory factor

Akt protein kinase B

Aldh1a1 Aldehyde Dehydrogenase 1 Family Member A1

AMPA alpha-amino-3-hydroxy-5-methyl-4-isoxazolepropionic acid

ANOVA analysis of variation

Anxa10 annexin A10

AP anterior posterior axis

aVTA anterior VTA

BLA basolateral amygdala

BNST bed nucleus of the stria terminalis

CA constitutively active

Calb1 Calbindin 1

CDC center for disease control

cDNA complementary DNA

Cg1 cingulate cortex 1

ChR2 channel rhodopsin 2

Chrna6 Cholinergic Receptor Nicotinic Alpha 6 Subunit

Chrn4 cholinergic receptor nicotinic beta 4 subunit

Cli central linear nucleus

CPA conditioned place aversion

CPM counts per million

CPP conditioned place preference

CSDS chronic social defeat stress

d.Str dorsal striatum

D1 dopamine receptor type 1

D2 dopamine receptor type 2

DA dopamine

DAT dopamine transporter

Ddc dopa decarboxylase

DEA drug enforcement agency

DEG differential gene expression

DIO double floxed inverse

dn dominant negative

DOR delta opioid receptor

DP dorsopeduncular cortex

DR dorsal Raphe

Drd dopamine receptor D2

DSM Diagnostic and Statistical Manual of Mental Disorders

DV dorsal ventral axis

EF1a human elongation factor-1 alpha

eGFP enhanced green fluorescent protein

eYFP enhanced yellow fluorescent protein

FC fold change

FITC Fluorescein isothiocyanate

fmi forceps minor of the corpus callosum

FP fluorescent protein

GABA gamma-Aminobutyric acid

GAD glutamate decarboxylase

GAPDH glyceraldehyde-3-phosphate dehydrogenase

Gcg glucagon

Gfap glial fibrillary acidic protein

Girk3 G protein-activated inward rectifier potassium channel 3

Glast1 glutamate/aspartate transporter 1

Glul glutamate-ammonia ligase

GluR1 glutamate-receptor 1

Glut glutamate

Gm gene model

GPCR G-coupled protein receptors

Grp gastrin releasing peptide

Hipp hippocampus

hr hour

HSV herpes simplex virus

IACUC Institutional animal use and care

ICSA intracranial self-administration

ICSS intracranial self-stimulation

IF interfascicular nucleus

Ih hyperpolarized-activated current

IHC immunohistochemistry

IL infralimbic cortex

ip intra paratoneal

IP immunoprecipitation

IPN interpeduncular nucleus

IRS2 insulin receptor substrate 2

IVSA intravenous self-administration

Kcnab Voltage-gated potassium channel subunit beta-1

Kcne1l potassium voltage-gated channel, Isk-related family, member 1-like,
pseudogene

KO knock out

KOR kappa opioid receptor

L.PN lateral paranigral nucleus

I.shell lateral shell

LC locus cerelius

LHb lateral habenula

LS/MS-MS Liquid chromatography mass-spectrometry

LTD lateral dorsal tegmentum

LTD long term depression

LTP long term potentiation

LUT look up table

M2 secondary motor cortex

m.shell medial shell

mCh mcherry

Mesp2 mesoderm posterior 2

MHb medial habenula

ML medial lateral axis

MME milligram morphine equivalent

MOR mu opioid receptor

mRNAmessenger ribonucleic acid

MSN medium spiny neuron

mTORC2 mammalian Target of Rapamycin complex 2

NAc nucleus accumbens

NDS normal donkey serum

NE norepinephrine neurons

NIDA national institute on drug abuse

NMDAN-methyl-D-aspartic acid

Nms neuromedin s

NO nitric oxide

NSDUH national survey on drug use and health

Nupr1 nuclear protein transcription regulator 1

Otx2 orthodenticle homeobox 2

PAG periaqueductal gray

PBP parabrachial pigmented nucleus

PBS phosphate buffered saline

PFC prefrontal cortex

PKA protein kinase A

PKG protein kinase G

PLC gamma phospholipase C gamma

PN paranigral nucleus

PPTg pedunculopontine tegmental nucleus

PrL prelimbic cortex

PTPRC protein tyrosine phosphatase receptor type, C

pVTA posterior VTA

Rik Riken

RIN RNA integrity number

RLi rostral linear nucleus

RMTg rostral medial tegmentum

RNAseq RNA sequencing

RRF retrorubral field

RT-PCR reverse-transcription polymerase chain reaction

SGK1 serum and glucocorticoid induced kinase 1

Smagp small cell adhesion glycoprotein

SNC substantia nigra pars compacta

Snca synuclein alpha

Sncg synuclein gamma

Sox6 sex-determining region Y-box 6

SUD substance use disorder

SUM supramammillary nucleus

Tal2 T cell acute lymphocytic leukemia 2

Tec tec protein tyrosine kinase

TH tyrosine hydroxylase

TRAP translating ribosome affinity purification

tVTA tail of the VTA

v.Str ventral striatum

VGAT vesicular GABA transporter

Vgf VGF nerve growth factor inducible

VGLUT2 vesicular glutamate transporter 2

vHipp ventral hippocampus

Vmat vesicular monoamine transporter

VTA ventral tegmental area

VTAR rostral part of VTA

wt wild type

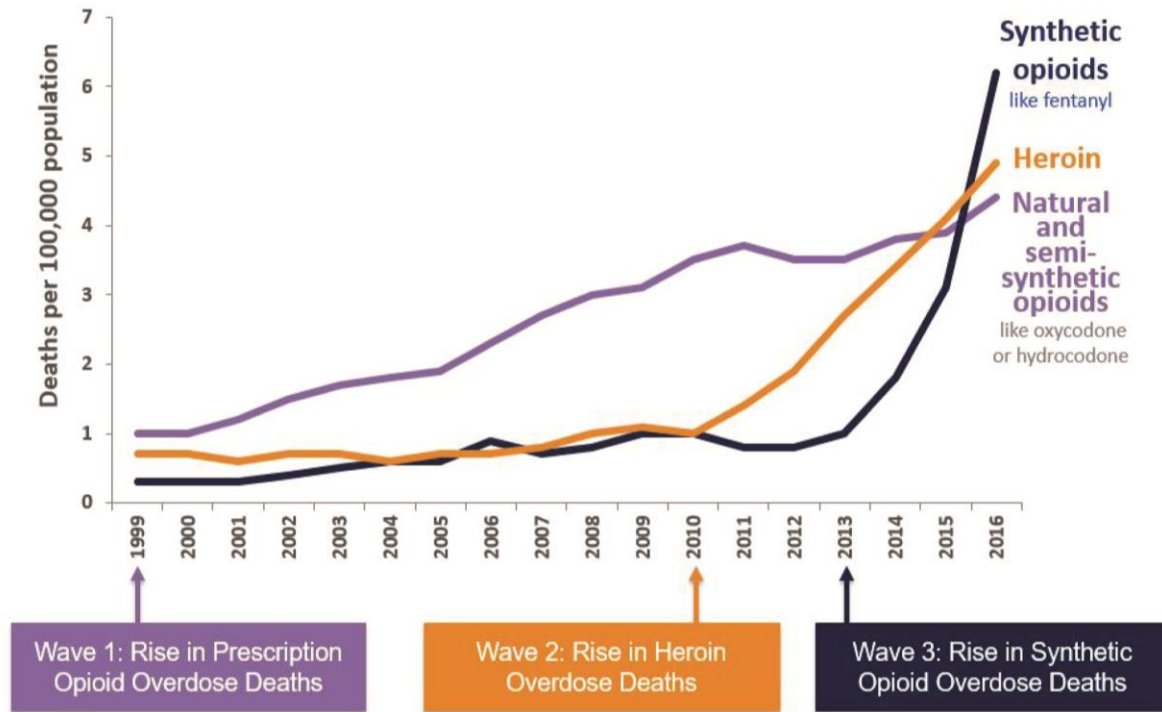
Chapter 1. Introduction

1.1. The United States Opioid Epidemic

Due to a dramatic increase in opioid overdose deaths in the United States over the last 20 years, 'Opioids and Addiction' rose to the top of the Surgeon General's priority list and has been officially termed a public health emergency (U.S. Dept of Health and Human Services (HHS), 2017). In fact, there has been a 500% increase in opioid-related overdose deaths from 1999 to 2016 with an average of 115 Americans dying every day (Center for Disease Control and Prevention (CDC), 2017). The opiate epidemic did not develop in a uniform, linear manner. Instead, it appears to have occurred in 3 distinct waves (Figure 1). Initially there was a significant increase in prescription opioids overdose deaths (1999-2010), followed by a dramatic increase in heroin overdose deaths in 2010, and finally an increase in overdoses involving synthetic opioids, particularly fentanyl, from 2013-2016 (CDC, 2017a). The progression of overdose deaths has been attributed in part to the overprescribing of opioids, which has led to a growing population of people with opioid dependence that also has increased risk for opioid addiction and misuse (Kanouse & Compton, 2015).

Beginning in the early 1990s, there was an increase in prescription rates of opioids due to increased concern for adequate pain management (Kanouse & Compton, 2015). Previously, prescription opioids were cautiously utilized for acute care following surgery within hospital settings or for chronic pain associated with terminal cancer treatment (Kanouse & Compton, 2015). In 1992, the Agency for Healthcare Quality Research issued a two-part statement which asserted that 50% of surgical patients were not receiving adequate pain treatment and that improved pain management was

3 Waves of the Rise in Opioid Overdose Deaths



SOURCE: National Vital Statistics System Mortality File.

Figure 1. 3 Waves of the Rise in Opioid Overdose Deaths. Opioid overdose death rates within the United States from 1999-2016. Figure Source: (CDC, 2017a). Data source: National Vital Statistics System Mortality File.

the patient's right (reviewed in (Kanouse & Compton, 2015; Kotecha & Sites, 2013)).

Also, during this time period, pharmaceutical companies were heavily promoting newly released formulations of prescription opioids, such as OxyContin (Oxycodone HCl), with claims of reduced abuse liability (reviewed in (Kanouse & Compton, 2015)). Collectively, this resulted in health care providers being encouraged to prescribe opioids for treatment of chronic pain with backing from both the pharmaceutical industry and medical societies such as the American Pain Society and American Academy of Pain Medicine (Haddox JD, 1997; Kolodny et al., 2015). This resulted in a profound increase

in opioid prescriptions, where sales of oxycodone, hydrocodone, and methadone from 1999-2005 increased by 533%, 198%, and 933%, respectively (Manchikanti, 2007).

The increased prescription of opioid drugs such as oxycodone has led to multiple lawsuits filed by several states, cities and counties. These suits allege that large pharmaceutical companies utilized advertising practices and propaganda that contributed to and encouraged the overprescribing of new prescription opioids (Jennings, 2018; Katie Benner, 2018; Semuels, 2017). This judicial action against pharmaceutical companies is similar to the campaign launched against major tobacco firms from 1954 to 1998 for recovery of tobacco-related health costs (Daynard, Bates, & Francey, 2000). These actions resulted in the largest civil litigation settlement in US history in 1998, where four major tobacco companies agreed to contribute annual payments to the states for tobacco-related health care costs in perpetuity and agreed to cease certain tobacco marketing practices (Daynard et al., 2000; Semuels, 2017). It remains to be seen if a similar legal tactic will be successful for compensation for opioid epidemic-related health care costs.

Regardless of where legal blame will fall for the current opioid epidemic, there is indisputable evidence for a substantial change in opioid prescribing practices beginning in the late 1990's. In 2010 total sales of opioid prescriptions were nearly 4 times greater than in 1999 (CDC, 2011). In fact, enough prescription opioids were sold in 2010 for each person in the United States to receive a typical dose of 5mg oxycodone every 4 hours for 1 month (CDC, 2011). Along with an increase in availability of prescription opioids there were also few regulations on prescription strength. In a study reporting on data from 1997-2005, the average daily prescribed opioid dose was between 30-60

morphine milligram equivalents per day (MME/day) (Von Korff et al., 2008). In a meta-analysis conducted in 2018, it was determined that there is a significant risk of unintentional overdose with doses greater than 20 MME/day (Adewumi, Hollingworth, Maravilla, Connor, & Alati, 2018). With such prolific prescribing practices, it is not surprising that incidence of unintentional overdose greatly increased given that the most frequent dose range (20 – 50 MME/day) was above this threshold. In an attempt to promote safe prescribing practices, the CDC recently modified published guidelines for prescribing opioids for chronic pain, suggesting caution when increasing dosage to ≥ 20 MME/day and to avoid increasing dosage to ≥ 90 MME/day (CDC, 2017b). This seems like a promising step, but it will be important to determine whether this new prescription guideline is ultimately sufficient to mitigate opioid overdose risk.

With over a decade of increased opioid prescription rates and overdose deaths, it is not surprising that the rates for opioid misuse and abuse have also increased. From 1997-2011 there was a dramatic 900% increase in admissions for treatment of prescription opioid addiction (Kolodny et al., 2015). Misused prescription opioids are often obtained from friends or family members in addition to personal prescriptions from a single doctor (Lipari, 2017). Critically, previous prescription opioid misuse is a significant risk factor for heroin abuse (Kanouse & Compton, 2015). It is estimated that those with previous prescription misuse are 40 times more likely to become addicted to heroin. This contrasts with other addictive drugs such as alcohol or cocaine, which are associated with 4- and 15-times risk for heroin addiction, respectively (Center for Disease Control and Prevention (CDC), 2017). Because of the incidence of opioid prescription sharing and diversion, public awareness and education on the risks of

overdose and the addictive properties of prescription opioids are an important first step in prevention of opioid abuse.

In response to the growing epidemic, the White House Administration under President Obama released the “National Drug Control Strategy” in 2010, which was expanded upon in 2011 with the “Prescription Drug Abuse Prevention Plan”. These official plans outlined four major strategies to reduce prescription drug abuse: education, monitoring, proper medication disposal, and enforcement (Kanouse & Compton, 2015; Office of National Drug Control Policy, 2010). While increased awareness of the addictive properties of opioids combined with increased regulations successfully reduced prescription numbers, it was perhaps too little too late. Concurrent with the increase in prescription regulations following 2010, there was a second wave of the opioid epidemic – a dramatic increase in heroin overdose deaths. Over the course of 5 years (2010-2015), heroin overdose deaths increased 5-fold, while prescription overdose death rates appeared to plateau (CDC, 2017a) (Figure 1). In a study conducted by the federal government’s National Survey on Drug Use and Health (NSDUH), nearly 80% of heroin initiates (defined as first use within 12 months) reported previous use of non-medical prescription pain relievers (Muhuri PK, 2013). It is likely that a subset of patients who had become dependent on high doses of opioids turned to illicit forms of the drug when faced with reduced prescription availability and increased costs (Kanouse & Compton, 2015; Lynch, 2016).

Finally, the third and most recent wave of the opioid epidemic is a severe increase in fentanyl-related fatal overdoses starting in 2015 (CDC, 2016b). Fentanyl is a synthetic opioid that is 50 times stronger than heroin and 100 times stronger than

morphine (CDC, 2016a). Pharmaceutical fentanyl was approved for treating severe pain, particularly associated with end-stage cancer (Algren et al., 2013). Its contribution to the opioid epidemic is not thought to be through prescription diversion, but rather an increase in its introduction into heroin and counterfeit prescription opioids during drug preparation (DEA, 2015). The spiked fentanyl not only gives the user a stronger drug-induced high but also greatly increases the risk of overdose. Therefore, increased fentanyl overdose rates are not a separate phenomenon from prescription and heroin overdose deaths but are an extension of the ongoing epidemic resulting from increased prevalence of this particularly potent form of opioid in illegal drug manufacturing. The clear increase in opioid overdose deaths within the United States, whether from prescription, heroin, or other synthetic forms, point to another significant health crisis: increased opioid dependence and abuse.

1.2. Substance Use Disorder (SUD): Dependence, Tolerance, and Abuse

There has been much discussion in the field of addiction over how to integrate the definitions of substance dependence, tolerance, and abuse into new diagnostic criteria for opioid SUD (Brady, McCauley, & Back, 2016; Heit & Gourlay, 2009). To discuss these distinctions, it is helpful to first define the terms. *Substance dependence* is characterized by the presence of physical withdrawal syndrome symptoms when the drug is stopped (Brady et al., 2016). *Drug tolerance*, frequently confused as substance dependence, is a physiological response where more drug is needed to achieve the same intensity of effect (Brady et al., 2016). *Substance abuse* refers to the maladaptive pattern of use causing significant impairment and distress in social and interpersonal

wellness. Finally, *addiction* as defined by the American Society of Addiction Medicine (ASAM) is,

“a primary, chronic disease of brain reward, motivation, memory and related circuitry. Dysfunction in these circuits leads to characteristic biological, psychological, social and spiritual manifestations. This is reflected in an individual pathologically pursuing reward and/or relief by a substance use and other behaviors” (Asam.org, n.d.).

An evolving understanding of substance abuse, dependence, and addiction as a spectrum rather than distinct and separate categories led to clarification and revisions in the criteria for SUD in the 5th edition of Diagnostic and Statistical Manual of Mental Disorders (DSM-5) (Brady et al., 2016; Hasin et al., 2013; Helzer, van den Brink, & Guth, 2006; Muthen, 2006). Previously, diagnosis of mild or early phase substance abuse required only one criteria to be met, usually involving social and interpersonal problems from substance use (DSM-IV-TR, (American Psychiatric Association, 2000)). Substance dependence was considered a more severe manifestation of substance use where diagnosis required evidence for uncontrolled use and physical dependence (i.e. tolerance, withdrawal symptoms) (Hasin et al., 2013). But following extensive review and revisions, the DSM-5 committee combined the previous DSM-IV-TR categories of substance dependence and substance abuse into a single diagnosis, substance use disorder (SUD), which is measured on a continuous scale (American Psychiatric Association, 2013). A comparison of diagnostic criteria of symptoms is displayed in Table 1.

Table 1. Comparison Between DSM-IV and DSM-5 Diagnostic Criteria: Substance Abuse, Dependence, and Substance Use Disorder (SUD).

Criterion Category	DSM-IV Abuse	DSM-IV Dependence	DSM-5 SUD
Hazardous Use	X	--	X
Social problems associated with use	X	--	X
Neglect of major roles (Family, Work, etc)	X	--	X
Legal Problems (removed from DSM-5)	X	--	--
Withdrawal	--	X	X
Tolerance	--	X	X
Larger amounts used/ or taken for longer	--	X	X
Repeated unsuccessful attempts to quit/control use	--	X	X
Large amount of time spent using	--	X	X
Physical/psychological problems related to use	--	X	X
Activities given up to use	--	X	X
Craving (new to DSM-5)	--	--	X
Diagnostic criterion:	≥ 1	≥ 3	≥2 *

* According to new DSM-5 criteria, SUD is graded on a scale of severity: mild (2-3 criterion), moderate (3-4 criterion), and severe (≥4 criterion).

The modified diagnostic criteria in DSM-5 allows for better representation of the spectrum of substance use and misuse within the population (Heit & Gourlay, 2009; Wu, Woody, Yang, Pan, & Blazer, 2011). For example, DSM-IV-TR criteria for substance dependence did not address the distinction that one can become physically dependent (i.e. experience withdrawal symptoms) on a substance with abuse potential, without having maladaptive or uncontrolled use. For example, opioid dependence and tolerance can easily occur with prescription opioids if used daily for more than 2-3 weeks, a common practice in treatment of chronic pain (Brady et al., 2016; CDC, 2017b). Meeting the previous criteria for substance dependence (i.e. withdrawal, tolerance, and

extended use) with prescription opioids may not necessarily indicate uncontrolled use or abuse if they are taken according to the instructions from the prescribing physician. It should be noted that preliminary studies have revealed similar numbers of opioid abuse diagnoses using either diagnostic criterion (Center for Behavioral Health Statistics and Quality, 2016), but clearly more studies are needed to address this potential discrepancy.

1.3. Opioid Receptors and Pharmacology

Opioids induce analgesia and reward by binding to opioid receptors in the nervous system. There are 3 main types of opioid receptors: μ (MOR), δ (DOR), and κ (KOR) (Minami & Satoh, 1995; Zaki et al., 1996). All opioid receptors are G-coupled protein receptors (GPCR), and activation via agonist binding initiates inhibitory cellular cascades mediated by $G_{i/o}$ signaling (Al-Hasani & Bruchas, 2011). Activation of opioid receptors results in decreased cellular activity. Specifically, this is primarily driven by reduced adenylate cyclase signaling which results in modified potassium channel function, calcium ion release, and reduced neurotransmitter release (Al-Hasani & Bruchas, 2011). In addition to changes in signaling, opioid receptor availability and sensitivity are also intricately regulated by exogenous opioids. For example, opioid drug tolerance is mediated in part by the desensitization of MORs (through increased receptor phosphorylation) and increased internalization of receptors (through β -arrestin binding) (Williams, Christie, & Manzoni, 2001).

Despite sharing sequence homology (~60%) and engaging similar GPCR signaling cascades, each receptor (MOR, DOR, and KOR) has distinct binding affinities for endogenous (e.g. endorphins, endomorphins, and dynorphins) and exogenous

opioids (e.g. morphine, oxycodone, and heroin) (Mansour, Hoversten, Taylor, Watson, & Akil, 1995; Williams et al., 2001). These affinities drive diverse roles for each receptor type in nociception, reward, and aversion. For example, exogenous opioids like morphine have high affinity for MOR and activation of this receptor is critical for reward. Interestingly, MOR activation is not only necessary for the rewarding aspects of opioids but can also modify the rewarding aspect of other drugs of abuse such as such as cannabinoids, nicotine, and alcohol (Berrendero, Kieffer, & Maldonado, 2002; Ghozland et al., 2002; Matthes et al., 1996; Roberts et al., 2000). Activation of DORs is thought to be particularly important for nociception, although there have been conflicting results suggesting they may also play a secondary or minor role in opioid reward and addiction (Charbogne, Kieffer, & Befort, 2014). Conversely, KOR activation by agonists such as dynorphin, may play an opposite role in behavior modification and is associated with aversion and dysphoria (Bruchas, Land, & Chavkin, 2010; Knoll & Carlezon, 2010; Land et al., 2008)

Most of our understanding of the behavioral significance of opioid receptors has been delineated from knockout studies (reviewed extensively in (Charbogne et al., 2014)). The key findings on reward and analgesia from these studies are summarized in Table 2. There are a few common behavioral assessments used to determine aspects of reward, or motivation, in rodents. In conditioned place preference (CPP), rodents learn to associate the rewarding stimulus (or aversive in the case conditioned place aversion, CPA) with a distinct context (Cunningham, Gremel, & Groblewski, 2006). For example, in a typical morphine CPP experiment, animals repeatedly receive saline and

Table 2. Opioid Receptor Knockout Effects on Reward-related Behavior.

KO Mice	Drug	Behavior Test	Effect	Reference
MOR KO	morphine	CPP	abolish	(Matthes et al., 1996; Nguyen, Marquez, Hamid, Kieffer, et al., 2012; Nguyen, Marquez, Hamid, & Lutfy, 2012; Sora et al., 2001)
		ICSA	decreased	(Becker et al., 2000; David et al., 2008)
		IVSA	abolish	(Sora et al., 2001)
		withdrawal	abolish	(Matthes et al., 1996)
		analgesia	abolish	(Fuchs, Roza, Sora, Uhl, & Raja, 1999; Loh et al., 1998; Matthes et al., 1996; Schuller et al., 1999; Sora, Li, Funada, Kinsey, & Uhl, 1999; Sora et al., 1997)
		hyper-locomotion	abolish	(Becker et al., 2000; Sora et al., 2001; Tian et al., 1997)
	heroin	CPP	abolish	(Contarino et al., 2002)
		withdrawal	abolish	(Kitanaka, Sora, Kinsey, Zeng, & Uhl, 1998)
		analgesia	no effect	(Schuller et al., 1999)
KOR KO	morphine	CPP	no effect	(Simonin et al., 1998)
		withdrawal	abolish	(Simonin et al., 1998)
		analgesia	no effect	(Simonin et al., 1998)

Abbreviations: conditioned place preference (CPP), intracranial self-administration (ICSA), intra-venous self-administration (IVSA), kappa opioid receptor knockout (KOR KO), mu opioid receptor knockout (MOR KO).

morphine injections in contextually distinct chambers. The animals are then allowed to explore both chambers in a drug-free state. Animals will spend more time in the morphine-paired chamber than in the saline-paired chamber due the rewarding aspects of morphine. A second common behavioral assessment for drug reward is operant conditioning, also referred to as drug self-administration (SA). In this assay, rodents learn to perform an operant task (e.g. nose-poke, lever press) to obtain a reward, in the case of drugs of abuse via intravenous (IVSA) or intracranial (ICSA) infusion (Goeders & Smith, 1987; Kmiolek, Baimel, & Gill, 2012; Panlilio & Goldberg, 2007). This is a powerful assay and variations of this task can be used to assess different aspects of addiction such as craving and relapse. Additionally, intracranial self-stimulation (ICSS), has been used extensively to determine not only specific brain regions implicated in reward processing, but also can be used to assess the abuse potential of many classes of drugs (Negus & Miller, 2014).

MOR agonists (e.g. morphine, heroin) are sufficient to form CPP and support IVSA and ICSA, along with the ability to induce pronounced analgesia (David & Cazala, 1994; Olmstead & Franklin, 1997). The necessity of MOR activity for morphine-induced reward and analgesia is supported by data from MOR knockout (MOR KO) mice, as these behavioral responses are abolished in KO mice (Hall et al., 2003; Matthes et al., 1996; Sora et al., 1997). In contrast, KOR KO had little to no effect on morphine or heroin reward but was sufficient to eliminate opioid withdrawal symptoms (Kitanaka et al., 1998; Simonin et al., 1998). In fact, KOR activation by agonists such as dynorphin is strongly associated with aversive events like stress and dysphoria. Moreover, chronic KOR activation has been shown to induce depressive-like behavior in rodents (Bruchas

et al., 2010; Knoll & Carlezon, 2010; Land et al., 2008). It has been suggested that KOR activation may regulate the negative side effects and dysphoria of opioid withdrawal and thereby contribute to the high risk of stress-induced drug relapse (Bruchas et al., 2010).

Along with differences in agonist affinity, variation in cellular expression pattern may also contribute to differential opioid receptor effects on behavior. All three types of opioid receptors are widely expressed in the CNS, including throughout the cortex, limbic system and brain stem (Arvidsson et al., 1995; Le Merrer, Becker, Befort, & Kieffer, 2009). This vast receptor distribution enables opioids to intricately modulate a multitude of responses including analgesia, reward, mood and aversion. For example, MOR and KOR receptors are densely distributed in mesocorticolimbic reward regions such as the ventral tegmental area (VTA) consistent with their role in opioid reward and addiction. However, while both receptor types are expressed in the VTA, they are largely expressed on separate neuronal populations. Specifically, MOR receptors are primarily expressed on GABA neurons in the VTA. Thus, MOR activation by agonists such as morphine reduces GABAergic tone on VTA DA neurons, leading to increased DA neuronal activity, or disinhibition. This results in increased DA release in VTA target structures such as the nucleus accumbens (NAc) and feelings of pleasure or reward. In contrast, KORs in the VTA are present on subsets of DA neurons. Thus, KOR agonists lead to decreased DA neuronal activity, consistent with aversive effects of kappa agonists such as dysphoria (Chefer, Backman, Gigante, & Shippenberg, 2013; Margolis, Lock, Chefer, et al., 2006). While much is known about the action of MOR agonists, such as morphine, at the receptor level, less is known about the downstream neuroadaptations that occur with chronic use.

1.4. Mesocorticolimbic Reward Circuitry

The mesocorticolimbic system is integral to the processing of reward, incentive salience, and aversion. The 6 major nodes of the reward circuitry (VTA, dorsal striatum (dStr), NAc, PFC, basolateral amygdala (BLA), and hippocampus (Hipp)) are represented in Figure 2. The VTA also receives important glutamatergic regulation from the lateral habenula (LHb), and both cholinergic and glutamatergic innervation from the lateral dorsal tegmentum (LDT) and the pedunculo pontine tegmental nucleus (PPTg), and GABAergic innervation from the rostral medial tegmentum (RMTg), dStr and NAc.

1.4.1. Ventral Tegmental Area (VTA)

The VTA is a heterogeneous region critical for processing natural and drug rewards. It is comprised mostly of dopamine (DA, 60-65%) and gamma-aminobutyric acid (GABA, ~30-35%) neurons, with a small proportion of glutamatergic neurons (2-3%) (Nair-Roberts et al., 2008; Swanson, 1982). The VTA is generally defined as a dopaminergic brain region and most studies of the VTA have focused on this class of neurons. However, VTA DA neurons can be further defined by their projection target (e.g. NAc, BLA, Hipp, PFC) and activation of specific circuits can elicit distinct behaviors.

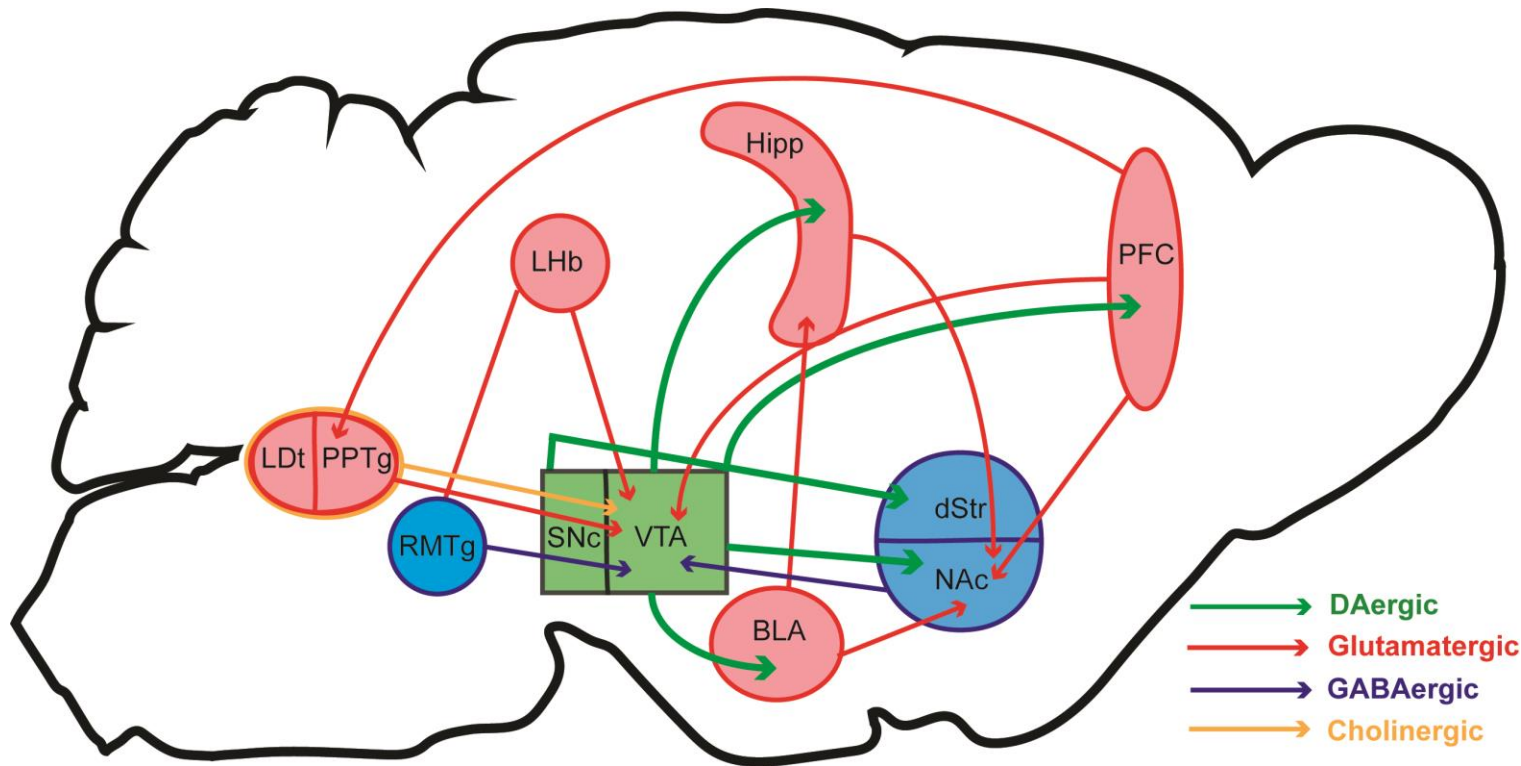


Figure 2. Mesocorticolimbic Reward Circuitry.

DAergic neurons (green) project from the VTA to the prefrontal cortex (PFC), nucleus accumbens (NAc), basolateral amygdala (BLA) and hippocampus (Hipp). DAergic neurons from the substantia nigra pars compacta (SNc) also project to the dorsal striatum (dStr). The VTA receives glutamatergic (red) input primarily from the PFC, lateral habenula (Lhb). The VTA also receives glutamatergic and cholinergic (yellow) input from laterodorsal tegmentum (Ldt) and pedunculo pontine tegmental nucleus (PPTg). VTA also receives GABAergic input from local VTA GABA neurons, NAc, and rostromedial tegmental nucleus (RMTg). Finally, the NAc receives glutamatergic input from the mPFC, BLA and Hipp.

In general, activation of VTA DA neurons increases the release of dopamine into projection regions (Nestler, 2005; Wise & Rompre, 1989). Virtually all known drugs of abuse increase DA levels in the NAc and direct activation of the VTA-NAc circuit through ICSS or optogenetic activation is sufficient to produce reward-related behaviors (Pascoli, Terrier, Hiver, & Luscher, 2015; Tsai et al., 2009; Witten et al., 2011). The DAergic VTA-NAc circuit has been the focus of numerous studies due to its critical involvement in drug and natural reward, but other VTA DA circuits (e.g. Hipp, BLA, PFC) have not received as much attention. This seems to be changing as appreciation for the distinct actions of subpopulations of VTA DA neurons grows, for example a number of recent studies have examined the DAergic VTA-PFC circuit. Interestingly, in opposition to the NAc circuit, activation of PFC-projecting VTA DA neurons is associated with the processing of aversive stimuli such as foot shock (Lammel, Ion, Roeper, & Malenka, 2011). Similar studies are now beginning to examine VTA DA projections to the Hipp and BLA. DA release in the Hipp is thought to mediate motivationally relevant learning and facilitate LTP (Lisman & Grace, 2005; McNamara, Tejero-Cantero, Trouche, Campo-Urriza, & Dupret, 2014; Rosen, Cheung, & Siegelbaum, 2015) and release in the BLA is integral for fear conditioning (de Oliveira et al., 2011; Fadok, Darvas, Dickerson, & Palmiter, 2010; Greba, Gifkins, & Kokkinidis, 2001). However, there is much work left to more fully understand the role of DA in these structures. The source of DA in the Hipp is under debate as recent evidence suggests it may be from catecholaminergic neurons residing in the locus coeruleus (LC), which also send projections to the Hipp, and not necessarily VTA DA neurons (McNamara & Dupret, 2017). Due to the wide variety of behavior elicited from specific VTA DA

projections it will be important to systematically examine how the function of each circuit is affected by different classes of drugs of abuse.

The VTA receives input from a variety of regions including glutamatergic input from the LDT, LHb, and PFC. The VTA also receives GABAergic input from NAc and RMTg, as well local VTA GABA interneurons (Figure 2). Of note, there is evidence of a relationship between VTA DA input and output circuitry associated with rewarding and aversive stimuli. For example, activation of the LDT→VTA DA→ NAc circuit promotes reward, while activation of the LHb→VTA DA→ PFC circuit is aversive (Lammel et al., 2012). While mapping specific VTA circuits is the focus of many current studies, there is still little data on how drugs of abuse affect the function of these distinct circuits. Given that VTA DA function is critical for drug reward, it will be essential to determine both cell- and circuit-specific effects of chronic opioid action in the VTA in order to better understand and treat opioid addiction.

1.4.2. Dorsal Striatum (dStr) and Nucleus Accumbens (NAc)

Another integral region for reward processing is the striatum, which can be divided into the dorsal striatum (dStr) and ventral striatum (i.e. the nucleus accumbens, NAc). These regions can be distinguished based on their predominant source of midbrain DA input: substantia nigra pars compacta (SNc) DA neurons project primarily to the dStr while VTA DA neurons project to the NAc (Oades & Halliday, 1987). The primary cell type within the dStr and NAc are GABAergic medium spiny neurons (MSNs), which can be further distinguished by D1- or D2-like DA receptor expression (Lu, Ghasemzadeh, & Kalivas, 1998). While both dStr and NAc have similar cellular

make up, region-specific D1 and D2 MSN regulation of reward processing is more nuanced across NAc and dStr projection circuitry.

It is well established that activation of D1 MSNs in the dStr increase thalamocortical drive through the direct pathway and ultimately increase motivated action. D2 MSNs, on the other hand, decrease thalamocortical drive through the indirect pathway and are associated with inhibiting goal-directed movement (Bolam, Hanley, Booth, & Bevan, 2000; Gerfen, 1984; Lenz & Lobo, 2013). In addition to regulation of movement, dopamine release in the dStr is necessary for the integration of reward and goal directed behavior, particularly in operant behaviors such as drug self-administration (Balleine, Delgado, & Hikosaka, 2007; Kreitzer & Malenka, 2008). And while dStr is integral in action selection, decision making and motor behavior output, there is some evidence for capability of direct reward-processing. Optogenetic activation of SNc neurons or their axon terminals in the dStr induces reward (operant place preference and optogenetic ICSS) while inactivation induces operant place avoidance similar to effects seen in direct VTA/NAc optogenetic ICSS studies (Ilango et al., 2014; Rossi, Sukharnikova, Hayrapetyan, Yang, & Yin, 2013). The rewarding effect of dStr activation may be mediated particularly by D1 MSNs. Optogenetic ICSS of D1 MSN neurons in the dStr resulted in CPP whereas no preference was formed by similar stimulation of D2 MSNs (Kravitz, Tye, & Kreitzer, 2012). Future studies will be needed to delineate the roles of dStr D1 and D2 MSN in reward processing separate from learning and motivated action selection.

While the role for DA release in the dStr in reward and initiation of motivated action is somewhat unclear, DA release in the NAc is critical for integrating the

rewarding and aversive aspects associated with a stimulus. The NAc is generally subdivided into the core and shell, with more recent studies distinguishing between medial (m.shell) and lateral shell (l.shell). Each subregion is implicated in overlapping aspects of reward behavior. Activation of the NAc m.shell induces strong reward-related behaviors and is thought to be the traditional hot-spot for hedonic value of reward (Castro & Berridge, 2014; Ikemoto, 2007; Sesack & Grace, 2010). It is well established that DA release into the NAc m.shell produces reward-related behavior, regardless of mode of activation (optogenetic, ICSS, systemic or ICSSA administration of drugs of abuse) (Carlezon, Devine, & Wise, 1995; Ikemoto, 2002; Ikemoto, Glazier, Murphy, & McBride, 1997). Activity of the NAc core is particularly important for the integration of reward with learning operant behavior, and the transition to compulsive action in drug abuse (Namburi, Al-Hasani, Calhoon, Bruchas, & Tye, 2016). In contrast, the l.shell has been implicated in the processing of reward and aversive stimuli, where direct activation of kappa opioid receptors results in pronounced CPA while conversely, DA-release into the l.shell is rewarding (Al-Hasani et al., 2015; Yang et al., 2018). Overall, the NAc is a key structure in the mesocorticolimbic reward circuitry, and much like the VTA, is critical in both reward, aversion and action selection processing.

In addition to VTA DA input, NAc MSNs also receive a large amount of glutamatergic input from the PFC, ventral HIPP (vHIPP), and basolateral amygdala (BLA) that is also important in reward processing (Floresco, 2015; Sesack & Grace, 2010). For example, direct activation of PFC glutamatergic input to the NAc core induces drug seeking behavior and increased glutamatergic plasticity in the NAc is

thought to mediate drug craving (Bossert, Marchant, Calu, & Shaham, 2013; Li, Caprioli, & Marchant, 2015).

1.4.3. Primary Sources of Glutamatergic Input: PFC, BLA and Hipp

The PFC is particularly noted for its role in executive control over reward behaviors such as drug seeking and provides glutamatergic innervation to multiple reward circuit structures including the VTA and NAc (Kalivas, Volkow, & Seamans, 2005). The medial PFC can be divided along the dorsal-ventral axis into the cingulate cortex (Cg1), prelimbic (PrL), infralimbic (IL) regions. Regulation of reward behavior is associated with specific PFC and NAc microcircuits, such as preferential projections from IL to NAc shell and PrL to NAc core (Sesack & Grace, 2010). As noted earlier, glutamatergic signaling from the PrL PFC to NAc core is critical in drug-seeking behavior (Bossert et al., 2013; Li et al., 2015). There is also evidence for glutamatergic drive of VTA DA neuron burst firing following cocaine and morphine treatment (Lammel et al., 2011; Lane et al., 2008; Sarti, Borgland, Kharazia, & Bonci, 2007). Additionally, since PFC glutamatergic neurons synapse onto PFC-projecting VTA DA neurons, there is potential for direct regulation of VTA DA-PFC circuitry (Carr & Sesack, 2000).

The Hipp and BLA also act as important sources of glutamatergic control of mesocortical reward circuitry and are implicated in aversive processing, locomotor effects of drugs and drug seeking behavior (Pascoli et al., 2014; Vezina & Kim, 1999). Specifically, glutamatergic projections to the NAc from the Hipp are critical for integrating contextual information in reward learning while projections from the BLA are important for integrating emotional salience information (French & Totterdell, 2003). Given the role of BLA and Hipp in integrating environmental information, it is not

surprising that they are integral in processing both rewarding and aversive stimuli (Correia & Goosens, 2016). Glutamatergic neurons of the BLA synapse onto NAc D1 MSNs and activation of this circuit is thought to mediate reward and seeking behaviors similarly to PFC – NAc stimulation (Ambroggi, Ishikawa, Fields, & Nicola, 2008; Charara & Grace, 2003; Janak & Tye, 2015; Stuber et al., 2011).

1.4.4. Regulation of VTA DA Neuronal Activity

There are multiple sources of GABAergic and glutamatergic input that regulate the activity of VTA DA neurons. Dense GABAergic innervation of VTA DA neurons serves to maintain a slow tonic firing rate, thereby mediating a continuous low supply of DA in projection regions (Floresco, West, Ash, Moore, & Grace, 2003; Grace, Floresco, Goto, & Lodge, 2007). In contrast, activation of glutamatergic inputs induces phasic or burst firing of VTA DA neurons, producing increased DA release in target regions that is associated with drug reward (Grace & Bunney, 1984; Grace et al., 2007). But VTA DA burst firing is not solely regulated by glutamatergic signaling. Separate glutamatergic and cholinergic projections from the lateral dorsal tegmentum (LDT) serve as “gates” to allow burst firing while cholinergic projections from the pedunculopontine tegmental nucleus (PPTg) regulate continual burst activity (Dautan et al., 2016; Floresco et al., 2003; Lodge & Grace, 2006; Lokwan, Overton, Berry, & Clark, 1999).

To orchestrate complex motivated behaviors there must be integration of afferent modulation across distinct anatomical and projection-specific subsets of VTA DA neurons. In the following sections, I will discuss VTA DA neuron heterogeneity and how defining specific subsets of VTA DA neurons is necessary to more fully understand the role of VTA DA neurons in reward processing.

1.5. VTA DA Neuron Heterogeneity and Function

The VTA has been at the center of a multitude of addiction related studies, with most work focusing on the DA neurons within this structure (Berridge & Robinson, 1998; Grace et al., 2007; Juarez & Han, 2016; Lammel, Lim, & Malenka, 2014; Luscher & Malenka, 2011; Saal, Dong, Bonci, & Malenka, 2003). Traditionally, VTA DA neurons were thought to be relatively homogenous in their electrophysiological properties and in their role in reward and motivated behavior. But with more precise techniques, including genetic isolation of specific neuron types, input/output circuitry mapping, and functional optogenetic studies, there has been a surge of evidence for VTA DA neuron heterogeneity. Two of the main sources of VTA DA neuron heterogeneity are: 1) cytoarchitecture of the VTA, 2) VTA neuronal cellular properties and projections.

1.5.1. Cytoarchitecture of the VTA

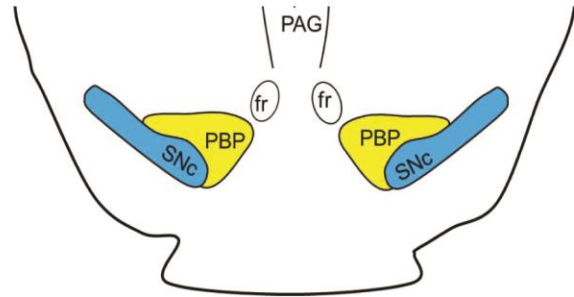
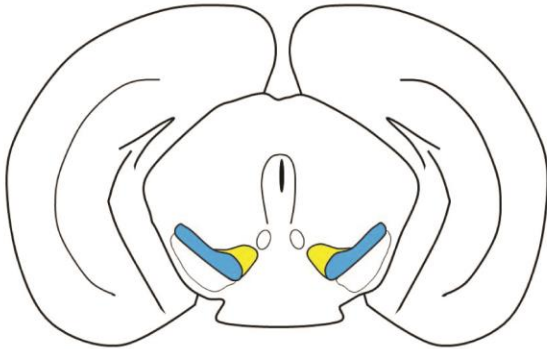
In early studies, midbrain dopamine neuron populations were originally divided into 3 loosely defined nuclei, A8, A9, and A10 (Dahlstrom & Fuxe, 1964). These numbered regions have since been renamed as retrorubral field (RRF, A8), SNc (A9), and VTA (A10) (Oades & Halliday, 1987). Each region was defined by a combination of tyrosine hydroxylase (TH) staining (TH is the rate-limiting enzyme in DA-synthesis), primary DA projection target, and drug reward processing. (Dahlstrom & Fuxe, 1964; Fallon, 1981; Fallon, Koziell, & Moore, 1978; Fallon & Moore, 1978a, 1978b; Ikemoto, 2007; Oades & Halliday, 1987). For example, DA neurons in A10 projected predominantly to the ventral striatum (NAc and olfactory tubercle) and direct infusion into this region elicited drug reward (Ikemoto & Wise, 2004). In contrast, A9 DA neurons projected predominantly to the dStr (Ikemoto, 2007). However, this nomenclature was

not without controversy, as there was a lack of consensus on whether to include other nuclei besides the VTA in the A10 division. For example, initially a number of midbrain nuclei (including interfascicular nucleus (IF), rostral linear nucleus (RLi), central linear nucleus (CLi), supramammillary nucleus (SUM), medial habenula (MHb), dorsal raphe (DR) and periaqueductal gray (PAG)) were collectively referred to as A10 (Oades & Halliday, 1987; Phillipson, 1979a, 1979b, 1979c; Swanson, 1982). However, recent studies generally use A10 to refer specifically to DA neurons in the VTA.

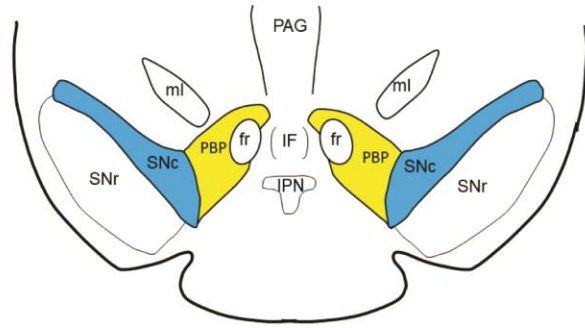
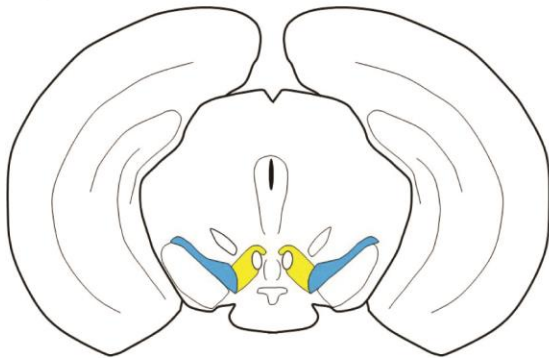
VTA cytoarchitecture was further defined into distinct subregions: the paranigral nucleus (PN) located anteriorly to the interpeduncular nucleus, the parabrachial pigmented nucleus (PBP) which extends dorsally from the PN, and the midline interfascicular nucleus (IF) as shown in Figures 3 and 4 (Fu et al., 2012; Ikemoto, 2007). DA neurons in the PN and PBP were easily distinguished from one another by cell morphology characteristics. PN DA neurons are predominantly medium size, oblong and have relatively uniform orientation toward the IF on an $\sim 45^\circ$ angle (Fu et al., 2012; Halliday & Tork, 1986; Ikemoto, 2007; Oades & Halliday, 1987). In contrast, PBP neurons appeared more heterogeneous, with medium to large cell bodies of varied shape and with no consistent orientation (Halliday & Tork, 1986; Ikemoto, 2007; Oades & Halliday, 1987). The IF subregion consists of small, round DA neurons with variable labeling for prominent DA cellular markers (e.g. TH and DAT) (Fu et al., 2012; Ikemoto, 2007). The PN and PBP are also distinguished by their topographical reciprocal circuitry with the NAc. Lateral PBP DA neurons project to, and receive GABAergic innervation from, the lateral shell of the NAc, and medial PN DA neurons primarily project to, and receive GABAergic innervation from, the m.shell of the NAc (Yang et al., 2018).

Anterior VTA Anatomy

Bregma -2.92



Bregma -3.08



Bregma -3.16

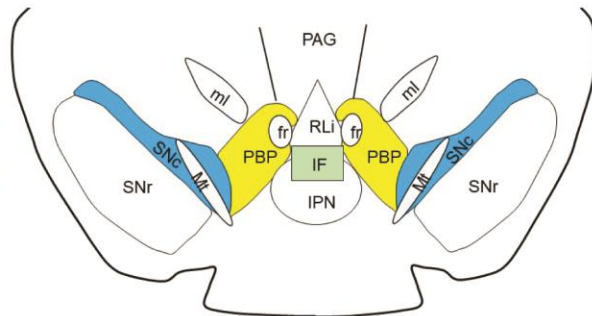
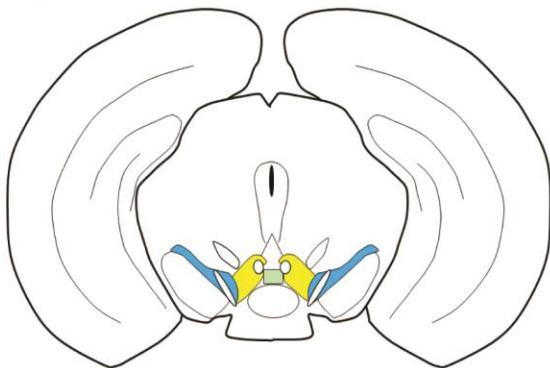
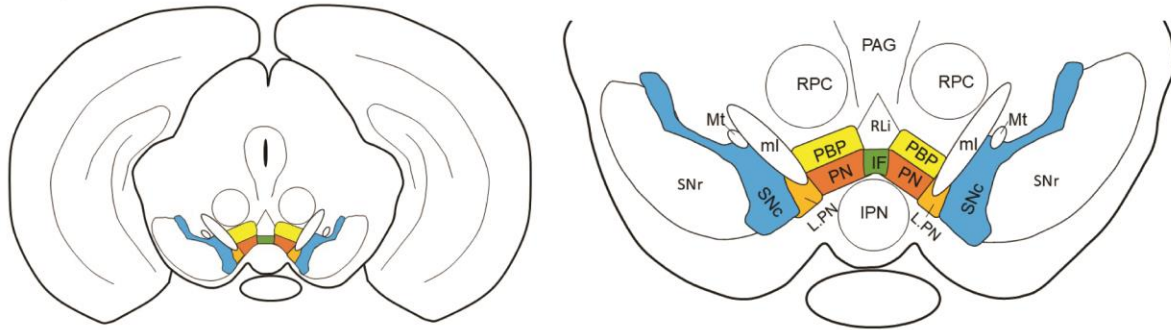


Figure 3. Anterior VTA Anatomy.

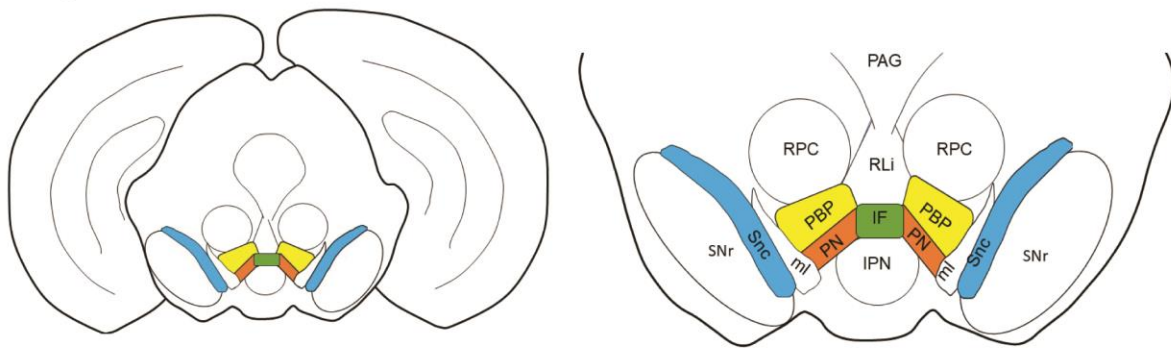
Substantia nigra pars compacta (SNc) is designated in blue, while aVTA, the parabrachial pigmented nucleus (PBP) is designated in yellow. Midline DA nuclei, interfesicular nucleus (IF) is shown in light green. Other non-DA regions are in white including: fasiculus retroflexis (fr), interpeduncular nucleus (IPN), medial lemniscus (ml), medial terminal nucleus of the optic tract (Mt), paraquedal gray (PAG), rostral linear nucleus (RLi), substantia nigra reticulata (SNr).

Posterior VTA Anatomy

Bregma -3.28



Bregma -3.52



Bregma -3.80

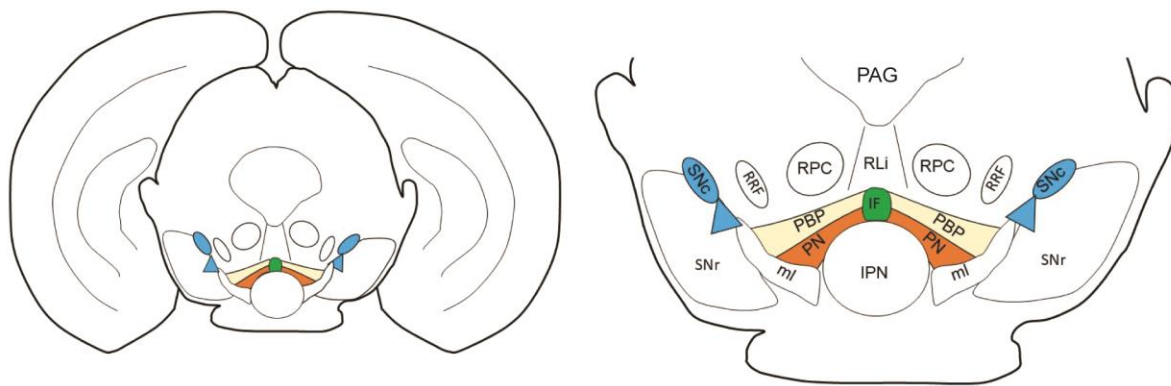


Figure 4. Posterior VTA Anatomy.

Substantia nigra pars compacta (SNc) is designated in blue. VTA DA subregions are distinguished by color: parabrachial pigmental nucleus (PBP) in yellow, paranigral nucleus (PN) in orange, and interfesicular nucleus (IF) in green. Other non-DA regions are in white including: interpeduncular nucleus (IPN), medial lemniscus (ml), medial terminal nucleus of the optic tract (Mt), paraquedal gray (PAG), red nucleus parvicellular part (RPC), retro rubral field (RRF), rostral linear nucleus (RLi), substantia nigra reticulata (SNr).

Complicating matters further, there is also a well-established literature delineating differences between the anterior (aVTA) and posterior VTA (pVTA). This includes differences in composition of VTA DA subregions, afferent/efferent connections, and reward function (Sanchez-Catalan, Kaufling, Georges, Veinante, & Barrot, 2014). Briefly, the aVTA is generally divided into the rostral anterior VTA which is medial and less DA-rich than the lateral aVTA, which is primarily an anterior extension of the PBP (Figure 3). The aVTA is mostly composed of mesolimbic DA neurons that project to the NAc core and lateral shell (Ikemoto, 2007; Lammel et al., 2008). In contrast the pVTA is more heterogeneous, containing DA neurons in the PBP, PN, and IF subregions (Figure 4) that project to a wide array of regions including the NAc (core, lateral and media shell), mPFC, and amygdala (Beier et al., 2015; Lammel et al., 2008).

The anterior-posterior distinctions were supported by multiple drug self-administration studies, where collectively, the pVTA supported intracranial self-administration of common drugs of abuse (ethanol, opioid, cocaine, methamphetamine, nicotine) while infusion in the aVTA did not (reviewed in Sanchez-Catalan et al. (2014)). While the aVTA may not directly support ICSS of opioids, it can modulate opioid reward. Morphine and heroin CPP were prevented or substantially reduced in studies where aVTA activity was inhibited either by lidocaine, GABA agonists, or blockade of glutamatergic AMPA receptors (Hutson et al., 2014; Moaddab, Haghparast, & Hassanpour-Ezatti, 2009; Shabat-Simon, Levy, Amir, Rehavi, & Zangen, 2008). Although the focus of this dissertation is primarily on opioid-induced plasticity in pVTA

DA neurons, a better understanding of the role of the aVTA in reward processing will be necessary for a more complete appreciation of the VTA in opioid reward.

1.5.2. VTA Neuron Cellular Properties and Projections

Traditionally, the VTA subregions have been defined primarily by the presence of DA-specific immunostaining (e.g. TH) (Ikemoto, 2007). But the VTA is not comprised of only DA neurons. While ~60-65% of neurons within the VTA are DAergic, there is also a large population of GABA neurons (30-35%) and a smaller population of glutamatergic neurons (~5%) (Nair-Roberts et al., 2008). However, these numbers are approximations and may depend on the criteria used to identify a neuron. For example, recent studies using electrophysiological markers and VGLUT2 expression suggest that there may actually be a higher proportion of glutamatergic neurons within the VTA (Kawano et al., 2006; Nair-Roberts et al., 2008; Yamaguchi, Sheen, & Morales, 2007; Yang et al., 2018). Critically, the three major neuronal populations (DA, GABA, Glut) are not equally distributed throughout the VTA. For example, glutamate neurons are predominantly within the anterior and medial structures (aVTA: PBP and RLi, and pVTA: IF, RLi and medial PN) (Morales & Margolis, 2017; Nair-Roberts et al., 2008). GABA neurons, on the other hand, are most concentrated within the pVTA PN and are less prominent in the aVTA and pVTA PBP regions (Edwards et al., 2017; Nair-Roberts et al., 2008).

The traditional distinct, single-neurotransmitter definition of VTA neuron populations may not accurately represent the heterogeneity of cell types within the VTA. Some DA neurons have the ability to co-release glutamate (Hnasko et al., 2010; Stuber, Hnasko, Britt, Edwards, & Bonci, 2010). These neurons (that express both TH and VGLUT2) were thought to be predominantly located in midline nuclei (IF, RLi and CLi)

and project to the PFC and NAc (Chuhma, Mingote, Moore, & Rayport, 2014; Morales & Margolis, 2017; Zhang et al., 2015). However, recent evidence suggests that these neurons may also represent a significant portion of VTA DA neurons in the PN that project to the NAc m.shell (Yang et al., 2018). Additionally, some populations of VTA DA neurons in midline nuclei (RLi, CLi) are capable of co-releasing GABA either through GABA-reuptake or the Aldha1a-dependent alternative GABA synthesis pathway (Kim et al., 2015; Tritsch, Oh, Gu, & Sabatini, 2014). It has been suggested that DA/GABA neurons (TH- and GAD-positive) in midline nuclei project to LHb, although there are conflicting reports based on the TH immunolabeling and the DA Cre-reporter line used (Lammel et al., 2015; Stamatakis et al., 2013). Importantly, these examples serve as a reminder that there are multiple VTA DA populations, many of which have not been directly studied in reward assays. Thus, it will be important to determine the roles of these specialized populations in future studies of reward-related behavior.

Prior to the discovery of co-neurotransmitter VTA DA neuron heterogeneity, VTA DA neurons were identified primarily based on the presence of tyrosine hydroxylase (TH) immunoreactivity and electrophysiological properties, most notably the presence of a robust hyperpolarization-activated current (I_h). Therefore, neurons in the VTA were divided into two types: type-1 neurons were considered dopaminergic as they displayed TH-immunolabeling and a high I_h current, while type-2 neurons were considered GABAergic and lacked TH-staining and/or displayed no or low I_h current (Grace & Onn, 1989; Johnson & North, 1992b). Other common criteria used to define DA neurons were low frequency pacemaker activity, broad action potentials, and hyperpolarization by DA via D2 receptors (Kitai, 1999). The use of these criteria to identify DA vs. GABA neurons

was predominant in the field and much of our understanding of VTA DA function in reward processing, such as increased phasic firing and DA release in the NAc, used these features in electrophysiological studies (Grace et al., 2007; Grace & Onn, 1989; Kalivas, 1993; Margolis, Lock, Hjelmstad, & Fields, 2006). But recent evidence suggests that using Ih to distinguish between GABAergic and DAergic VTA neurons is problematic. Specifically, use of Ih as the primary identifier of DA neurons may have been selective to only a few of the DA subtypes. For example, VTA DA neurons that project the l.shell NAc have high Ih, while DA neurons that project to the PFC and m.shell have low Ih. As summarized in Table 3, DA neurons vary in electrophysiological properties based on projection target (Ford, Mark, & Williams, 2006; Lammel et al., 2008; Lammel et al., 2011).

Table 3. Electrophysiological Properties Across DA Projection Target.

DA-projection:	nigro-striatal	NAc l.shell	NAc m.shell	PFC
Ih	high	high	low	low
D2 -mediated inhibition	yes	yes	yes	no
AMPA/NMDA	low	low	high	high

Abbreviations: ratio of α -amino-3-hydroxy-5-methyl-4-isoxazolepropionic acid (AMPA) to N-methyl-D-aspartic acid (NMDA) excitatory post-synaptic currents (AMPA/NMDA) dopamine (DA), dopamine receptor type 2 (D2), hyperpolarizing activated current (Ih), nucleus accumbens lateral shell (NAc l.shell), nucleus accumbens medial shell (NAc m.shell), prefrontal cortex (PFC).

In addition to differences in basal electrophysiological properties of projection-specific subsets DA neurons, there is also evidence for distinct responses to rewarding and aversive stimuli. For example, NAc-projecting VTA DA neurons are activated by rewarding stimuli such as cocaine, while PFC-projecting neurons are activated by aversive stimuli such as formalin paw injection or foot-shock (Lammel et al., 2011).

Additionally, optogenetic stimulation of LDT projections to VTA DA neurons that project

to NAc l.shell resulted in CPP, while activation of LHb inputs onto VTA DA neurons that project to PFC resulted in CPA (Lammel et al., 2012). Extensive research has been done to determine the role of VTA DA neurons in reward, but much of this research lacked VTA DA-projection specific distinctions (Juarez & Han, 2016). The new understanding of the diversity of VTA DA neurons raises questions about the interpretation of results from previous electrophysiological studies that used lh as a primary identifier of DA neurons. For example, the increase in phasic firing by drugs of abuse was predominantly identified in lh+ neurons. Therefore, these studies preferentially examined effects in VTA DA neurons that project to NAc l.shell and likely excluded VTA DA neurons that project to the NAc m.shell and PFC (Juarez & Han, 2016; Lammel et al., 2014). Additionally, the use of horizontal slices for electrophysiological studies made the distinction between VTA subregions difficult and likely led to the preferential selection of neurons in the lateral regions of the PBP (Lammel et al., 2014). To date, the majority of chronic opioid-related studies have not taken into account VTA DA neuron heterogeneity. Given that there is increasing evidence for separate VTA DA populations inducing opioid reward and dysphoria/withdrawal (See Section 1.6), it is important to systematically assess the possibility of projection-specific opioid plasticity.

1.6. Opioid Reward Circuitry

Opioid drugs induce changes in VTA function. Similar to other drugs of abuse such as cocaine, opioids induce excitatory plasticity in VTA DA neurons. For example, 24 hr. following a single treatment of morphine the ratio of α -amino-3-hydroxy-5-methyl-4isoxazolepropionic acid (AMPA) to N-methyl-D-aspartic acid (NMDA) excitatory post-

synaptic currents (AMPA/NMDA) is increased, indicative of increased synaptic strength onto DA neurons (Saal et al., 2003). Additionally, acute morphine increases insertion of GluA2-lacking AMPA receptors in VTA DA neurons (Brown et al., 2010). This glutamatergic plasticity is similar to that produced by other drugs of abuse and is associated with drug craving (Brown et al., 2010; Ungless, Whistler, Malenka, & Bonci, 2001).

1.6.1. DA-independent Mechanisms of Opioid Reward

While the action of VTA DA neurons are implicated in the effects of all drugs of abuse, opioid reward may be driven by both DA-dependent and -independent pathways (Fujita, Ide, & Ikeda, 2018). As described earlier, the DA-dependent pathway involves MOR-mediated inhibition of GABAergic input onto VTA DA neurons, leading to increased DA activity and DA release in the NAc (Fields & Margolis, 2015; Mazei-Robison & Nestler, 2012). However, evidence suggests that opioid reward can also be induced independently of DA release in the NAc. Rats treated with a DA receptor antagonist (alpha-flupentixol) or 6-OHDA-induced lesions of DA terminals in the NAc showed disrupted cocaine but not heroin IVSA (Ettenberg, Pettit, Bloom, & Koob, 1982; Pettit, Ettenberg, Bloom, & Koob, 1984). Additionally, DA-deficient mice can display morphine-induced CPP (Hnasko, Sotak, & Palmiter, 2005). One common factor in these studies is that the DA-independent opioid reward was induced only in previously drug-naïve rodents; blockade of DA receptor or DA release in rodents with previous drug dependence results in abolished or attenuated opioid reward (Fujita et al., 2018). This discrepancy with prior drug experience has contributed to theories for integrated yet

distinct circuitry for DA-independent acquisition and DA-dependent maintenance of opioid dependence (Fujita et al., 2018; Ting & van der Kooy, 2012).

DA-independent mechanisms of reward in opioid-naïve states involve regulation of the PPTg. Early studies identified a role for PPTg in DA-independent opioid reward through lesion studies. Specifically, lesion of PPTg blocked morphine-induced CPP in opioid-naïve rats, while having no effect on formation of CPP in opioid-dependent rats (Bechara & van der Kooy, 1989, 1992). The PPTg is a heterogenous region with GABAergic, glutamatergic and cholinergic neurons (Mena-Segovia & Bolam, 2017; Wang & Morales, 2009). Optogenetic activation of cholinergic and glutamatergic neurons in the PPTg induces reward and serve as promising mechanisms for DA-independent reward. The role of PPTg GABAergic neurons is still being elucidated (Xiao et al., 2016; Yoo et al., 2017). It is important to note that while the PPTg is implicated in DA-independent reward in drug-naïve rodents, PPTg glutamatergic and cholinergic neurons also send projections directly to VTA and SNc DA neurons. Optogenetic stimulation of PPTg cholinergic neurons induces DA release in the NAc (Mena-Segovia & Bolam, 2017). Therefore, PPTg-mediated reward may not be entirely DA-independent in its strictest definition. Taken together, these examples illustrate that while DA release in the NAc is sufficient for the acquisition of opioid reward, it may not be necessary. The discrepancy on the necessity of DA for opioid reward serves as a reminder that it is likely that no single brain region or cell type is solely responsible for opioid-induced reward, but rather that it results from the integration of many systems.

1.6.2. DA- and MOR-dependent Mechanisms of Opioid Reward

As mentioned previously, the predominant theory of DA-dependent opioid reward is through activation of MORs in the VTA to elicit disinhibition of VTA DA neurons. MORs are predominantly expressed on GABAergic neurons in the VTA, and MOR agonist binding directly inhibits GABA neuron function (Gysling & Wang, 1983; Johnson & North, 1992a). This ultimately leads to opioid-induced increases in tonic and phasic DA neuronal activity and DA release into the NAc (Georges, Le Moine, & Aston-Jones, 2006; Hutchinson et al., 2012; Koo et al., 2012; Mazei-Robison et al., 2011). However, recent research suggests that opioid receptor action in the VTA may be more complex than originally thought. There is now evidence MORs are not exclusively expressed on VTA GABA neurons but are also present on a subset of VTA DA neurons. Moreover, application of the MOR-agonist DAMGO in drug-naïve rats resulted in an increase in DA neuron firing rate independent of disrupted GABAergic signaling (Margolis, Hjelmstad, Fujita, & Fields, 2014). Additionally, both MOR and KOR expression has been identified on VTA DA neurons and receptor activation had opposing and some conflicting effects on neuronal activity. VTA application of a KOR agonist (U69593) increased whole-cell current in NAc m.shell-projecting, but not BLA-projecting, VTA DA neurons (Ford et al., 2006). Conversely, another study found KORs were expressed on PFC-projecting VTA DA neurons and application of KOR agonist reduced activity of this subset of neurons, while having no effect on VTA DA neurons that projected to the NAc (Margolis, Lock, Chefer, et al., 2006). While MOR-mediated inhibition of GABAergic signaling is critical for chronic opioid-induced plasticity, it will be important to determine the extent to which

direct and indirect MOR or KOR activation of subsets of VTA DA neurons may alter VTA DA activity and opioid reward.

1.6.3. Opioid-induced VTA GABA Signaling

While MOR-dependent GABAergic inhibition is sufficient to induce opioid reward, the origin of this GABAergic innervation remains somewhat unclear due to multiple inputs into the VTA (Fields & Margolis, 2015). Early evidence suggested that the GABAergic cell bodies in the VTA innervate nearby DA neurons, but these GABAergic neurons may also project to the NAc, mPFC and PPTg (Brown et al., 2012; Omelchenko & Sesack, 2005). It is therefore possible that VTA GABAergic inhibition by MOR agonists can alternatively disinhibit other distinct neuron populations, which in turn, innervate the VTA and are integral to reward processing. Additionally, VTA DA neurons also receive substantial inhibitory input from the NAc D1 MSN neurons (Yang et al., 2018), as well as from the RMTg (Balcita-Pedicino, Omelchenko, Bell, & Sesack, 2011; Barrot et al., 2012; Jalabert et al., 2011). Collectively, while much of what we understand about opioid-induced adaptations have delineated from pharmacological *ex vitro* experiments within the VTA, many of the *in vivo* experiments understandably use systemic drug treatment. Therefore, systemic opioid agonists (morphine, heroin, etc.) are likely to affect many systems and the integration of the projections described above add to the complexity of opioid dependence.

Traditionally the inhibitory GABAergic tone on VTA DA neurons was thought to be primarily driven by metabotropic GABA_B receptors on VTA DA neurons which mediate slower and prolonged inhibition through downstream regulation of potassium and calcium channels (Edwards et al., 2017; Kalivas, Duffy, & Eberhardt, 1990;

Laviolette & van der Kooy, 2001; Wirtshafter & Sheppard, 2001). Meanwhile, GABA_A ionotropic receptors are predominantly expressed on VTA GABA neurons and mediate fast-acting chloride-influx and therefore hyperpolarization and inhibition (Churchill, Dilts, & Kalivas, 1992; Kalivas, 1993). But recent evidence has shown projection-specific expression of both GABA_A and GABA_B receptors on VTA DA neurons (Yang et al., 2018). Yang et al. showed that NAc m.shell-projecting VTA DA neurons can be directly inhibited by NAc m.shell D1-MSNs through GABA_A signaling. This is in contrast to NAc l.shell D1 MSN inhibition of l.shell-projecting VTA DA neurons via GABA_B receptor activation.

Additionally, there is a switch from inhibitory to excitatory GABA_A receptor action during the transition from opioid-naïve to opioid-dependent states (Ting & van der Kooy, 2012). GABA_A channel ion flow can be reversed and depolarize (i.e. activate) the neuron if there is altered chloride and bicarbonate concentration gradients across the membrane (Kaila, 1994; Stein & Nicoll, 2003). In drug-naïve rats GABA_A agonists normally inhibit VTA GABA neurons, yet in the drug-dependent/withdrawal state the same treatment activates a subset of GABA neurons (Laviolette, Gallegos, Henriksen, & van der Kooy, 2004; Vargas-Perez et al., 2009). It is hypothesized that GABA_A reversal mediates a switch in opioid reward circuitry from DA-independent to DA-dependent mechanisms. In drug-naïve rats, GABA_A agonists facilitate DA dependent reward (DA disinhibition) while GABA_A antagonists may drive PPTg-mediated reward (Fujita et al., 2018; Ikemoto, Murphy, & McBride, 1998; Laviolette & van der Kooy, 2001). However, in the drug-dependent state, the primary target of agonist/antagonist action is reversed, as GABA_A agonists induce PPTg-reward and antagonists mediate increased DA activity.

Therefore, GABA_A regulation may be integral to the transition from drug-naïve (DA-independent PPTg pathways) to drug-dependent reward (GABA disinhibition mediated DA-dependent reward) discussed previously (Laviolette & van der Kooy, 2001).

1.6.4. Chronic Opioid-induced Structural Plasticity

In the previous sections I have outlined how opioids induce synaptic plasticity across a multitude of cell types and regions which in turn modulate VTA DA neuron activity. Long-term use of opioids induces lasting changes in VTA DA activity, output and structural morphology, which have been correlated with changes in reward behavior (e.g. reward tolerance during drug dependence). For instance, chronic (but not acute) opioid exposure reduces VTA DA soma size by approximately 20-25% (Chu et al., 2007; Mazei-Robison et al., 2011; Russo et al., 2007; Sklair-Tavron et al., 1996). Importantly, decreased soma size was correlated with increased DA activity and reward tolerance, as soma size changes were found to persist for at least 2 weeks following opiate administration (Mazei-Robison et al., 2011; Russo et al., 2007). A similar decrease in VTA DA soma size has also been observed in post-mortem samples from heroin addicts suggesting that this adaptation may be translationally relevant. This morphological adaptation does not occur with other drugs of abuse, such as cocaine, ethanol or nicotine (Mazei-Robison et al., 2014). However, decreased soma size is induced by multiple types of opioid drugs (morphine, heroin) and by multiple routes of administration (subcutaneous pellet, i.p. injections, self-administration). Moreover, the decrease in soma size can be blocked by systemic MOR antagonist treatment suggesting it is dependent on action at the MOR (Chu et al., 2007; Mazei-Robison et al., 2011; Russo et al., 2007; Sklair-Tavron et al., 1996; Spiga, Serra, Puddu, Foddai, &

Diana, 2003). The decrease in size is also activity-dependent such that over expression of a potassium channel subunit in VTA DA neurons prevents the morphine-induced change in soma size (Mazei-Robison et al., 2011). Collectively, this suggests that the chronic opioid-induced increase in activity of VTA DA neurons mediates a sequence of molecular changes in VTA DA neurons that ultimately induce structural plasticity which may underlie long-lasting changes in VTA DA function that drive addiction-related behavior.

1.6.5. Molecular Mediators of Opioid-induced VTA DA Structural Plasticity

Progress has been made in identification of molecular mediators of VTA DA structural plasticity. It was first suggested that the decrease in VTA DA soma size was driven by changes in actin remodeling particularly through altered brain-derived neurotrophic factor (BDNF) signaling. Indeed, chronic opioid administration alters the 3 main signaling pathways downstream of BDNF/TrkB in the VTA: phospholipase C gamma (PLC γ), insulin receptor substrate 2 (IRS2)-Akt and MAPK (Mazei-Robison et al., 2011; Russo et al., 2007; Russo, Mazei-Robison, Ables, & Nestler, 2009; Wolf, Nestler, & Russell, 2007; Wolf, Numan, Nestler, & Russell, 1999). Currently the data suggest that it is reduced signaling of the IRS2-Akt pathway that is critical for chronic-opioid induced changes in VTA DA neuron structure (Mazei-Robison et al., 2011; Russo et al., 2007; Russo et al., 2009; Wolf et al., 1999). Herpes simplex virus (HSV) expression of dominant-negative IRS2 in the VTA reduces phospho-Akt levels, reduces basal VTA DA soma size and attenuates morphine-induced CPP and locomotor sensitization (Russo et al., 2007). Conversely, overexpression of wild type IRS2 prevents chronic morphine-induced changes in DA soma size and morphine reward

(Russo et al., 2007). One possible mediator of VTA DA actin remodeling associated with IRS2/Akt signaling is mammalian target of rapamycin complex 2 (mTORC2). mTORC2 phosphorylates kinases implicated in opioid-reward and actin remodeling such as Akt, protein kinase C (PKC) and serum-and glucocorticoid-inducible kinase 1 (SGK1). In support of this, VTA overexpression of a component protein of mTORC2 (rapamycin insensitive companion of TOR, Rictor) is sufficient to prevent morphine-induced changes in VTA DA soma size and neuronal activity and attenuate morphine CPP (Mazei-Robison et al., 2011).

These candidate protein-based studies have helped to provide framework underlying opiate-induced neuroadaptations, but much remains unknown. Identification and confirmation of chronic opioid-induced molecular mediators of VTA DA plasticity is difficult due to the cellular complexity of the VTA. Several studies have utilized microarray and RNAsequencing of VTA following chronic opioid and withdrawal conditions and have identified some candidate genes (Heller et al., 2015; McClung, Nestler, & Zachariou, 2005). For example, SGK1 is of particular interest due to its induction in the VTA by chronic morphine, chronic cocaine, and chronic stress (Cooper et al., 2017; Heller et al., 2015; Koo et al., 2015; McClung et al., 2005). However, the interpretation of these studies is limited, as RNA was isolated from the whole VTA, so it is unclear if gene expression changes are driven specifically by VTA DA neurons or by other cell types.

Additionally, as discussed earlier, VTA DA neurons themselves are not homogenous and distinct projection-specific populations are involved in reward and aversion. In fact, increased VTA DA activity is not always synonymous with reward, as

subsets of VTA DA neurons are activated by aversive stimuli (foot-shock and formalin-paw injections) and chronic social defeat stress (Brischoux, Chakraborty, Brierley, & Ungless, 2009; Chaudhury et al., 2013; Lammel et al., 2011). Thus, changes in VTA DA plasticity may also be projection-specific. One particularly interesting study showed projection-specific glutamatergic synaptic plasticity in response to morphine. Specifically, GluA1 receptor expression was increased in PFC-projecting TH+ neurons in the PBP, but not in NAc-projecting TH+ neurons in the PN (Lane et al., 2008). This study also provides evidence for projection-specific changes in VTA DA neuron structure. Following chronic morphine administration, dendrites on NAc-projecting VTA DA neurons in the PN were significantly smaller than in saline-treated control, and dendrites on PFC-projecting VTA DA neurons in the PBP were significantly larger (Lane et al., 2008). Whether chronic opioid-induced changes in VTA DA soma size are also projection-specific has yet to be determined.

1.7. Hypothesis and Specific Aims

Despite the prevalent long-term use and abuse of opiate drugs, relatively little is known about the neuroadaptations that occur with chronic use. We previously determined that chronic opiate exposure decreases the soma size of VTA DA neurons (Mazei-Robison et al., 2011; Russo et al., 2007). This change was observed in post-mortem human samples as well as in rodent models where soma size was correlated with DA neuronal activity and reward behavior (Mazei-Robison et al., 2011). However, VTA DA neurons are heterogeneous; subsets of VTA DA neurons exhibit distinct electrophysiological properties and stimulation depending on their projection target (Chaudhury et al., 2013; Lammel et al., 2011; Lammel et al., 2012). While we know that

behaviorally relevant structural and functional changes are induced in VTA DA neurons in response to chronic opiates, we do not know if these changes are driven by specific VTA DA circuits. *I hypothesized that chronic opioids differentially regulate VTA DA neurons based on projection target and that the chronic opioid-induced decrease in soma size is present in NAc-projecting VTA DA neurons but not in PFC-projecting neurons.* Therefore, in Specific Aim 1, I tested this hypothesis using viral-mediated fluorophore expression to label specific VTA DA circuits and assess changes in morphology induced by chronic morphine.

The VTA is not only composed of dopaminergic neurons, but also includes GABAergic and glutamatergic neurons (Margolis, Toy, Himmels, Morales, & Fields, 2012; Morales & Root, 2014). Additionally, VTA DA and GABA neuron activity is oppositely regulated by chronic morphine such that VTA DA neuronal activity is increased while VTA GABA activity is decreased. Activation and inhibition of neuronal activity likely drives distinct molecular adaptations within DA and GABA neurons. However, all screening studies to date have been limited to homogenization of the entire VTA (Heller et al., 2015; Koo et al., 2015; McClung et al., 2005), potentially masking effects that occur in a single neuron type. *I hypothesized that chronic opioids induce a unique set of transcriptional changes in VTA DA neurons that result in actin remodeling, channel regulation, and ultimately increased activity.* I addressed this hypothesis in Specific Aim 2 by isolating actively translating mRNA specifically from DA neurons in the VTA using Translating Ribosome Affinity Purification (TRAP). Through combined RNAsequencing and RT-PCR validation, we identified novel transcript alterations, accelerating the current understanding of DA-specific response to opiates.

Together, Aims 1 and 2 address my central hypothesis, that chronic morphine induces structural plasticity in VTA DA neurons in a projection-specific manner and is mediated by transcriptional changes in VTA DA neurons. Importantly, this work significantly advances our understanding of how chronic opiate exposure alters the structure and function of VTA DA neurons and provides insight into novel mechanisms underlying mesocorticolimbic circuit dysfunction necessary for improved therapeutic strategies for drug abuse. Thus, the results of this dissertation research are a critical first step in a series of experiments to link structural adaptations to behavioral outcomes through cell type- and circuit-specific viral manipulation of candidate genes.

REFERENCES

REFERENCES

- Adewumi, A. D., Hollingworth, S. A., Maravilla, J. C., Connor, J. P., & Alati, R. (2018). Prescribed Dose of Opioids and Overdose: A Systematic Review and Meta-Analysis of Unintentional Prescription Opioid Overdose. *CNS Drugs*, 32(2), 101-116. doi:10.1007/s40263-018-0499-3
- Al-Hasani, R., & Bruchas, M. R. (2011). Molecular mechanisms of opioid receptor-dependent signaling and behavior. *Anesthesiology*, 115(6), 1363-1381. doi:10.1097/ALN.0b013e318238bba6
- Al-Hasani, R., McCall, J. G., Shin, G., Gomez, A. M., Schmitz, G. P., Bernardi, J. M., . . . Bruchas, M. R. (2015). Distinct Subpopulations of Nucleus Accumbens Dynorphin Neurons Drive Aversion and Reward. *Neuron*, 87(5), 1063-1077. doi:10.1016/j.neuron.2015.08.019
- Algren, D. A., Monteilh, C. P., Punja, M., Schier, J. G., Belson, M., Hepler, B. R., . . . Rubin, C. (2013). Fentanyl-associated fatalities among illicit drug users in Wayne County, Michigan (July 2005-May 2006). *J Med Toxicol*, 9(1), 106-115. doi:10.1007/s13181-012-0285-4
- Ambroggi, F., Ishikawa, A., Fields, H. L., & Nicola, S. M. (2008). Basolateral amygdala neurons facilitate reward-seeking behavior by exciting nucleus accumbens neurons. *Neuron*, 59(4), 648-661. doi:10.1016/j.neuron.2008.07.004
- American Psychiatric Association. (2000). *Diagnostic and statistical manual of mental disorders* (4th ed. Text Review ed.).
- American Psychiatric Association. (2013). *Diagnostic and statistical manual of mental disorders* (5th ed. ed.): American Psychiatric Association.
- Arvidsson, U., Riedl, M., Chakrabarti, S., Lee, J. H., Nakano, A. H., Dado, R. J., . . . Elde, R. (1995). Distribution and targeting of a mu-opioid receptor (MOR1) in brain and spinal cord. *J Neurosci*, 15(5 Pt 1), 3328-3341.
- Asam.org. (n.d.). Short Definition of Addiction. Retrieved from <https://www.asam.org/resources/definition-of-addiction>
- Balcita-Pedicino, J. J., Omelchenko, N., Bell, R., & Sesack, S. R. (2011). The inhibitory influence of the lateral habenula on midbrain dopamine cells: ultrastructural evidence for indirect mediation via the rostromedial mesopontine tegmental nucleus. *J Comp Neurol*, 519(6), 1143-1164. doi:10.1002/cne.22561

- Balleine, B. W., Delgado, M. R., & Hikosaka, O. (2007). The role of the dorsal striatum in reward and decision-making. *J Neurosci*, 27(31), 8161-8165.
doi:10.1523/JNEUROSCI.1554-07.2007
- Barrot, M., Sesack, S. R., Georges, F., Pistis, M., Hong, S., & Jhou, T. C. (2012). Braking dopamine systems: a new GABA master structure for mesolimbic and nigrostriatal functions. *J Neurosci*, 32(41), 14094-14101.
doi:10.1523/JNEUROSCI.3370-12.2012
- Bechara, A., & van der Kooy, D. (1989). The tegmental pedunculopontine nucleus: a brain-stem output of the limbic system critical for the conditioned place preferences produced by morphine and amphetamine. *J Neurosci*, 9(10), 3400-3409.
- Bechara, A., & van der Kooy, D. (1992). A single brain stem substrate mediates the motivational effects of both opiates and food in nondeprived rats but not in deprived rats. *Behav Neurosci*, 106(2), 351-363.
- Becker, A., Grecksch, G., Brodemann, R., Kraus, J., Peters, B., Schroeder, H., . . . Holtt, V. (2000). Morphine self-administration in mu-opioid receptor-deficient mice. *Naunyn Schmiedebergs Arch Pharmacol*, 361(6), 584-589.
- Beier, K. T., Steinberg, E. E., DeLoach, K. E., Xie, S., Miyamichi, K., Schwarz, L., . . . Luo, L. (2015). Circuit Architecture of VTA Dopamine Neurons Revealed by Systematic Input-Output Mapping. *Cell*, 162(3), 622-634.
doi:10.1016/j.cell.2015.07.015
- Berrendero, F., Kieffer, B. L., & Maldonado, R. (2002). Attenuation of nicotine-induced antinociception, rewarding effects, and dependence in mu-opioid receptor knock-out mice. *J Neurosci*, 22(24), 10935-10940.
- Berridge, K. C., & Robinson, T. E. (1998). What is the role of dopamine in reward: hedonic impact, reward learning, or incentive salience? *Brain Res Brain Res Rev*, 28(3), 309-369.
- Bolam, J. P., Hanley, J. J., Booth, P. A., & Bevan, M. D. (2000). Synaptic organisation of the basal ganglia. *J Anat*, 196 (Pt 4), 527-542.
- Bossert, J. M., Marchant, N. J., Calu, D. J., & Shaham, Y. (2013). The reinstatement model of drug relapse: recent neurobiological findings, emerging research topics, and translational research. *Psychopharmacology (Berl)*, 229(3), 453-476.
doi:10.1007/s00213-013-3120-y
- Brady, K. T., McCauley, J. L., & Back, S. E. (2016). Prescription Opioid Misuse, Abuse, and Treatment in the United States: An Update. *Am J Psychiatry*, 173(1), 18-26.
doi:10.1176/appi.ajp.2015.15020262

- Brischoux, F., Chakraborty, S., Brierley, D. I., & Ungless, M. A. (2009). Phasic excitation of dopamine neurons in ventral VTA by noxious stimuli. *Proc Natl Acad Sci U S A*, *106*(12), 4894-4899. doi:10.1073/pnas.0811507106
- Brown, M. T., Bellone, C., Mameli, M., Labouebe, G., Bocklisch, C., Balland, B., . . . Luscher, C. (2010). Drug-driven AMPA receptor redistribution mimicked by selective dopamine neuron stimulation. *PLoS One*, *5*(12), e15870. doi:10.1371/journal.pone.0015870
- Brown, M. T., Tan, K. R., O'Connor, E. C., Nikonenko, I., Muller, D., & Luscher, C. (2012). Ventral tegmental area GABA projections pause accumbal cholinergic interneurons to enhance associative learning. *Nature*, *492*(7429), 452-456. doi:10.1038/nature11657
- Bruchas, M. R., Land, B. B., & Chavkin, C. (2010). The dynorphin/kappa opioid system as a modulator of stress-induced and pro-addictive behaviors. *Brain Res*, *1314*, 44-55. doi:10.1016/j.brainres.2009.08.062
- Carlezon, W. A., Jr., Devine, D. P., & Wise, R. A. (1995). Habit-forming actions of nomifensine in nucleus accumbens. *Psychopharmacology (Berl)*, *122*(2), 194-197.
- Carr, D. B., & Sesack, S. R. (2000). Projections from the rat prefrontal cortex to the ventral tegmental area: target specificity in the synaptic associations with mesoaccumbens and mesocortical neurons. *J Neurosci*, *20*(10), 3864-3873.
- Castro, D. C., & Berridge, K. C. (2014). Opioid hedonic hotspot in nucleus accumbens shell: mu, delta, and kappa maps for enhancement of sweetness "liking" and "wanting". *J Neurosci*, *34*(12), 4239-4250. doi:10.1523/JNEUROSCI.4458-13.2014
- CDC. (2011). *Vital Signs: Overdoses of Prescription Opioid Pain Relievers. United States, 1999-2008*. Retrieved from <https://www.cdc.gov/mmwr/preview/mmwrhtml/mm6043a4.htm>
- CDC. (2016a, Dec 16, 2016). Synthetic Opioid Overdose Data. Retrieved from <https://www.cdc.gov/drugoverdose/data/fentanyl.html>
- CDC. (2016b). Wide-ranging online data for epidemiologic research (WONDER). from CDC, National Center for Health Statistics <http://wonder.cdc.gov>
- CDC. (2017a). 3 Waves of the Rise in Opioid Overdose Deaths. In.
- CDC. (2017b). *Guideline for Prescribing Opioids for Chronic Pain*. Atlanta, GA Retrieved from <https://www.cdc.gov/drugoverdose/prescribing/guideline.html>.
- Center for Behavioral Health Statistics and Quality. (2016). *Impact of the DSM-IV to DSM-5 Changes on the National Survey on Drug Use and Health*. Rockville, MD.

- Center for Disease Control and Prevention (CDC). (2017, August 30, 2017). Understanding the Epidemic. Retrieved from <https://www.cdc.gov/drugoverdose/epidemic/>
- Charara, A., & Grace, A. A. (2003). Dopamine receptor subtypes selectively modulate excitatory afferents from the hippocampus and amygdala to rat nucleus accumbens neurons. *Neuropsychopharmacology*, *28*(8), 1412-1421. doi:10.1038/sj.npp.1300220
- Charbogne, P., Kieffer, B. L., & Befort, K. (2014). 15 years of genetic approaches in vivo for addiction research: Opioid receptor and peptide gene knockout in mouse models of drug abuse. *Neuropharmacology*, *76 Pt B*, 204-217. doi:10.1016/j.neuropharm.2013.08.028
- Chaudhury, D., Walsh, J. J., Friedman, A. K., Juarez, B., Ku, S. M., Koo, J. W., . . . Han, M. H. (2013). Rapid regulation of depression-related behaviours by control of midbrain dopamine neurons. *Nature*, *493*(7433), 532-536. doi:10.1038/nature11713
- Chefer, V. I., Backman, C. M., Gigante, E. D., & Shippenberg, T. S. (2013). Kappa opioid receptors on dopaminergic neurons are necessary for kappa-mediated place aversion. *Neuropsychopharmacology*, *38*(13), 2623-2631. doi:10.1038/npp.2013.171
- Chu, N. N., Zuo, Y. F., Meng, L., Lee, D. Y., Han, J. S., & Cui, C. L. (2007). Peripheral electrical stimulation reversed the cell size reduction and increased BDNF level in the ventral tegmental area in chronic morphine-treated rats. *Brain Res*, *1182*, 90-98. doi:10.1016/j.brainres.2007.08.086
- Chuhma, N., Mingote, S., Moore, H., & Rayport, S. (2014). Dopamine neurons control striatal cholinergic neurons via regionally heterogeneous dopamine and glutamate signaling. *Neuron*, *81*(4), 901-912. doi:10.1016/j.neuron.2013.12.027
- Churchill, L., Dilts, R. P., & Kalivas, P. W. (1992). Autoradiographic localization of gamma-aminobutyric acidA receptors within the ventral tegmental area. *Neurochem Res*, *17*(1), 101-106.
- Contarino, A., Picetti, R., Matthes, H. W., Koob, G. F., Kieffer, B. L., & Gold, L. H. (2002). Lack of reward and locomotor stimulation induced by heroin in mu-opioid receptor-deficient mice. *Eur J Pharmacol*, *446*(1-3), 103-109.
- Cooper, S. E., Kechner, M., Caraballo-Perez, D., Kaska, S., Robison, A. J., & Mazei-Robison, M. S. (2017). Comparison of chronic physical and emotional social defeat stress effects on mesocorticolimbic circuit activation and voluntary consumption of morphine. *Sci Rep*, *7*(1), 8445. doi:10.1038/s41598-017-09106-3

- Correia, S. S., & Goosens, K. A. (2016). Input-specific contributions to valence processing in the amygdala. *Learn Mem*, 23(10), 534-543. doi:10.1101/lm.037887.114
- Cunningham, C. L., Gremel, C. M., & Groblewski, P. A. (2006). Drug-induced conditioned place preference and aversion in mice. *Nat Protoc*, 1(4), 1662-1670. doi:10.1038/nprot.2006.279
- Dahlstrom, A., & Fuxe, K. (1964). Localization of monoamines in the lower brain stem. *Experientia*, 20(7), 398-399.
- Dautan, D., Souza, A. S., Huerta-Ocampo, I., Valencia, M., Assous, M., Witten, I. B., . . . Mena-Segovia, J. (2016). Segregated cholinergic transmission modulates dopamine neurons integrated in distinct functional circuits. *Nat Neurosci*, 19(8), 1025-1033. doi:10.1038/nn.4335
- David, V., & Cazala, P. (1994). Differentiation of intracranial morphine self-administration behavior among five brain regions in mice. *Pharmacol Biochem Behav*, 48(3), 625-633.
- David, V., Matifas, A., Gavello-Baudy, S., Decorte, L., Kieffer, B. L., & Cazala, P. (2008). Brain regional Fos expression elicited by the activation of mu- but not delta-opioid receptors of the ventral tegmental area: evidence for an implication of the ventral thalamus in opiate reward. *Neuropsychopharmacology*, 33(7), 1746-1759. doi:10.1038/sj.npp.1301529
- Daynard, R. A., Bates, C., & Francey, N. (2000). Tobacco litigation worldwide. *BMJ*, 320(7227), 111-113.
- de Oliveira, A. R., Reimer, A. E., de Macedo, C. E., de Carvalho, M. C., Silva, M. A., & Brandao, M. L. (2011). Conditioned fear is modulated by D2 receptor pathway connecting the ventral tegmental area and basolateral amygdala. *Neurobiol Learn Mem*, 95(1), 37-45. doi:10.1016/j.nlm.2010.10.005
- DEA, D. E. A. (2015). *DEA Issues Nationwide Alert on Fentanyl as Threat to Health and Public Safety*. Retrieved from <https://www.dea.gov/divisions/hq/2015/hq031815.shtml>.
- Edwards, N. J., Tejada, H. A., Pignatelli, M., Zhang, S., McDevitt, R. A., Wu, J., . . . Bonci, A. (2017). Circuit specificity in the inhibitory architecture of the VTA regulates cocaine-induced behavior. *Nat Neurosci*, 20(3), 438-448. doi:10.1038/nn.4482
- Ettenberg, A., Pettit, H. O., Bloom, F. E., & Koob, G. F. (1982). Heroin and cocaine intravenous self-administration in rats: mediation by separate neural systems. *Psychopharmacology (Berl)*, 78(3), 204-209.

- Fadok, J. P., Darvas, M., Dickerson, T. M., & Palmiter, R. D. (2010). Long-term memory for pavlovian fear conditioning requires dopamine in the nucleus accumbens and basolateral amygdala. *PLoS One*, *5*(9), e12751. doi:10.1371/journal.pone.0012751
- Fallon, J. H. (1981). Collateralization of monoamine neurons: mesotelencephalic dopamine projections to caudate, septum, and frontal cortex. *J Neurosci*, *1*(12), 1361-1368.
- Fallon, J. H., Koziell, D. A., & Moore, R. Y. (1978). Catecholamine innervation of the basal forebrain. II. Amygdala, suprarhinal cortex and entorhinal cortex. *J Comp Neurol*, *180*(3), 509-532. doi:10.1002/cne.901800308
- Fallon, J. H., & Moore, R. Y. (1978a). Catecholamine innervation of the basal forebrain. III. Olfactory bulb, anterior olfactory nuclei, olfactory tubercle and piriform cortex. *J Comp Neurol*, *180*(3), 533-544. doi:10.1002/cne.901800309
- Fallon, J. H., & Moore, R. Y. (1978b). Catecholamine innervation of the basal forebrain. IV. Topography of the dopamine projection to the basal forebrain and neostriatum. *J Comp Neurol*, *180*(3), 545-580. doi:10.1002/cne.901800310
- Fields, H. L., & Margolis, E. B. (2015). Understanding opioid reward. *Trends Neurosci*, *38*(4), 217-225. doi:10.1016/j.tins.2015.01.002
- Floresco, S. B. (2015). The nucleus accumbens: an interface between cognition, emotion, and action. *Annu Rev Psychol*, *66*, 25-52. doi:10.1146/annurev-psych-010213-115159
- Floresco, S. B., West, A. R., Ash, B., Moore, H., & Grace, A. A. (2003). Afferent modulation of dopamine neuron firing differentially regulates tonic and phasic dopamine transmission. *Nat Neurosci*, *6*(9), 968-973. doi:10.1038/nn1103
- Ford, C. P., Mark, G. P., & Williams, J. T. (2006). Properties and opioid inhibition of mesolimbic dopamine neurons vary according to target location. *J Neurosci*, *26*(10), 2788-2797. doi:10.1523/JNEUROSCI.4331-05.2006
- French, S. J., & Totterdell, S. (2003). Individual nucleus accumbens-projection neurons receive both basolateral amygdala and ventral subicular afferents in rats. *Neuroscience*, *119*(1), 19-31.
- Fu, Y., Yuan, Y., Halliday, G., Rusznak, Z., Watson, C., & Paxinos, G. (2012). A cytoarchitectonic and chemoarchitectonic analysis of the dopamine cell groups in the substantia nigra, ventral tegmental area, and retrorubral field in the mouse. *Brain Struct Funct*, *217*(2), 591-612. doi:10.1007/s00429-011-0349-2
- Fuchs, P. N., Roza, C., Sora, I., Uhl, G., & Raja, S. N. (1999). Characterization of mechanical withdrawal responses and effects of mu-, delta- and kappa-opioid

- agonists in normal and mu-opioid receptor knockout mice. *Brain Res*, 821(2), 480-486.
- Fujita, M., Ide, S., & Ikeda, K. (2018). Opioid and nondopamine reward circuitry and state-dependent mechanisms. *Ann N Y Acad Sci*. doi:10.1111/nyas.13605
- Georges, F., Le Moine, C., & Aston-Jones, G. (2006). No effect of morphine on ventral tegmental dopamine neurons during withdrawal. *J Neurosci*, 26(21), 5720-5726. doi:10.1523/JNEUROSCI.5032-05.2006
- Gerfen, C. R. (1984). The neostriatal mosaic: compartmentalization of corticostriatal input and striatonigral output systems. *Nature*, 311(5985), 461-464.
- Ghozland, S., Matthes, H. W., Simonin, F., Filliol, D., Kieffer, B. L., & Maldonado, R. (2002). Motivational effects of cannabinoids are mediated by mu-opioid and kappa-opioid receptors. *J Neurosci*, 22(3), 1146-1154.
- Goeders, N. E., & Smith, J. E. (1987). Intracranial self-administration methodologies. *Neurosci Biobehav Rev*, 11(3), 319-329.
- Grace, A. A., & Bunney, B. S. (1984). The control of firing pattern in nigral dopamine neurons: burst firing. *J Neurosci*, 4(11), 2877-2890.
- Grace, A. A., Floresco, S. B., Goto, Y., & Lodge, D. J. (2007). Regulation of firing of dopaminergic neurons and control of goal-directed behaviors. *Trends Neurosci*, 30(5), 220-227. doi:10.1016/j.tins.2007.03.003
- Grace, A. A., & Onn, S. P. (1989). Morphology and electrophysiological properties of immunocytochemically identified rat dopamine neurons recorded in vitro. *J Neurosci*, 9(10), 3463-3481.
- Greba, Q., Gifkins, A., & Kokkinidis, L. (2001). Inhibition of amygdaloid dopamine D2 receptors impairs emotional learning measured with fear-potentiated startle. *Brain Res*, 899(1-2), 218-226.
- Gysling, K., & Wang, R. Y. (1983). Morphine-induced activation of A10 dopamine neurons in the rat. *Brain Res*, 277(1), 119-127.
- Haddox JD, J. D., Angarola RT, Brady A, Carr DB, Blonsky ER, Burchiel K, Giltin M, Midcap M, Payne R, Simon D, Vasudevan S, Wilson P. (1997). The use of opioids for the treatment of chronic pain. A consensus statement from the American Academy of Pain Medicine and the American Pain Society. *Clin J Pain*, 13(1), 6-8.
- Hall, F. S., Li, X. F., Goeb, M., Roff, S., Hoggatt, H., Sora, I., & Uhl, G. R. (2003). Congenic C57BL/6 mu opiate receptor (MOR) knockout mice: baseline and opiate effects. *Genes Brain Behav*, 2(2), 114-121.

- Halliday, G. M., & Tork, I. (1986). Comparative anatomy of the ventromedial mesencephalic tegmentum in the rat, cat, monkey and human. *J Comp Neurol*, 252(4), 423-445. doi:10.1002/cne.902520402
- Hasin, D. S., O'Brien, C. P., Auriacombe, M., Borges, G., Bucholz, K., Budney, A., . . . Grant, B. F. (2013). DSM-5 criteria for substance use disorders: recommendations and rationale. *Am J Psychiatry*, 170(8), 834-851. doi:10.1176/appi.ajp.2013.12060782
- Heit, H. A., & Gourlay, D. L. (2009). DSM-V and the definitions: time to get it right. *Pain Med*, 10(5), 784-786. doi:10.1111/j.1526-4637.2009.00654.x
- Heller, E. A., Kaska, S., Fallon, B., Ferguson, D., Kennedy, P. J., Neve, R. L., . . . Mazei-Robison, M. S. (2015). Morphine and cocaine increase serum- and glucocorticoid-inducible kinase 1 activity in the ventral tegmental area. *J Neurochem*, 132(2), 243-253. doi:10.1111/jnc.12925
- Helzer, J. E., van den Brink, W., & Guth, S. E. (2006). Should there be both categorical and dimensional criteria for the substance use disorders in DSM-V? *Addiction*, 101 Suppl 1, 17-22. doi:10.1111/j.1360-0443.2006.01587.x
- Hnasko, T. S., Chuhma, N., Zhang, H., Goh, G. Y., Sulzer, D., Palmiter, R. D., . . . Edwards, R. H. (2010). Vesicular glutamate transport promotes dopamine storage and glutamate corelease in vivo. *Neuron*, 65(5), 643-656. doi:10.1016/j.neuron.2010.02.012
- Hnasko, T. S., Sotak, B. N., & Palmiter, R. D. (2005). Morphine reward in dopamine-deficient mice. *Nature*, 438(7069), 854-857. doi:10.1038/nature04172
- Hutchinson, M. R., Northcutt, A. L., Hiranita, T., Wang, X., Lewis, S. S., Thomas, J., . . . Watkins, L. R. (2012). Opioid activation of toll-like receptor 4 contributes to drug reinforcement. *J Neurosci*, 32(33), 11187-11200. doi:10.1523/JNEUROSCI.0684-12.2012
- Hutson, L. W., Szczytkowski, J. L., Saurer, T. B., Lebonville, C., Fuchs, R. A., & Lysle, D. T. (2014). Region-specific contribution of the ventral tegmental area to heroin-induced conditioned immunomodulation. *Brain Behav Immun*, 38, 118-124. doi:10.1016/j.bbi.2014.01.008
- Ikemoto, S. (2002). Ventral striatal anatomy of locomotor activity induced by cocaine, D-amphetamine, dopamine and D1/D2 agonists. *Neuroscience*, 113(4), 939-955.
- Ikemoto, S. (2007). Dopamine reward circuitry: two projection systems from the ventral midbrain to the nucleus accumbens-olfactory tubercle complex. *Brain Res Rev*, 56(1), 27-78. doi:10.1016/j.brainresrev.2007.05.004

- Ikemoto, S., Glazier, B. S., Murphy, J. M., & McBride, W. J. (1997). Role of dopamine D1 and D2 receptors in the nucleus accumbens in mediating reward. *J Neurosci*, *17*(21), 8580-8587.
- Ikemoto, S., Murphy, J. M., & McBride, W. J. (1998). Regional differences within the rat ventral tegmental area for muscimol self-infusions. *Pharmacol Biochem Behav*, *61*(1), 87-92.
- Ikemoto, S., & Wise, R. A. (2004). Mapping of chemical trigger zones for reward. *Neuropharmacology*, *47 Suppl 1*, 190-201.
doi:10.1016/j.neuropharm.2004.07.012
- Ilango, A., Kesner, A. J., Keller, K. L., Stuber, G. D., Bonci, A., & Ikemoto, S. (2014). Similar roles of substantia nigra and ventral tegmental dopamine neurons in reward and aversion. *J Neurosci*, *34*(3), 817-822.
doi:10.1523/JNEUROSCI.1703-13.2014
- Jalabert, M., Bourdy, R., Courtin, J., Veinante, P., Manzoni, O. J., Barrot, M., & Georges, F. (2011). Neuronal circuits underlying acute morphine action on dopamine neurons. *Proc Natl Acad Sci U S A*, *108*(39), 16446-16450.
doi:10.1073/pnas.1105418108
- Janak, P. H., & Tye, K. M. (2015). From circuits to behaviour in the amygdala. *Nature*, *517*(7534), 284-292. doi:10.1038/nature14188
- Jennings, A. (2018, May 3, 2018). L.A. sues 9 drug companies, alleging unethical practices that worsened the opioid crisis. *Los Angeles Times*. Retrieved from <http://www.latimes.com/local/lanow/la-me-ln-opioid-city-lawsuit-20180503-story.html>
- Johnson, S. W., & North, R. A. (1992a). Opioids excite dopamine neurons by hyperpolarization of local interneurons. *J Neurosci*, *12*(2), 483-488.
- Johnson, S. W., & North, R. A. (1992b). Two types of neurone in the rat ventral tegmental area and their synaptic inputs. *J Physiol*, *450*, 455-468.
- Juarez, B., & Han, M. H. (2016). Diversity of Dopaminergic Neural Circuits in Response to Drug Exposure. *Neuropsychopharmacology*, *41*(10), 2424-2446.
doi:10.1038/npp.2016.32
- Kaila, K. (1994). Ionic basis of GABAA receptor channel function in the nervous system. *Prog Neurobiol*, *42*(4), 489-537.
- Kalivas, P. W. (1993). Neurotransmitter regulation of dopamine neurons in the ventral tegmental area. *Brain Res Brain Res Rev*, *18*(1), 75-113.
- Kalivas, P. W., Duffy, P., & Eberhardt, H. (1990). Modulation of A10 dopamine neurons by gamma-aminobutyric acid agonists. *J Pharmacol Exp Ther*, *253*(2), 858-866.

- Kalivas, P. W., Volkow, N., & Seamans, J. (2005). Unmanageable motivation in addiction: a pathology in prefrontal-accumbens glutamate transmission. *Neuron*, 45(5), 647-650. doi:10.1016/j.neuron.2005.02.005
- Kanouse, A. B., & Compton, P. (2015). The epidemic of prescription opioid abuse, the subsequent rising prevalence of heroin use, and the federal response. *J Pain Palliat Care Pharmacother*, 29(2), 102-114. doi:10.3109/15360288.2015.1037521
- Katie Benner, J. H. (2018, Feb 27, 2018). Justice Dept. Backs High-Stakes Lawsuit Against Opioid Makers. *The New York Times*. Retrieved from <https://www.nytimes.com/2018/02/27/us/politics/justice-department-opioid-lawsuit.html>
- Kawano, M., Kawasaki, A., Sakata-Haga, H., Fukui, Y., Kawano, H., Nogami, H., & Hisano, S. (2006). Particular subpopulations of midbrain and hypothalamic dopamine neurons express vesicular glutamate transporter 2 in the rat brain. *J Comp Neurol*, 498(5), 581-592. doi:10.1002/cne.21054
- Kim, J. I., Ganesan, S., Luo, S. X., Wu, Y. W., Park, E., Huang, E. J., . . . Ding, J. B. (2015). Aldehyde dehydrogenase 1a1 mediates a GABA synthesis pathway in midbrain dopaminergic neurons. *Science*, 350(6256), 102-106. doi:10.1126/science.aac4690
- Kitanaka, N., Sora, I., Kinsey, S., Zeng, Z., & Uhl, G. R. (1998). No heroin or morphine 6beta-glucuronide analgesia in mu-opioid receptor knockout mice. *Eur J Pharmacol*, 355(1), R1-3.
- Kmiotek, E. K., Baimel, C., & Gill, K. J. (2012). Methods for intravenous self administration in a mouse model. *J Vis Exp*(70), e3739. doi:10.3791/3739
- Knoll, A. T., & Carlezon, W. A., Jr. (2010). Dynorphin, stress, and depression. *Brain Res*, 1314, 56-73. doi:10.1016/j.brainres.2009.09.074
- Kolodny, A., Courtwright, D. T., Hwang, C. S., Kreiner, P., Eadie, J. L., Clark, T. W., & Alexander, G. C. (2015). The prescription opioid and heroin crisis: a public health approach to an epidemic of addiction. *Annu Rev Public Health*, 36, 559-574. doi:10.1146/annurev-publhealth-031914-122957
- Koo, J. W., Mazei-Robison, M. S., Chaudhury, D., Juarez, B., LaPlant, Q., Ferguson, D., . . . Nestler, E. J. (2012). BDNF is a negative modulator of morphine action. *Science*, 338(6103), 124-128. doi:10.1126/science.1222265
- Koo, J. W., Mazei-Robison, M. S., LaPlant, Q., Egervari, G., Braunscheidel, K. M., Adank, D. N., . . . Nestler, E. J. (2015). Epigenetic basis of opiate suppression of Bdnf gene expression in the ventral tegmental area. *Nat Neurosci*, 18(3), 415-422. doi:10.1038/nn.3932

- Kotecha, M. K., & Sites, B. D. (2013). Pain policy and abuse of prescription opioids in the USA: a cautionary tale for Europe. *Anaesthesia*, *68*(12), 1210-1215. doi:10.1111/anae.12450
- Kravitz, A. V., Tye, L. D., & Kreitzer, A. C. (2012). Distinct roles for direct and indirect pathway striatal neurons in reinforcement. *Nat Neurosci*, *15*(6), 816-818. doi:10.1038/nn.3100
- Kreitzer, A. C., & Malenka, R. C. (2008). Striatal plasticity and basal ganglia circuit function. *Neuron*, *60*(4), 543-554. doi:10.1016/j.neuron.2008.11.005
- Lammel, S., Hetzel, A., Hackel, O., Jones, I., Liss, B., & Roeper, J. (2008). Unique properties of mesoprefrontal neurons within a dual mesocorticolimbic dopamine system. *Neuron*, *57*(5), 760-773. doi:10.1016/j.neuron.2008.01.022
- Lammel, S., Ion, D. I., Roeper, J., & Malenka, R. C. (2011). Projection-specific modulation of dopamine neuron synapses by aversive and rewarding stimuli. *Neuron*, *70*(5), 855-862. doi:10.1016/j.neuron.2011.03.025
- Lammel, S., Lim, B. K., & Malenka, R. C. (2014). Reward and aversion in a heterogeneous midbrain dopamine system. *Neuropharmacology*, *76 Pt B*, 351-359. doi:10.1016/j.neuropharm.2013.03.019
- Lammel, S., Lim, B. K., Ran, C., Huang, K. W., Betley, M. J., Tye, K. M., . . . Malenka, R. C. (2012). Input-specific control of reward and aversion in the ventral tegmental area. *Nature*, *491*(7423), 212-217. doi:10.1038/nature11527
- Lammel, S., Steinberg, E. E., Foldy, C., Wall, N. R., Beier, K., Luo, L., & Malenka, R. C. (2015). Diversity of transgenic mouse models for selective targeting of midbrain dopamine neurons. *Neuron*, *85*(2), 429-438. doi:10.1016/j.neuron.2014.12.036
- Land, B. B., Bruchas, M. R., Lemos, J. C., Xu, M., Melief, E. J., & Chavkin, C. (2008). The dysphoric component of stress is encoded by activation of the dynorphin kappa-opioid system. *J Neurosci*, *28*(2), 407-414. doi:10.1523/JNEUROSCI.4458-07.2008
- Lane, D. A., Lessard, A. A., Chan, J., Colago, E. E., Zhou, Y., Schlussman, S. D., . . . Pickel, V. M. (2008). Region-specific changes in the subcellular distribution of AMPA receptor GluR1 subunit in the rat ventral tegmental area after acute or chronic morphine administration. *J Neurosci*, *28*(39), 9670-9681. doi:10.1523/JNEUROSCI.2151-08.2008
- Laviolette, S. R., Gallegos, R. A., Henriksen, S. J., & van der Kooy, D. (2004). Opiate state controls bi-directional reward signaling via GABAA receptors in the ventral tegmental area. *Nat Neurosci*, *7*(2), 160-169. doi:10.1038/nn1182

- Laviolette, S. R., & van der Kooy, D. (2001). GABA(A) receptors in the ventral tegmental area control bidirectional reward signalling between dopaminergic and non-dopaminergic neural motivational systems. *Eur J Neurosci*, *13*(5), 1009-1015.
- Le Merrer, J., Becker, J. A., Befort, K., & Kieffer, B. L. (2009). Reward processing by the opioid system in the brain. *Physiol Rev*, *89*(4), 1379-1412. doi:10.1152/physrev.00005.2009
- Lenz, J. D., & Lobo, M. K. (2013). Optogenetic insights into striatal function and behavior. *Behav Brain Res*, *255*, 44-54. doi:10.1016/j.bbr.2013.04.018
- Li, X., Caprioli, D., & Marchant, N. J. (2015). Recent updates on incubation of drug craving: a mini-review. *Addict Biol*, *20*(5), 872-876. doi:10.1111/adb.12205
- Lipari, R. H. A. (2017). *How People Obtain the Prescription Pain Relievers they Misuse*. Retrieved from Center for Behavioral Health Statistics and Quality, Substance Abuse and Mental Health Services Administration, Rockville, MD:
- Lisman, J. E., & Grace, A. A. (2005). The hippocampal-VTA loop: controlling the entry of information into long-term memory. *Neuron*, *46*(5), 703-713. doi:10.1016/j.neuron.2005.05.002
- Lodge, D. J., & Grace, A. A. (2006). The laterodorsal tegmentum is essential for burst firing of ventral tegmental area dopamine neurons. *Proc Natl Acad Sci U S A*, *103*(13), 5167-5172. doi:10.1073/pnas.0510715103
- Loh, H. H., Liu, H. C., Cavalli, A., Yang, W., Chen, Y. F., & Wei, L. N. (1998). mu Opioid receptor knockout in mice: effects on ligand-induced analgesia and morphine lethality. *Brain Res Mol Brain Res*, *54*(2), 321-326.
- Lokwan, S. J., Overton, P. G., Berry, M. S., & Clark, D. (1999). Stimulation of the pedunculo-pontine tegmental nucleus in the rat produces burst firing in A9 dopaminergic neurons. *Neuroscience*, *92*(1), 245-254.
- Lu, X. Y., Ghasemzadeh, M. B., & Kalivas, P. W. (1998). Expression of D1 receptor, D2 receptor, substance P and enkephalin messenger RNAs in the neurons projecting from the nucleus accumbens. *Neuroscience*, *82*(3), 767-780.
- Luscher, C., & Malenka, R. C. (2011). Drug-evoked synaptic plasticity in addiction: from molecular changes to circuit remodeling. *Neuron*, *69*(4), 650-663. doi:10.1016/j.neuron.2011.01.017
- Lynch, M. (2016). The Opioid Pendulum and the Need for Better Pain Care. *Pain Med*. doi:10.1093/pm/pnw085
- Manchikanti, L. (2007). National drug control policy and prescription drug abuse: facts and fallacies. *Pain Physician*, *10*(3), 399-424.

- Mansour, A., Hoversten, M. T., Taylor, L. P., Watson, S. J., & Akil, H. (1995). The cloned mu, delta and kappa receptors and their endogenous ligands: evidence for two opioid peptide recognition cores. *Brain Res*, *700*(1-2), 89-98.
- Margolis, E. B., Hjelmstad, G. O., Fujita, W., & Fields, H. L. (2014). Direct bidirectional mu-opioid control of midbrain dopamine neurons. *J Neurosci*, *34*(44), 14707-14716. doi:10.1523/JNEUROSCI.2144-14.2014
- Margolis, E. B., Lock, H., Chefer, V. I., Shippenberg, T. S., Hjelmstad, G. O., & Fields, H. L. (2006). Kappa opioids selectively control dopaminergic neurons projecting to the prefrontal cortex. *Proc Natl Acad Sci U S A*, *103*(8), 2938-2942. doi:10.1073/pnas.0511159103
- Margolis, E. B., Lock, H., Hjelmstad, G. O., & Fields, H. L. (2006). The ventral tegmental area revisited: is there an electrophysiological marker for dopaminergic neurons? *J Physiol*, *577*(Pt 3), 907-924. doi:jphysiol.2006.117069 [pii]
10.1113/jphysiol.2006.117069
- Margolis, E. B., Toy, B., Himmels, P., Morales, M., & Fields, H. L. (2012). Identification of rat ventral tegmental area GABAergic neurons. *PLoS One*, *7*(7), e42365. doi:10.1371/journal.pone.0042365
- Matthes, H. W., Maldonado, R., Simonin, F., Valverde, O., Slowe, S., Kitchen, I., . . . Kieffer, B. L. (1996). Loss of morphine-induced analgesia, reward effect and withdrawal symptoms in mice lacking the mu-opioid-receptor gene. *Nature*, *383*(6603), 819-823. doi:10.1038/383819a0
- Mazei-Robison, M. S., Appasani, R., Edwards, S., Wee, S., Taylor, S. R., Picciotto, M. R., . . . Nestler, E. J. (2014). Self-administration of ethanol, cocaine, or nicotine does not decrease the soma size of ventral tegmental area dopamine neurons. *PLoS One*, *9*(4), e95962. doi:10.1371/journal.pone.0095962
PONE-D-14-06041 [pii]
- Mazei-Robison, M. S., Koo, J. W., Friedman, A. K., Lansink, C. S., Robison, A. J., Vinish, M., . . . Nestler, E. J. (2011). Role for mTOR signaling and neuronal activity in morphine-induced adaptations in ventral tegmental area dopamine neurons. *Neuron*, *72*(6), 977-990. doi:10.1016/j.neuron.2011.10.012
- Mazei-Robison, M. S., & Nestler, E. J. (2012). Opiate-induced molecular and cellular plasticity of ventral tegmental area and locus coeruleus catecholamine neurons. *Cold Spring Harb Perspect Med*, *2*(7), a012070. doi:10.1101/cshperspect.a012070
- McClung, C. A., Nestler, E. J., & Zachariou, V. (2005). Regulation of gene expression by chronic morphine and morphine withdrawal in the locus ceruleus and ventral

- tegmental area. *J Neurosci*, 25(25), 6005-6015. doi:10.1523/JNEUROSCI.0062-05.2005
- McNamara, C. G., & Dupret, D. (2017). Two sources of dopamine for the hippocampus. *Trends Neurosci*, 40(7), 383-384. doi:10.1016/j.tins.2017.05.005
- McNamara, C. G., Tejero-Cantero, A., Trouche, S., Campo-Urriza, N., & Dupret, D. (2014). Dopaminergic neurons promote hippocampal reactivation and spatial memory persistence. *Nat Neurosci*, 17(12), 1658-1660. doi:10.1038/nn.3843
- Mena-Segovia, J., & Bolam, J. P. (2017). Rethinking the Pedunculo-pontine Nucleus: From Cellular Organization to Function. *Neuron*, 94(1), 7-18. doi:10.1016/j.neuron.2017.02.027
- Minami, M., & Satoh, M. (1995). Molecular biology of the opioid receptors: structures, functions and distributions. *Neurosci Res*, 23(2), 121-145.
- Moaddab, M., Haghparast, A., & Hassanpour-Ezatti, M. (2009). Effects of reversible inactivation of the ventral tegmental area on the acquisition and expression of morphine-induced conditioned place preference in the rat. *Behav Brain Res*, 198(2), 466-471. doi:10.1016/j.bbr.2008.11.030
- Morales, M., & Margolis, E. B. (2017). Ventral tegmental area: cellular heterogeneity, connectivity and behaviour. *Nat Rev Neurosci*, 18(2), 73-85. doi:10.1038/nrn.2016.165
- Morales, M., & Root, D. H. (2014). Glutamate neurons within the midbrain dopamine regions. *Neuroscience*, 282, 60-68. doi:10.1016/j.neuroscience.2014.05.032
- Muhuri PK, G. J., Daview MC. (2013). *Associations of Nonmedical Pain Reliever Use and Initiation of Heroin Use in the United States*. CBHSQ Data Review.
- Muthen, B. (2006). Should substance use disorders be considered as categorical or dimensional? *Addiction*, 101 Suppl 1, 6-16. doi:10.1111/j.1360-0443.2006.01583.x
- Nair-Roberts, R. G., Chatelain-Badie, S. D., Benson, E., White-Cooper, H., Bolam, J. P., & Ungless, M. A. (2008). Stereological estimates of dopaminergic, GABAergic and glutamatergic neurons in the ventral tegmental area, substantia nigra and retrorubral field in the rat. *Neuroscience*, 152(4), 1024-1031. doi:10.1016/j.neuroscience.2008.01.046
- Namburi, P., Al-Hasani, R., Calhoon, G. G., Bruchas, M. R., & Tye, K. M. (2016). Architectural Representation of Valence in the Limbic System. *Neuropsychopharmacology*, 41(7), 1697-1715. doi:10.1038/npp.2015.358
- Negus, S. S., & Miller, L. L. (2014). Intracranial self-stimulation to evaluate abuse potential of drugs. *Pharmacol Rev*, 66(3), 869-917. doi:10.1124/pr.112.007419

- Nestler, E. J. (2005). Is there a common molecular pathway for addiction? *Nat Neurosci*, 8(11), 1445-1449. doi:10.1038/nn1578
- Nguyen, A. T., Marquez, P., Hamid, A., Kieffer, B., Friedman, T. C., & Lutfy, K. (2012). The rewarding action of acute cocaine is reduced in beta-endorphin deficient but not in mu opioid receptor knockout mice. *Eur J Pharmacol*, 686(1-3), 50-54. doi:10.1016/j.ejphar.2012.04.040
- Nguyen, A. T., Marquez, P., Hamid, A., & Lutfy, K. (2012). The role of mu opioid receptors in psychomotor stimulation and conditioned place preference induced by morphine-6-glucuronide. *Eur J Pharmacol*, 682(1-3), 86-91. doi:10.1016/j.ejphar.2012.02.021
- Oades, R. D., & Halliday, G. M. (1987). Ventral tegmental (A10) system: neurobiology. 1. Anatomy and connectivity. *Brain Res*, 434(2), 117-165.
- Office of National Drug Control Policy. (2010). Prescription Drug Abuse Prevention Plan [Press release]. Retrieved from <https://obamawhitehouse.archives.gov/ondcp/national-drug-control-strategy-introduction>
- Olmstead, M. C., & Franklin, K. B. (1997). The development of a conditioned place preference to morphine: effects of microinjections into various CNS sites. *Behav Neurosci*, 111(6), 1324-1334.
- Omelchenko, N., & Sesack, S. R. (2005). Laterodorsal tegmental projections to identified cell populations in the rat ventral tegmental area. *J Comp Neurol*, 483(2), 217-235. doi:10.1002/cne.20417
- Panlilio, L. V., & Goldberg, S. R. (2007). Self-administration of drugs in animals and humans as a model and an investigative tool. *Addiction*, 102(12), 1863-1870. doi:10.1111/j.1360-0443.2007.02011.x
- Pascoli, V., Terrier, J., Espallergues, J., Valjent, E., O'Connor, E. C., & Luscher, C. (2014). Contrasting forms of cocaine-evoked plasticity control components of relapse. *Nature*, 509(7501), 459-464. doi:10.1038/nature13257
- Pascoli, V., Terrier, J., Hiver, A., & Luscher, C. (2015). Sufficiency of Mesolimbic Dopamine Neuron Stimulation for the Progression to Addiction. *Neuron*, 88(5), 1054-1066. doi:10.1016/j.neuron.2015.10.017
- Pettit, H. O., Ettenberg, A., Bloom, F. E., & Koob, G. F. (1984). Destruction of dopamine in the nucleus accumbens selectively attenuates cocaine but not heroin self-administration in rats. *Psychopharmacology (Berl)*, 84(2), 167-173.
- Phillipson, O. T. (1979a). Afferent projections to the ventral tegmental area of Tsai and interfascicular nucleus: a horseradish peroxidase study in the rat. *J Comp Neurol*, 187(1), 117-143. doi:10.1002/cne.901870108

- Phillipson, O. T. (1979b). The cytoarchitecture of the interfascicular nucleus and ventral tegmental area of Tsai in the rat. *J Comp Neurol*, 187(1), 85-98. doi:10.1002/cne.901870106
- Phillipson, O. T. (1979c). A Golgi study of the ventral tegmental area of Tsai and interfascicular nucleus in the rat. *J Comp Neurol*, 187(1), 99-115. doi:10.1002/cne.901870107
- Roberts, A. J., McDonald, J. S., Heyser, C. J., Kieffer, B. L., Matthes, H. W., Koob, G. F., & Gold, L. H. (2000). mu-Opioid receptor knockout mice do not self-administer alcohol. *J Pharmacol Exp Ther*, 293(3), 1002-1008.
- Rosen, Z. B., Cheung, S., & Siegelbaum, S. A. (2015). Midbrain dopamine neurons bidirectionally regulate CA3-CA1 synaptic drive. *Nat Neurosci*, 18(12), 1763-1771. doi:10.1038/nn.4152
- Rossi, M. A., Sukharnikova, T., Hayrapetyan, V. Y., Yang, L., & Yin, H. H. (2013). Operant self-stimulation of dopamine neurons in the substantia nigra. *PLoS One*, 8(6), e65799. doi:10.1371/journal.pone.0065799
- Russo, S. J., Bolanos, C. A., Theobald, D. E., DeCarolis, N. A., Renthal, W., Kumar, A., . . . Nestler, E. J. (2007). IRS2-Akt pathway in midbrain dopamine neurons regulates behavioral and cellular responses to opiates. *Nat Neurosci*, 10(1), 93-99. doi:10.1038/nn1812
- Russo, S. J., Mazei-Robison, M. S., Ables, J. L., & Nestler, E. J. (2009). Neurotrophic factors and structural plasticity in addiction. *Neuropharmacology*, 56 Suppl 1, 73-82. doi:10.1016/j.neuropharm.2008.06.059
- Saal, D., Dong, Y., Bonci, A., & Malenka, R. C. (2003). Drugs of abuse and stress trigger a common synaptic adaptation in dopamine neurons. *Neuron*, 37(4), 577-582.
- Sanchez-Catalan, M. J., Kauffling, J., Georges, F., Veinante, P., & Barrot, M. (2014). The antero-posterior heterogeneity of the ventral tegmental area. *Neuroscience*, 282, 198-216. doi:10.1016/j.neuroscience.2014.09.025
- Sarti, F., Borgland, S. L., Kharazia, V. N., & Bonci, A. (2007). Acute cocaine exposure alters spine density and long-term potentiation in the ventral tegmental area. *Eur J Neurosci*, 26(3), 749-756. doi:10.1111/j.1460-9568.2007.05689.x
- Schuller, A. G., King, M. A., Zhang, J., Bolan, E., Pan, Y. X., Morgan, D. J., . . . Pinar, J. E. (1999). Retention of heroin and morphine-6 beta-glucuronide analgesia in a new line of mice lacking exon 1 of MOR-1. *Nat Neurosci*, 2(2), 151-156. doi:10.1038/5706
- Samuels, A. (2017, June 2, 1017). Are Pharmaceutical Companies to Blame for the Opioid Epidemic? *The Atlantic*. Retrieved from

<https://www.theatlantic.com/business/archive/2017/06/lawsuit-pharmaceutical-companies-opioids/529020/>

- Sesack, S. R., & Grace, A. A. (2010). Cortico-Basal Ganglia reward network: microcircuitry. *Neuropsychopharmacology*, 35(1), 27-47. doi:10.1038/npp.2009.93
- Shabat-Simon, M., Levy, D., Amir, A., Rehavi, M., & Zangen, A. (2008). Dissociation between rewarding and psychomotor effects of opiates: differential roles for glutamate receptors within anterior and posterior portions of the ventral tegmental area. *J Neurosci*, 28(34), 8406-8416. doi:10.1523/JNEUROSCI.1958-08.2008
- Simonin, F., Valverde, O., Smadja, C., Slowe, S., Kitchen, I., Dierich, A., . . . Kieffer, B. L. (1998). Disruption of the kappa-opioid receptor gene in mice enhances sensitivity to chemical visceral pain, impairs pharmacological actions of the selective kappa-agonist U-50,488H and attenuates morphine withdrawal. *EMBO J*, 17(4), 886-897. doi:10.1093/emboj/17.4.886
- Sklair-Tavron, L., Shi, W. X., Lane, S. B., Harris, H. W., Bunney, B. S., & Nestler, E. J. (1996). Chronic morphine induces visible changes in the morphology of mesolimbic dopamine neurons. *Proc Natl Acad Sci U S A*, 93(20), 11202-11207.
- Sora, I., Elmer, G., Funada, M., Pieper, J., Li, X. F., Hall, F. S., & Uhl, G. R. (2001). Mu opiate receptor gene dose effects on different morphine actions: evidence for differential in vivo mu receptor reserve. *Neuropsychopharmacology*, 25(1), 41-54. doi:10.1016/S0893-133X(00)00252-9
- Sora, I., Li, X. F., Funada, M., Kinsey, S., & Uhl, G. R. (1999). Visceral chemical nociception in mice lacking mu-opioid receptors: effects of morphine, SNC80 and U-50,488. *Eur J Pharmacol*, 366(2-3), R3-5.
- Sora, I., Takahashi, N., Funada, M., Ujike, H., Revay, R. S., Donovan, D. M., . . . Uhl, G. R. (1997). Opiate receptor knockout mice define mu receptor roles in endogenous nociceptive responses and morphine-induced analgesia. *Proc Natl Acad Sci U S A*, 94(4), 1544-1549.
- Spiga, S., Serra, G. P., Puddu, M. C., Foddai, M., & Diana, M. (2003). Morphine withdrawal-induced abnormalities in the VTA: confocal laser scanning microscopy. *Eur J Neurosci*, 17(3), 605-612.
- Stamatakis, A. M., Jennings, J. H., Ung, R. L., Blair, G. A., Weinberg, R. J., Neve, R. L., . . . Stuber, G. D. (2013). A unique population of ventral tegmental area neurons inhibits the lateral habenula to promote reward. *Neuron*, 80(4), 1039-1053. doi:10.1016/j.neuron.2013.08.023
- Stein, V., & Nicoll, R. A. (2003). GABA generates excitement. *Neuron*, 37(3), 375-378.

- Stuber, G. D., Hnasko, T. S., Britt, J. P., Edwards, R. H., & Bonci, A. (2010). Dopaminergic terminals in the nucleus accumbens but not the dorsal striatum corelease glutamate. *J Neurosci*, *30*(24), 8229-8233. doi:10.1523/JNEUROSCI.1754-10.2010
- Stuber, G. D., Sparta, D. R., Stamatakis, A. M., van Leeuwen, W. A., Hardjoprajitno, J. E., Cho, S., . . . Bonci, A. (2011). Excitatory transmission from the amygdala to nucleus accumbens facilitates reward seeking. *Nature*, *475*(7356), 377-380. doi:10.1038/nature10194
- Swanson, L. W. (1982). The projections of the ventral tegmental area and adjacent regions: a combined fluorescent retrograde tracer and immunofluorescence study in the rat. *Brain Res Bull*, *9*(1-6), 321-353.
- Tian, M., Broxmeyer, H. E., Fan, Y., Lai, Z., Zhang, S., Aronica, S., . . . Yu, L. (1997). Altered hematopoiesis, behavior, and sexual function in mu opioid receptor-deficient mice. *J Exp Med*, *185*(8), 1517-1522.
- Ting, A. K. R., & van der Kooy, D. (2012). The neurobiology of opiate motivation. *Cold Spring Harb Perspect Med*, *2*(10). doi:10.1101/cshperspect.a012096
- Tritsch, N. X., Oh, W. J., Gu, C., & Sabatini, B. L. (2014). Midbrain dopamine neurons sustain inhibitory transmission using plasma membrane uptake of GABA, not synthesis. *Elife*, *3*, e01936. doi:10.7554/eLife.01936
- Tsai, H. C., Zhang, F., Adamantidis, A., Stuber, G. D., Bonci, A., de Lecea, L., & Deisseroth, K. (2009). Phasic firing in dopaminergic neurons is sufficient for behavioral conditioning. *Science*, *324*(5930), 1080-1084. doi:1168878 [pii] 10.1126/science.1168878
- U.S. Dept of Health and Human Services (HHS). (2017). HHS acting secretary declares public health emergency to address national opioid crisis [Press release]. Retrieved from <https://www.hhs.gov/about/news/2017/10/26/hhs-acting-secretary-declares-public-health-emergency-address-national-opioid-crisis.html>
- Ungless, M. A., Whistler, J. L., Malenka, R. C., & Bonci, A. (2001). Single cocaine exposure in vivo induces long-term potentiation in dopamine neurons. *Nature*, *411*(6837), 583-587. doi:10.1038/35079077
- Vargas-Perez, H., Ting, A. K. R., Walton, C. H., Hansen, D. M., Razavi, R., Clarke, L., . . . van der Kooy, D. (2009). Ventral tegmental area BDNF induces an opiate-dependent-like reward state in naive rats. *Science*, *324*(5935), 1732-1734. doi:10.1126/science.1168501
- Vegina, P., & Kim, J. H. (1999). Metabotropic glutamate receptors and the generation of locomotor activity: interactions with midbrain dopamine. *Neurosci Biobehav Rev*, *23*(4), 577-589.

- Von Korff, M., Saunders, K., Thomas Ray, G., Boudreau, D., Campbell, C., Merrill, J., . . . Weisner, C. (2008). De facto long-term opioid therapy for noncancer pain. *Clin J Pain*, *24*(6), 521-527. doi:10.1097/AJP.0b013e318169d03b
- Wang, H. L., & Morales, M. (2009). Pedunculo-pontine and laterodorsal tegmental nuclei contain distinct populations of cholinergic, glutamatergic and GABAergic neurons in the rat. *Eur J Neurosci*, *29*(2), 340-358. doi:10.1111/j.1460-9568.2008.06576.x
- Williams, J. T., Christie, M. J., & Manzoni, O. (2001). Cellular and synaptic adaptations mediating opioid dependence. *Physiol Rev*, *81*(1), 299-343. doi:10.1152/physrev.2001.81.1.299
- Wirtshafter, D., & Sheppard, A. C. (2001). Localization of GABA(B) receptors in midbrain monoamine containing neurons in the rat. *Brain Res Bull*, *56*(1), 1-5.
- Wise, R. A., & Rompre, P. P. (1989). Brain dopamine and reward. *Annu Rev Psychol*, *40*, 191-225. doi:10.1146/annurev.ps.40.020189.001203
- Witten, I. B., Steinberg, E. E., Lee, S. Y., Davidson, T. J., Zalocusky, K. A., Brodsky, M., . . . Deisseroth, K. (2011). Recombinase-driver rat lines: tools, techniques, and optogenetic application to dopamine-mediated reinforcement. *Neuron*, *72*(5), 721-733. doi:10.1016/j.neuron.2011.10.028
- Wolf, D. H., Nestler, E. J., & Russell, D. S. (2007). Regulation of neuronal PLCgamma by chronic morphine. *Brain Res*, *1156*, 9-20. doi:10.1016/j.brainres.2007.04.059
- Wolf, D. H., Numan, S., Nestler, E. J., & Russell, D. S. (1999). Regulation of phospholipase Cgamma in the mesolimbic dopamine system by chronic morphine administration. *J Neurochem*, *73*(4), 1520-1528.
- Wu, L. T., Woody, G. E., Yang, C., Pan, J. J., & Blazer, D. G. (2011). Abuse and dependence on prescription opioids in adults: a mixture categorical and dimensional approach to diagnostic classification. *Psychol Med*, *41*(3), 653-664. doi:10.1017/S0033291710000954
- Xiao, C., Cho, J. R., Zhou, C., Treweek, J. B., Chan, K., McKinney, S. L., . . . Gradinaru, V. (2016). Cholinergic Mesopontine Signals Govern Locomotion and Reward through Dissociable Midbrain Pathways. *Neuron*, *90*(2), 333-347. doi:10.1016/j.neuron.2016.03.028
- Yamaguchi, T., Sheen, W., & Morales, M. (2007). Glutamatergic neurons are present in the rat ventral tegmental area. *Eur J Neurosci*, *25*(1), 106-118. doi:10.1111/j.1460-9568.2006.05263.x
- Yang, H., de Jong, J. W., Tak, Y., Peck, J., Bateup, H. S., & Lammel, S. (2018). Nucleus Accumbens Subnuclei Regulate Motivated Behavior via Direct Inhibition and Disinhibition of VTA Dopamine Subpopulations. *Neuron*, *97*(2), 434-449 e434. doi:10.1016/j.neuron.2017.12.022

- Yoo, J. H., Zell, V., Wu, J., Punta, C., Ramajayam, N., Shen, X., . . . Hnasko, T. S. (2017). Activation of Pedunculopontine Glutamate Neurons Is Reinforcing. *J Neurosci*, *37*(1), 38-46. doi:10.1523/JNEUROSCI.3082-16.2016
- Zaki, P. A., Bilsky, E. J., Vanderah, T. W., Lai, J., Evans, C. J., & Porreca, F. (1996). Opioid receptor types and subtypes: the delta receptor as a model. *Annu Rev Pharmacol Toxicol*, *36*, 379-401. doi:10.1146/annurev.pa.36.040196.002115
- Zhang, S., Qi, J., Li, X., Wang, H. L., Britt, J. P., Hoffman, A. F., . . . Morales, M. (2015). Dopaminergic and glutamatergic microdomains in a subset of rodent mesoaccumbens axons. *Nat Neurosci*, *18*(3), 386-392. doi:10.1038/nn.3945

Chapter 2. Determination of Circuit-specific Morphological Adaptations in Ventral Tegmental Area Dopamine Neurons by Chronic Morphine

2.1. Introduction

There is increasing concern in both the scientific and public domains regarding the United States opioid epidemic, highlighted by a 500% increase in opioid overdose deaths from 1999 to 2016 (CDC, 2017). Long-term use of opioids (either in prescription or illicit forms) is frequently concurrent with escalating intake of drug and increased risk for physical drug dependence and addiction (Boscarino et al., 2010; Darnall, Stacey, & Chou, 2012). It is well established that the mesocorticolimbic circuitry is integral in the addictive properties of several drugs of abuse, including opiates, and that drug-induced changes to the mesocorticolimbic circuitry are central to the development of drug abuse (Cooper, Robison, & Mazei-Robison, 2017; Juarez & Han, 2016; Lammel, Lim, & Malenka, 2014).

Long-term use of opiates, such as morphine or heroin, can have lasting effects within the mesocorticolimbic circuitry, particularly the ventral tegmental area (VTA) dopamine (DA) neurons, which are essential for the processing of reward. For example, following chronic morphine administration VTA DA neurons exhibit increased spontaneous and burst firing rates (Koo et al., 2012; Mazei-Robison et al., 2011) and a unique morphological adaptation, specifically an ~20 - 25% reduction in soma size (Chu et al., 2007; Mazei-Robison et al., 2011; Russo et al., 2007; Sklair-Tavron et al., 1996). Given that this reduction can be blocked with opiate antagonists such as naltrexone (Sklair-Tavron et al., 1996) and that it does not occur following chronic administration of other commonly abused drugs such as cocaine, ethanol, or nicotine (Mazei-Robison et

al., 2014) suggests that this structural plasticity may be dependent on opioid signaling. Decreased VTA DA soma size has also been observed in post-mortem samples from heroin addicts, demonstrating translational relevance (Mazei-Robison et al., 2011). Importantly, this opiate-induced decrease in soma size is also correlated with behavioral changes such as reward tolerance; higher doses of morphine are required to elicit a conditioned place preference concomitant with decreased soma size (Russo et al., 2007). Together, these data suggest that chronic morphine elicits distinct morphological and electrophysiological responses in VTA DA neurons, and that these changes are concurrent with changes in the behavioral state of the subject.

While evidence supports opiate-induced changes in VTA DA morphology, whether these changes are limited to subpopulations of VTA DA neurons remains unclear. These distinctions may be critical as current work highlights that the activity of subpopulations of VTA DA neurons drive distinct behavioral states. For instance, activity of nucleus accumbens (NAc)-projecting VTA DA neurons has long been associated with rewarding aspects of stimuli (Sesack & Grace, 2010; Witten et al., 2011), but more recently increased activity of these neurons has been shown to promote susceptibility to chronic social defeat stress, a depressive-like phenotype (Chaudhury et al., 2013). In contrast, activity of prefrontal cortex (PFC)-projecting VTA DA neurons appears to regulate processing of aversive stimuli such as foot shock and formalin paw injection (Brischoux, Chakraborty, Brierley, & Ungless, 2009; Lammel, Ion, Roeper, & Malenka, 2011). Subpopulations of DA neurons also display different basal electrophysiological properties. For example, VTA DA neurons that project to the PFC, medial NAc shell (m.shell), and NAc core have a small hyperpolarization-activated current (I_h) and higher

maximal firing frequencies whereas neurons projecting to the lateral NAc shell (l.shell) have a high I_h and lower maximal firing frequency, similar to DA neurons in the substantia nigra (SN) that project to the dorsal striatum (Lammel et al., 2008; Lammel et al., 2011). This distinction is important due to the historical use of high I_h to identify VTA DA neurons from GABAergic neurons with low I_h (Margolis, Lock, Hjelmstad, & Fields, 2006). Research collected using this criterion may have disproportionately favored the l.shell NAc-projecting neurons, which may have different behavioral implications.

In spite of the growing literature describing specific circuits underlying reward and aversion, there is a surprising lack of information on circuit-specific adaptations to opiates in the mesocorticolimbic system. Thus, we sought to determine whether chronic morphine induces morphology changes within specific subsets of VTA DA neurons. NAc- and PFC-projecting VTA DA neurons were identified using Cre-dependent retrograde viral tracers in DA-Cre driver lines and basal and morphine-induced changes in morphology were assessed. Together, the results of this study further establish that VTA DA neurons are not homogeneous, as they show diverse basal morphology. Importantly, we reveal that chronic morphine induces opposing effects in discrete physiologically relevant VTA DA populations.

2.2. Materials and Methods

2.2.1. Animals and Stereotaxic Surgery

For all soma morphology experiments, we used adult (>8 weeks) male and female tyrosine hydroxylase (TH)-Cre (Jackson, 008601) and Slc6a (dopamine transporter, DAT)-Cre (Jackson, 006660) mice. All experimental animals had *ad libitum*

access to standard chow and water and were kept on a 12-hr. light-dark cycle. All experiments were approved by the Michigan State University Institutional Animal Use and Care (IACUC) committee and adhered to the guidelines set in the Guide for the Care and Use of Laboratory Animals of the National Institutes of Health. Stereotaxic surgeries were completed following standard protocols (Cetin, Komai, Eliava, Seeburg, & Osten, 2006; Juarez et al., 2017; Lammel et al., 2011). Briefly, mice (8-9 weeks) were anesthetized using ketamine (100mg/kg) and xylazine (10mg/kg) and viral vectors were bilateral infused (0.5ul over 5 min) into the brain projection region of interest (e.g. NAc or PFC). Specifically, retrograde viruses (AAV5-EF1a-DIO-eYFP-WPRE-hGH and AAV5-EF1a-DIO-mCherry, University of Pennsylvania and University of North Carolina Vector Cores, respectively) were targeted to either the NAc (AP: +1.6, ML: +1.5, DV: -4.4) or mPFC (AP: +1.8, ML: +0.65, DV: -2.0). Mice were then returned to their home cages (with conspecific littermates) for 6-8 weeks to allow for complete retrograde transport and stable fluorescent protein expression.

For dendritic morphology pilot experiments, we bilaterally injected viral constructs either directly into the VTA (AP: -3.2, ML: +1, DV: -4.6) or into the NAc (AP: +1.6, ML: +1.5, DV: -4.4). Specifically, HSV-GFP was bilaterally injected into the VTA of wild-type TH-Cre(-) mice (n5). For DA-specific dendritic morphology, a Cre-dependent viral construct that expresses channel rhodopsin (ChR2) at the injection site (AAV2-DIO-ChR2-eYFP [n3]) was bilaterally injected into the VTA of TH-Cre mice. For retrograde cell type-specific targeting of DA neurons, AAV5-DIO-ChR2-eYFP was injected into the NAc of DAT-Cre mice (n6). All mice were returned to their home cages until maximal viral expression and/or retrograde transport occurred (HSV-GFP: 36 hrs., AAV2: 2

weeks, retrograde AAV5: 6 weeks).

2.2.2. Morphine Treatment

For chronic morphine morphology studies, mice were subcutaneously implanted with either sham or morphine (25 mg) pellets (generously supplied by the NIDA Drug Supply Program). Morphine treatment was administered 6-8 weeks following stereotaxic surgery (14-17 weeks old) under isoflurane anesthesia as previously described (Fischer et al., 2008). Briefly, mice were implanted with single subcutaneous pellets on days 1 and 3 and were then sacrificed on day 5, a validated protocol to produce morphine dependence and changes in VTA DA neuronal activity, morphology, and signaling (Fischer et al., 2008; Koo et al., 2012; Mazei-Robison et al., 2011).

Analysis of blood morphine serum concentration was completed at the MSU Mass Spectrometry and Metabolomics Core. A separate cohort of mice (6 male and 8 female) was implanted with morphine pellets according to the procedure above. Trunk blood was collected following decapitation and serum was isolated using silicone-coated BD-Vacutainer tubes (BD-367812) and centrifuged at 1,300xg for 5min at 4°C. Free-morphine concentration was determined using Acquity TQ-D LS/MS-MS mass spectrometry utilizing an internal standard of Morphine-D3 (Lipomed, M39-FB-1LM) and standard curve generated with morphine sulfate (Sigma). Serum proteins were removed with 3:7 dilution into acetonitrile and centrifuged at 1,000xg for 3 min at 4°C and morphine-containing diluent were subsequently diluted in water for analysis. Final free-morphine serum concentrations were normalized to mouse weight (nM/g).

2.2.3. Immunohistochemistry (IHC)

Mice underwent transcardial perfusions with PBS and 4% paraformaldehyde (pH 7.4) under chloral hydrate anesthesia and brains were removed and post-fixed for 24 hrs. in 4% paraformaldehyde and then placed in 30% sucrose at 4°C until further processing. Brains were sectioned at 40 µm using a freezing microtome and sections were stored in PBS + 0.01% sodium azide in 4°C. Immunohistochemistry was completed on sections containing VTA, NAc, and PFC following standard procedures (Mazei-Robison et al., 2011). All incubations and washes were completed at room temperature, PBS was used for washes and sections were blocked in PBS with 3% normal donkey serum (NDS, Jackson Immunolab, 017-000-121) and 0.3% Triton X-100. Primary antibodies were prepared in PBS with 3% NDS and 0.3% Tween-20 and sections were incubated in primary antibody overnight at room temperature. The following primary antibodies and dilutions were used: mouse anti-TH (Sigma, T1299, 1:5000), rat anti-mCherry (Invitrogen, M11217, 1:20,000), rabbit anti-GFP (Life Tech, A11122, 1:18,000), rabbit anti-gamma synuclein (Sncg, Abcam, 55424, 1:2000), rabbit anti-sex determining region Y-box 6 (Sox6, Abcam, 30455, 1:500), and goat anti-orthodenticle homeobox 2 (Otx2, Neuromics, GT15095, 1:200). To determine viral spread in in NAc/PFC tissue of DAT-Cre mice, primary antibody concentrations for rat anti-mCherry and rabbit anti-GFP were increased to 1:10,000 due to weaker terminal signal. All secondary antibodies were from Jackson Immunolabs and diluted 1:500 in PBS: anti-Rabbit-488 (AF-711-545-152), anti-Rat-594 (AF-712-585-153), anti-Mouse-CY5 (AF-115-175-146), and anti-Goat-CY5 (AF-705-175-147): sections were incubated in secondary antibodies for 4 hrs. at room temperature. Sections were mounted on

standard slides, dehydrated in 70-100% ethanol, and cover-slipped using DPX mounting medium (Electron Microscopy Sciences, 13512).

For dendritic morphology experiments, mice underwent intracardial perfusion with PBS and 4% paraformaldehyde as described above. VTA were sectioned (100 μm) using a vibratome. For the HSV-GFP experiment, immunohistochemistry was performed using rabbit anti-GFP (Life Tech, A11122, 1:5,000) and anti-TH (Sigma, T1299, 1:5000). Sections were wet-mounted on glass slides using 0.12mm thick seal spacers (Electron microscopy sciences, 70327-13S) and VectaShield hardset mounting medium (Vector, H-1400). Slides were allowed to dry for >48 hr. prior to microscope image acquisition.

2.2.4. Microscope Image Acquisition

For soma size studies, VTA confocal z-stack images were taken using Olympus Fluoview FV1000 (version 4.2) and digital color camera (Olympus DP72) using a 60x PlanApoN (NA 1.42) oil objective and scan speed of 8.0 $\mu\text{s}/\text{pixel}$, Kalman average 4, step size 0.42 μm (MSU Center for Advanced Microscopy). Following confocal imaging, neurons expressing either eYFP or mCherry were reconstructed in three dimensions using Volocity software (Improvision) and the surface area was measured as described previously (Mazei-Robison et al., 2014; Mazei-Robison et al., 2011; Russo et al., 2007). Only neurons that were co-labeled with TH-IHC and fluorescent protein were included in the soma size study. For statistical analyses, soma surface areas of 4-38 neurons were averaged for each mouse. The n listed in figure graphics refers to the number of mice per group.

For determination of viral targeting, NAc, PFC, and VTA were imaged using a Nikon 600HL eclipse NiU upright microscope, Lumencof sola light engine, and

Photometrics cool SNAP Dyno camera. NAc and PFC were imaged using a 10X/0.3 Plan Fluor DIC LN1 objective and VTA was imaged using a 20X/0.5 Plan Fluor DIC MN2 objective. FITC, TexRed, and CY5 filters were used determine IHC-labeled eYFP, mCherry, and TH (Cy5) expression. Combined viral targeting images were created by overlaying images of the same Bregma region from each animal. Individual images for each region were acquired as follows: NAc medial shell and core (Bregma +1.10): FITC-400ms, TxRed-700ms; PFC (Bregma +1.78): FITC-400ms, TxRed-1s. The final combined images were converted into grey scale and then into a heat map (fire green blue). The final image LUTs were adjusted as follows: NAc medial shell- 500-1000, NAc core- 200-1000, PFC- 500-2000.

For colocalization studies, only neurons expressing Cre-driven mCherry (e.g. DA projection neurons) were assessed for Sncg, Otx2, or Sox6 colocalization within the VTA (PN, L.PN, and PBP) and SNc. Confocal z-stack images were taken using Olympus Fluoview FV1000 (version 4.2) and digital color camera (Olympus DP72) using a 20X and 40X dry objective and scan speed of 8.0 μ s/pixel, Kalman average 4, step size 1.8 μ m. Counts of mCherry expressing DA neurons positive for Sncg, Otx2, and Sox6 were obtained by an experimenter blind to conditions (n = 4/5 mice/group). All colocalization data are represented as the percentage of DA projection cells: (# cells positive for protein marker (e.g. Sncg) and mCherry) / (total # of mCherry-positive cells) x 100.

For dendritic morphology studies, confocal z-stack images were taken using Olympus Fluoview FV1000 (version 4.2) and digital color camera (Olympus DP72) using 60X and 100X oil objectives and scan speed of 8.0 μ s/pixel, Kalman average 2,

step size 0.2 μ m (100X objective) and 0.42 μ m (60X objective). Neuron morphology was assessed using NeuronStudio software with the rayburst algorithm using standard published settings (Christoffel et al., 2011; Robison et al., 2013).

2.2.5. Statistical Analyses

All statistical analyses were performed using GraphPad software (Prism, version 7). Results from experiments with two experimental groups were analyzed using an unpaired student t-test. Results from studies with 3 or more groups were assessed using one- or two-way ANOVAs followed by Tukey post-hoc tests, when appropriate. p values less than 0.05 were considered significant.

2.3. Results

2.3.1. Characterization of Basal Soma Size of VTA DA Projection Neurons

To first establish that both AAV5-DIO-eYFP and AAV5-DIO-mCherry similarly label VTA DA projection neurons, both vectors were stereotaxically injected into the NAc of TH-Cre and DAT-Cre mice (Figure 5A). Surface area measurements in VTA DA neurons expressing both eYFP and mCherry were assessed to validate that labeling with either fluorophore produced similar results. Indeed, surface area calculations were highly correlated (Pearson $r = 0.9883$, $p < 0.0001$), suggesting comparable cell labeling (Figure 5B). Therefore, in all future studies eYFP and mCherry were counter-balanced across all experimental groups and surface area data were combined. To address any differences in viral-mediated targeting of dopamine populations (Lammel et al., 2015; Stuber, Stamatakis, & Kantak, 2015), we compared VTA DA soma size using TH-Cre and DAT-Cre mice across VTA subregions (Barrot, 2014; Beier et al., 2015; Ikemoto,

2007). Using a two-way ANOVA, we determined a significant effect of VTA subregion ($F_{(2,31)} = 37.63$, $p < 0.0001$), but no effect of Cre-driver ($F_{(1,31)} = 0.5113$, $p > 0.05$) and no significant subregion x Cre-driver interaction ($F_{(2,31)} = 0.03668$, $p > 0.05$). Post-hoc analyses revealed that all subregions analyzed (interfascicular (IF), paranigral (PN) and lateral portion of the PN (L.PN), see Figure 5A lower panel) significantly differed from each other (Figure 5C, Tukey's multiple comparison test, $*p < 0.05$). Soma size increased along the medial-lateral axis such that the smallest VTA DA neurons were located within the medial IF and the largest neurons in the L.PN in both TH-Cre and DAT-Cre mice (Figure 5C). Since VTA DA neurons in TH-Cre and DAT-Cre mice were similar in size, a single model (TH-Cre) was used in subsequent morphine studies and distinct subregions were analyzed separately in order to avoid any confounds of basal differences in soma size. Finally, because previous soma size data was exclusively from males, we compared the basal soma size of male and female mice. We found no significant difference between the soma size of VTA DA neurons (PN subregion) of male and female DA-Cre mice (Figure 5D, student t-test, $t_{(13)} = 0.03797$, $p > 0.05$) consistent with observations that there are no sex differences in the basal electrophysiological properties, connectome or transcriptome of VTA DA neurons (A. S. Chung, Miller, Sun, Xu, & Zweifel, 2017). Thus, in subsequent experiments we combined data from males and females.

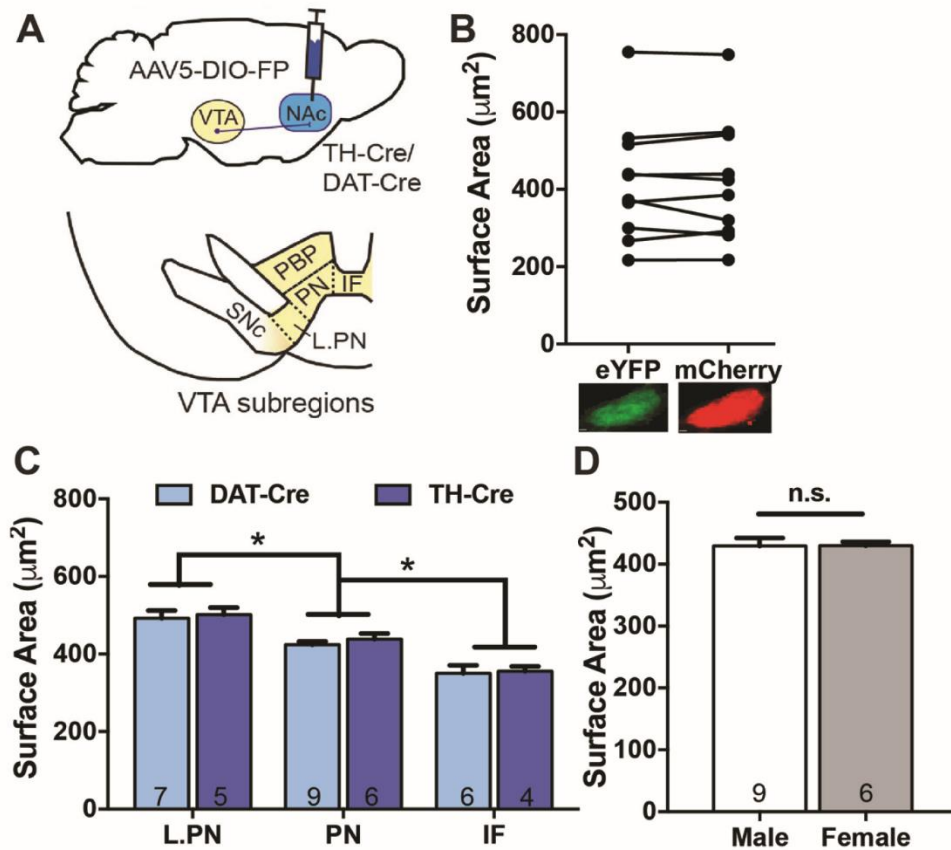


Figure 5. Basal Soma Size Characterization of NAc-projecting VTA DA Neurons. A. TH-Cre or DAT Cre-mice received bilateral infusions of retrograde AAV5-DIO-eYFP or –mCherry into the NAc and soma size of VTA DA neurons was analyzed in VTA subregions (interfascicular nucleus (IF), parabrachial pigmented nucleus (PBP), paranigral nucleus (PN), lateral portion of paranigral nucleus (L.PN)) B. VTA DA neurons expressing both fluorophores (FP, eYFP and mCherry) had comparable surface area measurements using either FP construct (n=8 neurons). Representative image of a VTA DA neuron expressing both FPs is shown below, field of view: 20 μm . C. Basal VTA DA soma size differed between VTA subregions in TH-Cre and DAT-Cre mice, with no differences observed between DA-driver lines. The number of mice in each group is noted within columns, 4-23 neurons were analyzed per mouse. *denotes significant subregion effects in both TH-Cre and DAT-Cre mice (two-way ANOVA, Tukey’s post-hoc test, $p < 0.05$). D. VTA DA soma size (PN subregion) did not differ between male and female mice. The number of mice in each group is noted within columns and 9-38 neurons were analyzed per mouse (student t-test, n.s., $p > 0.05$).

2.3.2. Morphine-induced Changes in Soma Size are Projection-specific

Chronic morphine decreases the soma size of VTA DA neurons, but it remains unclear whether all DA neurons display this response or if it is limited to subsets within the VTA. In order to determine if morphine-induced effects on morphology occur in a projection-specific manner, the surface area of NAc- and PFC-projecting VTA DA neurons were compared in sham- and chronic morphine-treated TH-Cre mice (Figure 6A). Prior experiments that implanted subcutaneous morphine pellets for chronic morphine exposure exclusively used male rodents (Mazei-Robison et al., 2014; Mazei-Robison et al., 2011; Russo et al., 2007). Therefore, we tested the drug administration paradigm in both sexes, and found no significant difference in free morphine (nM/g mouse) in isolated blood serum (Figure 6B, student t-test $t_{(13)}=0.171$, $p>0.05$). Given this, and the observation that basal soma size is equivalent between the sexes (Figure 5D), we combined data from male and female mice for morphine soma size measurements. Targeting of the projection site was validated by fluorescent protein (FP) expression; images of injection sites (heat map of fluorescence) are shown for NAc subregions (Figure 6C) and PFC (Figure 6E). Consistent with previous observations (Lammel et al., 2008; Lammel et al., 2011), injections centered in the NAc m.shell labeled VTA DA neurons predominately in the medial and ventral regions of the VTA (IF, PN, L.PN), while injections centered in the NAc core also labeled VTA DA neurons in PN and L.PN, but in addition labeled more neurons in the PBP, likely due to diffusion into the l.shell (Figure 6C). PFC injections were centered in the Cg1/Pr1 PFC and labeled VTA DA cells were predominately in the PBP, with sparse labeling in the PN. To control for basal differences between subregions (Figure 5C), NAc-projecting VTA DA

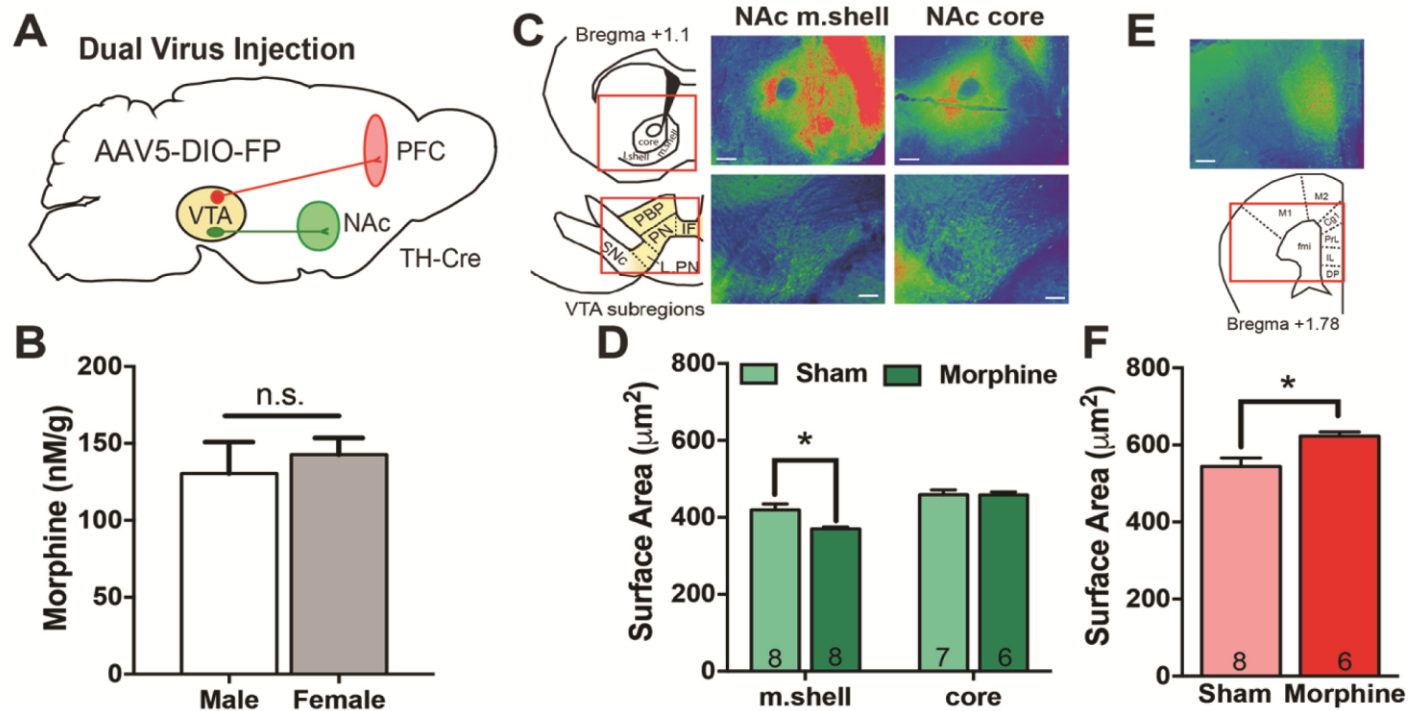


Figure 6. Chronic Morphine Effects on VTA DA Soma Size Differ Based on Projection Target. A. TH-Cre mice received bilateral infusions of retrograde AAV5-DIO-FP into the NAc or PFC and VTA DA neuron soma size was measured following chronic morphine or sham pellet administration. B. Male and female mice showed similar free morphine concentration in blood serum (student t-test, n.s., $p > 0.05$) C. Heatmaps of combined images used in morphine studies showing distinction in NAc medial shell (m.shell)- and core-projecting VTA DA neurons. Representative images were taken using 10X objective, scale bar = 100 μm . Top images: NAc infusion sites, Bottom images: labeled VTA DA neurons. D. Morphine decreases the soma size of NAc m.shell-projecting VTA DA PN neurons with no effect on VTA DA PN neurons that project to the NAc core. Number of mice in each group is noted within columns and 7-26 neurons were analyzed per mouse. *denotes significant effect of morphine on soma size (two-way ANOVA, Tukey's post-hoc test, $p < 0.05$). E. Heatmap of PFC infusion sites used in morphine studies. Representative images were taken using 10X objective, scale bar = 100 μm . F. Average soma size of VTA DA neurons that project to the PFC is increased following chronic morphine treatment. Number of mice in each group is noted within columns and 4-12 neurons were analyzed per mouse, (student t-test, $*p < 0.05$).

neurons (m.shell and core) were analyzed specifically within the PN region and PFC-projecting VTA DA neurons (within the PBP) were analyzed separately.

We found a significant main effect of drug ($F_{(1,25)}=4.872$, $p<0.05$), a main effect of projection ($F_{(1,25)}=30.93$, $p<0.0001$), and a significant drug x projection interaction ($F_{(1,25)}=4.382$, $p<0.05$) in VTA DA neurons projecting to the NAc m.shell and core (Figure 6D). Specifically, chronic morphine significantly reduced the soma size of NAc m.shell-projecting VTA DA neurons ($p<0.05$, Tukey's post-hoc test) but had no effect on NAc core-projecting neurons. There was a trend for increased size of core-projecting neurons compared to m.shell-projecting neurons in sham mice, but this did not reach statistical significance (sham m.shell: 419.7 ± 15.6 , sham core: 459.3 ± 12.7 , $p=0.08$, Tukey post-hoc test). Surprisingly, within the PFC-projecting population (Figure 6F), there was a significant increase in VTA DA soma size following chronic morphine (student t-test, $t_{(12)}=2.946$, $p<0.05$). PFC-projecting neurons were larger than NAc-projecting neurons in sham mice (PFC-sham: 544.5 ± 21.64 , m.shell-sham: 419.7 ± 15.6 , core-sham: 459.3 ± 12.7), consistent with differences in basal size between PBP and PN VTA DA neurons. Together, the data indicate that chronic morphine affects VTA DA soma size in a projection-specific manner: while soma size of NAc m.shell-projecting VTA DA neurons is decreased consistent with previous findings (Mazei-Robison et al., 2011; Russo et al., 2007; Sklair-Tavron et al., 1996), this is not observed in VTA DA cells projecting to the NAc core. Moreover, soma size of PFC-projecting neurons is significantly increased by morphine, which is, to our knowledge, the first observation of a stimulus-induced increase in VTA DA soma size.

2.3.3. Projection-specific Protein Expression Patterns in DA Neurons

Due to the surprising differences observed between VTA DA neurons projecting to NAc subregions, we next sought to determine if the NAc m.shell- and core-projecting VTA DA neurons are also molecularly distinct. DA neuron subpopulations differ transcriptionally based on single-cell RNA sequencing, including distinct gene expression patterns that distinguish striatal- and BNST-projecting neurons (Poulin et al., 2014). We therefore sought to determine if we could discriminate m.shell- from core-projecting VTA DA neurons using immunohistochemistry for two master transcriptional regulators (Otx2 and Sox6) which may differentiate SNc and VTA DA neurons (C. Y. Chung et al., 2010; Di Salvio, Di Giovannantonio, Omodei, Acampora, & Simeone, 2010; Panman et al., 2014) and gamma synuclein (Sncg), a protein involved in neurodevelopment, regulation of cell growth, division, and gene expression (Galvin, Schuck, Lee, & Trojanowski, 2001; Pan, Bruening, Giasson, Lee, & Godwin, 2002; Surguchev & Surguchov, 2017). We assessed colocalization in VTA DA neurons labeled with AAV5-DIO-mCherry that projected to NAc m.shell and core and SNc DA neurons that projected to the striatum. Due to antibody limitations, we compared colocalization in two IHC experiments, in the first experiment cells were assessed for Sncg and Otx2 expression (Figure 7A, B) and in the second experiment Sox6 and Otx2 were assessed (Figure 7C, D).

While no single protein was exclusive for a single type of DA projection, there were differences in expression patterns. For example, in set 1 (Sncg and Otx2) there was a significant effect of protein marker ($F_{(2,30)}=220.1$, $p<0.0001$), a significant marker x projection interaction ($F_{(4,30)}=85.83$, $p<0.0001$), but no overall effect of projection

($F_{(2,30)}=0$, $p>0.05$). Specifically, dorsal striatum-projecting neurons had a very different profile compared to NAc-projecting DA neurons. SNc DA neurons that projected to the dorsal striatum were almost exclusively only Sncg-positive (+) (99%, Figure 7A) while ~50% of NAc-projecting VTA neurons were also Otx2+ (m.shell-projecting: 65% Sncg+ and Otx2+, core-projecting: 47% Sncg+ and Otx2+). Interestingly, across all three regions, 99% all DA neurons assessed were Sncg+, such that only 1% of DA neurons were Sncg- and Otx2-, and there were no Otx2+ only neurons identified.

In the second set of IHC, Sox6 and Otx2 co-expression was assessed (Figure 7C, D). Using a two-way ANOVA, we determined there was a significant main effect of protein marker ($F_{(3,40)}=69.04$, $p<0.0001$), and protein marker x projection interaction ($F_{(6,40)}=64.94$, $p<0.0001$) but no overall effect of projection ($F_{(2,40)}=0$, $p>0.05$). Overall, we found that both NAc m.shell- and core-projecting neurons in the VTA had low Sox6 expression (5 and 7%, respectively) compared to dorsal striatal-projecting SNc neurons (71% Sox6+). Together, while these data suggest that the proportions of Sncg, Otx2, and Sox6 expression can distinguish NAc-projecting VTA DA neurons from striatum-projecting SNc DA neurons, these markers do not help to molecularly define the subsets of VTA DA neurons that are differentially affected by morphine exposure.

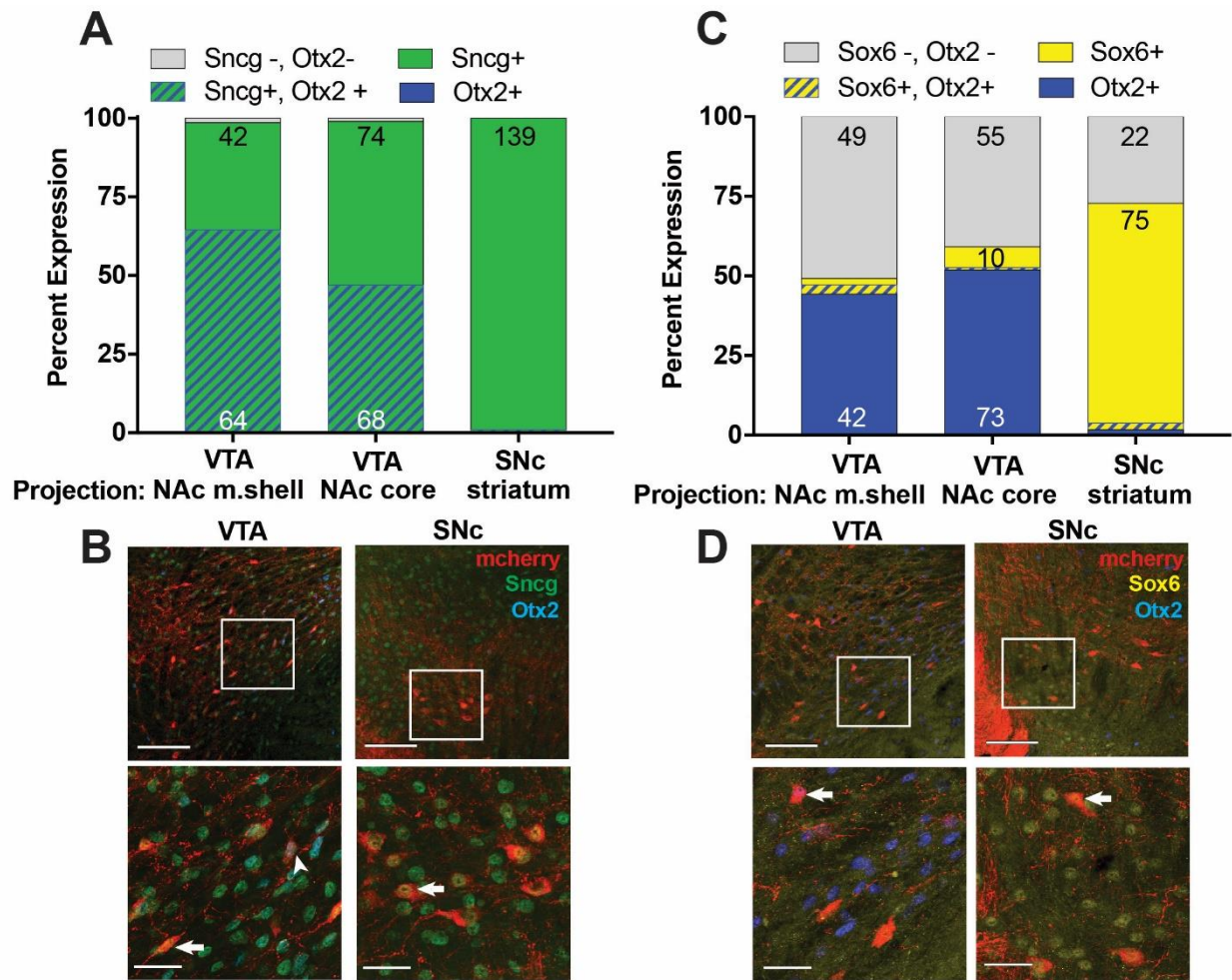


Figure 7. Protein Markers Differentiate SNc DA Neurons that Project to the dStr, but not VTA DA Neurons that Project to the NAc m.shell vs. core. A. Expression of Sncg (green) and Otx2 (blue) was assessed in VTA DA neurons that projected to the NAc m.shell or core or SNc DA neurons that projected the dorsal striatum (red). While ~50% of NAc-projecting VTA DA neurons expressed Otx2, this protein was absent from striatal-projecting SNc DA neurons. B. Representative images are shown of VTA (left) and SNc (right) neurons labeled with mCherry (red), Sncg (green), and Otx2 (blue). Arrowhead: Sncg+, Otx2+ cell, Arrows: Sncg+ cells. C. Expression of Sox6 (yellow) and Otx2 (blue) was assessed in VTA DA neurons that projected to the NAc m.shell or core or SNc DA neurons that projected the striatum (red). D. Representative images are shown of VTA (left) and SNc (right) neurons labeled with mCherry (red), Sox6 (yellow), and Otx2 (blue). Arrow: Otx2+ cell (VTA) or Sox6+ cell (SNc). A. and C. Data are expressed as the percent of DA projection neurons labeled, the number of neurons (for groups with >5 neurons) is noted within the columns. B. and D. Top images were taken using a 20X objective (scale bar = 100µm), white box illustrates image shown below (60X, scale bar = 30µm).

2.3.4. Viral-mediated Visualization of VTA DA Dendritic Spine Morphology

Very few experiments have been conducted to systematically assess VTA DA dendritic morphology. VTA DA neurons have a range of medium to low density of dendritic spines, although there is evidence for drug-induced changes in spine morphology (Phillipson, 1979; Sarti, Borgland, Kharazia, & Bonci, 2007). VTA DA neuron heterogeneity and robust neurite labeling are two main factors preventing significant progress on VTA DA dendritic morphology. In a study by Sarti et al., (2007) biocytin injection efficiently labeled VTA neuron soma and main dendrites but did not achieve the resolution required for individual spine morphology analysis. Conversely, Golgi-Cox staining did achieve the required resolution for spine analysis, but lacked molecular confirmation of the cell type analyzed. Using the same retrograde AAV5-DIO-eYFP/mCherry construct as in VTA DA soma morphology experiments, we noted extensive dendrite labeling (Figure 8). However, it was difficult to visualize any single dendrite beyond a short distance, or to accurately determine the dendrite's cell body of origin. Therefore, we tested additional AAV and HSV constructs to assess whether they could efficiently identify VTA DA neurons while also maintaining the required resolution for dendritic morphology assessment.

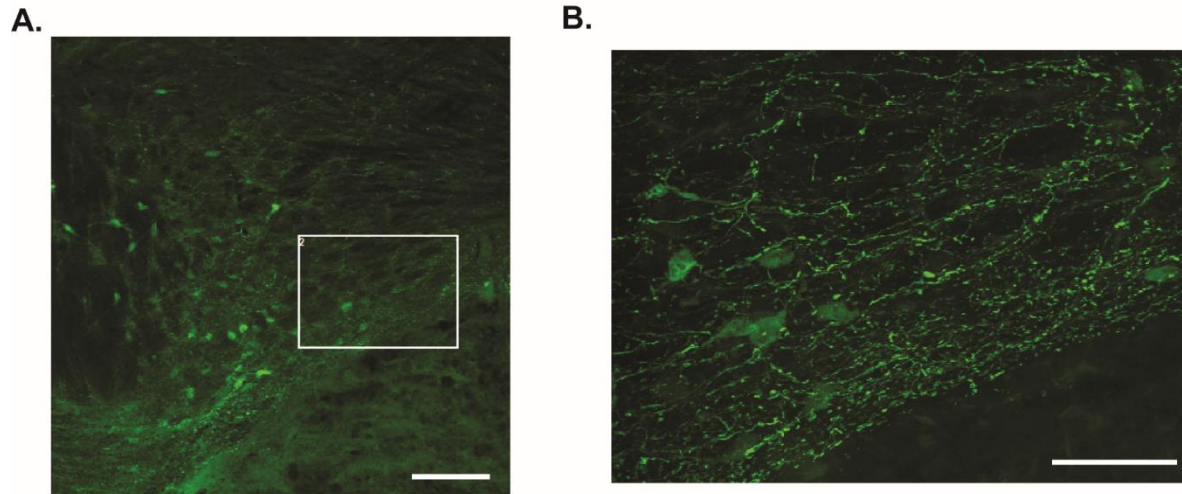


Figure 8. AAV5-DIO-eYFP Expression in VTA Fill Cell Soma but Have Variable Expression Across Dendrites. A. Representative image of VTA Bregma -3.28, 20X scale bar 100µm. B. 60X image of labeled dendrites displaying variable eYFP intensity and overcrowding of field view, scale bar 50µm.

In the first pilot experiment, we tested the efficacy of HSV-GFP labeling of VTA neurons for dendritic morphology in wild-type C57/BL6 mice. This method is not cell type-specific, so we verified DA neuron identity using TH-IHC. HSV produces a sparser neuronal labeling than AAV, so we hoped this might reduce the total number of cells labeled and therefore reduce the density and overlap of dendrites. The total density of dendrites expressing GFP was reduced compared to AAV5-DIO-eYFP (Figure 8), however most dendrites had variable or low GFP expression and dendritic morphology could not be reliably assessed. GFP IHC increased the intensity of GFP-labeling but also increased the background signal, which obscured dendrite spine identification and therefore the resolution was not improved (Figure 9A, B).

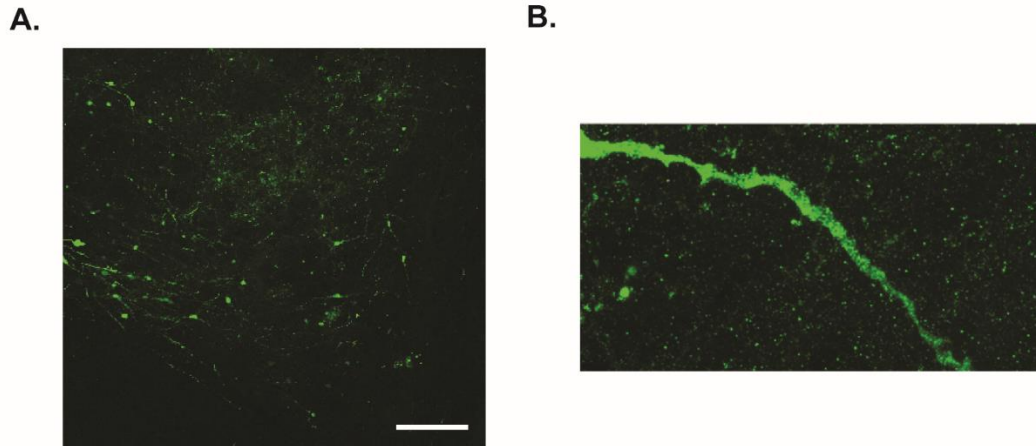
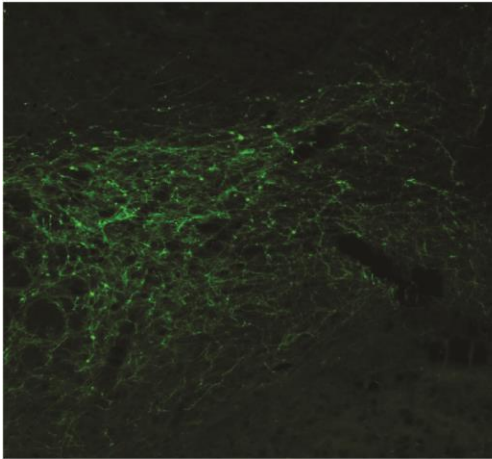


Figure 9. HSV-GFP Expression in VTA Fill Cell Soma but Have Variable Expression Across Dendrites. A. Representative image (10X) of HSV-GFP injected VTA Bregma -3.28, scale bar 200 μ m. B. Representative image of dendrite, 100X.

We next tested whether local expression of ChR2-eYFP would improve resolution. AAV2-DIO-ChR2-eYFP was injected directly into the VTA of TH-Cre mice. We were able to achieve improved spine resolution using this method (Figure 10), and could identify several types of spines (mushroom, thin and stubby) on a few VTA DA-specific dendrites (Figure 10B). However, we had similar extensive labeling as in the AAV5-DIO-eYFP experiments (Figure 8) making individual dendrite selection and visualization (Figure 10A) difficult. Therefore, while the use of ChR2-eYFP did increase the resolution of individual spines, it had similar problems in the ability to analyze single dendrites from a selected neuron.

A.



B.

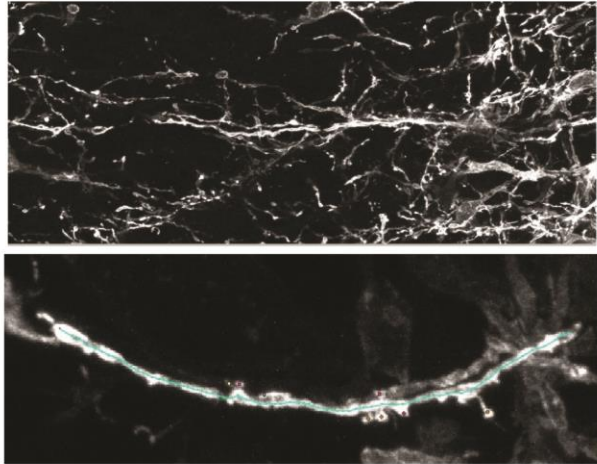


Figure 10. AAV2-DIO-ChR2-eYFP Expression in VTA DA Neurons Increase Dendritic Spine Resolution. A. Representative image of VTA Bregma -3.28, 10X. B. Representative images following NeuronStudio spine analysis of VTA DA dendrites expressing ChR2-eYFP, 60X (top) and 100X (bottom). Identified dendritic spines in bottom panel are labeled with colored circles according to spine types: mushroom (orange), stubby (pink), thin (yellow), and undetermined shape (grey).

In a final attempt to use viral-mediated fluorophore expression to identify spines, we injected retrograde AAV5-DIO-ChR2-eYFP into the NAc of DAT-Cre mice. This protocol did result in a lower number of VTA DA neurons labeled. Unfortunately, viral-mediated ChR2-eYFP intensity was relatively low in this cohort and extensive bleaching occurred during scanning. Therefore, whereas ChR2-eYFP expression could be observed at low magnification, with the higher magnification and longer scan time required imaging of dendritic spines, dendrites were quickly bleached and morphology was not able to be determined (data not shown).

2.4. Discussion

Chronic opioid exposure induces lasting structural and synaptic plasticity in the mesocorticolimbic reward circuitry, particularly within VTA DA neurons. Specifically, there is an increase in VTA DA firing rate following chronic morphine treatment, and a decrease in VTA DA soma size (Koo et al., 2012; Mazei-Robison et al., 2011). Yet VTA DA neurons are not homogeneous and recent studies that have characterized VTA DA neurons based on their projection target have noted both basal differences between subsets of VTA DA neurons as well as varied responses to rewarding and aversive stimuli. For instance, VTA DA neurons that project to the NAc I.shell are physiologically distinct from those that project to NAc m.shell or core, or to the PFC, exhibiting higher I_h currents, lower maximal firing rates, and reduced AMPA/NMDA ratio that are more similar to DA neurons in the SNc (Lammel et al., 2008; Lammel et al., 2011). However, despite these basal differences, cocaine increases the AMPA/NMDA ratio in VTA DA cells projecting to either the NAc m.shell or I.shell but does not impact the AMPA/NMDA ratio of PFC-projecting VTA DA neurons (Lammel et al., 2011). Differential regulation has also been noted for aversive stimuli, as AMPA/NMDA ratio is increased in PFC-projecting VTA DA neurons, but not in NAc m.shell-projecting VTA DA neurons despite their similar baseline properties (Lammel et al., 2011). These data highlight the complexity between subsets of DA neurons, where there are differences both basally and in response to stimuli. Additionally, these differences do not neatly align, for example the basal properties of NAc I.shell-projecting VTA neurons are similar to nigrostriatal neurons, but their responses to rewarding or aversive stimuli are not.

Our findings support that morphological complexity also exists, both basally and

in response to morphine exposure. Interestingly, we find that VTA DA neurons that project to the NAc m.shell exhibit the established morphine-induced decrease in soma size, while those that project mainly to the NAc core do not. This suggests results from previous studies were driven by changes in m.shell-projecting neurons, much in the way that data from electrophysiological studies using high I_h as a marker for DA neurons were driven by NAc l.shell-projecting DA neurons. Intriguingly, we also observed a morphine-induced increase in soma size of PFC-projecting VTA DA neurons. There are multiple reasons this effect could have been missed in previous studies. For example, there was a difference in the number of cells labeled. While NAc injections robustly labeled VTA DA cells, PFC injections resulted in much sparser labeling such that opposite regulation in this small subset of cells could have been obscured. Additionally, the VTA subregion examined likely also played a role. Previous work identifying opiate-induced decrease in soma size was primarily conducted within the PN of the VTA (Mazei-Robison et al., 2014; Mazei-Robison et al., 2011; Russo et al., 2007). While we did observe PFC-projecting DA neurons in the PN, the majority of cells were in the PBP, suggesting these cells were likely not included in the previous analyses. Therefore, it is probable that this opposing effect was masked in previous studies due to the high density of m.shell-projecting VTA DA neurons within the region analyzed. Overall, our data support current efforts to define changes within subsets of VTA DA neurons, as these are likely defined by differences both in their projection target as well as their input (Lammel et al., 2012; Yang et al., 2018).

There is a growing body of literature supporting the importance of analyzing VTA DA neurons based on their projections to NAc subregions (m.shell, l.shell, or core) due

to their distinct molecular and functional properties and behavioral responses. As noted previously, VTA DA neurons projecting to the NAc m.shell and l.shell have different basal electrophysiological properties (Lammel et al., 2011). Since we focused our efforts on the PN region of the VTA, we largely studied VTA DA neurons that projected to the NAc m.shell or core, although there was likely some l.shell-projecting neurons within the core group, consistent with previous categorization of PN VTA DA neurons (Beier et al., 2015; Lammel et al., 2008; Lammel et al., 2011). While differences in DAT/TH and DAT/vesicular monoamine expression have been noted between m.shell- and l.shell-projecting VTA DA neurons, these markers did not distinguish between m.shell- and core-projecting VTA DA neurons in the PN subregion (Lammel et al., 2008). We therefore tested whether m.shell- and core-projecting VTA DA neurons could be identified by protein markers (Otx2, Sox6, and Sncg) implicated in distinct molecular subtypes of VTA DA neurons (Poulin et al., 2014). While no protein showed exclusive projection-specific expression, these markers were sufficient to differentiate NAc-projecting VTA DA neurons from nigrostriatal neurons. Unfortunately, they did not allow differentiation between NAc m.shell- and core-projecting VTA DA neurons. Given that the m.shell- and core-projecting neurons are intermingled in the PN, future studies to identify distinct molecular markers between these neurons will be crucial to allow for more detailed analysis of the functional and behavioral importance of these neurons without the necessity of cumbersome tract-tracing methods.

Importantly, NAc subregion activity may drive distinct aspects of behavioral integration of reward and aversion processing. While it is well established that dopamine release, particularly in the NAc m.shell, is important for drug reward (Ikemoto,

2007; Sesack & Grace, 2010), there is increasing evidence that the NAc ventral and lateral shell may be involved in processing of both rewarding and aversive stimuli (Al-Hasani et al., 2015; McCutcheon, Ebner, Loriaux, & Roitman, 2012; Yang et al., 2018). More generally, stimuli-induced increases in DA the NAc shell are thought to be important for hedonic responses, while DA release in the NAc core role is prominently involved in the acquisition and expression of motivated behavior (Namburi, Al-Hasani, Calhoun, Bruchas, & Tye, 2016), particularly in instrumental behavior tasks involving reward prediction and outcome dichotomy. Morphine exposure is associated with changes in reward behavior and induces structural and activity changes in VTA DA neurons, but it is unclear whether all VTA DA neurons respond similarly. Here we show that chronic morphine induces structural changes in discrete NAc-projecting VTA DA populations, reducing the soma size of NAc m.shell-projecting VTA DA neurons while having no effect on nearby core/l.shell-projecting neurons. Therefore, these data suggest that behaviors associated with morphine-induced changes in morphology such as reward tolerance (Russo et al., 2007) may be driven by distinct VTA subcircuits.

Importantly, recent work on NAc m.shell and l.shell highlights that projection-specific subsets of VTA DA neurons also receive distinct NAc subregion GABAergic input (Yang et al., 2018). It is well established that chronic morphine increases VTA DA neuronal activity (Johnson & North, 1992; Koo et al., 2012; Mazei-Robison et al., 2011). But whether morphine-induced changes in GABAergic tone (Ford, Mark, & Williams, 2006; Johnson & North, 1992) or excitatory regulation (Chen et al., 2015; Margolis, Hjelmstad, Fujita, & Fields, 2014) differentially affect subsets of VTA DA neurons remains unclear. Taken together, these data make it clear that it will be necessary to

address whether specific forms of input drive projection-specific changes in VTA DA neuron structure and activation induced by morphine in future studies.

In addition to the differences in NAc-projecting VTA DA neurons, we also determined that the structure of PFC-projecting VTA DA neurons was altered by chronic morphine exposure, as soma size was increased. While multiple stimuli in addition to opiates have been found to decrease DA soma size (sexual experience, Clock gene mutation (Coque et al., 2011; Pitchers et al., 2014)), to our knowledge, this is the first observation of a stimulus-induced increase in VTA DA soma size. However, given that this effect was not evident in previous opiate studies likely due to the sparse labeling of these cells compared to NAc-projecting neurons, or the VTA subregion analyzed, it is possible that known stimuli could also produce a similar bidirectional effect on VTA DA soma size.

Opposing effects of chronic opioids on morphological adaptations across subsets of VTA DA neurons has been observed previously. An electron microscopy study found that chronic morphine increased the diameter of dendrites on VTA DA neurons in the PBP but decreased the diameter of dendrites on VTA DA neurons in the PN (Lane et al., 2008). Critically, these studies used retrograde tracers and found that PFC-projecting neurons were primarily found in the PBP while NAc-projecting neurons were more prominently labeled in in the PN. These results are consistent with the current data, where we observe a morphine-induced increase in PFC-projecting neurons (in PBP) and decrease in NAc m.shell-projecting neurons (in PN). Future studies verifying dendritic changes in PFC- vs. NAc-projecting DA neurons as well as studies of morphine-induced changes in synaptic plasticity will allow the development of a more

refined model of opiate-induced changes in mesocorticolimbic circuit activity. And while viral-mediated VTA DA dendritic morphology experiments outlined here did not achieve robust labeling of dendritic spines, the use of membrane-bound fluorophore constructs (ChR2-eYFP) substantially improved the resolution. In future studies, it may be possible to utilize a combined method of viral-mediated targeting and iontophoresis of VTA DA neurons for dendritic morphology. It will also be necessary to establish whether projection-specific changes in VTA DA morphology changes contribute to the behavioral changes associated with chronic opiate administration, such as reward tolerance (Mazei-Robison et al., 2011; Russo et al., 2007). Overall, the current results demonstrate that VTA DA neurons differ in soma size by both subregion and projection, and that these differences extend to their morphological responses to chronic opiate exposure. Moreover, our work supports the necessity of studying opiate-induced adaptations in VTA subcircuits, as changes are likely mediated by discrete sets of neurons, with opiate adaptations likely distinct from other stimuli (Mazei-Robison et al., 2014).

REFERENCES

REFERENCES

- Al-Hasani, R., McCall, J. G., Shin, G., Gomez, A. M., Schmitz, G. P., Bernardi, J. M., . . . Bruchas, M. R. (2015). Distinct Subpopulations of Nucleus Accumbens Dynorphin Neurons Drive Aversion and Reward. *Neuron*, *87*(5), 1063-1077. doi:10.1016/j.neuron.2015.08.019
- Barrot, M. (2014). The ventral tegmentum and dopamine: A new wave of diversity. *Neuroscience*, *282C*, 243-247. doi:10.1016/j.neuroscience.2014.10.017
- Beier, K. T., Steinberg, E. E., DeLoach, K. E., Xie, S., Miyamichi, K., Schwarz, L., . . . Luo, L. (2015). Circuit Architecture of VTA Dopamine Neurons Revealed by Systematic Input-Output Mapping. *Cell*, *162*(3), 622-634. doi:10.1016/j.cell.2015.07.015
- Boscarino, J. A., Rukstalis, M., Hoffman, S. N., Han, J. J., Erlich, P. M., Gerhard, G. S., & Stewart, W. F. (2010). Risk factors for drug dependence among out-patients on opioid therapy in a large US health-care system. *Addiction*, *105*(10), 1776-1782. doi:10.1111/j.1360-0443.2010.03052.x
- Brischoux, F., Chakraborty, S., Brierley, D. I., & Ungless, M. A. (2009). Phasic excitation of dopamine neurons in ventral VTA by noxious stimuli. *Proc Natl Acad Sci U S A*, *106*(12), 4894-4899. doi:10.1073/pnas.0811507106
- CDC. (2017, July 18, 2017). Opioid Overdose: Overview of an epidemic. Retrieved from <https://www.cdc.gov/drugoverdose/data/index.html>
- Cetin, A., Komai, S., Eliava, M., Seeburg, P. H., & Osten, P. (2006). Stereotaxic gene delivery in the rodent brain. *Nat Protoc*, *1*(6), 3166-3173. doi:10.1038/nprot.2006.450
- Chaudhury, D., Walsh, J. J., Friedman, A. K., Juarez, B., Ku, S. M., Koo, J. W., . . . Han, M. H. (2013). Rapid regulation of depression-related behaviours by control of midbrain dopamine neurons. *Nature*, *493*(7433), 532-536. doi:10.1038/nature11713

- Chen, M., Zhao, Y., Yang, H., Luan, W., Song, J., Cui, D., . . . Zheng, P. (2015). Morphine disinhibits glutamatergic input to VTA dopamine neurons and promotes dopamine neuron excitation. *Elife*, 4. doi:10.7554/eLife.09275
- Christoffel, D. J., Golden, S. A., Dumitriu, D., Robison, A. J., Janssen, W. G., Ahn, H. F., . . . Russo, S. J. (2011). I κ B kinase regulates social defeat stress-induced synaptic and behavioral plasticity. *J Neurosci*, 31(1), 314-321. doi:10.1523/JNEUROSCI.4763-10.2011
- Chu, N. N., Zuo, Y. F., Meng, L., Lee, D. Y., Han, J. S., & Cui, C. L. (2007). Peripheral electrical stimulation reversed the cell size reduction and increased BDNF level in the ventral tegmental area in chronic morphine-treated rats. *Brain Res*, 1182C, 90-98.
- Chung, A. S., Miller, S. M., Sun, Y., Xu, X., & Zweifel, L. S. (2017). Sexual congruency in the connectome and translome of VTA dopamine neurons. *Sci Rep*, 7(1), 11120. doi:10.1038/s41598-017-11478-5
- Chung, C. Y., Licznarski, P., Alavian, K. N., Simeone, A., Lin, Z., Martin, E., . . . Isacson, O. (2010). The transcription factor orthodenticle homeobox 2 influences axonal projections and vulnerability of midbrain dopaminergic neurons. *Brain*, 133(Pt 7), 2022-2031. doi:10.1093/brain/awq142
- Cooper, S., Robison, A. J., & Mazei-Robison, M. S. (2017). Reward Circuitry in Addiction. *Neurotherapeutics*, 14(3), 687-697. doi:10.1007/s13311-017-0525-z
- Coque, L., Mukherjee, S., Cao, J. L., Spencer, S., Marvin, M., Falcon, E., . . . McClung, C. A. (2011). Specific Role of VTA Dopamine Neuronal Firing Rates and Morphology in the Reversal of Anxiety-Related, but not Depression-Related Behavior in the ClockDelta19 Mouse Model of Mania. *Neuropsychopharmacology*, 36(7), 1478-1488. doi:npp201133 [pii] 10.1038/npp.2011.33
- Darnall, B. D., Stacey, B. R., & Chou, R. (2012). Medical and psychological risks and consequences of long-term opioid therapy in women. *Pain Med*, 13(9), 1181-1211. doi:10.1111/j.1526-4637.2012.01467.x
- Di Salvio, M., Di Giovannantonio, L. G., Omodei, D., Acampora, D., & Simeone, A. (2010). Otx2 expression is restricted to dopaminergic neurons of the ventral

tegmental area in the adult brain. *Int J Dev Biol*, 54(5), 939-945.
doi:10.1387/ijdb.092974ms

Fischer, S. J., Arguello, A. A., Charlton, J. J., Fuller, D. C., Zachariou, V., & Eisch, A. J. (2008). Morphine blood levels, dependence, and regulation of hippocampal subgranular zone proliferation rely on administration paradigm. *Neuroscience*, 151(4), 1217-1224. doi:10.1016/j.neuroscience.2007.11.035

Ford, C. P., Mark, G. P., & Williams, J. T. (2006). Properties and opioid inhibition of mesolimbic dopamine neurons vary according to target location. *J Neurosci*, 26(10), 2788-2797. doi:26/10/2788 [pii]

10.1523/JNEUROSCI.4331-05.2006

Galvin, J. E., Schuck, T. M., Lee, V. M., & Trojanowski, J. Q. (2001). Differential expression and distribution of alpha-, beta-, and gamma-synuclein in the developing human substantia nigra. *Exp Neurol*, 168(2), 347-355.
doi:10.1006/exnr.2000.7615

Ikemoto, S. (2007). Dopamine reward circuitry: two projection systems from the ventral midbrain to the nucleus accumbens-olfactory tubercle complex. *Brain Res Rev*, 56(1), 27-78. doi:10.1016/j.brainresrev.2007.05.004

Johnson, S. W., & North, R. A. (1992). Opioids excite dopamine neurons by hyperpolarization of local interneurons. *J Neurosci*, 12(2), 483-488.

Juarez, B., & Han, M. H. (2016). Diversity of Dopaminergic Neural Circuits in Response to Drug Exposure. *Neuropsychopharmacology*, 41(10), 2424-2446.
doi:10.1038/npp.2016.32

Juarez, B., Morel, C., Ku, S. M., Liu, Y., Zhang, H., Montgomery, S., . . . Han, M. H. (2017). Midbrain circuit regulation of individual alcohol drinking behaviors in mice. *Nat Commun*, 8(1), 2220. doi:10.1038/s41467-017-02365-8

Koo, J. W., Mazei-Robison, M. S., Chaudhury, D., Juarez, B., LaPlant, Q., Ferguson, D., . . . Nestler, E. J. (2012). BDNF is a negative modulator of morphine action. *Science*, 338(6103), 124-128. doi:10.1126/science.1222265

- Lammel, S., Hetzel, A., Hackel, O., Jones, I., Liss, B., & Roeper, J. (2008). Unique properties of mesoprefrontal neurons within a dual mesocorticolimbic dopamine system. *Neuron*, *57*(5), 760-773. doi:10.1016/j.neuron.2008.01.022
- Lammel, S., Ion, D. I., Roeper, J., & Malenka, R. C. (2011). Projection-specific modulation of dopamine neuron synapses by aversive and rewarding stimuli. *Neuron*, *70*(5), 855-862. doi:10.1016/j.neuron.2011.03.025
- Lammel, S., Lim, B. K., & Malenka, R. C. (2014). Reward and aversion in a heterogeneous midbrain dopamine system. *Neuropharmacology*, *76 Pt B*, 351-359. doi:10.1016/j.neuropharm.2013.03.019
- Lammel, S., Lim, B. K., Ran, C., Huang, K. W., Betley, M. J., Tye, K. M., . . . Malenka, R. C. (2012). Input-specific control of reward and aversion in the ventral tegmental area. *Nature*, *491*(7423), 212-217. doi:10.1038/nature11527
- Lammel, S., Steinberg, E. E., Foldy, C., Wall, N. R., Beier, K., Luo, L., & Malenka, R. C. (2015). Diversity of transgenic mouse models for selective targeting of midbrain dopamine neurons. *Neuron*, *85*(2), 429-438. doi:10.1016/j.neuron.2014.12.036
- Lane, D. A., Lessard, A. A., Chan, J., Colago, E. E., Zhou, Y., Schlussman, S. D., . . . Pickel, V. M. (2008). Region-specific changes in the subcellular distribution of AMPA receptor GluR1 subunit in the rat ventral tegmental area after acute or chronic morphine administration. *J Neurosci*, *28*(39), 9670-9681. doi:10.1523/JNEUROSCI.2151-08.2008
- Margolis, E. B., Hjelmstad, G. O., Fujita, W., & Fields, H. L. (2014). Direct bidirectional mu-opioid control of midbrain dopamine neurons. *J Neurosci*, *34*(44), 14707-14716. doi:10.1523/JNEUROSCI.2144-14.2014
- Margolis, E. B., Lock, H., Hjelmstad, G. O., & Fields, H. L. (2006). The ventral tegmental area revisited: is there an electrophysiological marker for dopaminergic neurons? *J Physiol*, *577*(Pt 3), 907-924. doi:jphysiol.2006.117069 [pii]
10.1113/jphysiol.2006.117069
- Mazei-Robison, M. S., Appasani, R., Edwards, S., Wee, S., Taylor, S. R., Picciotto, M. R., . . . Nestler, E. J. (2014). Self-administration of ethanol, cocaine, or nicotine does not decrease the soma size of ventral tegmental area dopamine neurons. *PLoS One*, *9*(4), e95962. doi:10.1371/journal.pone.0095962

PONE-D-14-06041 [pii]

- Mazei-Robison, M. S., Koo, J. W., Friedman, A. K., Lansink, C. S., Robison, A. J., Vinish, M., . . . Nestler, E. J. (2011). Role for mTOR signaling and neuronal activity in morphine-induced adaptations in ventral tegmental area dopamine neurons. *Neuron*, *72*(6), 977-990. doi:10.1016/j.neuron.2011.10.012
- McCutcheon, J. E., Ebner, S. R., Loriaux, A. L., & Roitman, M. F. (2012). Encoding of aversion by dopamine and the nucleus accumbens. *Front Neurosci*, *6*, 137. doi:10.3389/fnins.2012.00137
- Namburi, P., Al-Hasani, R., Calhoon, G. G., Bruchas, M. R., & Tye, K. M. (2016). Architectural Representation of Valence in the Limbic System. *Neuropsychopharmacology*, *41*(7), 1697-1715. doi:10.1038/npp.2015.358
- Pan, Z. Z., Bruening, W., Giasson, B. I., Lee, V. M., & Godwin, A. K. (2002). Gamma-synuclein promotes cancer cell survival and inhibits stress- and chemotherapy drug-induced apoptosis by modulating MAPK pathways. *J Biol Chem*, *277*(38), 35050-35060. doi:10.1074/jbc.M201650200
- Panman, L., Papathanou, M., Laguna, A., Oosterveen, T., Volakakis, N., Acampora, D., . . . Perlmann, T. (2014). Sox6 and Otx2 control the specification of substantia nigra and ventral tegmental area dopamine neurons. *Cell Rep*, *8*(4), 1018-1025. doi:10.1016/j.celrep.2014.07.016
- Phillipson, O. T. (1979). A Golgi study of the ventral tegmental area of Tsai and interfascicular nucleus in the rat. *J Comp Neurol*, *187*(1), 99-115. doi:10.1002/cne.901870107
- Pitchers, K. K., Coppens, C. M., Beloate, L. N., Fuller, J., Van, S., Frohmader, K. S., . . . Coolen, L. M. (2014). Endogenous opioid-induced neuroplasticity of dopaminergic neurons in the ventral tegmental area influences natural and opiate reward. *J Neurosci*, *34*(26), 8825-8836. doi:10.1523/JNEUROSCI.0133-14.2014
- Poulin, J. F., Zou, J., Drouin-Ouellet, J., Kim, K. Y., Cicchetti, F., & Awatramani, R. B. (2014). Defining midbrain dopaminergic neuron diversity by single-cell gene expression profiling. *Cell Rep*, *9*(3), 930-943. doi:10.1016/j.celrep.2014.10.008
- Robison, A. J., Vialou, V., Mazei-Robison, M., Feng, J., Kourrich, S., Collins, M., . . . Nestler, E. J. (2013). Behavioral and structural responses to chronic cocaine

- require a feedforward loop involving DeltaFosB and calcium/calmodulin-dependent protein kinase II in the nucleus accumbens shell. *J Neurosci*, 33(10), 4295-4307. doi:10.1523/JNEUROSCI.5192-12.2013
- Russo, S. J., Bolanos, C. A., Theobald, D. E., DeCarolis, N. A., Renthall, W., Kumar, A., . . . Nestler, E. J. (2007). IRS2-Akt pathway in midbrain dopamine neurons regulates behavioral and cellular responses to opiates. *Nat Neurosci*, 10(1), 93-99. doi:10.1038/nn1812
- Sarti, F., Borgland, S. L., Kharazia, V. N., & Bonci, A. (2007). Acute cocaine exposure alters spine density and long-term potentiation in the ventral tegmental area. *Eur J Neurosci*, 26(3), 749-756. doi:10.1111/j.1460-9568.2007.05689.x
- Sesack, S. R., & Grace, A. A. (2010). Cortico-Basal Ganglia reward network: microcircuitry. *Neuropsychopharmacology*, 35(1), 27-47. doi:10.1038/npp.2009.93
- Sklair-Tavron, L., Shi, W. X., Lane, S. B., Harris, H. W., Bunney, B. S., & Nestler, E. J. (1996). Chronic morphine induces visible changes in the morphology of mesolimbic dopamine neurons. *Proc Natl Acad Sci U S A*, 93(20), 11202-11207.
- Stuber, G. D., Stamatakis, A. M., & Kantak, P. A. (2015). Considerations when using cre-driver rodent lines for studying ventral tegmental area circuitry. *Neuron*, 85(2), 439-445. doi:10.1016/j.neuron.2014.12.034
- Surguchev, A. A., & Surguchov, A. (2017). Synucleins and Gene Expression: Ramblers in a Crowd or Cops Regulating Traffic? *Front Mol Neurosci*, 10, 224. doi:10.3389/fnmol.2017.00224
- Witten, I. B., Steinberg, E. E., Lee, S. Y., Davidson, T. J., Zalocusky, K. A., Brodsky, M., . . . Deisseroth, K. (2011). Recombinase-driver rat lines: tools, techniques, and optogenetic application to dopamine-mediated reinforcement. *Neuron*, 72(5), 721-733. doi:10.1016/j.neuron.2011.10.028
- Yang, H., de Jong, J. W., Tak, Y., Peck, J., Bateup, H. S., & Lammel, S. (2018). Nucleus Accumbens Subnuclei Regulate Motivated Behavior via Direct Inhibition and Disinhibition of VTA Dopamine Subpopulations. *Neuron*, 97(2), 434-449 e434. doi:10.1016/j.neuron.2017.12.022

Chapter 3. Chronic Morphine-induced Transcriptome of VTA DA Neurons

3.1. Introduction

The current opioid epidemic in the U.S. has been termed a national health crisis, as opioid overdose deaths have increased over 500% from 1999 to 2016 (Center for Disease Control and Prevention (CDC), 2017; U.S. Dept of Health and Human Services (HHS), 2017). Long-term use of prescription opioids greatly increases risk of drug tolerance which can lead to dependence, drug addiction and an increase in risk for accidental overdose (CDC, 2017; Scripts, 2014). Despite the prevalent long-term use and abuse of opiate drugs, relatively little is known about the neuroadaptations that occur with chronic use. We previously determined that chronic opiate exposure decreases the soma size of dopamine (DA) neurons in the ventral tegmental area (VTA), a key structure in the mesocorticolimbic reward circuit (Mazei-Robison et al., 2011). This change was observed in post-mortem human samples as well as in rodent models, where soma size was correlated with increased DA activity and reward behavior (Mazei-Robison et al., 2011).

Importantly, the structural effects of chronic opioids appear to be drug-class specific, where chronic treatment with alcohol, nicotine or cocaine did not produce the same effects (Mazei-Robison et al., 2014). This suggests distinct molecular changes occur in chronic opioid-induced plasticity in the VTA. Consistent with this idea, in an RNAsequencing (RNAseq) screen we identified 152 genes whose expression was significantly increased following chronic morphine injections and expression of only 5 of these genes were similarly increased following cocaine injections (Heller et al., 2015).

This highlights that while both morphine and cocaine increase VTA DA activity and induce drug-related reward, these effects may be driven by molecular adaptations unique to each drug.

Identification of molecular mediators of chronic opioid effects specific to DA neurons is difficult due to cellular heterogeneity within the VTA. While approximately 60% of VTA neurons are DAergic, a significant fraction of GABAergic neurons (~30%) are also present (Margolis, Toy, Himmels, Morales, & Fields, 2012; Morales & Root, 2014; Nair-Roberts et al., 2008). Opioids primarily increase VTA DA neuronal activity via disinhibition, specifically decreased GABAergic tone (Gysling & Wang, 1983; Stinus, Koob, Ling, Bloom, & Le Moal, 1980). Therefore, it is likely that opioids induce different molecular adaptations (such as ion channel regulation, LTP and LTD associated signaling cascades) within DA and GABA neurons. To date, large-scale screening studies for chronic opioid-induced changes in gene expression have been limited to the homogenization of the entire VTA (Heller et al., 2015; Koo et al., 2015; McClung, Nestler, & Zachariou, 2005). Thus, data from previous studies did not distinguish between GABA and DA genetic material. Therefore, it is largely unknown whether previously identified morphine-induced changes in gene expression are driven by expression in one or multiple cell types. This includes genes such as serum- and glucocorticoid-regulated kinase 1 (Sgk1) which is significantly induced by drugs of abuse and chronic social defeat stress (CSDS) in the VTA (Cooper et al., 2017; Heller et al., 2015) as well as potassium channels such as Kcnab and Girk3 which have been implicated in opioid reward (Mazei-Robison et al., 2011).

Therefore, in this study we addressed this knowledge gap using translating ribosome affinity purification (TRAP) to isolate actively translating mRNA specifically from VTA DA neurons. Using RNAseq, we were able to identify the DA-specific transcriptome of both sham and chronic morphine-treated DAT^{L10a-GFP} mice. Using differential gene expression analysis, we identified basal DA-specific transcriptome, morphine-induced alterations in whole VTA, and the morphine-induced transcriptome in VTA DA neurons specifically. Additionally, we validated previously identified morphine-regulated genes, such as *Sgk1* and *Kcnab* expression, as well as multiple new candidate genes for chronic morphine induced adaptations in VTA. The results of this study highlight the importance of determining VTA cell type-specific adaptations to drugs of abuse and provide substantial insight into novel mechanisms underlying chronic opioid-induced mesocorticolimbic circuit dysfunction.

3.2. Materials and Methods

3.2.1. Animals

All experiments were approved by the Michigan State University Institutional Animal Use and Care (IACUC) committee and adhered to the guidelines set in the Guide for the Care and Use of Laboratory Animals of the National Institutes of Health. All experimental animals had *ad libitum* access to standard chow and water and were kept on a 12-hr. light-dark cycle. Two DA-specific Cre-driver lines, tyrosine hydroxylase (TH)-Cre (Jackson, 008601) and *Slc6a3* (dopamine transporter, DAT)-Cre (Jackson, 006660) mice were crossed with Rosa26-L10a-eGFP (Jackson, B6;129S4-Gt(ROSA)26Sor^{tm9(EGFP/Rpl10a)Amc}/J, 024750) mice for Cre-dependent and cell-specific

ribosome subunit L10a-GFP fusion protein (referred to as DAT^{L10a-eGFP} and TH^{L10a-eGFP}, respectively). Genotyping for each line was confirmed, mice heterozygous for both cell-specific Cre-driver and L10a-GFP were used for all experiments. Group numbers are noted for each experiment and ranged from 24-40 mice.

3.2.2. Morphine Treatment

10-11wk old male and female DAT^{L10a-eGFP} and TH^{L10a-eGFP} mice were subcutaneously implanted with either sham or morphine (25 mg) pellets (generously supplied by the NIDA Drug Supply Program) under isoflurane anesthesia as previously described (Fischer et al., 2008). Briefly, mice were implanted with single subcutaneous pellets on days 1 and 3 and were then sacrificed on day 5, a validated protocol to produce morphine dependence and changes in VTA DA neuronal activity, morphology, and signaling (Fischer et al., 2008; Koo et al., 2012; Mazei-Robison et al., 2011).

3.2.3. Immunohistochemistry (IHC) and Microscope Image Acquisition

For validation of Cre-dependent L10a-GFP expression, mice underwent transcardial perfusions with PBS and 4% paraformaldehyde (pH 7.4) under chloral hydrate anesthesia and brains were removed and post-fixed for 24 hrs. in 4% paraformaldehyde and then placed in 30% sucrose at 4°C until further processing. Brains were sectioned at 35 µm using a freezing microtome and sections were stored in PBS + 0.01% sodium azide at 4°C. Immunohistochemistry was performed as described previously (Chapter 2, page 70). The following primary antibodies and dilutions were used: mouse anti-TH (Sigma, T1299, 1:5000), rabbit anti-GFP (Life Tech, A11122, 1:18,000), anti-Nms (Peninsula Lab [Bachem], T-4814, 1:500). All secondary antibodies

were from Jackson Immunolabs and diluted 1:500 in PBS: anti-Rabbit-488 (AF-711-545-152), anti-Mouse-CY5 (AF-115-175-146), and anti-Ms-CY3 (AF-715-165-150).

Images were obtained using Cell Sens software and Qi-Click 12 Bit camera with Olympus BX53 fluorescence microscope. VTA was imaged using a 10X objective, while mPFC and NAc containing sections were imaged with 4X objective. FITC, TexRed filters were used determine IHC-labeled eGFP and TH (Cy3) expression.

3.2.4. Translating Ribosome Affinity Purification (TRAP)

In order to isolate actively translating mRNA, TRAP purification was performed according to published protocols (Heiman, Kulicke, Fenster, Greengard, & Heintz, 2014) with the following minor alterations to isolate RNA from DA VTA neurons. VTA was microdissected from coronal slices of DAT^{L10a-eGFP} and TH^{L10a-eGFP} mice using a 14G blunt needle and tissue was immediately frozen on dry ice and stored at -80°C until further processing. VTA from 4 mice were pooled for each immunoprecipitation (IP) and homogenized in 1 ml of tissue lysis buffer. 100 µl of this tissue was aliquoted for input control analysis. Affinity matrix beads were incubated with anti-GFP antibodies (Memorial Sloan-Kettering Monoclonal Antibody Facility: Htz-GFP-19F7 and Htz-GFP-19C8, 50ug/ml each) for 2-4 hr. at 4°C. Isolation of DA-specific translating mRNA was achieved by incubation of VTA lysate with anti-GFP affinity matrix overnight at 4°C.

Final RNA purification was performed using the RNeasy Micro Kit (Qiagen, 74004) according to the kit protocol with the following adjustments. Input and pulldown samples were incubated for 10 min at 4°C with 10% β-ME in RLT buffer (Qiagen, RNeasy micro kit, 74004) and briefly vortexed. RNA was then precipitated using 70%

ethanol and immediately placed in the Qiagen centrifuge isolation tube and the Qiagen kit protocol was followed for remaining steps. Final purified RNA was extracted from columns using 12 μ l (for qPCR), or 14 μ l (for RNAseq) 60°C RNase-free water.

3.2.5. RT-PCR Analysis

RNA quality was immediately assessed using nanodrop and 8-10 ng of RNA was reversed transcribed into cDNA using the High Capacity Reverse Transcription kit (Applied Biosystems, 4368814). Final cDNA samples were diluted with DNase/RNase free water to ~140ng/ μ l and stored at -20°C until further processing. RT-PCR analysis was performed using SYBR-green (CFX-connect, Biorad). Samples were run in triplicate and normalized to glyceraldehyde-3-phosphate dehydrogenase (GAPDH) using the $\Delta\Delta$ Ct method (Tsankova et al., 2006). 4 μ l of cDNA was used for most genes, except for low abundance genes (Gcg, Anxa10) where cDNA volume was increased to 6 μ l. Primers were designed using Primer-BLAST (Ye et al., 2012) and validated via RT-PCR; primer specificity and product size were confirmed by DNA gel electrophoresis. Sequences of validated primers are listed in Table 4.

Table 4. Experimental Primer Sequences.

Gene name	Forward Primer (5'-3')	Reverse Primer (5'-3')
Acta2	AAG AGC ATC CGA CAC TGC TG	CAG CAC AAT ACC AGT TGT ACG TC
Anxa10	CGC CAG AAG TGA AAT AGA CC	GGG TGC CTA TAA AGA AGA TCG
Chrn4	GCT CAC TCG CGG TTC CAT	TCA GGT TGT TGT AGC GGG TT
Slc6a3 (DAT)	GCG ACC CAA CCT GTA CTG	GGA AGA TGT AGG CTC CAT AGT G
GAD2	TGC GCA CTC TGG AAG ACA AT	GTG AGT TGC TGC AGG GTT TG
GAPDH	AGG TCG GTG TGA ACG GAT TTG	TGT AGA CCA TGT AGT TGA GGT CA
Gcg	GAT GAG ATG AAT GAA GAC AAA CG	AAC TCA CAT CAC TAA AGG
Kcnab	GGC CAG ATC ACG GAT GAG ATG	AGC TTT TCC AGC AGC GTA GAC
Kcne1l	CAG TCT GCA CAG CTA ATG G	TCT TCC TTT CCC ATT GAA CC
Mesp2	CAG TCA CCC TTA CAC CAG TCC	AGA CAC AGA AAG ACT CTG ATA CAC T
Nms	CCA ACC TAA GGA AAA CCA GGA TGT A	CCC CAG GCT GGT AGT AGG AT
Nupr1	CGG AAA GGT CGG ACC AAG AG	GTC TGG CCT TAT CTC CAG CTC
Smagp	CGT CGG ACT GGA AAG ATC TGA	CAA CTG CAA TGA GCG CTG TG
Sgk1	CGT CAA AGC CGA GGC TGC TCG AAG C	GGT TTG GCG TGA GGG TTG GAG GAC
Tal2	CGC TGC GAC AGC TAC CTT G	AGC TTG GCA AAG GCA TTG TTG
TH	CAG AGC AGG ATA CCA AGC AGG	CTC GAA TAC CAC AGC CTC CAA
Slc32a1 (VGAT)	GGG GTC ACG ACA AAC CCA A	GTG GAG GAT GGC GTA GGG TA
Slc17a6 (VGLUT2)	TAT GCG CAG AAT CCG TCT TTC	TCT CTC GGT TGT CCT GCT TC
Vgf	AAA CTC GCA GGC AAT CC	ACA GCA ATT TGG AGA AGA GG

3.2.6. RNA Sequencing (RNAseq)

VTA samples were processed from female DAT^{L10a-GFP} 10-11wk mice (n=16 sham and 16 morphine-treated mice) identical to the above procedures. As described above, 4 VTA samples were pooled for each IP, resulting in 4 replicates for each treatment group (sham input, sham IP, morphine input, morphine IP, note final analysis included an n=3 for the morphine input due to loss of one replicate during library processing). RNA quantity and quality were assessed via Illumina Bioanalyzer, and all samples had RIN >8 and IP samples had total RNA yields of at least 9-10 ng total RNA. Final sample processing and RNAseq were performed by the Univ. Maryland Genomics Core. cDNA libraries were generated using a strand-specific library kit (low input NEB kit with polyA enrichment) followed by amplification. Samples were pooled (8 input and 8 IP) and RNA was sequenced across two lanes (Illumina HiSeq4000, 75bp paired end read). RNAseq alignment statistics confirmed an average of 47 million total reads per sample with high proportion (90%) of unique mapped reads per sample. Differential gene expression was assessed by Dr. Qiwen Hu (Heller Lab, Univ. Pennsylvania) using edgeR/DEseq program software (Bioconductor 3.7).

3.2.7. Statistical Analyses

All RT-PCR statistical analyses were performed using GraphPad software (Prism, version 7). RT-PCR validation of candidate genes were analyzed with two-way ANOVAs (fraction x drug) followed by Sidak post-hoc test when appropriate. Significance was set at $p < 0.05$, p values of 0.05-0.1 are listed as non-significant trends. For RNAsequencing data, differential gene expression was assessed using

edgeR/DEseq program and $p_{\text{adj}} < 0.05$ were considered significant. All genes identified were included in Volcano-plot analysis.

3.3. Results

3.3.1. Determination of DA-specific Expression of L10a-GFP

Multiple models have been used to identify and manipulate the activity of dopaminergic neurons, the two most common transgenic mouse lines use tyrosine hydroxylase (TH) or dopamine transporter (Slc6a3, DAT) to drive Cre-recombinase expression (Cre). While TH can identify norepinephrine (NE) neurons, within the VTA TH is considered to be DA-specific due to the absence of NE neurons. However, recent evidence suggests TH-Cre driver lines may not be as specific for VTA DA neurons as originally thought (Lammel et al., 2015; Stuber, Stamatakis, & Kantak, 2015). Specifically, VTA neurons that lack identifiable TH protein expression, TH(-), are labeled in TH-Cre mice with Cre-dependent viral constructs (Lammel et al., 2015). These TH(-)/Cre(+) neurons are most prominent in midline VTA structures (IPN, RLi and CLi), and predominantly project to the lateral habenula (LHb) (Lammel et al., 2015; Stamatakis et al., 2013). Thus, DAT-Cre mice might more reliably label DA neurons in the VTA as studies suggest a more uniform co-labeling of TH and DAT protein in adult mice (Lammel et al., 2015).

Therefore, in this study we compared the specificity of Cre-dependent eGFP-tagged ribosome protein (L10a) expression by crossing Rosa26-L10a-eGFP mice with TH-Cre (TH^{L10a-GFP}) or DAT-Cre (DAT^{L10a-GFP}) mice. Due to noted Cre-driver variability in DA-specific expression across the VTA, we first compared GFP expression across VTA

subregions. GFP and TH protein expression was visualized via IHC on VTA sections from adult mice (Figure 11). There was no evidence for ectopic L10a-GFP expression in control L10a-GFP(+)/Cre(-) mice, and both Cre driver lines (DAT^{L10a-GFP} and TH^{L10a-GFP}) exhibited robust GFP signal in the VTA.

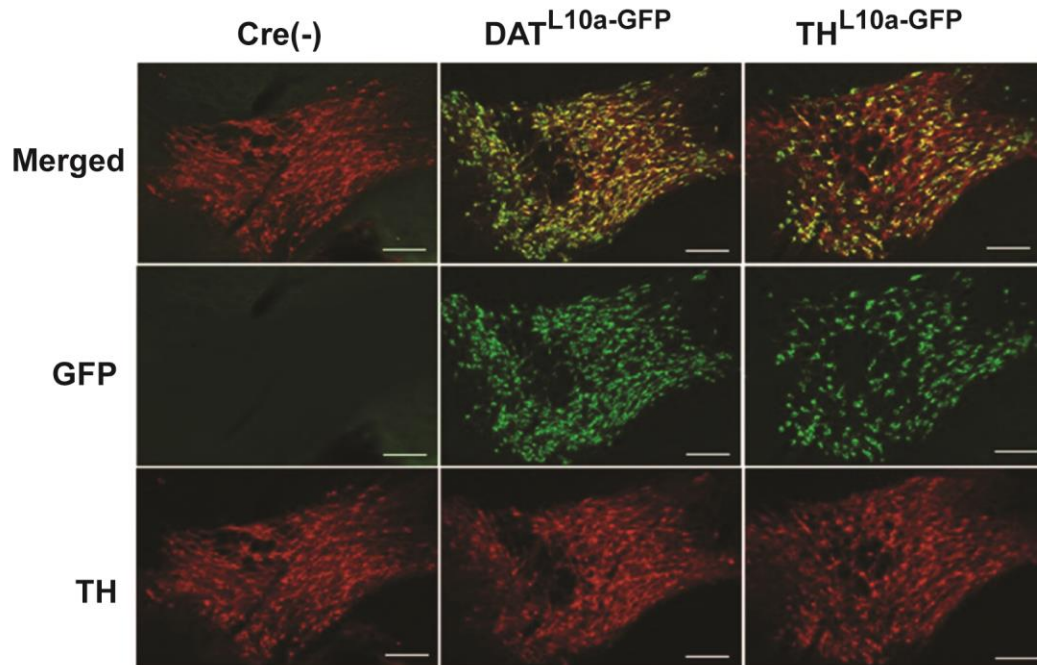


Figure 11. Dopamine-specific Expression of L10a-GFP in the VTA.

No evidence for ectopic L10a-GFP (green) expression in control L10a-GFP(+)/Cre(-) VTA (left column). Robust L10a-GFP expression and colocalization with tyrosine hydroxylase, TH (red) in DAT^{L10a-GFP} (middle column) and TH^{L10a-GFP} (right column). Bregma -3.28, Scale bar = 100um.

L10a-GFP expression was also assessed across the anterior and posterior VTA (Figure 12). Consistent with previous reports (Lammel et al., 2015), we observed GFP-labeled neurons in the midline nuclei (IPN, RLi) of TH^{L10a-GFP} mice, however there was little GFP label in the IPN or RLi of DAT^{L10a-GFP} mice. We also assessed L10a-GFP expression patterns across mPFC and NAc containing sections. There was notable

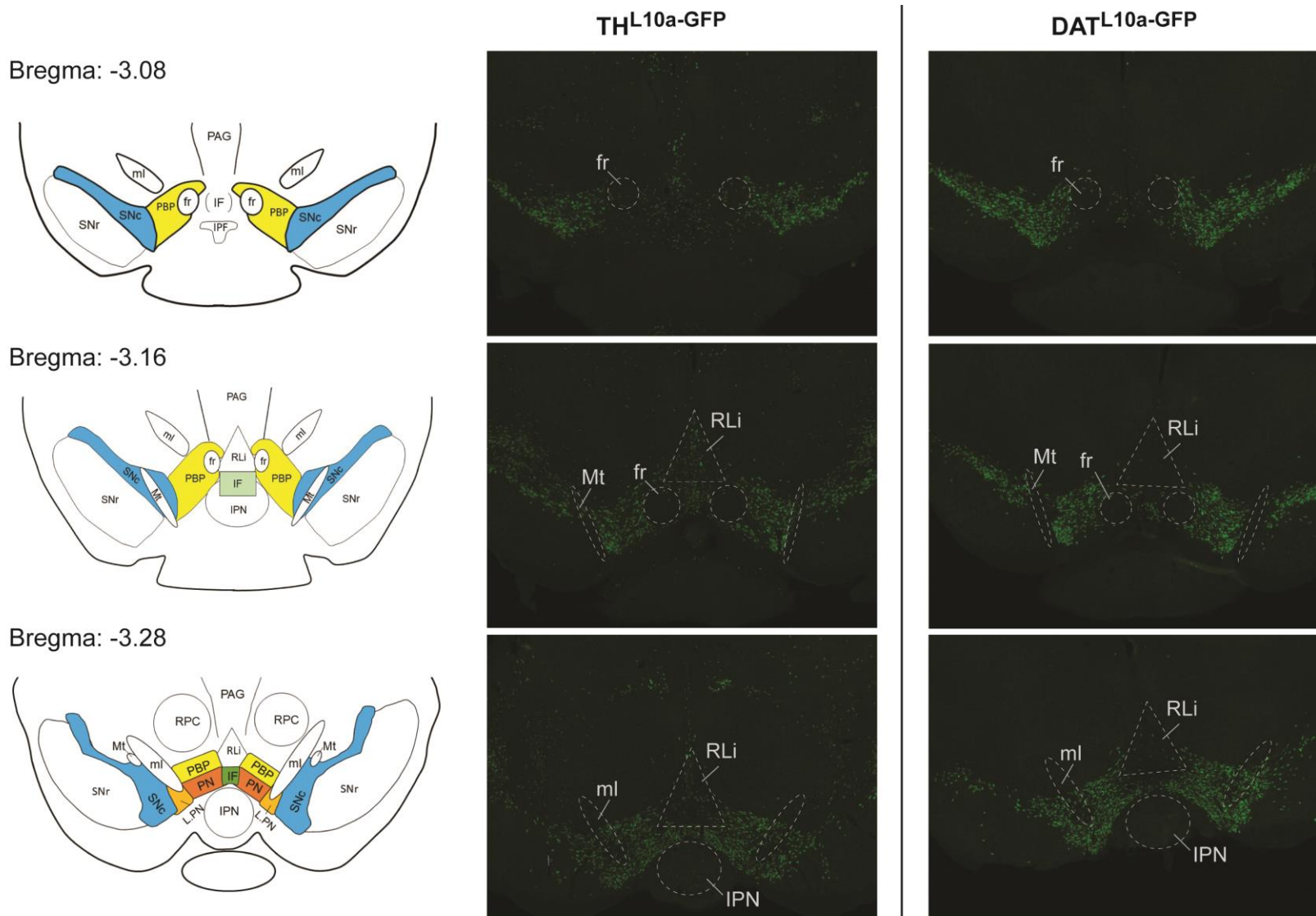
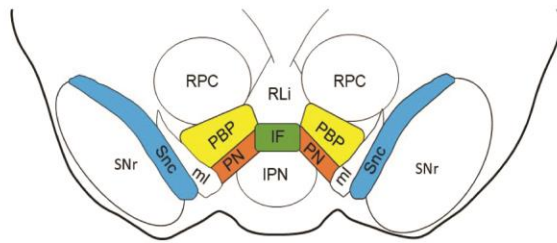


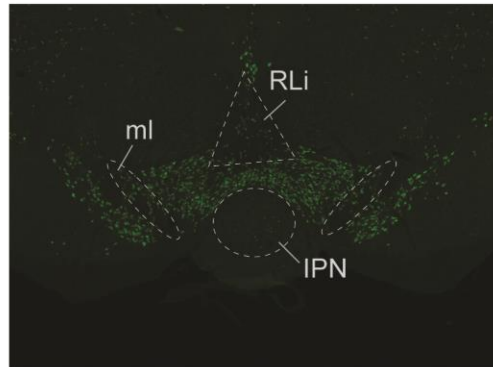
Figure 12. Comparison of GFP Expression Across VTA Nuclei in TH^{L10a}-GFP and DAT^{L10a}-GFP Mice.

Figure 12. (Cont'd)

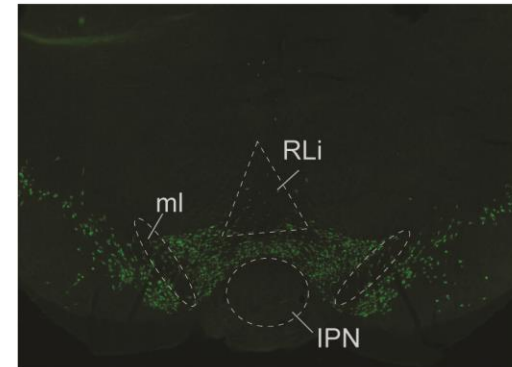
Bregma: -3.52



TH^{L10a}-GFP



DAT^{L10a}-GFP



Corresponding diagrams of VTA-containing sections are shown (left column). Representative anti-GFP immunohistochemistry stained sections from TH^{L10a}-GFP mice (middle column) and DAT^{L10a}-GFP mice (right column). List of abbreviations: fessulus retroflexis (fr), interfesicular nucleus (IF), interpeduncular nucleus (IPN), lateral paranigral nucleus (L.PN), medial lemniscus (ml), medial terminal nucleus of the optic tract (Mt), paraquedal gray (PAG), para-brachial pigmental nucleus (PBP), paranigral nucleus (PN), red nucleus parvicellular part (RPC), rostral linear nucleus (RLi), substantia nigra pars compacta (SNc), substantia nigra reticulata (SNr).

GFP expression in the mPFC, olfactory tubercle, NAc, and lateral septum in TH^{L10a-GFP} mice with no detected expression in identical regions in DAT^{L10a-GFP} mice (Appendix A). Collectively, we show that TH promoter driven expression of L10a-GFP has similar ectopic expression patterns across non-DA midline structures (IPN, RLi, etc) as previously characterized with Cre-dependent viral-mediated fluorophore expression (Lammel et al., 2015). Therefore, the use of DAT^{L10a-GFP} may be better suited for isolation of VTA DA-specific mRNA due to the lack of substantial expression in non-DA midline structures, which would be included in a midline VTA tissue punch dissection.

3.3.2. Validation of TRAP Enrichment of DA Markers

We first verified that TRAP purification from VTA of DAT^{L10a-GFP} and TH^{L10a-GFP} mice resulted enrichment and depletion of DA and GABAergic markers, respectively. Expression of DA-specific genes (DAT, TH) and the GABAergic marker (GAD) was assessed in input and IP samples from sham and morphine treated mice (DAT^{L10a-GFP} n7 and TH^{L10a-GFP} n6-8) using RT-PCR. Gene expression levels were normalized to sham input and data were analyzed using two-way ANOVA (drug x fraction) followed by Sidak post-hoc tests when appropriate.

As expected, in DAT^{L10a-GFP} IP samples DA-specific markers (DAT and TH) were significantly enriched (~7-fold) compared to input controls (Figure 13). Additionally, the GABAergic-marker GAD was significantly decreased in the IP compared to the input control (~88%, Figure 13). Morphine treatment did not affect either enrichment or depletion, as there was no effect of drug treatment on TH, DAT or GAD expression. The summary of statistical analysis for each two-way ANOVA are listed in Table 5.

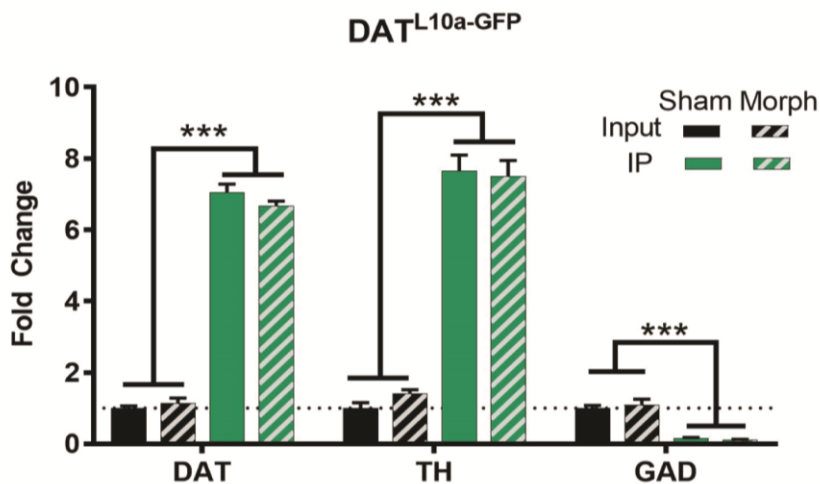


Figure 13. RT-PCR of Cell-specific Marker Expression in DAT^{L10a-GFP} Input and IP. Significant enrichment of DA-specific markers (TH and DAT) and significant reduction in GABAergic marker (GAD) in DA-specific IP fraction compared to input control in DAT^{L10a-GFP}(n7), ***p<0.0001. No effect of drug across all genes, p>0.05, (2-way ANOVA ea., Sidak post hoc test).

Table 5. Statistical Values of 2-way ANOVA DAT^{L10a-GFP} Cell-specific Markers.

Gene	Drug	p value	Fraction	p value	Interaction	p value
DAT	F _(1,24) =0.52	>0.05	F _(1,24) =1334	<0.0001	F _(1,24) =2.66	>0.05
TH	F _(1,24) =0.15	>0.05	F _(1,24) =362.3	<0.0001	F _(1,24) =0.74	>0.05
GAD	F _(1,24) =0.007	>0.05	F _(1,24) =107.5	<0.0001	F _(1,24) =0.30	>0.05

TH^{L10a-GFP} samples produced similar results in cell-specific marker expression as DAT^{L10a-GFP} samples. Specifically, DAT and TH expression were increased in IP samples (6-fold) and GAD expression was significantly reduced (60%, Figure 14). Again, there was no significant effect of drug treatment on TH, DAT or GAD expression.

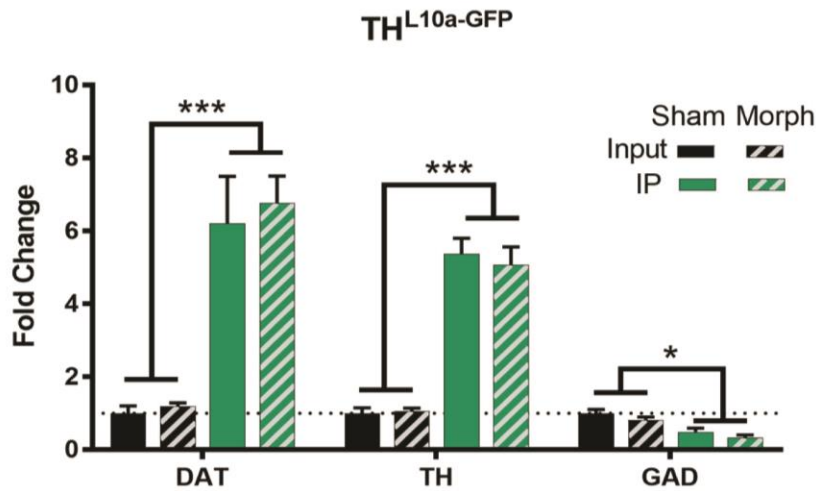


Figure 14. RT-PCR of Cell-specific Marker Expression in TH^{L10a-GFP} Input and IP. Significant enrichment of DA-specific markers (TH and DAT) and significant reduction in GABAergic marker (GAD) in DA-specific IP fraction compared to input control in TH^{L10a-GFP}(n6-8). ***p<0.0001, * p<0.05 No effect of drug across all genes. (2-way ANOVA ea., Sidak post hoc test).

Table 6. Statistical Values of 2-way ANOVA TH^{L10a-GFP} Cell-specific Markers.

Gene	Drug	p value	Fraction	p value	Interaction	p value
DAT	F _(1,23) =0.19	>0.05	F _(1,23) =37.76	<0.0001	F _(1,23) =0.04	>0.05
TH	F _(1,23) =0.12	>0.05	F _(1,23) =143.9	<0.0001	F _(1,23) =0.27	>0.05
GAD	F _(1,23) =3.30	>0.05	F _(1,23) =27.98	<0.0001	F _(1,23) =0.01	>0.05

Together, these data suggest that both mouse models sufficiently enrich for DA-specific markers (TH and DAT). However, we did notice some differences between the two models. While DAT enrichment was very similar in DAT^{L10a-GFP} and TH^{L10a-GFP} samples (7-fold and 6-fold, respectively), TH appeared more enriched in DAT^{L10a-GFP} samples compared to TH^{L10a-GFP} (7-fold vs. 5-fold enrichment, respectively). Additionally, GAD levels were more greatly reduced in DAT^{L10a-GFP} vs. TH^{L10a-GFP} samples (85% vs 51% reduction, respectively) suggesting a more robust depletion of GABAergic cells in the DAT^{L10a-GFP} model (Figure 15). Given the improved profile of DA:

GABA expression in the DAT^{L10a-GFP} samples, this mouse line was utilized for all further experiments (RNAseq and RT-PCR validation).

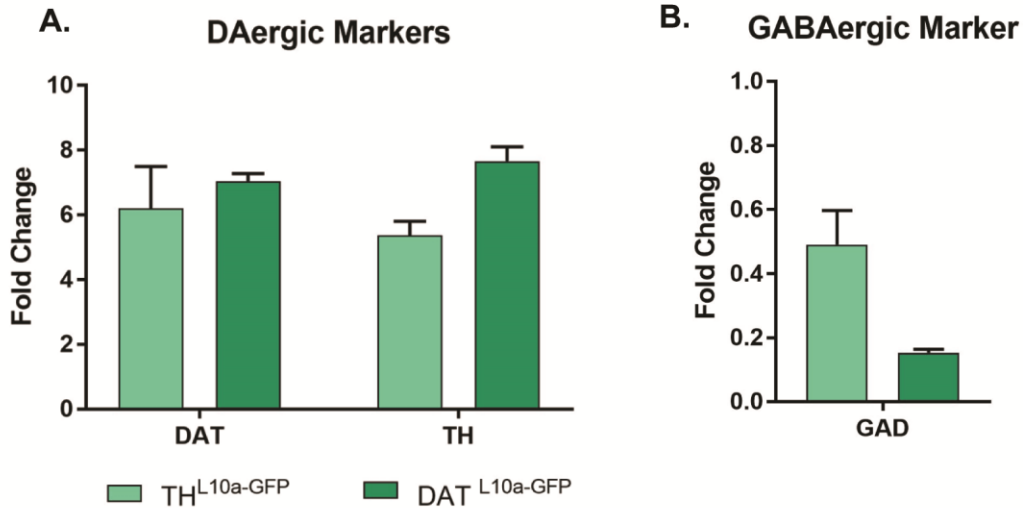


Figure 15. Cre-driver Differences in DAergic and GABAergic Marker Enrichment and Depletion. Visual comparison of A) DAT, TH and B) GAD expression levels across sham treated TH^{L10a-GFP} (light green, n6-8) and DAT^{L10a-GFP} (dark green, n7) samples.

3.3.3. RNA Sequencing of VTA from DAT^{L10a-GFP} Following Sham and Morphine Treatment

Previous studies utilized microarray or RNAseq techniques to determine morphine-induced changes in VTA gene expression (Heller et al., 2015; McClung et al., 2005). But these studies utilized whole VTA tissue and the cell-specificity of the candidate genes identified from these studies remains unclear. The use of TRAP eliminates this confound by isolating actively translating mRNA from specific cell types, allowing identification of gene expression changes specifically in VTA DA neurons, for example. To identify the chronic morphine-induced transcriptome, 10-week old female DAT^{L10a-GFP} mice were given subcutaneous sham or morphine pellets (n16 ea.) and

VTA was extracted on day 5 of chronic drug administration. TRAP RNA was isolated from pooled samples (n4 VTA each) using standard procedures and libraries were prepared for RNAsequencing. Due to one sample loss during sample preparation, final RNAseq sample numbers are as follows: sham input (n4), morphine input (n3), sham IP (n4), morphine IP (n4). We used DEG analyses to determine: 1) the VTA DA transcriptome (sham input vs. sham IP), 2) morphine-induced changes in gene expression in whole VTA (sham input vs. morphine input), and 3) morphine-induced changes in VTA DA neuron specific transcriptome (sham IP vs. morphine IP).

3.3.3.1. Determination of VTA DA Transcriptome (Sham Input vs. Sham IP)

In order to identify the basal DA-specific mRNA transcriptome, we performed DEG analysis of sham input vs. sham IP fractions. In total, there were 23,058 genes identified: 2,164 genes were significantly enriched and 5,493 genes were significantly depleted ($p_{adj} < 0.05$). All results are represented as a Volcano plot ($\text{Log}[FC]$ vs $-\text{Log}[p_{adj}]$) in Figure 16.

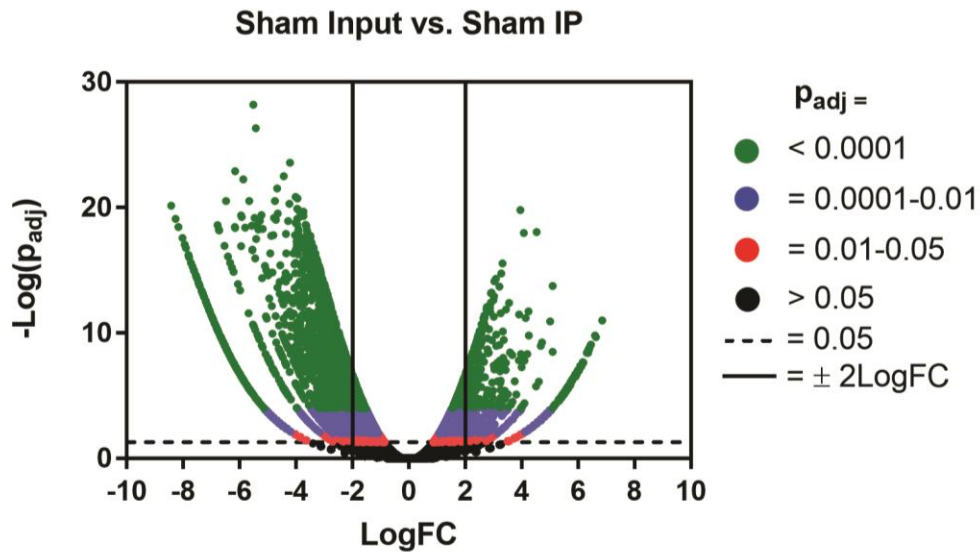


Figure 16. Volcano Plot of Differential Gene Expression Analysis of Sham Input vs. Sham IP. A. Volcano plot of total 23,058 identified genes are represented by LogFC (x-axis) and $-\text{Log}(p_{\text{adj}})$ (y-axis). Genes are grouped by significance: $p_{\text{adj}} < 0.0001$ (green), 0.0001-0.01, (blue), 0.01-0.05 (red) and > 0.05 black. Vertical solid lines are displayed at $\pm 2 \text{LogFC}$ and horizontal dotted line designating $\text{Log}(p_{\text{adj}} = 0.05)$.

While 7,657 total genes were identified as significantly enriched or depleted, a portion of these were driven by extreme values in single replicates or due to variable low expression near the limit of detection. In order to focus on genes changes that were not driven by variability, we conducted student t-tests as a gross measure of sample variability. Thus, the t-test threshold ($p < 0.2$) was not used to assess significance (all genes were already labeled as significantly different using the appropriate $p_{\text{adj}} < 0.05$) but as a screening tool to identify genes most likely to be replicable as enriched or depleted in DA neurons. Using this added condition, the gene list was narrowed down to 5,966 total genes. Finally, we removed any genomic DNA segments, predicted/pseudo-genes and genes with canonical names (Gm-, -Rik annotation) to further refine the gene list. The resulting final list of significantly regulated confirmed and annotated genes included

a total of 4,499 genes (1083 significantly enriched and 3,416 depleted genes).

Visualization of the proportion of excluded genes during this analysis process is shown in Figure 17.

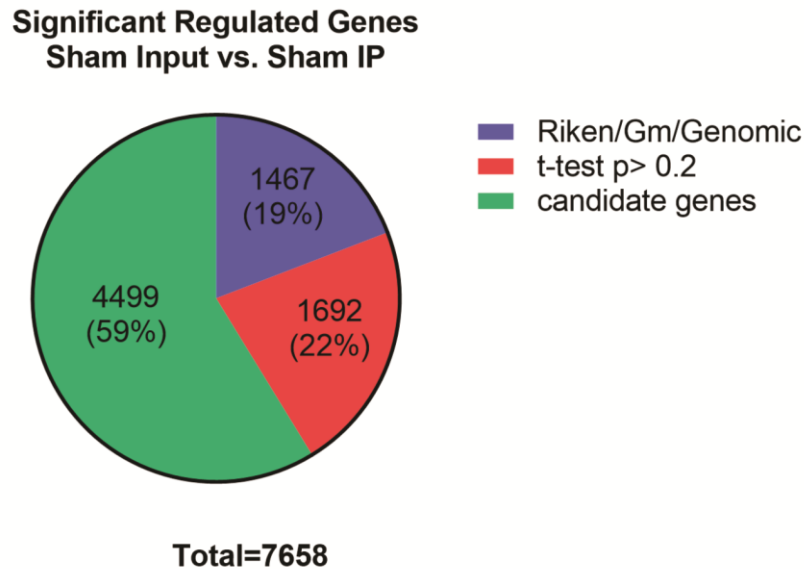


Figure 17. Distribution of Significantly Enriched and Depleted Genes in Sham IP.

7,658 total significantly enriched/depleted genes were identified in the VTA IP fraction, 1692 genes (22%-red) displayed high variability with student-t test >0.2 . 1467 genes were pseudo-genes (-Riken), Genome model (Gm) or genomic DNA contamination (19%-blue). 4499 significant enriched/depleted genes (59%-green) were included in the final analysis.

Importantly, known DA-specific markers (e.g. TH, DAT, dopamine receptor D2 [Drd2], dopa decarboxylase [Ddc], and vesicular monoamine transporter [Vmat]) were significantly enriched in the DA-specific IP (>2 LogFC, $\text{padj} < 0.0001$, Figure 18). As expected, GABAergic markers (e.g. GAD1, GAD2, vesicular GABA transporter [VGAT]), glutamatergic markers (e.g. vesicular glutamate transporter 2 [VGLUT2]), and glial markers (e.g. glutamate-ammonia ligase [Glu1], glial fibrillary acidic protein [Gfap], glutamate/aspartate transporter 1 [Glast1], Protein tyrosine phosphatase, receptor type,

C [PTPRC] and allograft inflammatory factor [Aif1]) were all significantly depleted in the IP fraction (<-1.8 LogFC, $p_{adj}<0.0001$, Figure 18).

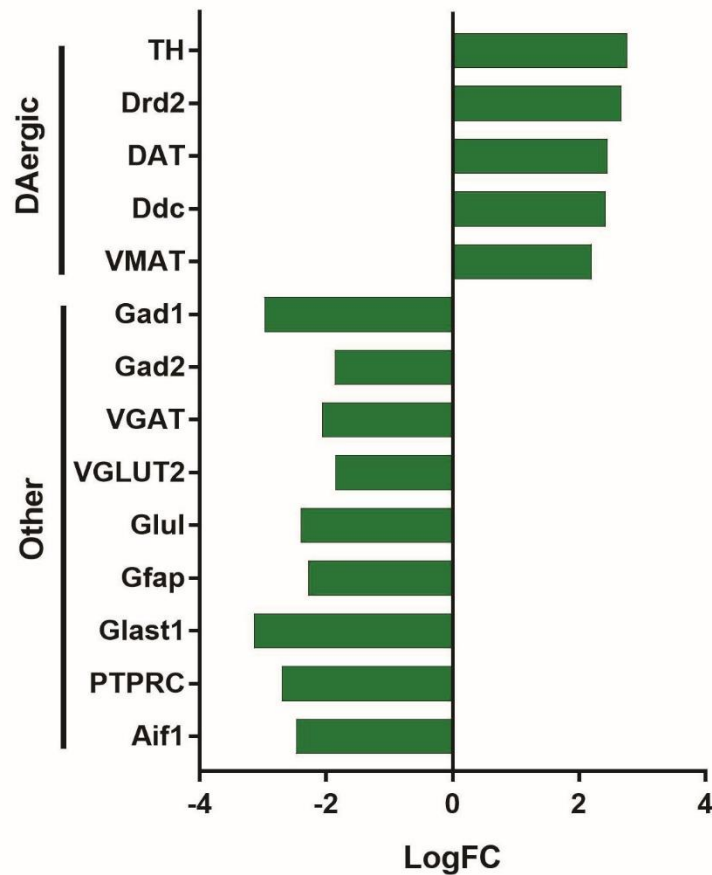


Figure 18. Significant Enrichment of DA Markers and Depletion of Non-DA Markers in Sham IP. LogFC of common cell-specific markers show significant DA enrichment (TH, Drd2, DAT, Ddc, VMAT), GABAergic depletion (Gad1, Gad2, VGAT), Glutamatergic depletion (VGLUT2), and Glial marker depletion (Gfap, Glast1, PTPRC, Aif1). All genes differential gene expression analysis, $p_{adj} < 0.0001$.

Significantly enriched genes ($p_{adj}<0.05$, >1.5 LogFC) were sorted by prevalence (counts per Million [CPM]) and the top 25 enriched genes in the DA-specific fraction are shown in Figure 19. Of note, there are several genes that are not traditionally identified as DA-specific markers (Snca, Grp, Calb1, Chrna6). These identified genes are in

agreement with recent reports using similar technology to define the VTA DA transcriptome (Chung, Miller, Sun, Xu, & Zweifel, 2017; Ekstrand et al., 2014). Additionally, it is worth noting *Aldh1a1*, which has been implicated in an alternate pathway for GABA synthesis (Kim et al., 2015), is also highly enriched in the DA-fraction (2.3 LogFC). Other genes of interest in enriched in the DA fraction include two nicotinic receptor subunits (*Chrna6*, and *Chrna4*, 2.6 and 1.9 Log FC, respectively). The top 150 DA-specific enriched genes ($p_{adj} < 0.05$, $t\text{-test} < 0.2$) and top 150 depleted genes ($p_{adj} < 0.05$, $t\text{-test} < 0.2$) are shown in Appendix B.

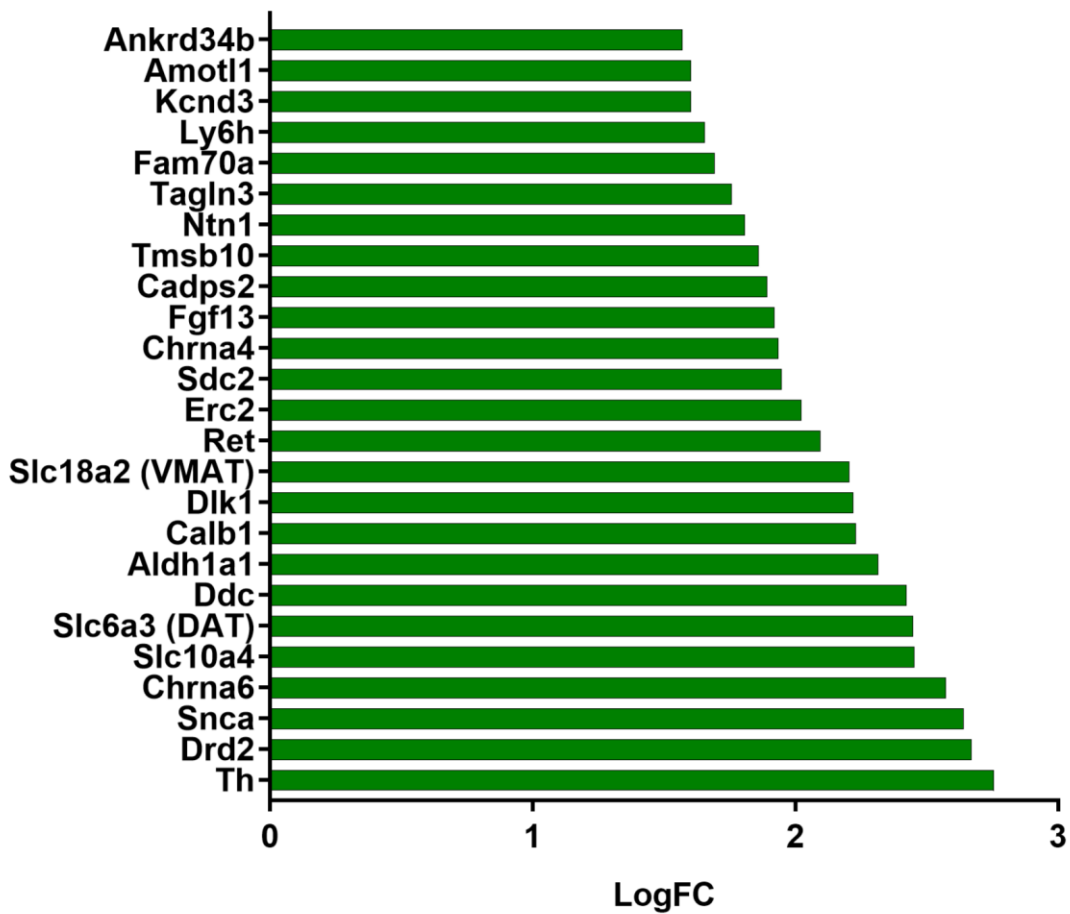


Figure 19. Top 25 Enriched Genes in Sham VTA DA-IP.

3.3.3.2. Global Changes in VTA Gene Expression (Sham Input vs. Morphine Input)

We then compared sham input to morphine input fractions using DEG analysis to identify gene expression changes induced by chronic morphine in the VTA. In total, 23,062 genes were identified and of those 2,103 genes were significantly regulated by chronic morphine ($p_{adj} < 0.05$). Specifically, there were 948 significantly up-regulated and 1,155 significantly down-regulated genes ($p_{adj} < 0.05$). Results are displayed in Figure 20 as a Volcano Plot ($-\text{Log}(p_{adj})$ vs LogFC).

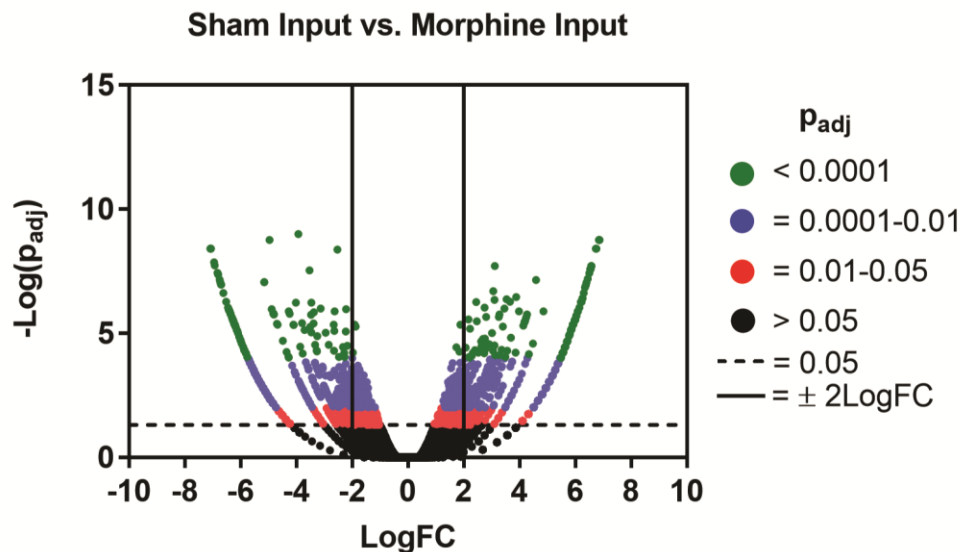


Figure 20. Volcano Plot of Differential Gene Expression Analysis of Sham Input vs. Morphine Input. Volcano plot of total 23,062 identified genes are represented by LogFC (x-axis) and $-\text{Log}(p_{adj})$ (y-axis). Genes are displayed according to significant enrichment/depletion groups: $p_{adj} < 0.0001$ (green), $0.0001-0.01$ (blue), $0.01-0.05$ (red) and > 0.05 black. Vertical solid lines are displayed at $\pm 2 \text{LogFC}$ and horizontal dotted line designating $\text{Log}(p_{adj} = 0.05)$.

We performed a similar screening process as described previously ($p_{adj} < 0.05$, t-test $p < 0.2$) to eliminate highly variable genes in order to rank potential candidate genes. Using this screen, we narrowed the pool to 228 genes up-regulated following morphine

treatment and 182 down-regulated genes. The top 100 up-regulated and down-regulated genes ($p_{adj} < 0.05$, t-test $p < 0.2$) are listed in Appendix C. The top 25 chronic morphine up-regulated and down-regulated genes ($p_{adj} < 0.05$, t-test $p < 0.2$) are displayed in Figure 21.

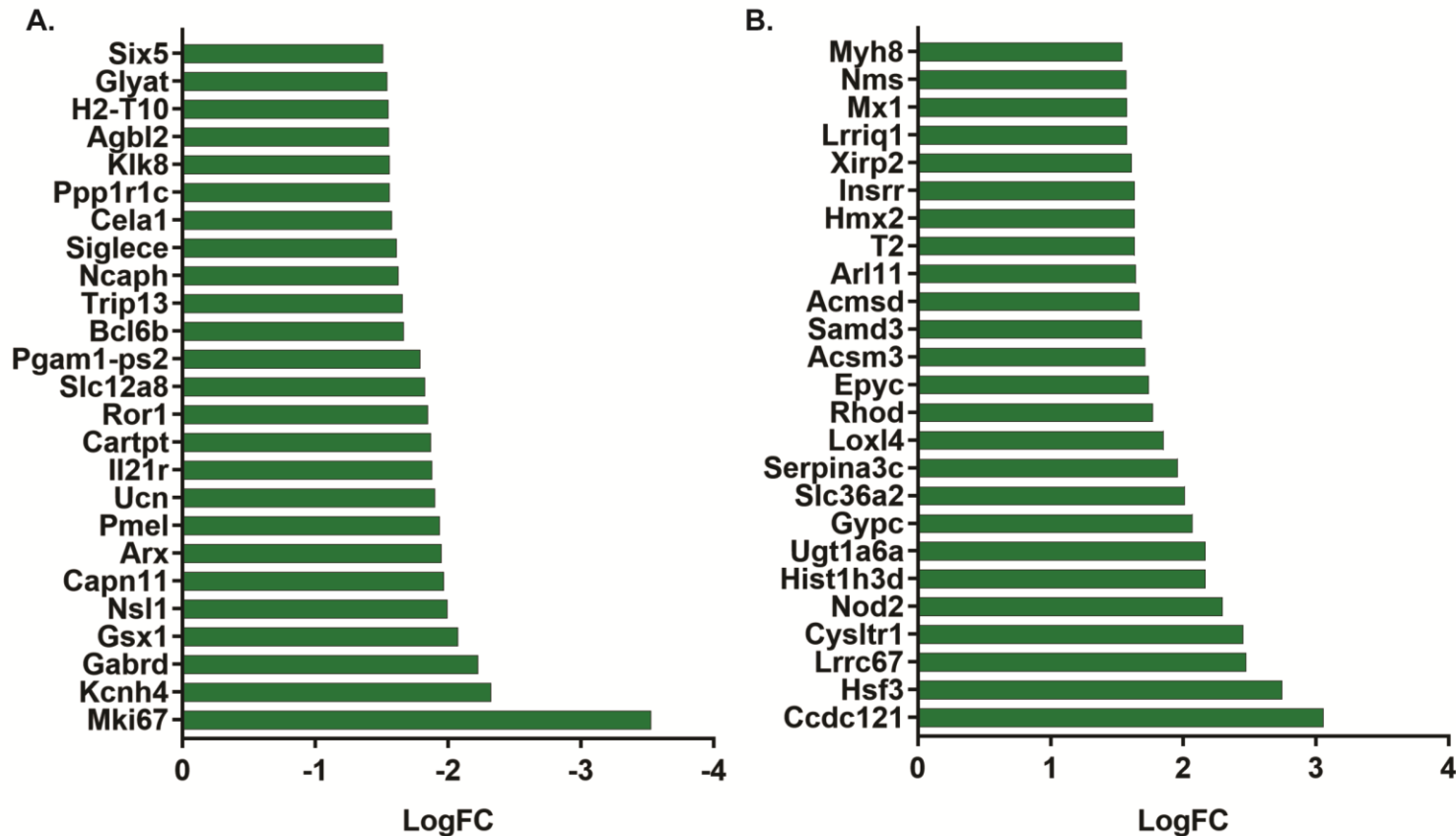


Figure 21. Top 25 Significant Morphine-regulated Genes in RNAseq of VTA Inputs.
 A. Significantly down-regulated genes B. Significantly up-regulated genes.

3.3.3.3. Morphine-induced Transcriptome in VTA DA Neurons (Sham IP vs. Morphine IP)

In the final analysis, we identified gene expression changes induced specifically in VTA DA neurons by morphine by comparing sham and morphine IP samples. Of the 21,754 total genes identified, 998 were significantly up-regulated and 794 were significantly down-regulated ($p_{adj} < 0.05$, Figure 22).

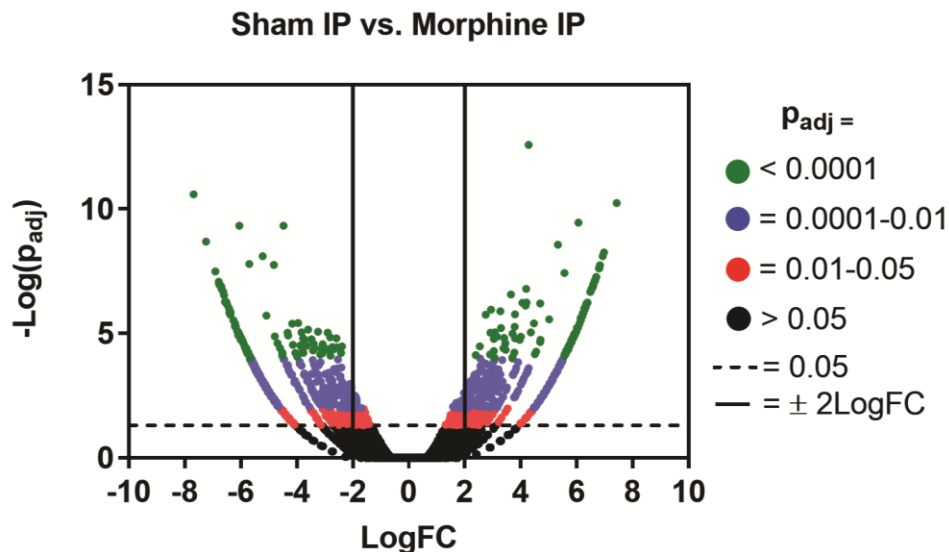


Figure 22. Volcano Plot of Differential Gene Expression Analysis of Sham IP vs. Morphine IP. Volcano plot of total 21,754 identified genes are represented by LogFC(x-axis) and $-\text{Log}(p_{adj})$ (y-axis). Genes are displayed according to significant enrichment/depletion groups: $p_{adj} < 0.0001$ (green), 0.0001-0.01 (blue), 0.01-0.05 (red) and > 0.05 black. Vertical solid lines are displayed at $\pm 2 \text{ LogFC}$ and horizontal dotted line designating $\text{Log}(p_{adj} = 0.05)$.

Using combined parameters of $p < 0.05$ and t-test $p < 0.2$, we generated a candidate gene list containing 125 up-regulated genes and 268 down-regulated genes. The top 100 morphine up- and down-regulated genes are listed in Appendix D. For ease of comparison, the first 25 upregulated and downregulated genes are displayed in Figure 23 ($p < 0.0001$, t-test $p < 0.1$).

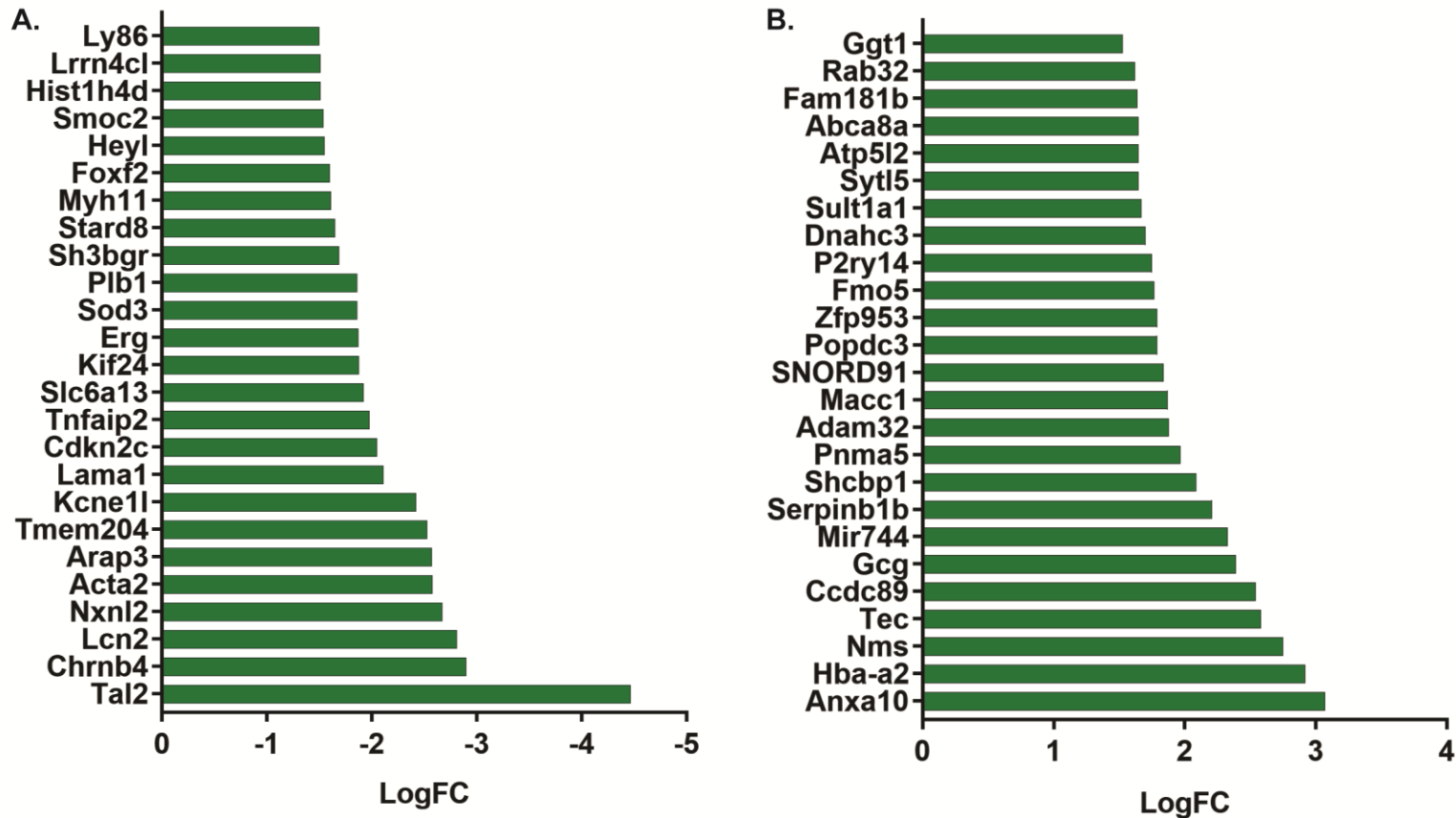


Figure 23. Top 25 Significant Morphine-regulated Genes in RNAseq of VTA DA IP.

A. Significantly down-regulated genes B. Significantly up-regulated genes.

We next sought to compare the identified morphine-regulated candidate genes ($p_{adj} < 0.05$, $t < 0.2$) in whole-VTA (Input) and the DAergic fraction (IP). There was surprisingly little overlap between the morphine-regulated genes identified in the input (whole VTA) and IP (DA specific) analyses (Figure 24). Only 7% of the morphine-regulated genes (30 genes)

were identified in both input and IP analyses while ~93% of total chronic morphine regulated genes were unique to the input and DA-specific IP fractions.

Significant Morphine-regulated Genes

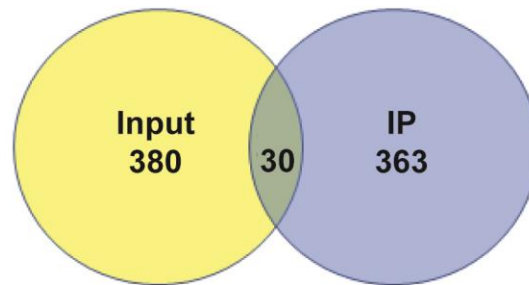


Figure 24. Identification of Highly Distinct Morphine-regulated Genes in Whole VTA Input Compared to DA-specific IP. Venn Diagram representation of overlap between identified significantly regulated genes in whole VTA Input and DA-specific IP fractions. Number of genes identified displayed in each section.

These differences highlight the importance for cell-specific analysis, as chronic morphine effects driven by DA neurons are distinct from cumulative effects in the entire VTA. In fact, the previously identified increase in Sgk1 expression by chronic morphine is an excellent example of the sample content differences. Sgk1 induction in VTA by chronic morphine was identified previously in microarray and RNAseq analysis of the VTA (Heller et al., 2015; McClung et al., 2005), although in our study this difference did not reach statistical significance due to one outlier sham replicate (Grubbs outlier test, $\alpha=0.05$). Surprisingly, Sgk1 was significantly depleted from sham IP compared to sham input (LogFC -1.7, $p_{adj} < 0.0001$), and there was no evidence for morphine-induction of Sgk1 in the DA-specific DEG analysis. To confirm the increase in Sgk1 expression was not driven by changes in VTA DA neurons, we completed a RT-PCR validation experiment on DAT^{L10a-GFP} input and IP (n7-8) samples. We found a significant effect of

drug ($F_{(1,26)}=16.58$, $p<0.05$), a significant effect of fraction ($F_{(1,26)}=90.02$, $p<0.0001$) and a significant drug x fraction interaction ($F_{(1,26)}=13.4$, $p<0.05$) via 2-way ANOVA.

Specifically, chronic morphine-induced Sgk1 expression in the whole VTA (input, 2-fold), but Sgk1 was not induced in VTA DA neurons (IP). In fact, Sgk1 was significantly depleted in the sham DA fraction (~80%) compared to the sham input (Sidak post-hoc test, $p<0.05$), similar to the reduction of GAD gene (~88%) in the DA-specific IP (Figure 13). This result highlights the importance of addressing cell-type specificity of gene expression changes identified in heterogenous samples, because the significant gene may or may not occur within the predominant cell type.

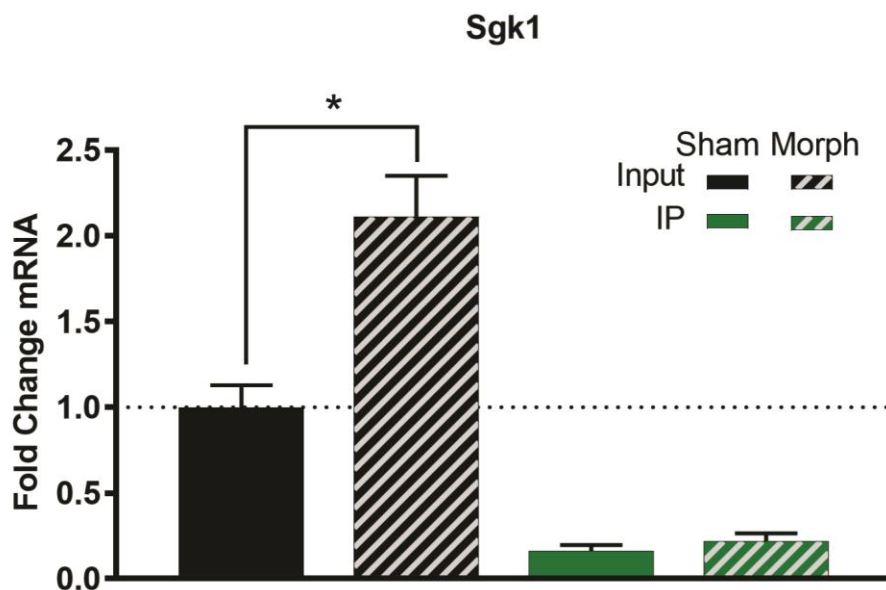


Figure 25. RT-PCR of Sgk1 Gene Expression in Input and IP of Sham- and Morphine-treated DAT^{L10a-GFP}. Chronic morphine-treatment (dashed-bars) significantly induces Sgk1 gene expression in whole-VTA input (black) while having no effect in the DA-specific IP (green) compared to sham-treated controls (solid-bars). Sgk1 expression was also significantly depleted from IP fractions. * $p<0.05$ (two-way ANOVA, Sidak post hoc test, n6-8 ea.)

3.3.4. Validation of Morphine-Induced Changes in Gene Expression in VTA DA IP

We next sought to validate chronic morphine-regulated genes identified in the DA-specific DEG analysis. Selected candidate genes and their average sham and morphine relative expression ratios and p_{adj} from the RNAsequencing screen are listed in Table 7. Genes were selected from multiple functional groups including: neuropeptides (Gcg, Nms, Vgf), cytoskeletal proteins (Acta2, Anxa10), receptors and channels (Chrn4, Kcnab2, Kcne1l), and transcription factors (Nupr1, Smagp, Tal2). The increased expression of a number of neuropeptides was a surprise, especially since this is the first time to our knowledge that some of these neuropeptides (e.g. Nms, Vgf, and Gcg) have been described in the VTA. In fact, both Nms and Gcg are significantly enriched in the sham IP compared to sham inputs (1.5-fold and 1.4-fold, respectively, $p_{adj}<0.05$) and therefore are basally enriched in VTA DA neurons.

Table 7. Significant Morphine-regulated Genes in RNAseq DA-IP.

Gene	Sham IP (Ave \pm SEM)	Morph IP (Ave \pm SEM)	logFC	logCPM	p_{adj}	t-test p value
Acta2	1.56 \pm 0.38	0.26 \pm 0.09	-2.58	0.74	<0.0001	0.015
Anxa10	0.05 \pm 0.02	0.49 \pm 0.11	3.07	-0.93	<0.0001	0.008
Chrn4	0.37 \pm 0.09	0.05 \pm 0.01	-2.90	-0.36	<0.0001	0.014
Gcg	0.36 \pm 0.09	1.89 \pm 0.41	2.39	0.37	<0.0001	0.011
Kcnab2*	104.68 \pm 1.84	93.32 \pm 7.03	-0.15	8.61	1.00	0.17
Kcne1l†	1.48 \pm 0.56	0.26 \pm 0.09	-2.42	0.46	<0.0001	0.076
Mesp2†	0.26 \pm 0.05	0.01 \pm 0.01	-3.95	-1.66	<0.0001	0.003
Nms	0.78 \pm 0.19	5.17 \pm 0.82	2.75	1.62	<0.0001	0.002
Nupr1†	0.29 \pm 0.04	0.01 \pm 0.01	-4.82	-1.25	<0.0001	0.001
Smagp†	0.63 \pm 0.27	0.01 \pm 0.01	-6.05	-1.29	<0.0001	0.061
Tal2†	0.46 \pm 0.12	0.02 \pm 0.01	-4.47	-0.41	<0.0001	0.012
Vgf*	65.07 \pm 9.54	148.27 \pm 26.11	1.20	8.10	0.09	0.02

* denotes genes selected with $p>0.05$, but were included due to suspected outlier effects. † denotes genes which were below RT-PCR detection range, and therefore removed from the study.

RT-PCR conditions were first verified on samples from whole VTA to ensure primer specificity (melt curve analysis and DNA gel electrophoresis) and that the gene expression was within detection range. Multiple candidate genes (Kcne1l, Mesp2, Nupr1, Smagp, and Tal2) were below the detection range using standard RT-PCR settings (data not shown). This is not surprising due to their relative low abundance in the RNAsequencing data set (values $<-1\text{LogCPM}$). Therefore, these genes may require amplification (or altered primer design) for optimal detection. RT-PCR was used to assess the expression of the remaining genes in sham and morphine-treated DAT^{L10a-GFP} input and IP samples. Because RNAseq was performed on female DAT^{L10a-GFP} mice, candidate genes were examined in both male (n3-4) and female (n3-5) samples in separate experiments. Each candidate gene tested was normalized to sham input for ease of comparison, and results are shown in Table 8. The results of 2-way ANOVA are represented in Table 9 (predicted up-regulated genes) and Table 10 (predicted down-regulated genes).

Table 8. RT-PCR of Candidate Genes (Normalized to Sham Input).

Gene	Sham Input	Morph Input	Sham IP	Morph IP
Nms	1.00 ± 0.05, n3	2.33 ± 0.65, n4	1.31 ± 0.19, n4	*11.40 ± 1.54, n4
Gcg	1.00 ± 0.36, n4	1.78 ± 0.58, n3	1.13 ± 0.2, n4	*4.62 ± 0.17, n4
Vgf	1.00 ± 0.22, n4	1.41 ± 0.21, n4	#0.70 ± 0.12, n4	1.15 ± 0.10, n4
Anxa10	1.00 ± 0.10, n4	1.70 ± 0.69, n3	1.37 ± 0.18, n4	*3.85 ± 0.69, n4
Chrn4	1.00 ± 0.18, n4	1.19 ± 0.06, n4	†0.15 ± 0.03, n4	0.06 ± 0.01, n4
Kcnab	1.00 ± 0.15, n4	1.00 ± 0.15, n4	0.91 ± 0.11, n4	0.70 ± 0.04, n4
Acta2	1.00 ± 0.76, n4	0.63 ± 0.42, n4	#0.07 ± 0.04, n4	0.04 ± 0.02, n4

*Drug effect within fraction, †effect of fraction, # trend in effect of fraction

Table 9. Results of 2-way ANOVA of Up-regulated Genes.

2-way ANOVA	Nms		Gcg		Vgf		Anxa10	
	Fvalue	p value	Fvalue	p value	Fvalue	p value	Fvalue	p value
Effect of Drug	$F_{(1,28)}= 32.69$	<0.0001	$F_{(1,11)}= 32.31$	0.0001	$F_{(1,25)}=10.44$	<0.01	$F_{(1,11)}= 13.05$	<0.01
Effect of Fraction	$F_{(1,28)}= 23.92$	<0.0001	$F_{(1,11)}= 16.24$	<0.01	$F_{(1,25)}=0.035$	>0.05	$F_{(1,11)}= 8.196$	<0.05
Interaction	$F_{(1,28)}= 23.92$	<0.0001	$F_{(1,11)}= 16.24$	<0.01	$F_{(1,25)}=0.035$	>0.05	$F_{(1,11)}= 4.089$	#0.07
Sidak Post-hoc	significant?	p value	significant?	p value	significant?	p value	significant?	p value
Sham Input vs. IP	no	>0.05	no	>0.05	no	>0.05	no	>0.05
Input Sham vs. Morph	no	>0.05	no	>0.05	no	>0.05	no	>0.05
IP Sham vs. Morph	yes	<0.0001	yes	<0.0001	no	>0.05	yes	<0.01

Trending Effect

Table 10. Results of 2-way ANOVA of Down-regulated Genes.

2-way ANOVA	Chrn4		Kcnab		Acta2	
	Fvalue	p value	Fvalue	p value	Fvalue	p value
Effect of Drug	$F_{(1,12)}= 0.27$	>0.05	$F_{(1,12)}= 0.74$	>0.05	$F_{(1,12)}= 0.21$	>0.05
Effect of Fraction	$F_{(1,12)}= 104.3$	<0.0001	$F_{(1,12)}= 2.55$	>0.05	$F_{(1,12)}= 3.05$	#0.11
Interaction	$F_{(1,12)}= 2.09$	>0.05	$F_{(1,12)}= 0.74$	>0.05	$F_{(1,12)}= 0.15$	>0.05
Sidak Post-hoc	significant?	p value	significant?	p value	significant?	p value
Sham Input vs. IP	yes	<0.01	no	>0.05	no	>0.05
Input Sham vs. Morph	no	>0.05	no	>0.05	no	>0.05
IP Sham vs. Morph	no	>0.05	no	>0.05	no	>0.05

Trending Effect

Specifically, there were no significant effects of drug across all input fractions, but there was a significant effect of drug in DA-specific IP of Nms, Gcg, and Anxa10 genes. Interestingly, several genes were decreased in the sham IP compared to sham input. Specifically, Chrn4 was significantly depleted and there was a trend for decreased Vgf and Acta2 expression in sham IP. Acta2 sham input expression was highly variable and while it appears to be downregulated following chronic morphine this effect did not reach statistical significance. Select candidate gene expression changes (Nms, Vgf, Anxa10) were also validated in female DAT^{L10a-GFP} mice (n3-5) and therefore were combined in the final analysis. In order to better visualize the final results, gene expression was normalized to average sham (within fraction) and all predicted upregulated genes (Nms, Vgf, Gcg, Anxa10) are shown in Figure 26A, and predicted downregulated genes (Acta2, Chrn4, Kcnab) are displayed in Figure 26B. Because each gene was normalized within fractions, t-tests were used to assess chronic morphine effects on expression of each gene and results are summarized in Table 11.

Of note, all the neuropeptides analyzed (Nms, Gcg, and Vgf) were significantly induced by chronic morphine in the IP fractions. Chronic morphine also significantly induced Nms and Vgf in the input fractions, although it should be noted that the magnitude of Nms morphine induction was much greater in the IP (14-fold change) compared to the input (2-fold). The morphine-induced increase in Gcg and Anxa10 expression was only significant in the DA-specific IP fraction. As shown in Figure 26B,

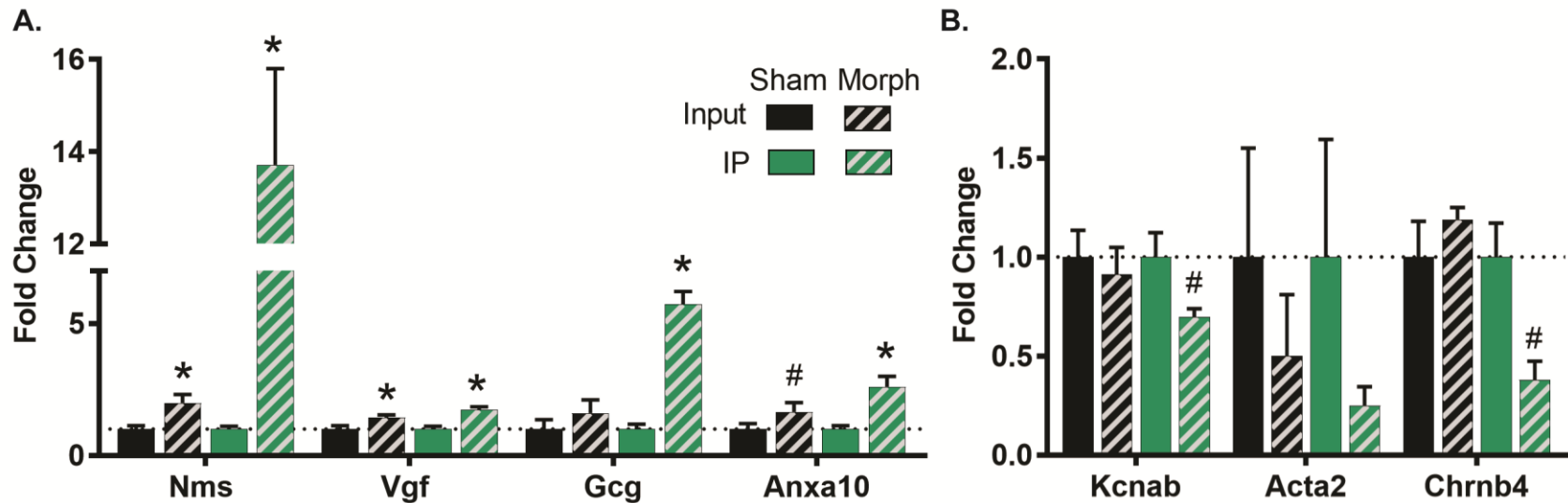


Figure 26. Combined RT-PCR Validation of Chronic Morphine-induced Genes in DAT^{L10a}-GFP Input and IP.

A. Significant morphine induction in IP of all predicted up-regulated genes (Nms, Vgf, Gcg, and Anxa10). Nms and Vgf were significantly increased in the morphine-treated input fraction while there was a trend for induction of Anxa10 in the input. B. No significant down-regulation was detected across predicted down-regulated genes. There was a trend for chronic morphine decrease in Kcnab (multiple t-test, $p=0.12$), and Chrn4 (multiple t-test, $p=0.05$). Significance determined by Multiple t-tests; * = $p<0.05$ trend # = $0.05<p<0.15$.

Table 11. Combined RT-PCR Validation of Candidate Genes, Multiple T-tests.

Gene	Input: Morphine Effect	IP: Morphine effect
Nms	$t_{(12)} = 2.53, (n7), *p < 0.05$	$t_{(13)} = 5.79, (n7-8), *p < 0.05$
Vgf	$t_{(13)} = 2.29, (n7-8), *p < 0.05$	$t_{(12)} = 2.72, (n7), *p < 0.05$
Gcg	$t_{(5)} = 1.11, (n3-4), p > 0.05$	$t_{(6)} = 7.26, (n4), *p < 0.05$
Anxa10	$t_{(12)} = 1.75, (n6-8), \#p = 0.105$	$t_{(13)} = 3.01, (n7-8), *p < 0.05$
Chrn4	$t_{(6)} = 1.00, (n4), p > 0.05$	$t_{(6)} = 2.45, (n4), \#p = 0.05$
Kcnab	$t_{(6)} = 0.00, (n4), p > 0.05$	$t_{(6)} = 1.80, (n4), p = 0.12$
Acta2	$t_{(6)} = 0.45, (n4), p > 0.05$	$t_{(6)} = 0.75, (n4), p > 0.05$

* significant effect $p < 0.05$, # trending effect, $p < 0.1$

there were no significant drug effects in input samples of all genes tested. Only Chrn4 showed a strong trend for reduction in the morphine IP compared to sham IP (~40% decrease, t-test $p = 0.050$). Morphine-induced downregulation of Kcnab in the IP fraction did not meet statistical significance (t-test $p = 0.12$), although our effect (24% reduction) is similar to published results of ~15-20% from chronic morphine in whole VTA (Mazei-Robison et al., 2011). Acta2 did show a trend for decreased expression in the DA fraction, however expression was highly variable in the input controls, limiting the ability to detect significant differences.

3.4. Discussion

The VTA is a cellularly heterogenous, with not only distinct DA, GABA and glutamatergic neuron populations, but also neurons that may co-express neurotransmitters (TH/GABA(+), TH/GLUT(+)) (Margolis, Lock, Hjelmstad, & Fields, 2006; Nair-Roberts et al., 2008; Stamatakis et al., 2013; Stuber et al., 2015). Previous genetic screens (RNAseq, microarray) to identify chronic opioid-induced molecular changes examined the whole VTA, including midline structures. While these analyses

were useful for identification of initial candidate genes, the cell type- and circuit-specificity of such differences have yet to be directly tested. Therefore, in this study we used TRAP to specifically identify morphine-induced adaptations in DA neurons within the VTA.

TRAP utilizes a GFP-tagged ribosome subunit (L10a-GFP) to immunoprecipitate actively translating RNA, expression of the L10a-GFP transgene can be driven in a cell type specific manner via Cre-recombinase driver lines. Therefore, we achieved DA-specific expression by crossing the Rosa26-L10a-GFP reporter line with TH-Cre and DAT-Cre mice. We first assessed DA-specific expression of TH^{L10a-GFP} and DAT^{L10a-GFP} for GFP expression patterns across the VTA, mPFC and NAc. TH^{L10a-GFP} mice exhibited notable GFP expression in TH(-) midline nuclei (IPN and RLi) in VTA as well as expression in the mPFC, Ventral Pallidum (VP), Lateral Septum (LS) and NAc. In contrast, L10a-GFP expression in DAT^{L10a-GFP} mice was restricted primarily to VTA and SNc, with little to no expression detected in mPFC and NAc containing sections. RT-PCR analysis confirmed that either DA-driver line (DAT^{L10a-GFP} or TH^{L10a-GFP}) was sufficient to significantly enrich DA-specific markers and reduce GABAergic genes in IP samples, although DAT^{L10a-GFP} samples appeared to achieve a purer DA-specific fraction (88% reduction of GAD) compared to TH^{L10a-GFP} (40% reduction of GAD). The results of this study are consistent with previous reports suggesting TH-Cre mice express Cre-recombinase not only in VTA DA neurons but also in the midline structures (IF, IPN, and RLi) which have either low or no TH expression (Lammel et al., 2015). This anatomical distinction is particularly important if using tissue punch extraction for

VTA RNA isolation, which in TH^{L10a-GFP} mice would include midline structures with variable TH-Cre expression. Therefore, due to these distinctions in Cre-driver expression of L10a-GFP, we used DAT^{L10a-GFP} line to determine chronic morphine-induced transcriptome in VTA DA neurons

We performed RNAseq analysis of VTA from sham and morphine-treated DAT^{L10a-GFP} mice which resulted in the identification of >20,000 genes which is approximately 99% coverage of the 20,210 protein-coding genes in the mouse genome (Church et al., 2009). Following RNAseq, we utilized DEG expression analysis to identify significantly regulated genes across three main analyses: 1) sham input vs. sham IP to identify the basal DA transcriptome, 2) sham input vs. morphine input for morphine-induced changes in whole VTA and 3) sham IP vs. morphine IP to determine the morphine-induced DA transcriptome.

In the first analysis, we compared DA-specific transcriptome to whole VTA, and determined that more genes were significantly depleted than enriched in the DA-specific IP. This is expected not only due to the heterogeneity of the VTA (ie. multiple cell types), but also due to the specificity of the IP fraction to contain only actively translating mRNA transcripts and therefore remove small regulatory RNA (miRNA, snRNA) (Heiman et al., 2014). Importantly, we show that DA-specific transcripts (DAT, TH, D2d, VMAT) were significantly enriched >2-fold in the IP while GABAergic, glutamatergic and glial cell markers were significantly reduced. This confirms that we were able to achieve a relatively pure DA-specific transcriptome in our experiments, similar to other published DA-specific TRAP techniques (Chung et al., 2017; Ekstrand et al., 2014). Of note,

Aldh1a1 gene was significantly enriched >2-fold in the DA-specific IP in our samples. Aldh1a1 has also been identified in single-cell DA-specific mRNA analysis (Poulin et al., 2014) and in situ hybridization confirmed Aldh1a1 expression in ~15% of VTA DA neurons (Kim et al., 2015). Aldh1a1 has been implicated in GABA synthesis and co-release properties of d.Str- and NAc-projecting DA neurons (Kim et al., 2015) and has also been described in LHb projecting-TH(-) neurons in midline nuclei (IF and RLi) (Lammel et al., 2015; Stamatakis et al., 2013; Tritsch, Oh, Gu, & Sabatini, 2014). However, since the SNc marker Sox6 (Panman et al., 2014; Poulin et al., 2014) was not enriched in our IP samples and use of DAT^{L10a-GFP} model removes IPN and RLi mRNA contamination from our samples, our IP likely contained predominantly VTA (PBP and PN) DA neuron mRNA without substantial SNc, IPN, or RLi mRNA. Because Aldha1a was enriched in the IP (>2-fold), this may suggest that either a higher proportion of VTA DA neurons express Aldha1a than previously suggested or that it is expressed in relatively high levels in a small proportion of VTA DA neurons.

In order to determine global morphine-induced gene expression in whole VTA, we used DEG analysis to compare sham input to morphine input samples. This analysis identified 410 significantly regulated genes. While most of these genes are novel, we identified a few candidate targets belonging to functional pathways which had been implicated in previous studies (e.g. BDNF/TrkB signaling, actin remodeling, and K⁺ channel regulation). For example, decreased Kcnab and Girk3 channel expression following chronic morphine were implicated as possible mediators of increased activity of DA neurons (Mazei-Robison et al., 2011). Additionally, Sgk1 expression is

significantly induced in the VTA following both chronic morphine and cocaine exposure and is a downstream target of mTORC2/Akt pathways implicated in morphine reward (Heller et al., 2015; McClung et al., 2005).

Therefore, we first sought to determine whether genes previously identified to be regulated by morphine in the VTA (*Girk3*, *Kcnab*, *Sgk1*) were present in DA neurons. We found that *Girk3* expression was significantly increased in the input fraction by chronic morphine in our RNAsequencing results, similar to the induction reported previously (Heller et al., 2015), but was not regulated in the DA fraction. In contrast, chronic morphine-induced downregulation of *Kcnab* does appear to be DA-specific. Using RT-PCR we confirmed a trend for ~25% reduction, similar to the reduction reported in the whole VTA (~15-20%). Due to the relatively modest effect, validation may require higher power (increased n) to confirm that effects are significant. Surprisingly, the robust induction of *Sgk1* by morphine was not driven by increased expression in VTA DA neurons. This suggests that *Sgk1* may be induced in a separate cellular population (such as glial, GABA, or Glutamatergic VTA neurons), or it may not be actively translated into protein in the cell soma but rather transported to distal dendrites or axons until further activation through translational pausing mechanisms (Kanai, Dohmae, & Hirokawa, 2004; Richter & Coller, 2015). Therefore, the cellular specificity of *Sgk1* induction and its physiological relevance will require further testing. Collectively, these results illustrate the necessity of validating candidate genes using cell type-specific approaches, as changes may occur in a specific subpopulation of neurons.

We next identified 393 genes that were significantly regulated by morphine in the specifically in VTA DA neurons. Surprisingly, when morphine-regulated genes identified in the input analysis are compared to the DA-specific IP analysis, there was little overlap. Only ~7% of genes significantly regulated by morphine in the input were also identified to be DA-specific, and of these only 50% were regulated in the same the direction (increased or decreased). These data clearly illustrate that gene expression changes that occur in DA neurons can easily be masked when examining whole VTA. For example, while Nms expression was modestly increased by morphine in the input fraction (~ 2-fold), a much more robust induction was observed in DA neurons (14-fold). Thus, more modest gene expression changes in DA neurons could easily be missed in whole VTA analysis unless the gene in question is specific to only DA neurons (such as TH or Aldh1a1) or is very highly induced (e.g. Nms).

Several novel morphine-regulated genes were identified in the DA-specific IP analysis. Specifically, three neuropeptides (Nms, Gcg, and Vgf) were significantly upregulated following chronic morphine treatment in VTA DA neurons. Nms was first identified in the suprachiasmatic nucleus (SCN) and has been implicated in circadian rhythm maintenance, feeding behavior, and pituitary hormone secretion (Ida et al., 2005; Lee et al., 2015; Mori et al., 2005; Shousha et al., 2006; Vigo et al., 2007). This is the first time, to our knowledge, that Nms production has been detected in VTA DA neurons. Interestingly, both Nms and Gcg-related peptides (glucagon, and glucagon-like peptide 1 [GLP-1]) have similar identified roles in regulation of feeding behavior and energy homeostasis (Cork et al., 2015; Ida et al., 2005; Wang et al., 2015). Moreover,

Gcg has been implicated in food and drug reward. For example, GLP-1 receptor (GLP-1R) is expressed in the VTA and intra-VTA infusion of GLP-1R agonist significantly reduces cocaine self-administration (Cork et al., 2015; Schmidt et al., 2016). GLP-1 peptide is primarily expressed in the nucleus tractus solitarius (NTS) which projects to the VTA and NAc to regulate highly palatable food intake (Alhadeff, Rupprecht, & Hayes, 2012; Dickson et al., 2012). It remains to be determined if chronic morphine-induced increases in Nms and Gcg expression have a similar physiological role in the VTA as seen in other brain regions, such as regulation of feeding behavior or circadian oscillations (Ida et al., 2005; Lee et al., 2015; Mori et al., 2005). Either may be likely, as chronic morphine induces substantial weight loss and changes in feeding behavior (Levine, Morley, Gosnell, Billington, & Bartness, 1985; Ren et al., 2013), as well as alterations in circadian rhythm (Li et al., 2010; Pacesova, Novotny, & Bendova, 2016).

The identification of Vgf expression in VTA DA neurons is also a novel candidate for morphine-induced adaptations in the VTA. Vgf protein and its derived neuropeptides regulate BDNF/TrkB and CREB pathways in neurons and play a role in a number of processes such as, hyperalgesia, inflammation, depression, energy homeostasis, and synaptic plasticity (Behnke et al., 2017; Bozdagi et al., 2008; Chen et al., 2013; Fairbanks et al., 2014; W. J. Lin et al., 2015; Sadari et al., 2014). Additionally, Vgf has been implicated as a molecular mediator of antidepressant action as well as pro-depressant effects in different brain regions (Jiang et al., 2017; Malberg & Monteggia, 2008). For example, Vgf is induced in the hippocampus following both exercise and antidepressant administration, both of which promote alleviation of mood disorder-

related symptoms through alteration of BDNF/TrkB and Akt/mTORC signaling pathways (Hunsberger et al., 2007; P. Lin et al., 2014; Thakker-Varia et al., 2007). Conversely, Vgf induction in the NAc is associated with pro-depressive behavior (Jiang et al., 2017). Both BDNF/TrkB and Akt/mTORC2 signaling pathways are integral to chronic morphine-induced synaptic plasticity, morphology and behavioral reward (Koo et al., 2012; Koo et al., 2015; Mazei-Robison et al., 2011; Russo et al., 2007; Russo, Mazei-Robison, Ables, & Nestler, 2009) suggesting that Vgf and BDNF/TrkB signaling may be differentially regulated in distinct VTA DA populations.

It is important to note that previous genetic screens to determine chronic morphine effects in the VTA were completed only in male mice (Heller et al., 2015; Koo et al., 2015; McClung et al., 2005). It is largely unknown whether opioids produce the same molecular response in VTA DA neurons of females. This is particularly important due to known sex-specific and hormone state-dependent effects of cocaine on VTA DA activity and behavior (Calipari et al., 2017; Zhang, Yang, Yang, Jin, & Zhen, 2008). Few studies have directly assessed sex-specific effects of chronic morphine. To address this knowledge gap in the field, we performed RNAseq analysis on samples from females and candidate genes validation utilized both sexes. Overall, we found no sex-specific effects across all genes validated similar with a recent study which found similar VTA DA transcriptome across sex (Chung et al., 2017), but it will be important to continue to systematically assess any sexual dimorphism of VTA DA responses to chronic opioids in future studies.

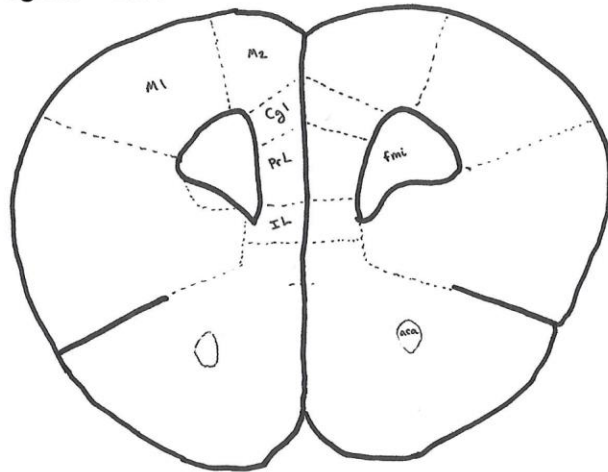
The identification of multiple new gene targets identified in this study highlight both the power and the importance of cell-specific genetic screens in identifying novel targets for drug-induced neuroplasticity. For example, our RNAsequencing analysis of VTA DA neurons identified a morphine-induced decrease in nicotinic receptor expression (Chrnb4) . Given that nicotinic modulation of VTA DA neurons is necessary for glutamatergic-dependent burst firing, Chrnb4 may serve as critical mediator of morphine-induced changes in VTA DA neuron activity. Additionally, further analysis of the RNAsequencing dataset may elucidate whether there is shared transcriptional regulation across regulated genes or whether changes exist across distinct signaling pathways. Together with the projection-specific effects of chronic morphine on VTA DA morphology (see Chapter 2 for details), we can now systematically examine new candidate genes in projection-specific subsets of VTA DA neurons utilizing combined cell- and projection-specific viral methods. For example, projection-specific gene editing using Crispr-Cas9 viral systems can be utilized for functional validation of target genes in specific DA-projections. Together the results of this study progress our understanding of chronic-morphine induced adaptations in whole VTA and VTA DA neuros specifically, furthering the ultimate goal of identifying novel targets for therapeutic intervention in opioid dependence and addiction.

APPENDICES

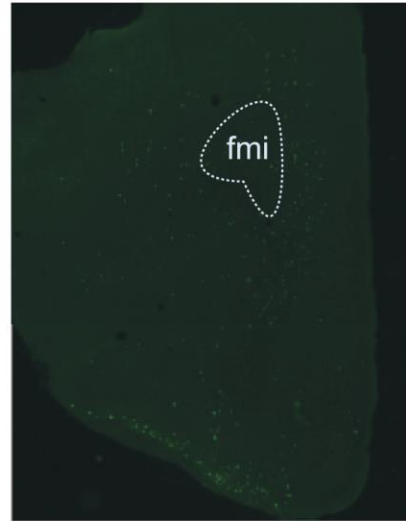
Appendix A.

L10a-GFP Expression Patterns Across Prefrontal Cortex and Nucleus Accumbens

Bregma +1.98



THL10a-GFP



DATL10a-GFP



Bregma +1.78

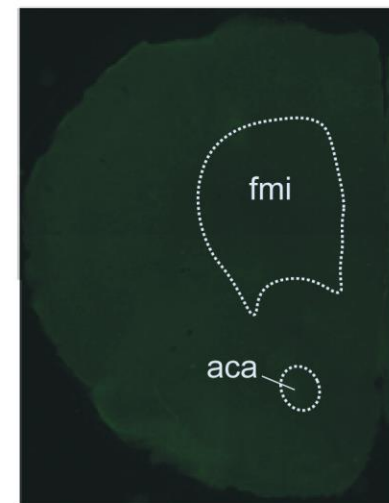
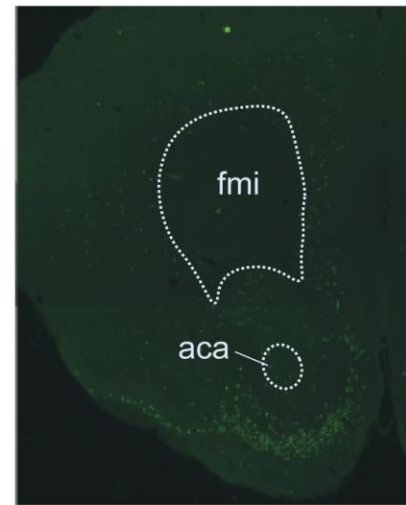
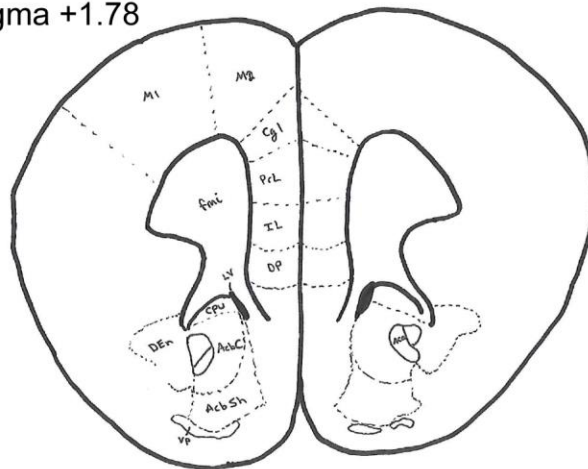
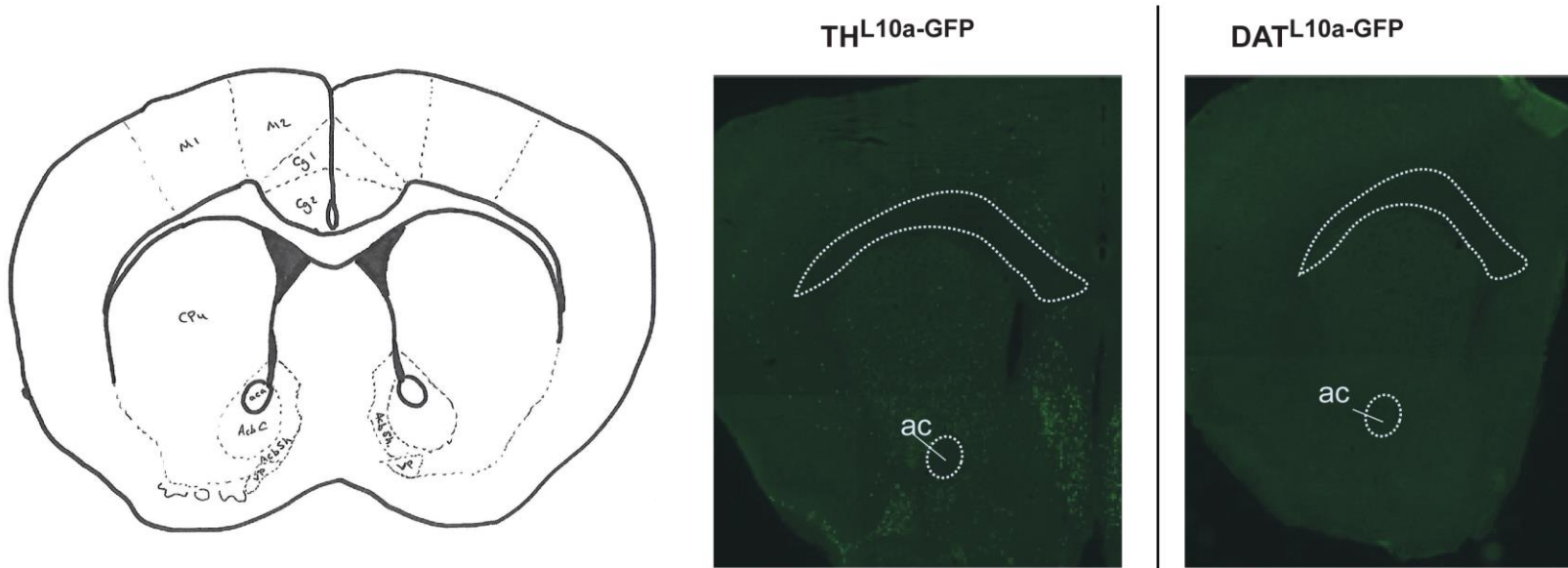


Figure 27. Comparison of GFP Expression Across PFC and NAc in TH^{L10a}-GFP and DAT^{L10a}-GFP Mice.

Figure 27. (Cont'd)



Abbreviations: anterior commissural nucleus (ac), nucleus accumbens core (AcbC, aka NAc core), nucleus accumbens shell (AcbSh, aka NAc m.shell) caudate putamen (CPU, aka striatum), cingulate cortex 1 (Cg1), cingulate cortex 2 (Cg2), dorsopeduncular cortex (DP), forceps minor of the corpus callosum (fmi), infralimbic cortex (IL), primary motor cortex (M1), secondary motor cortex (M2), prelimbic cortex (PrL), ventral pallidum (VP),

Appendix B.

Significant Enriched and Depleted Genes in VTA DA neurons:

Sham Input vs. Sham IP

Table 12. Top 100 Significantly Enriched Genes in Sham VTA DA Neurons.

No.	Gene Symbol	Sham Input AVE \pm SEM	Sham IP AVE \pm SEM	LogFC	LogCPM	LR	P.adj
1	Th	343.1 \pm 27.1	2147.3 \pm 97.2	2.8	11.3	59.7	<0.0001
2	Ddc	365.4 \pm 17.1	1815.0 \pm 97.2	2.4	11.1	47.3	<0.0001
3	Aldh1a1	350.3 \pm 11.4	1612.0 \pm 91.5	2.3	11.0	43.5	<0.0001
4	Ret	75.7 \pm 7.3	299.5 \pm 11.4	2.1	10.5	36.3	<0.0001
5	Slc6a3 (DAT)	118.3 \pm 15.9	596.2 \pm 46.1	2.4	10.3	48.2	<0.0001
6	Dlk1	96.7 \pm 9.2	416.4 \pm 32.2	2.2	10.3	40.3	<0.0001
7	Slc18a2 (VMAT)	115.5 \pm 8.2	492.4 \pm 38.5	2.2	10.2	39.8	<0.0001
8	Sncg	202.8 \pm 2.4	1171.8 \pm 43.4	2.6	9.8	55.2	<0.0001
9	Tagln3	289.6 \pm 11.4	907.2 \pm 50.6	1.8	9.6	26.1	<0.0001
10	Cadps2	49.1 \pm 0.9	169.0 \pm 1.6	1.9	9.1	29.9	<0.0001
11	Fgf13	84.5 \pm 1.2	296.7 \pm 5.3	1.9	8.9	30.8	<0.0001
12	Amotl1	25.4 \pm 1.0	71.7 \pm 3.1	1.6	8.8	21.9	<0.0001
13	Tmsb10	253.6 \pm 6.3	853.4 \pm 37.3	1.9	8.6	29.0	<0.0001
14	Erc2	25.1 \pm 1.1	94.8 \pm 3.7	2.0	8.6	34.0	<0.0001
15	Chrna6	38.9 \pm 3.1	214.3 \pm 14.7	2.6	8.6	52.8	<0.0001
16	Chrna4	35.6 \pm 2.8	126.0 \pm 6.9	1.9	8.6	31.2	<0.0001
17	Calb1	32.1 \pm 0.9	140.2 \pm 6.0	2.2	8.5	40.7	<0.0001
18	Ankrd 34b	46.6 \pm 1.8	128.8 \pm 3.4	1.6	8.5	21.0	<0.0001
19	Drd2	38.2 \pm 3.4	225.5 \pm 11.5	2.7	8.4	56.3	<0.0001
20	Ly6h	61.3 \pm 3.0	178.7 \pm 10.6	1.7	8.4	23.3	<0.0001
21	Kcnd3	24.4 \pm 1.2	68.8 \pm 1.7	1.6	8.4	21.9	<0.0001
22	Sdc2	42.9 \pm 2.6	153.7 \pm 7.2	1.9	8.4	31.6	<0.0001
23	Ntn1	25.2 \pm 2.0	81.7 \pm 2.5	1.8	8.3	27.5	<0.0001
24	Slc10a4	26.3 \pm 1.6	133.1 \pm 11.1	2.5	8.3	48.4	<0.0001
25	Fam70a	41.0 \pm 2.3	122.9 \pm 4.6	1.7	8.3	24.3	<0.0001
26	Sncg	158.9 \pm 10.9	534.7 \pm 46.7	1.9	8.2	29.1	<0.0001
27	En1	26.3 \pm 1.0	115.7 \pm 5.0	2.2	8.2	41.2	<0.0001
28	Scn3b	31.2 \pm 2.4	92.0 \pm 3.2	1.7	8.2	23.6	<0.0001
29	Cck	116.2 \pm 13.8	516.3 \pm 53.7	2.3	8.0	41.8	<0.0001
30	Gfra1	26.4 \pm 0.7	69.6 \pm 4.8	1.5	7.8	19.3	0.0001
31	Cpne7	26.2 \pm 2.0	98.4 \pm 2.5	2.0	7.8	33.8	<0.0001
32	Cdh13	25.7 \pm 1.2	70.9 \pm 5.4	1.6	7.8	21.2	<0.0001
33	Chrn3	18.1 \pm 0.9	74.7 \pm 5.4	2.2	7.8	38.2	<0.0001
34	Nr4a2	27.9 \pm 0.8	87.3 \pm 3.2	1.8	7.7	26.0	<0.0001
35	Clptm1l	41.1 \pm 2.8	129.1 \pm 5.5	1.8	7.6	26.2	<0.0001

Table 12. (Cont'd)

No.	Gene Symbol	Sham Input AVE \pm SEM	Sham IP AVE \pm SEM	LogFC	LogCPM	LR	P.adj
36	Gng4	33.0 \pm 1.1	86.7 \pm 4.5	1.5	7.6	19.3	0.0001
37	Grik3	10.5 \pm 0.8	30.9 \pm 0.7	1.7	7.6	23.4	<0.0001
38	Ntsr1	14.1 \pm 1.4	77.5 \pm 7.0	2.6	7.5	52.6	<0.0001
39	Klhl1	22.8 \pm 0.9	63.7 \pm 1.0	1.6	7.5	21.4	<0.0001
40	Tacr3	20.3 \pm 1.6	73.2 \pm 5.5	2.0	7.5	32.1	<0.0001
41	Satb1	12.8 \pm 0.8	39.7 \pm 1.9	1.7	7.4	25.6	<0.0001
42	Whrn	20.7 \pm 0.9	58.1 \pm 1.3	1.6	7.3	21.6	<0.0001
43	Dkk3	22.8 \pm 1.8	66.0 \pm 4.8	1.6	7.3	23.0	<0.0001
44	Col25a1	10.2 \pm 0.7	33.8 \pm 2.9	1.8	7.2	28.4	<0.0001
45	Syt17	41.1 \pm 2.3	142.0 \pm 7.8	1.9	7.2	30.0	<0.0001
46	Gch1	18.2 \pm 1.0	85.6 \pm 3.0	2.3	7.2	44.5	<0.0001
47	Bahcc1	3.0 \pm 0.2	23.3 \pm 4.8	3.0	7.2	70.3	<0.0001
48	Lmo4	41.6 \pm 1.4	114.2 \pm 5.4	1.6	7.1	20.9	<0.0001
49	Foxp2	10.2 \pm 0.7	27.8 \pm 1.2	1.6	7.0	20.6	<0.0001
50	Gsg1l	15.2 \pm 1.4	49.5 \pm 3.7	1.8	7.0	27.7	<0.0001
51	Syt5	37.5 \pm 3.0	105.4 \pm 7.4	1.6	7.0	21.8	<0.0001
52	Tnrc18	7.1 \pm 0.8	30.3 \pm 5.6	2.2	7.0	39.1	<0.0001
53	Ctxn1	47.8 \pm 0.8	126.8 \pm 2.9	1.5	6.8	19.6	0.0001
54	Fam167a	8.1 \pm 0.8	37.6 \pm 1.2	2.3	6.6	43.6	<0.0001
55	Ajap1	14.0 \pm 0.6	46.3 \pm 1.2	1.8	6.6	28.2	<0.0001
56	Gse1	6.4 \pm 0.7	20.0 \pm 3.2	1.7	6.5	25.4	<0.0001
57	Lpl	6.7 \pm 0.6	35.4 \pm 3.4	2.5	6.5	50.2	<0.0001
58	Rac3	40.0 \pm 1.8	118.0 \pm 4.9	1.7	6.4	23.6	<0.0001
59	Lmx1b	9.8 \pm 0.3	25.9 \pm 0.5	1.5	6.4	19.4	0.0001
60	Oprk1	8.2 \pm 0.4	26.9 \pm 1.7	1.8	6.4	27.7	<0.0001
61	Nxph3	19.3 \pm 1.2	57.4 \pm 4.8	1.7	6.4	23.9	<0.0001
62	Ctxn2	36.0 \pm 2.1	114.1 \pm 2.3	1.8	6.3	26.4	<0.0001
63	Glce	8.3 \pm 0.6	22.9 \pm 1.2	1.6	6.2	20.9	<0.0001
64	F2r	10.7 \pm 0.6	32.4 \pm 0.8	1.7	6.2	24.6	<0.0001
65	Nup98	6.5 \pm 0.3	18.9 \pm 3.0	1.6	6.2	22.5	<0.0001
66	Msh3	7.7 \pm 0.5	25.2 \pm 0.9	1.8	6.1	27.9	<0.0001
67	Fxyd7	53.8 \pm 2.0	142.0 \pm 4.2	1.5	6.1	19.5	0.0001
68	Foxa1	10.3 \pm 0.4	30.3 \pm 1.0	1.7	6.0	23.5	<0.0001
69	Vwc2l	7.1 \pm 0.5	20.2 \pm 1.0	1.6	6.0	22.1	<0.0001
70	Lrrc55	11.4 \pm 0.5	30.9 \pm 0.9	1.5	6.0	20.3	<0.0001
71	Grp	15.8 \pm 2.1	110.4 \pm 11.2	2.9	6.0	65.3	<0.0001
72	Il13ra1	6.6 \pm 0.4	25.1 \pm 1.8	2.0	5.9	34.5	<0.0001
73	Adra1b	8.5 \pm 0.5	26.2 \pm 2.7	1.7	5.9	25.3	<0.0001

Table 12. (Cont'd)

No.	Gene Symbol	Sham Input AVE ± SEM	Sham IP AVE ± SEM	LogFC	LogCPM	LR	P.adj
74	Bcor	2.8 ± 0.2	13.2 ± 1.2	2.3	5.8	44.0	<0.0001
75	Wipf3	5.9 ± 0.5	17.6 ± 0.7	1.7	5.8	23.9	<0.0001
76	Gucy2c	4.4 ± 0.5	21.4 ± 1.9	2.4	5.7	46.0	<0.0001
77	Lrrc3b	14.1 ± 1.8	47.6 ± 3.0	1.9	5.7	29.1	<0.0001
78	Gabra4	6.2 ± 0.4	17.7 ± 0.7	1.6	5.7	22.5	<0.0001
79	Zfp503	6.0 ± 0.4	16.9 ± 1.0	1.6	5.6	21.8	<0.0001
80	Spint2	16.8 ± 1.0	48.6 ± 4.2	1.6	5.6	22.9	<0.0001
81	S100a10	34.1 ± 0.1	104.1 ± 7.3	1.7	5.6	24.7	<0.0001
82	Fkbp1b	25.4 ± 1.2	67.5 ± 1.0	1.5	5.5	19.7	0.0001
83	Gpr83	5.3 ± 0.3	15.3 ± 1.6	1.6	5.5	22.5	<0.0001
84	Kcns3	6.3 ± 0.1	22.4 ± 1.4	1.9	5.4	30.8	<0.0001
85	Ghr	4.9 ± 0.4	13.9 ± 0.6	1.6	5.3	22.0	<0.0001
86	Anxa1	6.2 ± 0.8	38.6 ± 7.6	2.7	5.3	58.8	<0.0001
87	Bend5	6.9 ± 0.7	29.7 ± 1.1	2.2	5.1	40.0	<0.0001
88	Asb4	4.0 ± 0.1	15.6 ± 1.9	2.1	5.0	35.7	<0.0001
89	Prima1	15.7 ± 1.1	42.3 ± 2.0	1.5	5.0	20.1	<0.0001
90	Trpc6	3.7 ± 0.3	18.3 ± 1.5	2.4	5.0	46.9	<0.0001
91	Tll1	2.7 ± 0.3	9.7 ± 0.8	1.9	5.0	30.9	<0.0001
92	Arhgap6	2.9 ± 0.2	8.2 ± 0.2	1.6	5.0	22.2	<0.0001
93	Pitx3	5.2 ± 0.6	36.8 ± 2.4	2.9	5.0	65.5	<0.0001
94	Npbwr1	2.6 ± 0.1	13.7 ± 0.9	2.5	5.0	49.1	<0.0001
95	Vit	5.9 ± 0.4	17.0 ± 0.9	1.6	5.0	22.5	<0.0001
96	Pappa	1.4 ± 0.1	3.8 ± 0.5	1.6	4.9	20.7	<0.0001
97	Bcl11a	2.4 ± 0.1	6.8 ± 0.4	1.6	4.8	21.9	<0.0001
98	Ntn4	4.0 ± 0.4	11.0 ± 0.2	1.6	4.8	20.6	<0.0001
99	Scml4	2.6 ± 0.1	8.2 ± 0.5	1.8	4.8	26.5	<0.0001
100	Fchsd1	3.1 ± 0.3	8.3 ± 0.3	1.5	4.6	19.3	0.0001

Table 13. Top 100 Significantly Depleted Genes in Sham VTA DA Neurons.

No.	Gene Symbol	Sham Input AVE \pm SEM	Sham IP AVE \pm SEM	LogFC	LogCPM	LR	P.adj
1	mt-Co1	4946.8 \pm 528.3	534.2 \pm 127.2	-3.1	12.0	74.1	<0.0001
2	Plp1	1040.6 \pm 68.8	102.9 \pm 20.7	-3.2	11.4	79.3	<0.0001
3	mt-Cytb	3193.4 \pm 324.3	223.9 \pm 48.3	-3.7	10.9	100.8	<0.0001
4	Mbp	679.6 \pm 36.0	124.4 \pm 29.6	-2.4	10.9	45.1	<0.0001
5	Meg3	195.0 \pm 50.4	14.8 \pm 1.3	-3.6	10.5	95.0	<0.0001
6	mt-Rnr2	1700.7 \pm 200.9	209.5 \pm 51.8	-2.9	10.5	66.5	<0.0001
7	mt-Nd1	2789.1 \pm 281.0	364.9 \pm 72.6	-2.8	10.5	62.9	<0.0001
8	mt-Nd5	1388.6 \pm 119.1	69.9 \pm 10.5	-4.2	10.3	122.3	<0.0001
9	mt-Nd2	2272.8 \pm 222.6	235.7 \pm 45.9	-3.2	10.3	76.4	<0.0001
10	Glul	783.6 \pm 33.7	138.7 \pm 13.3	-2.4	10.3	46.5	<0.0001
11	Sparcl1	749.6 \pm 16.6	77.4 \pm 16.3	-3.2	10.3	76.7	<0.0001
12	Mtap1a	147.0 \pm 7.7	42.4 \pm 2.6	-1.7	10.1	24.2	<0.0001
13	mt-Nd4	1246.1 \pm 116.5	114.4 \pm 21.8	-3.4	9.8	83.7	<0.0001
14	ApoE	1219.1 \pm 35.3	114.8 \pm 21.7	-3.3	9.8	82.2	<0.0001
15	Mobp	395.1 \pm 25.9	91.9 \pm 22.8	-2.0	9.6	33.7	<0.0001
16	Aldoc	463.3 \pm 12.7	93.7 \pm 8.4	-2.2	9.6	39.8	<0.0001
17	mt-Rnr1	1408.8 \pm 163.3	212.1 \pm 52.3	-2.6	9.6	55.3	<0.0001
18	Nefm	334.3 \pm 31.2	69.6 \pm 10.4	-2.2	9.5	38.4	<0.0001
19	NdrG2	549.1 \pm 16.0	103.9 \pm 9.6	-2.3	9.4	43.1	<0.0001
20	Atp1a2	202.7 \pm 7.3	21.4 \pm 3.9	-3.2	9.4	75.3	<0.0001
21	Sparc	495.4 \pm 32.9	55.3 \pm 9.1	-3.1	9.3	72.0	<0.0001
22	Cnp	307.8 \pm 7.9	38.9 \pm 6.2	-2.9	8.9	64.7	<0.0001
23	Vamp1	174.5 \pm 13.9	40.3 \pm 7.1	-2.0	8.8	33.9	<0.0001
24	Gpm6b	143.7 \pm 12.3	29.4 \pm 3.9	-2.2	8.7	39.4	<0.0001
25	Atp1b2	172.7 \pm 7.8	38.1 \pm 3.7	-2.1	8.6	35.7	<0.0001
26	Qk	96.4 \pm 8.6	18.0 \pm 3.2	-2.3	8.6	44.1	<0.0001
27	Snhg11	113.3 \pm 16.9	10.7 \pm 0.8	-3.3	8.5	81.6	<0.0001
28	Slc6a1	132.2 \pm 5.4	34.3 \pm 0.6	-1.8	8.5	28.4	<0.0001
29	Slc6a11	149.8 \pm 2.0	22.3 \pm 1.9	-2.6	8.4	55.4	<0.0001
30	Csrp1	304.0 \pm 5.1	39.9 \pm 6.8	-2.8	8.3	62.6	<0.0001
31	Macf1	19.4 \pm 2.7	6.1 \pm 1.3	-1.6	8.2	21.3	<0.0001
32	Mal	194.4 \pm 7.6	22.2 \pm 4.9	-3.0	8.2	70.7	<0.0001
33	Plekhb1	182.0 \pm 7.4	31.1 \pm 6.6	-2.5	8.2	48.6	<0.0001
34	Cartpt	627.1 \pm 202.1	57.4 \pm 21.0	-3.4	8.2	83.7	<0.0001
35	Gad2	76.6 \pm 3.3	19.6 \pm 2.5	-1.9	8.1	29.2	<0.0001
36	mt-Nd6	852.5 \pm 94.2	79.7 \pm 8.2	-3.3	7.9	82.2	<0.0001
37	Abca2	46.0 \pm 3.3	13.1 \pm 0.3	-1.7	7.9	24.5	<0.0001
38	Epb4.113	85.6 \pm 2.9	18.5 \pm 1.9	-2.1	7.9	36.6	<0.0001

Table 13. (Cont'd)

No.	Gene Symbol	Sham Input AVE \pm SEM	Sham IP AVE \pm SEM	LogFC	LogCPM	LR	P.adj
39	Mag	177.9 \pm 8.6	14.8 \pm 2.9	-3.5	7.8	89.7	<0.0001
40	Syne1	12.3 \pm 2.9	4.0 \pm 0.9	-1.5	7.8	19.9	<0.0001
41	Kcnj10	72.3 \pm 3.4	8.4 \pm 1.7	-3.0	7.7	69.8	<0.0001
42	Scd1	72.2 \pm 5.8	15.7 \pm 2.1	-2.1	7.7	36.4	<0.0001
43	Enpp2	98.5 \pm 4.1	24.1 \pm 1.2	-1.9	7.7	31.0	<0.0001
44	Syn2	82.5 \pm 2.9	23.4 \pm 1.3	-1.7	7.6	24.8	<0.0001
45	Gad1	101.8 \pm 10.3	12.2 \pm 3.0	-3.0	7.6	68.0	<0.0001
46	Nacc2	44.4 \pm 2.0	14.6 \pm 1.2	-1.5	7.6	19.3	0.0001
47	S100b	227.9 \pm 10.1	38.2 \pm 8.0	-2.5	7.6	49.6	<0.0001
48	Ptgds	262.9 \pm 22.2	31.1 \pm 4.4	-3.0	7.6	68.2	<0.0001
49	Apod	167.9 \pm 25.7	17.6 \pm 3.6	-3.2	7.6	75.3	<0.0001
50	Tspan2	64.0 \pm 2.5	20.9 \pm 2.2	-1.5	7.5	19.7	0.0001
51	Rasgrf1	79.7 \pm 6.6	10.6 \pm 0.7	-2.8	7.5	61.2	<0.0001
52	Cntn2	29.4 \pm 1.8	9.5 \pm 0.1	-1.5	7.5	19.9	<0.0001
53	Kcnc1	36.4 \pm 1.7	10.5 \pm 0.9	-1.7	7.5	24.2	<0.0001
54	Mt1	468.1 \pm 10.6	103.0 \pm 11.2	-2.1	7.5	35.9	<0.0001
55	Slc4a4	40.2 \pm 0.9	5.3 \pm 1.3	-2.8	7.5	62.2	<0.0001
56	Cldn11	176.3 \pm 7.3	18.0 \pm 2.4	-3.2	7.4	77.1	<0.0001
57	Gprc5b	60.7 \pm 2.2	15.9 \pm 1.0	-1.8	7.4	28.1	<0.0001
58	Sepp1	147.8 \pm 18.9	18.3 \pm 3.6	-2.9	7.4	66.1	<0.0001
59	Car2	168.6 \pm 6.6	24.2 \pm 3.9	-2.7	7.4	57.6	<0.0001
60	Syt2	41.9 \pm 3.7	7.3 \pm 1.5	-2.4	7.4	47.7	<0.0001
61	Slc17a6	56.1 \pm 3.8	14.5 \pm 1.1	-1.8	7.2	28.6	<0.0001
62	Paqr8	44.6 \pm 3.4	13.2 \pm 0.9	-1.7	7.2	23.1	<0.0001
63	Phldb1	46.8 \pm 3.2	6.5 \pm 1.1	-2.8	7.2	59.5	<0.0001
64	Olig1	122.7 \pm 5.3	13.2 \pm 2.9	-3.1	7.2	74.1	<0.0001
65	Kcna1	27.0 \pm 1.3	5.0 \pm 1.1	-2.3	7.1	44.1	<0.0001
66	Neat1	11.8 \pm 1.0	1.9 \pm 0.3	-2.6	7.1	52.8	<0.0001
67	Kcnc3	44.0 \pm 4.3	9.4 \pm 1.0	-2.1	7.1	37.3	<0.0001
68	Scn1a	26.3 \pm 0.8	6.5 \pm 0.7	-1.9	7.1	30.8	<0.0001
69	Acsl6	35.2 \pm 0.5	11.0 \pm 0.6	-1.6	7.0	21.3	<0.0001
70	Miat	26.4 \pm 7.3	3.6 \pm 0.4	-2.8	7.0	59.5	<0.0001
71	Gatm	94.2 \pm 2.0	14.6 \pm 2.8	-2.6	7.0	53.5	<0.0001
72	Ernm	61.4 \pm 4.3	7.8 \pm 1.8	-2.9	6.9	64.9	<0.0001
73	Gja1	72.1 \pm 3.5	8.4 \pm 1.6	-3.0	6.9	69.2	<0.0001
74	Psat1	75.4 \pm 1.9	18.4 \pm 1.5	-1.9	6.9	31.0	<0.0001
75	Pip4k2a	55.3 \pm 1.4	15.3 \pm 1.5	-1.8	6.9	26.0	<0.0001
76	Acsbg1	77.9 \pm 4.0	7.8 \pm 2.1	-3.2	6.9	78.2	<0.0001

Table 13. (Cont'd)

No.	Gene Symbol	Sham Input AVE ± SEM	Sham IP AVE ± SEM	LogFC	LogCPM	LR	P.adj
77	Clic4	51.3 ± 1.3	7.1 ± 1.6	-2.8	6.9	60.0	<0.0001
78	Kndc1	25.0 ± 1.6	7.0 ± 0.6	-1.7	6.8	25.4	<0.0001
79	Gfap	74.3 ± 2.2	14.5 ± 7.0	-2.3	6.8	42.2	<0.0001
80	Gstm1	159.0 ± 1.3	21.9 ± 2.5	-2.8	6.8	59.6	<0.0001
81	Ppap2b	64.9 ± 1.6	8.0 ± 1.8	-2.9	6.8	66.2	<0.0001
82	Tph2	73.5 ± 16.1	10.5 ± 2.4	-2.7	6.8	57.8	<0.0001
83	Sash1	24.4 ± 1.2	5.9 ± 0.7	-2.0	6.7	32.0	<0.0001
84	Aqp4	37.8 ± 3.2	4.9 ± 1.7	-2.9	6.7	64.0	<0.0001
85	Epas1	34.5 ± 1.0	6.5 ± 2.0	-2.3	6.7	43.9	<0.0001
86	Edil3	34.7 ± 2.7	5.6 ± 0.4	-2.5	6.7	51.2	<0.0001
87	Bcan	58.7 ± 1.3	6.2 ± 1.1	-3.1	6.7	74.6	<0.0001
88	Slc1a3	42.9 ± 2.0	4.6 ± 0.9	-3.1	6.7	74.6	<0.0001
89	Phlpp1	26.9 ± 1.0	6.5 ± 1.2	-2.0	6.7	31.8	<0.0001
90	Golgb1	14.5 ± 0.6	4.2 ± 0.5	-1.7	6.7	23.8	<0.0001
91	Kif1c	23.1 ± 0.5	6.6 ± 1.5	-1.7	6.6	25.1	<0.0001
92	Daam2	30.5 ± 2.5	2.6 ± 0.6	-3.5	6.6	88.6	<0.0001
93	ErbB2ip	23.3 ± 1.3	6.5 ± 1.0	-1.8	6.6	26.0	<0.0001
94	Gpr37l1	80.3 ± 0.8	7.2 ± 1.6	-3.4	6.6	84.8	<0.0001
95	Numa1	20.4 ± 0.8	6.7 ± 0.4	-1.5	6.6	19.3	0.0001
96	Mt2	298.1 ± 11.1	52.8 ± 7.7	-2.4	6.6	46.4	<0.0001
97	Myh14	22.2 ± 2.3	7.2 ± 0.7	-1.5	6.6	19.6	0.0001
98	Slc12a2	24.2 ± 0.9	5.3 ± 0.6	-2.1	6.6	36.0	<0.0001
99	Myo6	21.3 ± 0.5	3.0 ± 0.7	-2.7	6.6	58.0	<0.0001
100	Itpkb	25.9 ± 0.9	5.0 ± 1.1	-2.3	6.6	41.8	<0.0001

Appendix C.

Significant Morphine-regulated Genes in Whole VTA: Sham Input vs. Morphine Input

Table 14. Top 100 Significant Morphine Up-regulated Genes in VTA Input.

No.	Gene Symbol	Sham Input AVE \pm SEM	Sham IP AVE \pm SEM	LogFC	LogCPM	LR	P.adj
1	Epyc	0.4 \pm 0.1	1.5 \pm 0.1	1.7	1.2	26.8	<0.0001
2	Xirp2	0.0 \pm 0.0	0.1 \pm 0.0	1.6	0.0	19.7	0.0006
3	Hist1h3d	0.3 \pm 0.1	1.3 \pm 0.4	2.2	-0.1	33.5	<0.0001
4	Lrriq1	0.1 \pm 0.0	0.3 \pm 0.1	1.6	-0.1	18.5	0.0010
5	T2	0.2 \pm 0.1	0.7 \pm 0.3	1.6	-0.4	18.7	0.0009
6	Cysltr1	0.0 \pm 0.0	0.2 \pm 0.0	2.5	-0.5	38.0	<0.0001
7	Myh8	0.1 \pm 0.0	0.2 \pm 0.0	1.5	-0.5	16.3	0.0024
8	Insrr	0.1 \pm 0.0	0.2 \pm 0.1	1.6	-0.6	17.5	0.0015
9	Nms	0.3 \pm 0.0	0.9 \pm 0.1	1.6	-0.7	16.3	0.0025
10	Mx1	0.1 \pm 0.0	0.3 \pm 0.1	1.6	-0.7	16.2	0.0025
11	Gypc	0.1 \pm 0.1	0.5 \pm 0.2	2.1	-0.7	26.8	<0.0001
12	Rhod	0.2 \pm 0.1	0.6 \pm 0.0	1.8	-0.8	19.5	0.0007
13	Acmsd	0.1 \pm 0.0	0.3 \pm 0.0	1.7	-0.9	17.1	0.0017
14	Hmx2	0.1 \pm 0.1	0.4 \pm 0.2	1.6	-1.0	15.8	0.0029
15	Lrrc67	0.1 \pm 0.0	0.6 \pm 0.4	2.5	-1.0	32.9	<0.0001
16	Acsm3	0.1 \pm 0.0	0.2 \pm 0.1	1.7	-1.1	16.6	0.0022
17	Hsf3	0.0 \pm 0.0	0.3 \pm 0.1	2.7	-1.2	36.7	<0.0001
18	Arl11	0.1 \pm 0.0	0.4 \pm 0.1	1.6	-1.3	14.7	0.0046
19	Serpina 3c	0.1 \pm 0.1	0.3 \pm 0.0	2.0	-1.3	20.1	0.0005
20	Loxl4	0.0 \pm 0.0	0.2 \pm 0.0	1.9	-1.3	18.0	0.0012
21	Ccdc121	0.0 \pm 0.0	0.4 \pm 0.2	3.1	-1.4	40.5	<0.0001
22	Slc36a2	0.1 \pm 0.0	0.2 \pm 0.1	2.0	-1.4	20.1	0.0005
23	Nod2	0.0 \pm 0.0	0.1 \pm 0.1	2.3	-1.4	25.0	<0.0001
24	Samd3	0.1 \pm 0.0	0.2 \pm 0.1	1.7	-1.5	14.4	0.0053
25	Ugt1a6a	0.0 \pm 0.0	0.2 \pm 0.1	2.2	-1.5	22.3	0.0002
26	Asb5	0.1 \pm 0.0	0.4 \pm 0.2	2.4	-1.5	26.3	<0.0001
27	Zfp185	0.0 \pm 0.0	0.2 \pm 0.1	3.1	-1.5	38.6	<0.0001
28	Ripk3	0.1 \pm 0.0	0.2 \pm 0.1	1.9	-1.6	17.4	0.0016
29	Trem14	0.1 \pm 0.0	0.3 \pm 0.1	2.0	-1.6	18.7	0.0009
30	Gdnf	0.0 \pm 0.0	0.1 \pm 0.0	1.5	-1.6	11.0	0.0206
31	Cldn15	0.1 \pm 0.0	0.2 \pm 0.0	1.7	-1.7	13.1	0.0092
32	Bpil2	0.0 \pm 0.0	0.2 \pm 0.1	2.3	-1.7	22.5	0.0002
33	Tmem 174	0.0 \pm 0.0	0.2 \pm 0.1	2.2	-1.7	20.2	0.0005
34	Dmc1	0.0 \pm 0.0	0.2 \pm 0.1	2.5	-1.7	25.7	<0.0001
35	SNORA5	1.0 \pm 0.4	2.9 \pm 0.3	1.5	-1.7	10.6	0.0252
36	Cdca5	0.06 \pm 0.03	0.20 \pm 0.03	1.79	-1.76	14.06	0.0061

Table 14. (Cont'd)

No.	Gene Symbol	Sham Input AVE \pm SEM	Sham IP AVE \pm SEM	LogFC	LogCPM	LR	P.adj
37	Oas1a	0.1 \pm 0.0	0.2 \pm 0.1	1.7	-1.8	12.6	0.0110
38	Figf	0.0 \pm 0.0	0.2 \pm 0.1	2.8	-1.8	28.8	<0.0001
39	Adam7	0.0 \pm 0.0	0.1 \pm 0.0	1.7	-1.8	12.2	0.0128
40	Catsper4	0.1 \pm 0.0	0.2 \pm 0.1	2.1	-1.8	17.4	0.0016
41	Osgin1	0.1 \pm 0.0	0.2 \pm 0.0	1.6	-1.9	11.5	0.0179
42	Rsph6a	0.0 \pm 0.0	0.2 \pm 0.0	2.0	-1.9	15.5	0.0033
43	Myh2	0.0 \pm 0.0	0.1 \pm 0.0	3.5	-1.9	38.7	<0.0001
44	Mov10l1	0.0 \pm 0.0	0.1 \pm 0.1	3.3	-1.9	34.7	<0.0001
45	Kiss1	0.1 \pm 0.1	0.5 \pm 0.0	1.8	-1.9	12.7	0.0103
46	Fgfbp1	0.0 \pm 0.0	0.4 \pm 0.1	3.3	-1.9	34.1	<0.0001
47	SNORA 44	0.2 \pm 0.2	3.3 \pm 2.1	3.7	-2.0	38.2	<0.0001
48	Wfikkn1	0.0 \pm 0.0	0.2 \pm 0.1	2.7	-2.0	25.4	<0.0001
49	Prss16	0.0 \pm 0.0	0.2 \pm 0.1	2.9	-2.0	27.6	<0.0001
50	Cby3	0.1 \pm 0.0	0.5 \pm 0.1	2.1	-2.0	15.8	0.0029
51	Akr1c19	0.1 \pm 0.1	0.2 \pm 0.1	2.0	-2.1	15.2	0.0037
52	Amdhd1	0.0 \pm 0.0	0.2 \pm 0.0	3.9	-2.1	39.3	<0.0001
53	Oip5	0.0 \pm 0.0	0.2 \pm 0.1	2.0	-2.1	13.9	0.0064
54	Rdh16	0.0 \pm 0.0	0.1 \pm 0.0	4.6	-2.2	43.1	<0.0001
55	Tat	0.0 \pm 0.0	0.1 \pm 0.0	3.0	-2.2	26.1	<0.0001
56	Kcnj15	0.0 \pm 0.0	0.0 \pm 0.0	1.7	-2.3	9.6	0.0378
57	Myh4	0.0 \pm 0.0	0.1 \pm 0.0	4.0	-2.3	35.7	<0.0001
58	Tssk1	0.0 \pm 0.0	0.2 \pm 0.1	1.9	-2.3	12.4	0.0120
59	Armc4	0.0 \pm 0.0	0.1 \pm 0.0	2.9	-2.3	23.9	0.0001
60	Hist1h 2bp	0.1 \pm 0.0	0.5 \pm 0.3	2.4	-2.3	17.7	0.0014
61	Dfnb59	0.0 \pm 0.0	0.2 \pm 0.0	2.9	-2.4	22.2	0.0002
62	Vmn1r- ps32	0.0 \pm 0.0	0.3 \pm 0.2	2.6	-2.4	19.3	0.0008
63	Hist1h2al	0.2 \pm 0.1	0.7 \pm 0.3	2.1	-2.4	13.7	0.0071
64	Hal	0.0 \pm 0.0	0.1 \pm 0.0	2.8	-2.4	21.3	0.0003
65	Ascl4	0.1 \pm 0.1	0.2 \pm 0.0	1.8	-2.4	9.8	0.0349
66	Rpl27- ps3	0.1 \pm 0.0	0.6 \pm 0.2	2.8	-2.4	20.5	0.0005
67	Dyrk4	0.0 \pm 0.0	0.1 \pm 0.0	3.1	-2.4	23.5	0.0001
68	Tgm3	0.0 \pm 0.0	0.1 \pm 0.0	2.8	-2.4	20.5	0.0005
69	Cd200r1	0.0 \pm 0.0	0.1 \pm 0.0	2.3	-2.4	15.0	0.0042
70	Itih4	0.0 \pm 0.0	0.1 \pm 0.0	1.9	-2.4	10.7	0.0235

Table 14. (Cont'd)

No.	Gene Symbol	Sham Input AVE \pm SEM	Sham IP AVE \pm SEM	LogFC	LogCPM	LR	P.adj
71	Hist1h3i	0.1 \pm 0.1	0.6 \pm 0.3	3.0	-2.4	22.8	0.0002
72	Zfp819	0.0 \pm 0.0	0.1 \pm 0.1	4.3	-2.5	34.7	<0.0001
73	Wfdc3	0.0 \pm 0.0	0.2 \pm 0.1	2.7	-2.5	18.7	0.0009
74	Rpl35a- ps5	0.1 \pm 0.1	0.8 \pm 0.4	3.0	-2.5	21.7	0.0003
75	Ccl3	0.0 \pm 0.0	0.4 \pm 0.2	4.2	-2.5	33.0	<0.0001
76	Tas2r137	0.0 \pm 0.0	0.3 \pm 0.2	4.2	-2.5	32.7	<0.0001
77	Fosl1	0.0 \pm 0.0	0.1 \pm 0.1	2.9	-2.5	20.1	0.0005
78	Mettl4- ps1	0.0 \pm 0.0	0.2 \pm 0.1	6.5	-2.5	45.9	<0.0001
79	Olf1128	0.0 \pm 0.0	0.3 \pm 0.2	6.5	-2.5	45.9	<0.0001
80	Styx11	0.0 \pm 0.0	0.1 \pm 0.1	2.1	-2.5	12.1	0.0136
81	RP23- 38P5.9	0.3 \pm 0.1	1.1 \pm 0.4	1.9	-2.5	9.9	0.0333
82	Qrich2	0.0 \pm 0.0	0.1 \pm 0.0	1.8	-2.6	9.2	0.0447
83	Akr1cl	0.0 \pm 0.0	0.1 \pm 0.1	3.1	-2.6	21.5	0.0003
84	Akr1c12	0.0 \pm 0.0	0.2 \pm 0.1	2.8	-2.6	18.3	0.0011
85	Trim6	0.0 \pm 0.0	0.1 \pm 0.0	2.5	-2.6	15.1	0.0040
86	Cd300ld	0.0 \pm 0.0	0.1 \pm 0.1	2.7	-2.6	17.1	0.0017
87	Trim40	0.0 \pm 0.0	0.1 \pm 0.0	2.3	-2.7	12.7	0.0104
88	Ager	0.0 \pm 0.0	0.1 \pm 0.0	2.3	-2.7	12.8	0.0100
89	Klrb1f	0.0 \pm 0.0	0.1 \pm 0.1	2.0	-2.7	10.2	0.0300
90	Fam115e	0.0 \pm 0.0	0.1 \pm 0.0	2.2	-2.7	11.9	0.0145
91	Akap2	0.0 \pm 0.0	0.0 \pm 0.0	2.2	-2.8	11.0	0.0211
92	Lao1	0.0 \pm 0.0	0.1 \pm 0.0	6.2	-2.8	38.0	<0.0001
93	Fgg	0.0 \pm 0.0	0.1 \pm 0.0	2.5	-2.8	13.6	0.0073
94	Rpl36- ps3	0.1 \pm 0.0	0.5 \pm 0.2	2.5	-2.8	13.5	0.0076
95	Ptx3	0.0 \pm 0.0	0.1 \pm 0.0	2.0	-2.8	9.2	0.0443
96	Hmgb1- ps5	0.1 \pm 0.0	0.3 \pm 0.1	2.0	-2.8	9.2	0.0443
97	Il2rg	0.0 \pm 0.0	0.1 \pm 0.1	3.1	-2.8	18.1	0.0012
98	Apol9b	0.0 \pm 0.0	0.1 \pm 0.1	6.0	-2.9	34.4	<0.0001
99	RP24- 89N4.5	0.0 \pm 0.0	0.2 \pm 0.1	2.6	-2.9	12.8	0.0099
100	Slc22a22	0.0 \pm 0.0	0.1 \pm 0.0	6.0	-2.9	33.3	<0.0001

Table 15. Top 100 Significant Morphine Down-regulated Genes in VTA Input.

No.	Gene Symbol	Sham Input AVE \pm SEM	Sham IP AVE \pm SEM	LogFC	LogCPM	LR	P.adj
1	Cartpt	627.1 \pm 202.1	168.7 \pm 54.8	-1.9	8.6	31.5	<0.0001
2	Ucn	102.0 \pm 35.5	26.8 \pm 8.0	-1.9	5.1	32.1	<0.0001
3	Cela1	3.6 \pm 0.5	1.2 \pm 0.2	-1.6	1.5	20.4	0.0005
4	Pgam1-ps2	2.4 \pm 0.6	0.7 \pm 0.2	-1.8	0.4	22.5	0.0002
5	Capn11	0.6 \pm 0.0	0.2 \pm 0.0	-2.0	0.3	25.7	<0.0001
6	Bcl6b	0.4 \pm 0.1	0.1 \pm 0.0	-1.7	0.1	18.9	0.0009
7	Agbl2	0.3 \pm 0.1	0.1 \pm 0.0	-1.6	0.0	16.2	0.0026
8	Six5	0.4 \pm 0.1	0.1 \pm 0.0	-1.5	-0.1	15.0	0.0042
9	Nsl1	0.4 \pm 0.1	0.1 \pm 0.0	-2.0	-0.1	24.3	0.0001
10	H2-T10	0.3 \pm 0.0	0.1 \pm 0.1	-1.6	-0.2	15.6	0.0032
11	Il21r	0.5 \pm 0.0	0.1 \pm 0.0	-1.9	-0.2	21.7	0.0003
12	Ppp1r1c	0.3 \pm 0.0	0.1 \pm 0.1	-1.6	-0.3	15.3	0.0036
13	Klk8	0.7 \pm 0.2	0.2 \pm 0.0	-1.6	-0.4	14.8	0.0046
14	Siglece	0.5 \pm 0.2	0.2 \pm 0.1	-1.6	-0.5	15.4	0.0035
15	Arx	0.3 \pm 0.0	0.1 \pm 0.0	-2.0	-0.6	20.6	0.0005
16	Slc12a8	0.3 \pm 0.0	0.1 \pm 0.0	-1.8	-0.7	18.4	0.0011
17	Ncaph	0.3 \pm 0.1	0.1 \pm 0.0	-1.6	-0.7	15.0	0.0042
18	Ror1	0.1 \pm 0.0	0.0 \pm 0.0	-1.8	-0.7	18.6	0.0010
19	Kcnh4	0.2 \pm 0.0	0.0 \pm 0.0	-2.3	-0.7	27.0	<0.0001
20	Glyat	0.2 \pm 0.0	0.1 \pm 0.0	-1.5	-0.8	13.2	0.0086
21	Mki67	0.1 \pm 0.0	0.0 \pm 0.0	-3.5	-0.9	45.5	<0.0001
22	Trip13	0.3 \pm 0.1	0.1 \pm 0.0	-1.7	-0.9	14.6	0.0049
23	Gsx1	0.4 \pm 0.1	0.1 \pm 0.0	-2.1	-1.0	20.7	0.0004
24	Gabrd	0.3 \pm 0.0	0.1 \pm 0.0	-2.2	-1.0	22.9	0.0002
25	Pmel	0.3 \pm 0.1	0.1 \pm 0.0	-1.9	-1.0	18.2	0.0012
26	Dnahc11	0.0 \pm 0.0	0.0 \pm 0.0	-1.5	-1.0	12.4	0.0121
27	Gnat2	0.2 \pm 0.0	0.1 \pm 0.0	-2.0	-1.1	19.0	0.0009
28	Adamts19	0.1 \pm 0.0	0.0 \pm 0.0	-1.7	-1.2	13.7	0.0068
29	Gpr160	0.2 \pm 0.0	0.1 \pm 0.0	-1.8	-1.2	14.8	0.0046
30	Sim2	0.3 \pm 0.1	0.1 \pm 0.0	-1.9	-1.2	17.0	0.0018
31	Gabbr1	0.2 \pm 0.1	0.1 \pm 0.0	-2.1	-1.2	19.5	0.0007
32	Omp	0.2 \pm 0.1	0.1 \pm 0.0	-1.9	-1.3	15.4	0.0035
33	Ldha-ps2	0.6 \pm 0.1	0.0 \pm 0.0	-3.5	-1.3	37.7	<0.0001
34	Psma8	0.3 \pm 0.1	0.1 \pm 0.1	-1.6	-1.3	12.3	0.0127
35	Hrct1	0.4 \pm 0.1	0.1 \pm 0.0	-2.1	-1.3	19.3	0.0008
36	Rangrf	0.6 \pm 0.1	0.1 \pm 0.1	-2.2	-1.3	20.7	0.0004

Table 15. (Cont'd)

No.	Gene Symbol	Sham Input AVE \pm SEM	Sham IP AVE \pm SEM	LogFC	LogCPM	LR	P.adj
37	Tarm1	0.6 \pm 0.2	0.1 \pm 0.1	-2.1	-1.3	18.7	0.0009
38	Ccl12	0.9 \pm 0.3	0.2 \pm 0.2	-2.0	-1.3	16.5	0.0022
39	Wdr27	0.2 \pm 0.1	0.0 \pm 0.0	-2.3	-1.3	21.7	0.0003
40	Dsp	0.1 \pm 0.0	0.0 \pm 0.0	-3.4	-1.4	35.3	<0.0001
41	Capn9	0.2 \pm 0.1	0.0 \pm 0.0	-2.2	-1.4	19.0	0.0008
42	Col13a1	0.1 \pm 0.0	0.0 \pm 0.0	-1.5	-1.4	10.4	0.0278
43	H2-Aa	0.5 \pm 0.2	0.1 \pm 0.0	-2.8	-1.4	27.5	<0.0001
44	Krt83	0.3 \pm 0.1	0.0 \pm 0.0	-3.5	-1.5	34.6	<0.0001
45	Fam167b	0.5 \pm 0.1	0.2 \pm 0.2	-1.5	-1.5	10.0	0.0324
46	Tecrl	0.2 \pm 0.0	0.1 \pm 0.0	-1.5	-1.5	10.0	0.0322
47	Haoa	0.4 \pm 0.1	0.1 \pm 0.1	-2.1	-1.5	17.0	0.0018
48	SNORA 67	2.8 \pm 0.9	0.8 \pm 0.8	-1.8	-1.5	13.6	0.0074
49	RP23- 392I3.14	0.5 \pm 0.1	0.1 \pm 0.1	-2.1	-1.5	16.5	0.0022
50	B3gnt3	0.2 \pm 0.1	0.0 \pm 0.0	-3.4	-1.6	32.4	<0.0001
51	Plaur	0.3 \pm 0.1	0.1 \pm 0.1	-2.1	-1.6	16.8	0.0020
52	Ccr2	0.1 \pm 0.0	0.0 \pm 0.0	-2.4	-1.6	20.4	0.0005
53	Snora30	3.2 \pm 1.3	0.7 \pm 0.7	-2.2	-1.6	17.8	0.0014
54	Selp	0.1 \pm 0.0	0.0 \pm 0.0	-1.7	-1.6	11.2	0.0197
55	Abca13	0.0 \pm 0.0	0.0 \pm 0.0	-1.6	-1.6	10.0	0.0324
56	Ccdc146	0.1 \pm 0.1	0.0 \pm 0.0	-2.2	-1.7	17.1	0.0017
57	Hist2h2a a2	0.7 \pm 0.2	0.2 \pm 0.1	-1.8	-1.7	12.2	0.0130
58	Hsd3b3	0.2 \pm 0.1	0.1 \pm 0.1	-1.6	-1.7	10.3	0.0283
59	Nkx6-3	0.2 \pm 0.0	0.0 \pm 0.0	-1.8	-1.7	12.4	0.0121
60	Wdr16	0.2 \pm 0.0	0.0 \pm 0.0	-2.0	-1.7	14.0	0.0062
61	Nkx1-1	0.3 \pm 0.1	0.1 \pm 0.0	-2.5	-1.7	20.1	0.0005
62	Pkd111	0.1 \pm 0.0	0.0 \pm 0.0	-3.5	-1.7	31.4	<0.0001
63	Fbxl22	0.1 \pm 0.0	0.0 \pm 0.0	-1.7	-1.7	10.6	0.0251
64	Ii27ra	0.1 \pm 0.0	0.0 \pm 0.0	-2.1	-1.8	14.7	0.0048
65	Hrc	0.2 \pm 0.0	0.0 \pm 0.0	-2.6	-1.8	21.3	0.0003
66	Prr15l	0.1 \pm 0.0	0.0 \pm 0.0	-5.2	-1.8	42.6	<0.0001
67	C78197	0.6 \pm 0.3	0.0 \pm 0.0	-5.2	-1.8	42.6	<0.0001
68	RP23- 27D5.11	0.5 \pm 0.2	0.0 \pm 0.0	-4.3	-1.8	35.6	<0.0001
69	Apol6	0.1 \pm 0.1	0.0 \pm 0.0	-2.3	-1.8	16.7	0.0021
70	Mc5r	0.3 \pm 0.1	0.0 \pm 0.0	-3.3	-1.9	27.5	<0.0001

Table 15. (Cont'd)

No.	Gene Symbol	Sham Input AVE \pm SEM	Sham IP AVE \pm SEM	LogFC	LogCPM	LR	P.adj
71	Tmprss6	0.1 \pm 0.0	0.0 \pm 0.0	-4.2	-1.9	34.9	<0.0001
72	Galnt5	0.1 \pm 0.0	0.0 \pm 0.0	-7.0	-1.9	47.9	<0.0001
73	Clec7a	0.1 \pm 0.0	0.0 \pm 0.0	-2.1	-1.9	13.7	0.0069
74	Batf3	0.5 \pm 0.3	0.0 \pm 0.0	-6.9	-1.9	47.2	<0.0001
75	SNORA 71	2.7 \pm 0.8	0.3 \pm 0.3	-3.3	-1.9	26.0	<0.0001
76	Foxf1a	0.3 \pm 0.1	0.0 \pm 0.0	-3.2	-1.9	25.5	<0.0001
77	Ap3s1- ps2	0.2 \pm 0.1	0.1 \pm 0.0	-1.9	-2.0	12.0	0.0139
78	Pnlip	0.2 \pm 0.1	0.0 \pm 0.0	-2.3	-2.0	16.2	0.0026
79	Serinc2	0.2 \pm 0.1	0.0 \pm 0.0	-6.8	-2.0	44.9	<0.0001
80	Ect2l	0.1 \pm 0.0	0.0 \pm 0.0	-2.8	-2.0	20.4	0.0005
81	Kctd19	0.1 \pm 0.0	0.0 \pm 0.0	-4.8	-2.1	35.0	<0.0001
82	Hkdc1	0.1 \pm 0.0	0.0 \pm 0.0	-4.8	-2.1	34.7	<0.0001
83	Il1b	0.2 \pm 0.0	0.0 \pm 0.0	-6.7	-2.1	42.5	<0.0001
84	Clec4n	0.2 \pm 0.1	0.0 \pm 0.0	-6.7	-2.1	41.9	<0.0001
85	Amica1	0.1 \pm 0.0	0.0 \pm 0.0	-3.0	-2.1	20.2	0.0005
86	Aqp5	0.2 \pm 0.0	0.0 \pm 0.0	-3.3	-2.2	23.2	0.0002
87	Il20rb	0.1 \pm 0.0	0.0 \pm 0.0	-6.6	-2.2	40.1	<0.0001
88	Ush1c	0.1 \pm 0.0	0.0 \pm 0.0	-3.8	-2.2	25.3	<0.0001
89	Krt76	0.1 \pm 0.0	0.0 \pm 0.0	-2.2	-2.2	12.3	0.0124
90	P2rx1	0.1 \pm 0.0	0.0 \pm 0.0	-6.4	-2.3	36.2	<0.0001
91	Ltbp2	0.0 \pm 0.0	0.0 \pm 0.0	-6.4	-2.3	35.7	<0.0001
92	Srms	0.1 \pm 0.0	0.0 \pm 0.0	-6.4	-2.3	35.6	<0.0001
93	Ush2a	0.0 \pm 0.0	0.0 \pm 0.0	-2.3	-2.4	12.5	0.0112
94	Eif4ebp3	0.3 \pm 0.1	0.0 \pm 0.0	-3.0	-2.4	17.9	0.0013
95	Slc7a15	0.1 \pm 0.1	0.0 \pm 0.0	-3.6	-2.4	21.7	0.0003
96	Ankle1	0.1 \pm 0.0	0.0 \pm 0.0	-6.3	-2.4	34.1	<0.0001
97	Nlrp4f	0.1 \pm 0.0	0.0 \pm 0.0	-6.3	-2.4	33.5	<0.0001
98	Npffr2	0.1 \pm 0.1	0.0 \pm 0.0	-6.3	-2.4	33.5	<0.0001
99	Snord 35b	2.5 \pm 1.2	0.3 \pm 0.3	-3.0	-2.4	17.2	0.0016
100	MyI2	0.3 \pm 0.1	0.0 \pm 0.0	-4.4	-2.4	25.8	<0.0001

Appendix D.

Significant Morphine-regulated Genes in VTA DA neurons:

Sham IP vs. Morphine IP

Table 16. Top 100 Significant Morphine Up-regulated Genes in VTA DA Neurons.

No.	Gene Symbol	Sham Input AVE \pm SEM	Sham IP AVE \pm SEM	LogFC	LogCPM	LR	P.adj
1	Nms	0.8 \pm 0.2	5.2 \pm 0.8	2.7	1.6	34.9	<0.0001
2	Abca8a	0.2 \pm 0.0	0.5 \pm 0.2	1.6	0.8	13.2	0.0096
3	Sytl5	0.3 \pm 0.0	1.1 \pm 0.4	1.7	0.8	13.3	0.0094
4	Atp5l2	2.0 \pm 0.2	6.4 \pm 1.9	1.7	0.7	13.2	0.0096
5	Fam181b	0.4 \pm 0.1	1.1 \pm 0.4	1.6	0.5	13.0	0.0107
6	Gcg	0.4 \pm 0.1	1.9 \pm 0.4	2.4	0.4	25.1	<0.0001
7	Fmo5	0.1 \pm 0.0	0.3 \pm 0.1	1.8	0.2	14.4	0.0059
8	Ccdc89	0.1 \pm 0.1	0.8 \pm 0.3	2.5	0.1	27.4	<0.0001
9	Sult1a1	0.3 \pm 0.1	1.0 \pm 0.4	1.7	-0.1	12.7	0.0122
10	Tec	0.1 \pm 0.1	0.6 \pm 0.2	2.6	-0.2	27.3	<0.0001
11	Rab32	0.2 \pm 0.1	0.6 \pm 0.3	1.6	-0.2	11.8	0.0174
12	Ggt1	0.2 \pm 0.1	0.5 \pm 0.1	1.5	-0.2	10.4	0.0305
13	Pnma5	0.1 \pm 0.0	0.5 \pm 0.2	2.0	-0.3	16.5	0.0025
14	Adam32	0.1 \pm 0.1	0.4 \pm 0.2	1.9	-0.4	14.9	0.0049
15	SNORD91	3.1 \pm 1.1	10.9 \pm 2.3	1.8	-0.5	14.1	0.0066
16	Hba-a2	0.2 \pm 0.1	2.0 \pm 1.0	2.9	-0.6	30.8	<0.0001
17	Popdc3	0.1 \pm 0.1	0.5 \pm 0.2	1.8	-0.6	13.3	0.0094
18	Serpina1b	0.1 \pm 0.1	0.6 \pm 0.2	2.2	-0.7	19.2	0.0008
19	Zfp953	0.1 \pm 0.0	0.2 \pm 0.1	1.8	-0.7	12.7	0.0121
20	P2ry14	0.1 \pm 0.1	0.5 \pm 0.2	1.8	-0.8	12.2	0.0146
21	Dnahc3	0.0 \pm 0.0	0.1 \pm 0.0	1.7	-0.9	11.6	0.0185
22	Macc1	0.1 \pm 0.0	0.2 \pm 0.1	1.9	-0.9	13.7	0.0079
23	Mir744	1.5 \pm 0.8	8.1 \pm 2.7	2.3	-0.9	20.0	0.0006
24	Shcbp1	0.1 \pm 0.0	0.4 \pm 0.1	2.1	-0.9	16.6	0.0024
25	Anxa10	0.1 \pm 0.0	0.5 \pm 0.1	3.1	-0.9	31.0	<0.0001
26	Lrrc39	0.1 \pm 0.0	0.2 \pm 0.1	2.0	-1.0	15.1	0.0043
27	Cenpf	0.0 \pm 0.0	0.1 \pm 0.0	1.7	-1.0	11.2	0.0223
28	Fen1	0.1 \pm 0.0	0.3 \pm 0.1	1.9	-1.0	14.1	0.0066
29	Drd3	0.1 \pm 0.0	0.5 \pm 0.2	2.6	-1.0	22.6	0.0002
30	Prr22	0.1 \pm 0.0	0.4 \pm 0.2	2.2	-1.1	17.1	0.0020
31	Dcdc2b	0.1 \pm 0.1	0.7 \pm 0.1	2.3	-1.1	19.0	0.0009
32	Cxcr4	0.1 \pm 0.0	0.4 \pm 0.2	1.9	-1.1	13.2	0.0097
33	Epyc	0.0 \pm 0.0	0.3 \pm 0.2	3.0	-1.1	29.2	<0.0001
34	Ang	0.1 \pm 0.0	0.7 \pm 0.3	3.3	-1.2	31.9	<0.0001
35	Cbfa2t2-ps1	0.2 \pm 0.1	0.9 \pm 0.4	2.1	-1.2	16.1	0.0030

Table 16. (Cont'd)

No.	Gene Symbol	Sham Input AVE \pm SEM	Sham IP AVE \pm SEM	LogFC	LogCPM	LR	P.adj
36	Mei4	0.0 \pm 0.0	0.2 \pm 0.1	2.0	-1.2	13.9	0.0072
37	Htr1b	0.1 \pm 0.1	0.5 \pm 0.2	2.0	-1.2	14.3	0.0062
38	Epcam	0.1 \pm 0.0	0.3 \pm 0.1	2.5	-1.3	21.2	0.0004
39	Msh5	0.0 \pm 0.0	0.2 \pm 0.1	2.2	-1.3	16.3	0.0027
40	Larp1b	0.0 \pm 0.0	0.1 \pm 0.1	1.7	-1.3	10.8	0.0262
41	Nhedc1	0.1 \pm 0.0	0.3 \pm 0.1	2.1	-1.3	14.7	0.0052
42	Trim43a	0.0 \pm 0.0	0.3 \pm 0.0	2.8	-1.4	23.2	0.0002
43	Rasef	0.0 \pm 0.0	0.1 \pm 0.0	2.0	-1.4	14.3	0.0061
44	Exo1	0.0 \pm 0.0	0.1 \pm 0.0	2.1	-1.4	14.4	0.0059
45	Itgb7	0.0 \pm 0.0	0.2 \pm 0.1	2.1	-1.4	15.3	0.0040
46	Sh2d6	0.1 \pm 0.0	0.5 \pm 0.2	2.9	-1.4	25.2	<0.0001
47	Trim47	0.0 \pm 0.0	0.2 \pm 0.1	2.1	-1.5	14.3	0.0060
48	H2-T10	0.0 \pm 0.0	0.1 \pm 0.0	1.8	-1.5	11.1	0.0233
49	Tmem88	0.0 \pm 0.0	0.3 \pm 0.2	3.1	-1.5	26.3	<0.0001
50	Qrfpr	0.1 \pm 0.0	0.3 \pm 0.1	1.9	-1.5	12.5	0.0127
51	Fpr2	0.1 \pm 0.0	0.4 \pm 0.2	2.7	-1.6	21.2	0.0004
52	Cuzd1	0.0 \pm 0.0	0.2 \pm 0.1	2.0	-1.6	13.0	0.0107
53	Orc1	0.0 \pm 0.0	0.1 \pm 0.0	2.2	-1.7	14.6	0.0056
54	Zfp831	0.0 \pm 0.0	0.0 \pm 0.0	2.1	-1.8	12.9	0.0111
55	Fam132b	0.0 \pm 0.0	0.1 \pm 0.1	2.0	-1.8	12.3	0.0140
56	Mtag2	0.1 \pm 0.1	0.6 \pm 0.2	1.8	-1.8	9.9	0.0385
57	Tnni3k	0.0 \pm 0.0	0.1 \pm 0.0	1.8	-1.8	10.6	0.0278
58	Cbr2	0.1 \pm 0.0	0.3 \pm 0.1	2.1	-1.8	13.4	0.0089
59	Ascl2	0.0 \pm 0.0	0.3 \pm 0.2	5.6	-1.9	45.0	<0.0001
60	Rrh	0.0 \pm 0.0	0.2 \pm 0.1	2.8	-1.9	20.3	0.0005
61	Ect2	0.0 \pm 0.0	0.1 \pm 0.0	1.8	-1.9	9.3	0.0476
62	Ahrr	0.0 \pm 0.0	0.1 \pm 0.0	2.9	-1.9	21.3	0.0004
63	Slc22a12	0.0 \pm 0.0	0.2 \pm 0.1	2.2	-2.0	13.7	0.0080
64	Wee2	0.0 \pm 0.0	0.1 \pm 0.0	1.9	-2.0	10.3	0.0321
65	Zc3h12d	0.0 \pm 0.0	0.1 \pm 0.0	2.4	-2.1	15.1	0.0043
66	Tmco5	0.1 \pm 0.0	0.2 \pm 0.1	1.9	-2.1	10.2	0.0339
67	Col4a3	0.0 \pm 0.0	0.0 \pm 0.0	3.0	-2.1	20.6	0.0005
68	Col6a4	0.0 \pm 0.0	0.0 \pm 0.0	1.9	-2.1	10.0	0.0363
69	Accn3	0.0 \pm 0.0	0.2 \pm 0.1	4.5	-2.1	33.0	<0.0001
70	Colq	0.0 \pm 0.0	0.1 \pm 0.1	3.2	-2.2	21.9	0.0003
71	Mfsd7a	0.0 \pm 0.0	0.1 \pm 0.1	3.1	-2.2	20.8	0.0004
72	Krt19	0.0 \pm 0.0	0.2 \pm 0.1	2.0	-2.2	10.4	0.0300
73	Mir335	0.0 \pm 0.0	3.1 \pm 2.1	6.6	-2.3	42.1	<0.0001

Table 16. (Cont'd)

No.	Gene Symbol	Sham Input AVE ± SEM	Sham IP AVE ± SEM	LogFC	LogCPM	LR	P.adj
74	Naa11	0.0 ± 0.0	0.1 ± 0.0	3.0	-2.3	19.0	0.0009
75	Ildr1	0.0 ± 0.0	0.1 ± 0.0	2.3	-2.3	12.6	0.0122
76	Trpm8	0.0 ± 0.0	0.1 ± 0.0	6.5	-2.3	40.9	<0.0001
77	Pnpla1	0.0 ± 0.0	0.1 ± 0.0	3.7	-2.3	24.7	<0.0001
78	Slfn9	0.0 ± 0.0	0.1 ± 0.0	3.3	-2.4	20.8	0.0004
79	B4galnt2	0.0 ± 0.0	0.1 ± 0.0	2.1	-2.4	10.6	0.0282
80	Catsper3	0.0 ± 0.0	0.2 ± 0.1	2.8	-2.4	16.4	0.0025
81	Tnfaip8l3	0.0 ± 0.0	0.1 ± 0.1	3.2	-2.4	18.9	0.0010
82	Ptpn22	0.0 ± 0.0	0.1 ± 0.0	2.8	-2.4	16.0	0.0030
83	Anpep	0.0 ± 0.0	0.1 ± 0.0	2.0	-2.5	9.4	0.0458
84	Muc1	0.0 ± 0.0	0.1 ± 0.0	2.2	-2.5	11.0	0.0245
85	Otos	0.0 ± 0.0	0.1 ± 0.0	3.9	-2.5	23.5	0.0001
86	Stat4	0.0 ± 0.0	0.1 ± 0.0	3.3	-2.6	19.2	0.0008
87	Chrna10	0.0 ± 0.0	0.1 ± 0.1	6.2	-2.6	34.3	<0.0001
88	Marco	0.0 ± 0.0	0.1 ± 0.1	3.8	-2.6	22.3	0.0002
89	Vnn3	0.0 ± 0.0	0.1 ± 0.0	3.3	-2.6	18.5	0.0011
90	Rdh1	0.0 ± 0.0	0.1 ± 0.0	3.3	-2.6	18.4	0.0011
91	Qrich2	0.0 ± 0.0	0.1 ± 0.1	3.3	-2.6	18.1	0.0013
92	Gstm2	0.0 ± 0.0	0.2 ± 0.1	4.5	-2.6	25.3	<0.0001
93	Tgif1	0.0 ± 0.0	0.1 ± 0.1	3.2	-2.7	16.8	0.0022
94	Gckr	0.0 ± 0.0	0.1 ± 0.0	6.0	-2.7	31.9	<0.0001
95	Dnm3os	0.0 ± 0.0	0.0 ± 0.0	6.0	-2.7	31.9	<0.0001
96	Amac1	0.0 ± 0.0	0.1 ± 0.1	5.9	-2.7	30.2	<0.0001
97	Gabbr1	0.0 ± 0.0	0.1 ± 0.0	2.9	-2.8	13.7	0.0080
98	Mybpc1	0.0 ± 0.0	0.0 ± 0.0	5.7	-2.9	27.2	<0.0001
99	Psma8	0.0 ± 0.0	0.1 ± 0.1	5.7	-2.9	27.2	<0.0001
100	Cyp2c70	0.0 ± 0.0	0.1 ± 0.1	5.7	-2.9	26.9	<0.0001

Table 17. Top 100 Significant Morphine Down-regulated Genes in VTA DA Neurons.

No.	Gene Symbol	Sham Input AVE ± SEM	Sham IP AVE ± SEM	LogFC	LogCPM	LR	P.adj
1	Myh11	0.6 ± 0.2	0.2 ± 0.2	-1.6	1.4	13.0	0.0107
2	Heyl	0.8 ± 0.2	0.3 ± 0.3	-1.6	1.3	12.1	0.0151
3	Acta2	1.6 ± 0.4	0.3 ± 0.2	-2.6	0.7	29.3	<0.0001
4	Lrrn4cl	0.8 ± 0.1	0.3 ± 0.2	-1.5	0.6	11.0	0.0246
5	Kcne1l	1.5 ± 0.6	0.3 ± 0.2	-2.4	0.5	25.6	<0.0001
6	Ly86	1.8 ± 0.8	0.6 ± 0.5	-1.5	0.3	10.7	0.0273
7	Sh3bgr	1.3 ± 0.5	0.4 ± 0.2	-1.7	0.2	13.1	0.0099
8	Arap3	0.3 ± 0.2	0.1 ± 0.0	-2.6	0.1	27.1	<0.0001
9	Smoc2	0.5 ± 0.1	0.2 ± 0.1	-1.5	0.1	11.0	0.0246
10	Kif24	0.3 ± 0.1	0.1 ± 0.0	-1.9	0.0	15.6	0.0037
11	Stard8	0.3 ± 0.1	0.1 ± 0.1	-1.7	-0.1	12.2	0.0145
12	Sod3	0.4 ± 0.1	0.1 ± 0.0	-1.9	-0.1	15.1	0.0045
13	Cdkn2c	0.6 ± 0.3	0.1 ± 0.1	-2.0	-0.1	17.7	0.0015
14	Slc6a13	0.6 ± 0.1	0.1 ± 0.1	-1.9	-0.2	15.9	0.0033
15	Lama1	0.1 ± 0.1	0.0 ± 0.0	-2.1	-0.2	18.5	0.0011
16	Foxf2	0.5 ± 0.1	0.2 ± 0.1	-1.6	-0.3	11.2	0.0217
17	Lcn2	1.0 ± 0.5	0.1 ± 0.1	-2.8	-0.3	29.6	<0.0001
18	Erg	0.3 ± 0.1	0.1 ± 0.1	-1.9	-0.4	14.7	0.0052
19	Chrn4	0.4 ± 0.1	0.0 ± 0.0	-2.9	-0.4	30.8	<0.0001
20	Plb1	0.2 ± 0.1	0.1 ± 0.0	-1.9	-0.4	14.4	0.0060
21	Tal2	0.5 ± 0.1	0.0 ± 0.0	-4.5	-0.4	55.4	<0.0001
22	Hist1h4d	2.5 ± 0.6	0.9 ± 0.9	-1.5	-0.5	9.8	0.0390
23	Nxn12	1.0 ± 0.4	0.1 ± 0.1	-2.7	-0.5	26.6	<0.0001
24	Tmem204	0.6 ± 0.3	0.1 ± 0.1	-2.5	-0.5	24.2	0.0001
25	Tnfaip2	0.3 ± 0.0	0.1 ± 0.1	-2.0	-0.6	15.7	0.0035
26	Fam19a4	0.5 ± 0.2	0.1 ± 0.1	-2.7	-0.6	27.2	<0.0001
27	Adap2	0.5 ± 0.2	0.1 ± 0.1	-1.7	-0.6	11.9	0.0163
28	Dppa5a	1.5 ± 0.2	0.4 ± 0.9	-1.7	-0.6	12.3	0.0143
29	Hmha1	0.2 ± 0.1	0.1 ± 0.0	-1.7	-0.7	12.2	0.0146
30	Ush1g	0.3 ± 0.1	0.1 ± 0.1	-1.8	-0.7	12.6	0.0123
31	Dnmt3b	0.2 ± 0.1	0.1 ± 0.0	-1.5	-0.8	9.4	0.0458
32	Mir137	8.4 ± 3.0	1.8 ± 3.1	-2.1	-0.8	17.0	0.0021
33	Mmp23	0.6 ± 0.2	0.2 ± 0.2	-1.7	-0.8	11.1	0.0234
34	Sdcbp2	0.6 ± 0.1	0.2 ± 0.2	-1.7	-0.8	12.0	0.0159
35	Thsd1	0.2 ± 0.0	0.0 ± 0.0	-2.0	-0.8	15.4	0.0038
36	Tnfrsf10b	0.2 ± 0.1	0.1 ± 0.1	-1.6	-0.9	10.0	0.0376
37	Ttll8	0.3 ± 0.1	0.1 ± 0.1	-1.6	-0.9	10.4	0.0307

Table 17. (Cont'd)

No.	Gene Symbol	Sham Input AVE \pm SEM	Sham IP AVE \pm SEM	LogFC	LogCPM	LR	P.adj
38	Ly96	1.2 \pm 0.3	0.4 \pm 0.6	-1.6	-0.9	9.8	0.0393
39	Ogn	0.3 \pm 0.1	0.1 \pm 0.1	-1.8	-0.9	12.7	0.0121
40	Rorc	0.3 \pm 0.1	0.1 \pm 0.1	-1.8	-0.9	12.3	0.0142
41	Hyal1	0.2 \pm 0.1	0.1 \pm 0.1	-2.0	-1.0	14.5	0.0057
42	Eya4	0.2 \pm 0.1	0.0 \pm 0.0	-2.1	-1.0	16.3	0.0027
43	Grap	0.4 \pm 0.1	0.1 \pm 0.2	-1.8	-1.0	12.4	0.0131
44	Il28ra	0.2 \pm 0.0	0.0 \pm 0.0	-1.9	-1.0	13.7	0.0082
45	Tuba1c	0.4 \pm 0.1	0.1 \pm 0.0	-2.1	-1.0	15.4	0.0039
46	Pik3cg	0.1 \pm 0.0	0.0 \pm 0.0	-1.9	-1.0	13.2	0.0097
47	Slc22a8	0.2 \pm 0.1	0.1 \pm 0.0	-1.7	-1.0	10.4	0.0304
48	Cybrd1	0.1 \pm 0.0	0.0 \pm 0.0	-2.4	-1.1	20.3	0.0005
49	Papln	0.2 \pm 0.1	0.0 \pm 0.0	-1.9	-1.1	12.8	0.0118
50	Filip1l	0.2 \pm 0.0	0.0 \pm 0.0	-2.2	-1.1	16.9	0.0022
51	Vmn2r- ps19	1.2 \pm 0.4	0.2 \pm 0.3	-2.8	-1.1	25.0	<0.0001
52	mmu-mir- 2134-2	11.2 \pm 3.3	2.2 \pm 2.0	-2.3	-1.1	17.8	0.0015
53	Mfng	0.3 \pm 0.2	0.1 \pm 0.1	-1.9	-1.1	13.1	0.0100
54	RP23- 27D5.11	0.7 \pm 0.1	0.2 \pm 0.2	-1.7	-1.2	10.4	0.0304
55	Tmem 190	1.1 \pm 0.2	0.2 \pm 0.3	-2.3	-1.2	18.3	0.0012
56	S1pr2	0.2 \pm 0.0	0.0 \pm 0.0	-2.6	-1.2	21.5	0.0003
57	Lgals3	0.4 \pm 0.1	0.1 \pm 0.1	-1.8	-1.2	12.1	0.0151
58	Nupr1	0.3 \pm 0.0	0.0 \pm 0.0	-4.8	-1.3	47.0	<0.0001
59	Pate2	0.3 \pm 0.1	0.1 \pm 0.1	-2.1	-1.3	14.7	0.0053
60	Hdc	0.1 \pm 0.1	0.0 \pm 0.0	-3.1	-1.3	27.4	<0.0001
61	Hsf2bp	0.2 \pm 0.0	0.0 \pm 0.0	-2.1	-1.3	15.4	0.0038
62	Smagp	0.6 \pm 0.3	0.0 \pm 0.0	-6.1	-1.3	55.4	<0.0001
63	Pth2r	0.2 \pm 0.1	0.1 \pm 0.1	-1.7	-1.3	10.1	0.0359
64	Il12rb1	0.2 \pm 0.1	0.0 \pm 0.1	-2.0	-1.3	14.2	0.0064
65	Hs3st6	0.4 \pm 0.1	0.1 \pm 0.1	-2.7	-1.3	22.0	0.0003
66	Mcm10	0.1 \pm 0.1	0.0 \pm 0.0	-7.7	-1.3	62.5	<0.0001
67	Plscr2	0.4 \pm 0.2	0.0 \pm 0.0	-5.2	-1.3	48.9	<0.0001
68	Ninj2	0.6 \pm 0.2	0.2 \pm 0.2	-1.7	-1.3	10.6	0.0283
69	Ak3l2-ps	0.8 \pm 0.2	0.2 \pm 0.1	-1.9	-1.4	12.9	0.0110
70	Rin3	0.1 \pm 0.1	0.0 \pm 0.0	-1.9	-1.4	12.4	0.0133
71	Ptgr1	0.2 \pm 0.1	0.1 \pm 0.1	-1.8	-1.4	11.5	0.0195

Table 17. (Cont'd)

No.	Gene Symbol	Sham Input AVE \pm SEM	Sham IP AVE \pm SEM	LogFC	LogCPM	LR	P.adj
72	Emx2os	0.1 \pm 0.0	0.0 \pm 0.0	-2.1	-1.4	14.5	0.0058
73	Fscn2	0.3 \pm 0.1	0.1 \pm 0.1	-1.7	-1.4	10.3	0.0317
74	Wfikkn2	0.2 \pm 0.1	0.0 \pm 0.0	-2.3	-1.4	17.0	0.0021
75	Cryba2	0.7 \pm 0.2	0.2 \pm 0.2	-1.7	-1.4	9.5	0.0438
76	Lrg1	0.4 \pm 0.2	0.1 \pm 0.1	-1.9	-1.4	12.2	0.0148
77	Tspan11	0.1 \pm 0.0	0.0 \pm 0.0	-2.1	-1.4	14.3	0.0061
78	Ccl17	1.0 \pm 0.2	0.2 \pm 0.3	-2.1	-1.4	14.0	0.0069
79	Gbgt1	0.4 \pm 0.2	0.1 \pm 0.1	-1.9	-1.5	11.8	0.0170
80	Hist2h3b	1.0 \pm 0.2	0.2 \pm 0.3	-2.0	-1.5	12.8	0.0115
81	Amdhd1	0.2 \pm 0.1	0.0 \pm 0.0	-2.4	-1.5	17.2	0.0019
82	Ptpn18	0.3 \pm 0.1	0.1 \pm 0.1	-2.2	-1.5	15.0	0.0047
83	Six5	0.2 \pm 0.1	0.0 \pm 0.0	-2.1	-1.6	13.6	0.0084
84	Atoh7	0.9 \pm 0.3	0.3 \pm 0.2	-1.7	-1.6	9.8	0.0393
85	Aim1	0.1 \pm 0.0	0.0 \pm 0.0	-2.1	-1.6	13.9	0.0075
86	Crhr2	0.2 \pm 0.0	0.0 \pm 0.0	-3.5	-1.6	29.1	<0.0001
87	Rdh9	0.2 \pm 0.1	0.0 \pm 0.0	-2.3	-1.6	15.5	0.0038
88	Glb1l2	0.1 \pm 0.0	0.0 \pm 0.0	-1.7	-1.6	9.5	0.0446
89	Cdhr2	0.1 \pm 0.1	0.0 \pm 0.0	-3.4	-1.6	27.9	<0.0001
90	Rapsn	0.3 \pm 0.1	0.0 \pm 0.1	-2.5	-1.6	17.7	0.0015
91	Neurod2	0.1 \pm 0.1	0.0 \pm 0.0	-2.1	-1.6	13.1	0.0099
92	Ptprq	0.1 \pm 0.0	0.0 \pm 0.0	-3.2	-1.6	25.2	<0.0001
93	Unc45b	0.1 \pm 0.0	0.0 \pm 0.0	-1.8	-1.7	9.8	0.0398
94	Mesp2	0.3 \pm 0.0	0.0 \pm 0.0	-4.0	-1.7	33.1	<0.0001
95	Cpxm2	0.1 \pm 0.1	0.0 \pm 0.0	-3.4	-1.7	26.9	<0.0001
96	Clec12a	0.1 \pm 0.1	0.0 \pm 0.0	-2.4	-1.7	16.2	0.0029
97	S100a8	1.1 \pm 0.4	0.2 \pm 0.2	-2.8	-1.7	20.9	0.0004
98	Cr2	0.1 \pm 0.0	0.0 \pm 0.0	-2.0	-1.7	11.7	0.0175
99	Rpl39l	0.6 \pm 0.3	0.1 \pm 0.1	-2.9	-1.7	21.1	0.0004
100	Tgm7	0.2 \pm 0.1	0.0 \pm 0.1	-1.8	-1.7	10.3	0.0321

REFERENCES

REFERENCES

- Alhadeff, A. L., Rupprecht, L. E., & Hayes, M. R. (2012). GLP-1 neurons in the nucleus of the solitary tract project directly to the ventral tegmental area and nucleus accumbens to control for food intake. *Endocrinology*, *153*(2), 647-658. doi:10.1210/en.2011-1443
- Behnke, J., Cheedalla, A., Bhatt, V., Bhat, M., Teng, S., Palmieri, A., . . . Alder, J. (2017). Neuropeptide VGF Promotes Maturation of Hippocampal Dendrites That Is Reduced by Single Nucleotide Polymorphisms. *Int J Mol Sci*, *18*(3). doi:10.3390/ijms18030612
- Bozdagi, O., Rich, E., Tronel, S., Sadahiro, M., Patterson, K., Shapiro, M. L., . . . Salton, S. R. (2008). The neurotrophin-inducible gene *Vgf* regulates hippocampal function and behavior through a brain-derived neurotrophic factor-dependent mechanism. *J Neurosci*, *28*(39), 9857-9869. doi:10.1523/JNEUROSCI.3145-08.2008
- Calipari, E. S., Juarez, B., Morel, C., Walker, D. M., Cahill, M. E., Ribeiro, E., . . . Nestler, E. J. (2017). Dopaminergic dynamics underlying sex-specific cocaine reward. *Nat Commun*, *8*, 13877. doi:10.1038/ncomms13877
- CDC. (2017). *Guideline for Prescribing Opioids for Chronic Pain*. Atlanta, GA Retrieved from <https://www.cdc.gov/drugoverdose/prescribing/guideline.html>.
- Center for Disease Control and Prevention (CDC). (2017, August 30, 2017). Understanding the Epidemic. Retrieved from <https://www.cdc.gov/drugoverdose/epidemic/>
- Chen, Y. C., Pristera, A., Ayub, M., Swanwick, R. S., Karu, K., Hamada, Y., . . . Okuse, K. (2013). Identification of a receptor for neuropeptide VGF and its role in neuropathic pain. *J Biol Chem*, *288*(48), 34638-34646. doi:10.1074/jbc.M113.510917
- Chung, A. S., Miller, S. M., Sun, Y., Xu, X., & Zweifel, L. S. (2017). Sexual congruency in the connectome and translome of VTA dopamine neurons. *Sci Rep*, *7*(1), 11120. doi:10.1038/s41598-017-11478-5
- Church, D. M., Goodstadt, L., Hillier, L. W., Zody, M. C., Goldstein, S., She, X., . . . Mouse Genome Sequencing, C. (2009). Lineage-specific biology revealed by a finished genome assembly of the mouse. *PLoS Biol*, *7*(5), e1000112. doi:10.1371/journal.pbio.1000112

- Cooper, S. E., Kechner, M., Caraballo-Perez, D., Kaska, S., Robison, A. J., & Mazei-Robison, M. S. (2017). Comparison of chronic physical and emotional social defeat stress effects on mesocorticolimbic circuit activation and voluntary consumption of morphine. *Sci Rep*, 7(1), 8445. doi:10.1038/s41598-017-09106-3
- Cork, S. C., Richards, J. E., Holt, M. K., Gribble, F. M., Reimann, F., & Trapp, S. (2015). Distribution and characterisation of Glucagon-like peptide-1 receptor expressing cells in the mouse brain. *Mol Metab*, 4(10), 718-731. doi:10.1016/j.molmet.2015.07.008
- Dickson, S. L., Shirazi, R. H., Hansson, C., Bergquist, F., Nissbrandt, H., & Skibicka, K. P. (2012). The glucagon-like peptide 1 (GLP-1) analogue, exendin-4, decreases the rewarding value of food: a new role for mesolimbic GLP-1 receptors. *J Neurosci*, 32(14), 4812-4820. doi:10.1523/JNEUROSCI.6326-11.2012
- Ekstrand, M. I., Nectow, A. R., Knight, Z. A., Latcha, K. N., Pomeranz, L. E., & Friedman, J. M. (2014). Molecular profiling of neurons based on connectivity. *Cell*, 157(5), 1230-1242. doi:10.1016/j.cell.2014.03.059
- Fairbanks, C. A., Peterson, C. D., Speltz, R. H., Riedl, M. S., Kitto, K. F., Dykstra, J. A., . . . Vulchanova, L. (2014). The VGF-derived peptide TLQP-21 contributes to inflammatory and nerve injury-induced hypersensitivity. *Pain*, 155(7), 1229-1237. doi:10.1016/j.pain.2014.03.012
- Fischer, S. J., Arguello, A. A., Charlton, J. J., Fuller, D. C., Zachariou, V., & Eisch, A. J. (2008). Morphine blood levels, dependence, and regulation of hippocampal subgranular zone proliferation rely on administration paradigm. *Neuroscience*, 151(4), 1217-1224. doi:10.1016/j.neuroscience.2007.11.035
- Gysling, K., & Wang, R. Y. (1983). Morphine-induced activation of A10 dopamine neurons in the rat. *Brain Res*, 277(1), 119-127.
- Heiman, M., Kulicke, R., Fenster, R. J., Greengard, P., & Heintz, N. (2014). Cell type-specific mRNA purification by translating ribosome affinity purification (TRAP). *Nat Protoc*, 9(6), 1282-1291. doi:10.1038/nprot.2014.085
- Heller, E. A., Kaska, S., Fallon, B., Ferguson, D., Kennedy, P. J., Neve, R. L., . . . Mazei-Robison, M. S. (2015). Morphine and cocaine increase serum- and glucocorticoid-inducible kinase 1 activity in the ventral tegmental area. *J Neurochem*, 132(2), 243-253. doi:10.1111/jnc.12925
- Hunsberger, J. G., Newton, S. S., Bennett, A. H., Duman, C. H., Russell, D. S., Salton, S. R., & Duman, R. S. (2007). Antidepressant actions of the exercise-regulated gene VGF. *Nat Med*, 13(12), 1476-1482. doi:10.1038/nm1669

- Ida, T., Mori, K., Miyazato, M., Egi, Y., Abe, S., Nakahara, K., . . . Murakami, N. (2005). Neuromedin s is a novel anorexigenic hormone. *Endocrinology*, *146*(10), 4217-4223. doi:10.1210/en.2005-0107
- Jiang, C., Lin, W. J., Sadahiro, M., Labonte, B., Menard, C., Pfau, M. L., . . . Salton, S. R. (2017). VGF function in depression and antidepressant efficacy. *Mol Psychiatry*. doi:10.1038/mp.2017.233
- Kanai, Y., Dohmae, N., & Hirokawa, N. (2004). Kinesin transports RNA: isolation and characterization of an RNA-transporting granule. *Neuron*, *43*(4), 513-525. doi:10.1016/j.neuron.2004.07.022
- Kim, J. I., Ganesan, S., Luo, S. X., Wu, Y. W., Park, E., Huang, E. J., . . . Ding, J. B. (2015). Aldehyde dehydrogenase 1a1 mediates a GABA synthesis pathway in midbrain dopaminergic neurons. *Science*, *350*(6256), 102-106. doi:10.1126/science.aac4690
- Koo, J. W., Mazei-Robison, M. S., Chaudhury, D., Juarez, B., LaPlant, Q., Ferguson, D., . . . Nestler, E. J. (2012). BDNF is a negative modulator of morphine action. *Science*, *338*(6103), 124-128. doi:10.1126/science.1222265
- Koo, J. W., Mazei-Robison, M. S., LaPlant, Q., Egervari, G., Braunscheidel, K. M., Adank, D. N., . . . Nestler, E. J. (2015). Epigenetic basis of opiate suppression of Bdnf gene expression in the ventral tegmental area. *Nat Neurosci*, *18*(3), 415-422. doi:10.1038/nn.3932
- Lammel, S., Steinberg, E. E., Foldy, C., Wall, N. R., Beier, K., Luo, L., & Malenka, R. C. (2015). Diversity of transgenic mouse models for selective targeting of midbrain dopamine neurons. *Neuron*, *85*(2), 429-438. doi:10.1016/j.neuron.2014.12.036
- Lee, I. T., Chang, A. S., Manandhar, M., Shan, Y., Fan, J., Izumo, M., . . . Yanagisawa, M. (2015). Neuromedin s-producing neurons act as essential pacemakers in the suprachiasmatic nucleus to couple clock neurons and dictate circadian rhythms. *Neuron*, *85*(5), 1086-1102. doi:10.1016/j.neuron.2015.02.006
- Levine, A. S., Morley, J. E., Gosnell, B. A., Billington, C. J., & Bartness, T. J. (1985). Opioids and consummatory behavior. *Brain Res Bull*, *14*(6), 663-672.
- Li, S. X., Liu, L. J., Jiang, W. G., Sun, L. L., Zhou, S. J., Le Foll, B., . . . Lu, L. (2010). Circadian alteration in neurobiology during protracted opiate withdrawal in rats. *J Neurochem*, *115*(2), 353-362. doi:10.1111/j.1471-4159.2010.06941.x
- Lin, P., Wang, C., Xu, B., Gao, S., Guo, J., Zhao, X., . . . Zhou, W. (2014). The VGF-derived peptide TLQP62 produces antidepressant-like effects in mice via the BDNF/TrkB/CREB signaling pathway. *Pharmacol Biochem Behav*, *120*, 140-148. doi:10.1016/j.pbb.2014.03.003

- Lin, W. J., Jiang, C., Sadahiro, M., Bozdagi, O., Vulchanova, L., Alberini, C. M., & Salton, S. R. (2015). VGF and Its C-Terminal Peptide TLQP-62 Regulate Memory Formation in Hippocampus via a BDNF-TrkB-Dependent Mechanism. *J Neurosci*, *35*(28), 10343-10356. doi:10.1523/JNEUROSCI.0584-15.2015
- Malberg, J. E., & Monteggia, L. M. (2008). VGF, a new player in antidepressant action? *Sci Signal*, *1*(18), pe19. doi:10.1126/stke.118pe19
- Margolis, E. B., Lock, H., Hjelmstad, G. O., & Fields, H. L. (2006). The ventral tegmental area revisited: is there an electrophysiological marker for dopaminergic neurons? *J Physiol*, *577*(Pt 3), 907-924. doi:jphysiol.2006.117069 [pii]
10.1113/jphysiol.2006.117069
- Margolis, E. B., Toy, B., Himmels, P., Morales, M., & Fields, H. L. (2012). Identification of rat ventral tegmental area GABAergic neurons. *PLoS One*, *7*(7), e42365. doi:10.1371/journal.pone.0042365
- Mazei-Robison, M. S., Appasani, R., Edwards, S., Wee, S., Taylor, S. R., Picciotto, M. R., . . . Nestler, E. J. (2014). Self-administration of ethanol, cocaine, or nicotine does not decrease the soma size of ventral tegmental area dopamine neurons. *PLoS One*, *9*(4), e95962. doi:10.1371/journal.pone.0095962
PONE-D-14-06041 [pii]
- Mazei-Robison, M. S., Koo, J. W., Friedman, A. K., Lansink, C. S., Robison, A. J., Vinish, M., . . . Nestler, E. J. (2011). Role for mTOR signaling and neuronal activity in morphine-induced adaptations in ventral tegmental area dopamine neurons. *Neuron*, *72*(6), 977-990. doi:10.1016/j.neuron.2011.10.012
- McClung, C. A., Nestler, E. J., & Zachariou, V. (2005). Regulation of gene expression by chronic morphine and morphine withdrawal in the locus ceruleus and ventral tegmental area. *J Neurosci*, *25*(25), 6005-6015. doi:10.1523/JNEUROSCI.0062-05.2005
- Morales, M., & Root, D. H. (2014). Glutamate neurons within the midbrain dopamine regions. *Neuroscience*, *282*, 60-68. doi:10.1016/j.neuroscience.2014.05.032
- Mori, K., Miyazato, M., Ida, T., Murakami, N., Serino, R., Ueta, Y., . . . Kangawa, K. (2005). Identification of neuromedin S and its possible role in the mammalian circadian oscillator system. *EMBO J*, *24*(2), 325-335. doi:10.1038/sj.emboj.7600526
- Nair-Roberts, R. G., Chatelain-Badie, S. D., Benson, E., White-Cooper, H., Bolam, J. P., & Ungless, M. A. (2008). Stereological estimates of dopaminergic, GABAergic and glutamatergic neurons in the ventral tegmental area, substantia nigra and

- retrotrubral field in the rat. *Neuroscience*, 152(4), 1024-1031.
doi:10.1016/j.neuroscience.2008.01.046
- Pacesova, D., Novotny, J., & Bendova, Z. (2016). The effect of chronic morphine or methadone exposure and withdrawal on clock gene expression in the rat suprachiasmatic nucleus and AA-NAT activity in the pineal gland. *Physiol Res*, 65(3), 517-525.
- Panman, L., Papanthou, M., Laguna, A., Oosterveen, T., Volakakis, N., Acampora, D., . . . Perlmann, T. (2014). Sox6 and Otx2 control the specification of substantia nigra and ventral tegmental area dopamine neurons. *Cell Rep*, 8(4), 1018-1025.
doi:10.1016/j.celrep.2014.07.016
- Poulin, J. F., Zou, J., Drouin-Ouellet, J., Kim, K. Y., Cicchetti, F., & Awatramani, R. B. (2014). Defining midbrain dopaminergic neuron diversity by single-cell gene expression profiling. *Cell Rep*, 9(3), 930-943. doi:10.1016/j.celrep.2014.10.008
- Ren, X., Lutfy, K., Mangubat, M., Ferrini, M. G., Lee, M. L., Liu, Y., & Friedman, T. C. (2013). Alterations in phosphorylated CREB expression in different brain regions following short- and long-term morphine exposure: relationship to food intake. *J Obes*, 2013, 764742. doi:10.1155/2013/764742
- Richter, J. D., & Collier, J. (2015). Pausing on Polyribosomes: Make Way for Elongation in Translational Control. *Cell*, 163(2), 292-300. doi:10.1016/j.cell.2015.09.041
- Russo, S. J., Bolanos, C. A., Theobald, D. E., DeCarolis, N. A., Renthal, W., Kumar, A., . . . Nestler, E. J. (2007). IRS2-Akt pathway in midbrain dopamine neurons regulates behavioral and cellular responses to opiates. *Nat Neurosci*, 10(1), 93-99. doi:10.1038/nn1812
- Russo, S. J., Mazei-Robison, M. S., Ables, J. L., & Nestler, E. J. (2009). Neurotrophic factors and structural plasticity in addiction. *Neuropharmacology*, 56 Suppl 1, 73-82. doi:10.1016/j.neuropharm.2008.06.059
- Saderi, N., Buijs, F. N., Salgado-Delgado, R., Merkenstein, M., Basualdo, M. C., Ferri, G. L., . . . Buijs, R. M. (2014). A role for VGF in the hypothalamic arcuate and paraventricular nuclei in the control of energy homeostasis. *Neuroscience*, 265, 184-195. doi:10.1016/j.neuroscience.2014.01.060
- Schmidt, H. D., Mietlicki-Baase, E. G., Ige, K. Y., Maurer, J. J., Reiner, D. J., Zimmer, D. J., . . . Hayes, M. R. (2016). Glucagon-Like Peptide-1 Receptor Activation in the Ventral Tegmental Area Decreases the Reinforcing Efficacy of Cocaine. *Neuropsychopharmacology*, 41(7), 1917-1928. doi:10.1038/npp.2015.362

- Scripts, E. (2014). *A Nation in Pain: Focusing on U.S. Opioid Trends for treatment of short-term and longer-term pain* Retrieved from <http://lab.express-scripts.com/publications/a-nation-in-pain>
- Shousha, S., Nakahara, K., Sato, M., Mori, K., Miyazato, M., Kangawa, K., & Murakami, N. (2006). Effect of neuromedin S on feeding regulation in the Japanese quail. *Neurosci Lett*, 391(3), 87-90. doi:10.1016/j.neulet.2005.08.033
- Stamatakis, A. M., Jennings, J. H., Ung, R. L., Blair, G. A., Weinberg, R. J., Neve, R. L., . . . Stuber, G. D. (2013). A unique population of ventral tegmental area neurons inhibits the lateral habenula to promote reward. *Neuron*, 80(4), 1039-1053. doi:10.1016/j.neuron.2013.08.023
- Stinus, L., Koob, G. F., Ling, N., Bloom, F. E., & Le Moal, M. (1980). Locomotor activation induced by infusion of endorphins into the ventral tegmental area: evidence for opiate-dopamine interactions. *Proc Natl Acad Sci U S A*, 77(4), 2323-2327.
- Stuber, G. D., Stamatakis, A. M., & Katak, P. A. (2015). Considerations when using cre-driver rodent lines for studying ventral tegmental area circuitry. *Neuron*, 85(2), 439-445. doi:10.1016/j.neuron.2014.12.034
- Thakker-Varia, S., Krol, J. J., Nettleton, J., Bilimoria, P. M., Bangasser, D. A., Shors, T. J., . . . Alder, J. (2007). The neuropeptide VGF produces antidepressant-like behavioral effects and enhances proliferation in the hippocampus. *J Neurosci*, 27(45), 12156-12167. doi:10.1523/JNEUROSCI.1898-07.2007
- Tritsch, N. X., Oh, W. J., Gu, C., & Sabatini, B. L. (2014). Midbrain dopamine neurons sustain inhibitory transmission using plasma membrane uptake of GABA, not synthesis. *Elife*, 3, e01936. doi:10.7554/eLife.01936
- Tsankova, N. M., Berton, O., Renthal, W., Kumar, A., Neve, R. L., & Nestler, E. J. (2006). Sustained hippocampal chromatin regulation in a mouse model of depression and antidepressant action. *Nat Neurosci*, 9(4), 519-525. doi:10.1038/nn1659
- U.S. Dept of Health and Human Services (HHS). (2017). HHS acting secretary declares public health emergency to address national opioid crisis [Press release]. Retrieved from <https://www.hhs.gov/about/news/2017/10/26/hhs-acting-secretary-declares-public-health-emergency-address-national-opioid-crisis.html>
- Vigo, E., Roa, J., Lopez, M., Castellano, J. M., Fernandez-Fernandez, R., Navarro, V. M., . . . Tena-Sempere, M. (2007). Neuromedin s as novel putative regulator of luteinizing hormone secretion. *Endocrinology*, 148(2), 813-823. doi:10.1210/en.2006-0636

- Wang, X. F., Liu, J. J., Xia, J., Liu, J., Mirabella, V., & Pang, Z. P. (2015). Endogenous Glucagon-like Peptide-1 Suppresses High-Fat Food Intake by Reducing Synaptic Drive onto Mesolimbic Dopamine Neurons. *Cell Rep*, 12(5), 726-733. doi:10.1016/j.celrep.2015.06.062
- Ye, J., Coulouris, G., Zaretskaya, I., Cutcutache, I., Rozen, S., & Madden, T. L. (2012). Primer-BLAST: a tool to design target-specific primers for polymerase chain reaction. *BMC Bioinformatics*, 13, 134. doi:10.1186/1471-2105-13-134
- Zhang, D., Yang, S., Yang, C., Jin, G., & Zhen, X. (2008). Estrogen regulates responses of dopamine neurons in the ventral tegmental area to cocaine. *Psychopharmacology (Berl)*, 199(4), 625-635. doi:10.1007/s00213-008-1188-6

Chapter 4. Conclusions and Future Directions

4.1. Summary of Dissertation

Opioids have been used for thousands of years for the treatment of pain despite their highly addictive properties. But over the last 20 years, opioid use in the United States has dramatically increased, such that 80% of the world's supply of opioids are being used by Americans (Manchikanti, 2007). Long-term use of opiate drugs induces lasting changes in the mesocorticolimbic reward circuit (Dacher & Nugent, 2011b; Fields & Margolis, 2015; Mazei-Robison & Nestler, 2012). For example, we previously determined that chronic opiate exposure decreases the soma size of DA neurons in the VTA, a key structure in the mesocorticolimbic reward circuit (Mazei-Robison et al., 2011). This change was observed in post-mortem human samples as well as in rodent models where soma size was correlated with DA neuronal activity and reward behavior (Mazei-Robison et al., 2011). VTA DA neurons are not homogenous, however, as subsets of neurons can form distinct functional circuits (e.g. NAc-projecting neurons are associated with reward, while PFC-projecting neurons are associated with aversion). Critically, the projection-specificity of opioid-induced structural plasticity is not yet known. Additionally, our previous work suggests that neurotrophic signaling plays an important role in morphine-induced actin-remodeling and functional adaptations of VTA DA neurons (Heller et al., 2015; Koo et al., 2012; Mazei-Robison & Nestler, 2012). However, identification of molecular mediators specific to DA neurons has been difficult due to the cellular heterogeneity within the VTA. Therefore, this dissertation identified morphine-induced structural adaptations in specific VTA DA circuits important for both

reward and aversive processing as well as identified novel candidate genes in VTA DA neurons that will inform future studies investigating novel therapeutic approaches for opioid dependence and addiction.

4.2. Chronic Morphine-induced Soma Size Change is Projection-specific

In the experiments outlined in Chapter 2, we showed that VTA DA neuron morphology is not homogenous, differing both basally and in response to chronic morphine. VTA DA basal morphology is distinct across VTA subregions, where basal soma size decreases along the medial-lateral axis such that the largest VTA DA neurons were predominantly in the lateral regions (L.PN) and smallest in the medial regions (IF). This agrees with other studies, which used soma diameter as a proxy for cell soma size (Y. Fu et al., 2012). Our use of viral-expressed fluorophore increased not only the efficacy of soma morphology measurements but also allowed for projection-specific isolation of DA neurons. Similar to NAc core- and m.shell-projecting neurons, VTA DA neurons projecting to the PFC also displayed subregion specificity and primarily project to the PrL/Cg1 subregions of the PFC. Little-to-no PFC-projecting DA neurons were identified from stereotaxic injections into the anterior Cg1/secondary motor cortex (M2) or from injections into the ventral PFC (IL or dorsopeduncular cortex [DP]). Importantly, we also showed that chronic morphine drives distinct effects on VTA DA morphology across NAc m.shell, NAc core, and PFC projections. Specifically, chronic morphine decreases the soma size of m.shell-projecting DA neurons, while having no effect on NAc core-projections. Conversely, PFC-projecting DA neurons increased soma size following chronic morphine. Collectively, our study suggests that

opioid-induced regulation of VTA DA morphology is not homogenous, and occurs in distinct, projection-specific subsets and VTA subregions.

Chronic morphine-induced morphology changes of PFC-projecting DA neurons may have been masked in previous studies due to their VTA subregion distribution and relative scarcity compared to NAc-projecting neurons (Margolis et al., 2006; Swanson, 1982). In our study, PFC-projecting VTA DA neurons were predominantly in the PBP and dorsal regions of the PN, while NAc core- and m.shell-projecting VTA DA neurons were measured only in the PN. Previous studies have seen similar projection distribution although there are some differences in the total number of identified PFC-projecting neurons (Beier et al., 2015; Lammel et al., 2008). We identified 4-12 PFC-projecting neurons per mouse and these neurons were located predominantly in the PBP and dorsal regions of the PN. This is in stark contrast to the NAc-projecting population where more than 30 neurons within the PN were labeled per mouse. The scarcity of labeled PFC-projections may be attributed to differences in efficiency of viral uptake and expression, although our results mirror studies using other retro-labeling methods (e.g. Retrobeads, fluorogold, Dil) that also show a greater number of NAc-projecting neurons compared to PFC-projecting neurons (Ford, Mark, & Williams, 2006; Ikemoto, 2007; Lammel et al., 2008; Lammel, Ion, Roeper, & Malenka, 2011; Margolis et al., 2006). One study estimated that the total number of PFC-projecting neurons may be 50% less than NAc-projecting neurons in the VTA. Additionally, only 45% of the PFC-projecting neurons were TH(+) compared to 66% of the NAc-projecting neurons (Margolis et al., 2006). While PFC-projecting DA neurons are only a small subset of neurons in the VTA, there is increasing evidence that they play an important role in

aversive processing (Lammel et al., 2011; Margolis et al., 2006). But many studies on drug-reward have not distinguished PFC-projecting neurons from other VTA DA populations and more studies are needed to precisely determine their functional significance.

4.3. Determine NAc I.shell-projecting VTA DA Morphological Response to Chronic Morphine.

Chapter 2 results also support the importance of distinguishing between NAc subregions for understanding drug reward. NAc m.shell has been traditionally viewed as a hedonic hot-spot where DA release is primarily responsible for the rewarding and motivational effects of a drug or stimulus (Ikemoto, 2007; Sesack & Grace, 2010). NAc core is associated with the integration of reward with a particular learned motivated action (e.g. operant conditioning) (Namburi, Al-Hasani, Calhoon, Bruchas, & Tye, 2016). NAc I.shell may be involved in processing of both rewarding and aversive stimuli (Al-Hasani et al., 2015; Hikida, Morita, & Macpherson, 2016; Yang et al., 2018) and opioid-induced adaptations in this population may be important for opioid reward and/or dysphoria in opioid withdrawal (Al-Hasani et al., 2015; Hikida et al., 2016).

In this dissertation we predominantly targeted NAc core and m.shell, with only minimal labeling of NAc I.shell. We have some preliminary evidence that I.shell projecting-DA neurons in the aVTA PBP may be intermediate in size (488.4 ± 19.77), although these measurements were only from 3 mice. In order to better assess the morphology of VTA DA neurons projecting to the NAc I.shell (basal and chronic-opioid induced), it would be plausible to repeat the experimental procedures outlined in Chapter 2 using adjusted stereotaxic coordinates to more efficiently target NAc I.shell

(Lammel et al., 2008). The use of a retrograde viral tracer, AAV5-DIO-eYFP/mCh, was ideal in our experiments for cell-type and regional specificity, while also allowing for direct 3D reconstruction of DA neuron morphology. However, substantial and careful post-hoc analysis of viral spread at the injection site is required to accurately determine NAc-subregion specificity.

An alternative to retro-virus targeting is the use of fluorescent retrobeads (lumaFluor) which have a smaller diameter of spread across the injection site (<1mm) compared to many viral constructs which can have a range from 1-1.8mm (Lumafuor, ND; Watakabe et al., 2015). While this addresses the issue of subregion specificity, retrobead labeling is not cell type-specific. Since VTA DA and GABAergic neurons send direct projections to the NAc and to the PFC, retrobeads would be present in both populations (Carr & Sesack, 2000a; Van Bockstaele & Pickel, 1995). Therefore, a combined technique of injecting both virus and retrobeads may be useful to improve the confidence level of NAc-subregion and cell-type specificity of VTA projections. For example, if viral expression spreads across both NAc core and I.shell, but retrobeads were retained only in the I.shell, we can assume that VTA DA neurons with both viral expressed-eYFP and retrobeads are VTA DA neurons that project to the NAc I.shell.

Using these techniques would allow us to determine whether opiate-plasticity also occurs in NAc I.shell-projecting neurons. As mentioned previously, this projection has been implicated in both reward and aversion, and DA release dynamics across projections may encode the value of a stimulus (Bassareo, De Luca, & Di Chiara, 2002; Bassareo & Di Chiara, 1999). Chronic morphine increases the tonic and phasic firing rates of VTA DA neurons although projection specificity was not assessed. Therefore, I

predict that chronic morphine induces molecular adaptations in NAc I.shell projecting VTA DA neurons important for opioid-reward and identification of morphological plasticity in this subset of neurons would further our understanding in the integration of each circuit.

4.4. Determine Projection-specific Chronic Opioid-induced Activity

The findings of this dissertation not only shed light on the distinct projection-specific morphology of VTA DA neurons, but also highlight the importance of directly testing previously held assumptions that VTA DA neurons respond uniformly to opioids. It was initially surprising to find distinctions between neurons that project to NAc core and m.shell in our study. Given their known differences in physiology and function, it will be important to determine whether NAc I.shell-projecting VTA DA neurons also display distinct morphological response to chronic opioids. But this projection-specific structural response to opioids does not resolve whether the morphology change (reduced soma size) occurs in the same population of neurons with increased activity. Previous data on chronic opioid-induced changes in morphology and activity were correlated in separate experiments and while it is clear that both phenomena occur we have not yet directly confirmed whether they are concomitant in the same cell (Koo et al., 2012; Mazei-Robison et al., 2011; Russo et al., 2007). The opioid-induced increase in phasic and tonic activity of VTA DA neurons used presence of high I_h to identify putative DA neurons with low I_h cells presumed to be GABAergic (Gysling & Wang, 1983; Johnson & North, 1992; Koo et al., 2012; Mazei-Robison et al., 2011). But VTA DA neurons that project to the NAc m.shell and core exhibit low I_h currents, while I.shell projecting DA neurons have high I_h (Lammel et al., 2011). Therefore, the common practice of sorting

DA from GABAergic neurons using Ih could lead to recording primarily I.shell-projecting VTA DA neurons. While our study shows that chronic opioids decrease soma size of m.shell-projecting neurons, the effects on I.shell projections are unknown. Due to the diversity of behaviors associated to NAc subregions, it will be important to test whether opioids induce similar activity changes across all NAc projections, or whether they are projection-specific like changes in soma size.

There is also evidence for diversity in the source and strength of glutamatergic regulation of VTA DA activity based on projection target. PFC-projecting VTA DA neurons appear to receive direct glutamatergic input and have higher basal AMPA/NMDA ratios, while glutamatergic regulation of NAc-projecting neurons may be indirect (Carr & Sesack, 2000b; Lammel et al., 2008; Lammel et al., 2011; Takahata & Moghaddam, 2000). Many studies on drug-induced glutamatergic plasticity have focused on acute effects of stimulant drugs (cocaine or amphetamines), which strengthen excitatory synapses on VTA DA neurons (e.g. increase AMPA/NMDA ratio and GluR1 expression) (Fitzgerald, Ortiz, Hamedani, & Nestler, 1996; Luscher & Malenka, 2011; Ungless, Whistler, Malenka, & Bonci, 2001). Similar strengthening is observed in response to acute opioid treatment (Lane et al., 2008; Saal, Dong, Bonci, & Malenka, 2003).

While several studies have measured increased phasic and tonic firing of VTA DA neurons following chronic opioids, there is a distinct knowledge gap in determining the underlying post-synaptic changes which drive this plasticity. Experiments outlined below (section 4.5) to identify opioid-induced changes in VTA DA neuron dendritic morphology could be used as an initial proxy for synaptic plasticity. There is some

evidence for differences in chronic opioid-induced glutamatergic plasticity based on projection target. In a study by (Lane et al., 2008), GluR1 immunogold labeling (a marker for glutamatergic plasticity) was directly compared in projection-specific subsets of VTA DA neurons following either acute or chronic morphine treatment. Acute morphine increased the number of GluR1-labeled synapses in both PFC- and NAc-projecting TH(+) and TH(-) neurons in the PBP and PN of the VTA. Conversely, chronic morphine-induced GluR1 labeling only in PFC-projecting VTA DA neurons (Lane et al., 2008), suggesting projection-specific glutamatergic regulation of DA neurons. Additionally, the fact that acute, but not chronic morphine, increased GluR1 labeling in NAc-projecting DA neurons suggests distinct plasticity can be induced depending on state of drug dependence. It is possible that in response to the initial high activation of NAc m.shell-projecting VTA DA neurons by acute morphine homeostatic mechanisms are engaged which may counter the initial plasticity, such as potassium channel regulation, decreased axonal transport, and destabilization of actin cytoarchitecture (Beitner-Johnson & Nestler, 1993; Diana, Pistis, Muntoni, & Gessa, 1995; Mazei-Robison et al., 2011). Therefore, it will be important to assess whether changes in morphology and activity occur in a similar projection-specific manner.

4.5. Determine Basal and Opioid-induced VTA DA Dendritic Morphology

Chronic morphine-induced changes in VTA DA soma size likely reflect altered regulation of cytoskeletal remodeling. Chronic opioids induce changes in BDNF/TrkB signaling in VTA DA neurons, which in turn alter both cytoskeletal dynamics and activity (Koo et al., 2012; Koo et al., 2015; Liu et al., 2017). Some progress has been made in elucidating the downstream mediators of actin remodeling in VTA DA neurons, including

reduced IRS/Akt and mTORC2/Rictor signaling which is associated with increased F-actin destabilization (Mazei-Robison et al., 2011; Russo et al., 2007; Russo, Mazei-Robison, Ables, & Nestler, 2009; Wolf, Numan, Nestler, & Russell, 1999). Additionally, chronic opioids induce actin-remodeling in other brain regions integral to reward processing (Robinson & Kolb, 2004). For example, dendritic branching and spine complexity is reduced in both NAc MSN neurons and PFC pyramidal neurons following chronic opiate administration (Robinson, Gorny, Savage, & Kolb, 2002; Robinson & Kolb, 1999b). This is in contrast to other drugs of abuse such as stimulants (cocaine and amphetamines), which robustly increase dendritic spine number and complexity in the NAc and PFC (Robinson & Kolb, 1999a, 2004). Therefore, we hypothesized that the dendritic morphology of VTA DA neurons is altered along with soma size following opiate exposure.

There have been very few studies on the dendritic morphology of VTA neurons primarily due to limitations in techniques and VTA complexity. VTA DA neuron soma and dendrites are densely distributed across the VTA. As noted in Chapter 2 morphology studies, virally-labeled VTA DA neurons and their dendrites are particularly dense within the PBP and PN, which can be problematic in identifying the origin of specific dendrites. Additionally, VTA DA neurons have been suggested to have a low density of dendritic spines, although spine density may be dependent on the methodology used (Phillipson, 1979; Sarti, Borgland, Kharazia, & Bonci, 2007). Despite relatively low spine numbers, VTA DA neurons do show robust glutamatergic regulation to control tonic and phasic firing and DA release (Floresco, West, Ash, Moore, & Grace, 2003; Grace & Bunney, 1984; Grace, Floresco, Goto, & Lodge, 2007; Grace & Onn,

1989), and dendritic morphology is generally used as a proxy for glutamatergic plasticity (A. K. Fu & Ip, 2017; Konietzny, Bar, & Mikhaylova, 2017; Robinson & Kolb, 2004).

To our knowledge very few studies have addressed drug-induced changes in dendritic morphology directly in VTA DA neurons. In a study by (Sarti et al., 2007), Golgi-Cox impregnation was used to determine VTA neuron dendritic spine density 24 hours following cocaine treatment. This study showed a cocaine-induced increase in dendritic spine density in type 1 neurons, with no changes observed in type 2 neurons. Type 1 neurons were relatively small in size with extensive proximal and distal varicosities and were likely m.shell projecting DA neurons. Type 2 neurons were distinguished primarily by dendrites that remained thick throughout their length with few varicosities and due to the presence of high Ih and TH staining, and were likely l.shell-projecting DA neurons. Collectively this study highlights the possibility of increased dendritic branching and spine complexity in VTA DA neurons similar to effects seen in the NAc and PFC following cocaine treatment. Therefore, given the opposing effects of opioids and stimulants on NAc and PFC dendritic spines complexity (Robinson & Kolb, 1999b, 2004), as well as evidence for altered actin remodeling in VTA DA neurons (soma size) (Mazei-Robison et al., 2011; Russo et al., 2007), we hypothesized that chronic opioids would likely decrease VTA DA dendritic spine number and/or complexity.

4.6. Viral-Mediated Visualization of VTA DA Dendritic Morphology

To first characterize basal VTA DA dendritic morphology, we piloted several viral techniques to label VTA DA neurons. As described in Chapter 2 we used retrograde AAV5-DIO-eYFP/mCherry to assess VTA DA soma morphology, which also resulted in

extensive dendrite labeling. But this robust labeling resulted in an inability to accurately trace a single dendrite back to its cell body of origin. Therefore, we tested other AAV and HSV constructs to determine whether we could efficiently identify VTA DA neurons while also maintaining the required resolution for dendritic morphology assessment. In summary, AAV2-DIO-eYFP and AAV2-DIO-ChR2-eYFP showed robust cell-specific labeling of VTA DA neurons but with reduced ability to trace of individual dendrites as was observed with retrograde AAV5-DIO-eYFP. HSV-LSL1-GFP failed to robustly label VTA DA dendrites and therefore we could not obtain the required resolution to resolve spine morphology. It should be noted that use of a membrane-bound fluorophore (such as AAV2-DIO-ChR2-eYFP) substantially improved spine resolution although again overcrowding in the field of view served as a major hurdle. Therefore, across multiple experiments, the issues in fluorescent intensity, photobleaching, and high transduction efficiency (i.e. too many DA cells labeled) limited the collective usefulness of these techniques. Therefore, methods such as Golgi-cox staining or microinjection of a fluorophore that allow sparse neuronal labeling may be required to effectively resolve VTD DA dendritic morphology.

4.7. Projection-specific Labeling of VTA DA Neurons for Dendritic Morphology and Electrophysiological Studies

One way to directly link opioid-induced changes in VTA DA morphology and activity is through combined retrograde tracing and *in vivo* or *in vitro* electrophysiology. In collaboration with Dr. Lee Cox and Dr. Joe Beatty, we attempted VTA DA projection-specific dendritic morphology and activity measurements. We used our same retrograde constructs to label NAc-projecting VTA DA neurons as discussed in Chapter

2, combined with *ex vivo* whole-cell patch clamp and microinjection of a dye (AlexaFluor-594, AF-594) using a 2-photon microscope-fitted electrophysiology unit. NAc-projecting VTA DA neurons (eYFP+) were identified in the VTA and Ih and basal firing rate were measured via whole-cell patch clamp (data not shown). Directly following electrophysiological measurements cells were microinjected with AF-594 and immediately scanned using high-resolution 2-photon microscope imaging. This powerful method combines cell type-specificity, high resolution imaging, and measurement of electrophysiological properties such as firing frequency and Ih. However, this experiment was technically challenging, and across 4 mice, only 3 neurons were successfully measured and microinjected with AF-594. An example image of AF-594 filled NAc-projecting VTA DA neuron and dendritic morphology is shown in Figure 28.

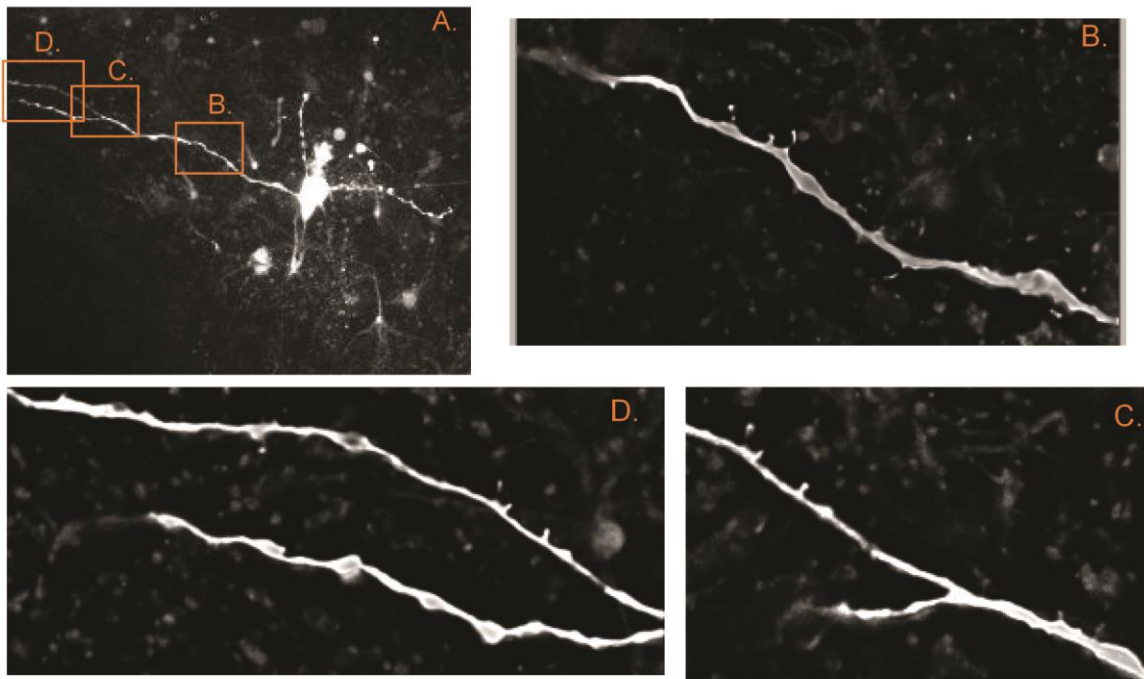


Figure 28. VTA DA Dendritic Spine Morphology of Projection-specific Microinjected VTA DA neuron. A. Example NAc-projecting VTA DA neuron microinjected with Alexafluor-594. B-D. 100X images of dendritic morphology.

In this pilot experiment, issues included poor tissue viability and low visibility of viral-mediated eYFP in fiber-dense VTA regions in >14wk old mice. Additionally, the total number of eYFP-labeled neurons was particularly low, and the probability of a neuron being both eYFP(+) and at an appropriate depth for efficient patch-clamp and iontophoresis was low. However, modifications in this approach may yield better results. For example, an alternate DA-specific model such as DAT^{L10a-GFP} combined with retrobeads labeling of projection-specific subsets of neurons may increase the total number of fluorophore-expressing VTA DA neurons at an appropriate tissue-depth. This would eliminate any problems due to viral efficiency and due to primary localization of L10a-GFP expression in the cell soma (see Chapter 3, Figure 11), there would be less obstruction of view from extensive dendritic branching allowing for easier targeting of VTA DA soma required for whole-cell patch clamp methods. Additionally, the use of retrobeads tracers, as opposed to our viral-mediated method, may reduce the time required for robust retrograde labeling from 6 weeks (AAV) to 3 weeks (retrobeads). The use of younger mice would likely increase the viability of *ex vivo* VTA slices. Finally, use of horizontal (as opposed to coronal) sections may allow for more complete VTA DA morphology assessment similar to methods used by others (Sarti et al., 2007), which noted longer dendrite lengths using horizontal sections.

4.8. Identification of Novel VTA DA Chronic Morphine-induced Molecular Changes

The molecular changes driving DA morphology and activity regulation are difficult to identify in such a heterogenous molecular environment. To date, unbiased screening studies for molecular mediators of chronic opioid induced plasticity have been limited to

homogenization of the entire VTA (Heller et al., 2015; Koo et al., 2015; McClung, Nestler, & Zachariou, 2005), which includes GABAergic and dopaminergic neurons (Margolis, Toy, Himmels, Morales, & Fields, 2012; Morales & Root, 2014; Nair-Roberts et al., 2008). I addressed this knowledge gap by using a transgenic mouse line (DAT^{L10a-GFP}) to isolate actively translating mRNA specifically from VTA DA neurons using TRAP as described in Chapter 3.

A similar TRAP method was developed to achieve both cell type- and projection-specific transcriptome isolation by combining cell-specific expression of an anti-GFP nanobody-fused L10a ribosome protein and targeted retrograde CAV-GFP expression (i.e. Retro-TRAP) (Ekstrand et al., 2014). While this would be ideal to investigate mechanisms underlying my morphine-induced morphology changes, it would be technically challenging for a couple of reasons. This technique would require extensive post-hoc analysis of injection targets while also relying on viral expression efficiency for overall yield. Additionally, we needed to pool 4 VTA for each TRAP pulldown in order to have sufficient RNA for RNAsequencing analysis, reduction in the total number of labeled DA neurons would significantly increase the number animals needed. This would be particularly problematic for isolation of PFC-projecting VTA DA neurons, which are scarce compared to their NAc-projecting counterparts.

Therefore, we went forward with standard TRAP with the rationale that since NAc-projecting VTA DA neurons are the predominant DA cell type, changes in gene expression would likely be driven by this population, and projection-specificity of identified candidate genes could be easily validated through *in situ*-hybridization and IHC. Additionally, we felt that separation of the DAergic fraction from other neurons in

the VTA was particularly important due to the noted opposing opioid-induced adaptations in GABA vs. DA cells (e.g. inhibition of GABA neurons and excitation of DA neurons) (Dacher & Nugent, 2011a; Mazei-Robison et al., 2011; Nugent, Penick, & Kauer, 2007). Thus, separation of DA neurons from the abundant other cellular populations (GABAergic, glutamatergic neurons and glial populations) is a logical and critical first step in understanding opioid-induced plasticity in the cellularly heterogeneous VTA.

We first validated the efficiency and cell-specificity of TRAP using TH^{L10a-GFP} and DAT^{L10a-GFP} mice to isolate the DA-specific fraction in the VTA. VTA from chronic morphine- and sham-treated DAT^{L10a-GFP} mice were dissected and RNA from the whole VTA (input) and specifically from VTA DA neurons (IP) was sequenced. Using differential gene expression analysis, we identified 1,792 DA-specific transcript alterations induced by morphine. This is the first time to our knowledge that genome-wide analysis has been completed for VTA DA neurons following drug treatment, accelerating the field's current understanding of DA-specific response to opiates. Additionally, in the whole VTA (input) analysis, we identified 2,103 genes significantly regulated by morphine. While we focused on validating candidate genes in VTA DA neurons, we can use similar techniques to validate morphine-induced genes identified in the input fraction. Therefore, the results of these studies are critical for the advancement of the field in elucidating new molecular mechanisms underlying morphine reward and VTA DA plasticity.

4.9. Validation of DA-specific Morphine-induced Genes

Thus far we have validated 7 morphine-regulated genes in VTA DA neurons using RT-PCR analysis. Surprisingly, these findings include several neuropeptides (Nms, Gcg, and Vgf) whose expression is induced by morphine. Expression of these neuropeptides in the VTA has not been investigated previously. We could use western blot or IHC to validate that the neuropeptides are expressed, although given the fast-axonal transport of vesicles containing neuropeptides, protein concentrations in the cell soma in the VTA may be low. One method to increase neuropeptide concentrations in the cell soma is to halt vesicle trafficking through colchicine interruption of microtubule dynamics (Vandecandelaere, Martin, & Engelborghs, 1997). Intracerebroventricular injection of colchicine increases neuropeptide concentrations in the cell soma and thus allows for increased immunofluorescent labeling. This method has been successfully utilized to label Nms-producing neurons in the SCN (Lee et al., 2015), and may be sufficient for protein validation of morphine-induced neuropeptides (Nms, Gcg, Vgf) in the VTA.

Previously, BDNF/TrkB and Akt/mTORC pathways have been have been the focus of many studies on chronic opioid-induced adaptations in the VTA. Specifically, BDNF signaling in the VTA is reduced following chronic morphine treatment and is correlated with actin remodeling and increased DA activity (Koo et al., 2012; Koo et al., 2015; Mazei-Robison et al., 2011; Russo et al., 2007; Russo et al., 2009; Wolf, Nestler, & Russell, 2007; Wolf et al., 1999). Therefore, identification of a morphine-induced increase in Vgf expression in VTA DA neurons is somewhat counterintuitive given that Vgf induction is seen following increased BDNF/TrkB signaling in other regions (Behnke

et al., 2017; Bozdagi et al., 2008; P. Lin et al., 2014; W. J. Lin et al., 2015; Lu et al., 2014). This is the first time to our knowledge that Vgf mRNA was described in DA neurons. It is possible that Vgf induction may occur within distinct subpopulations of DA neurons. This could have behavioral implications similar to the region-specific effects of Vgf on stress and anti-depressant action as Vgf has been implicated in chronic social defeat stress in both in NAc and Hipp (Jiang et al., 2017; Lu et al., 2014). Specifically, increased Vgf in the NAc is associated with pro-depressant behavior while Vgf in the Hipp is thought to mediate anti-depressant action (Jiang et al., 2017; P. Lin et al., 2014). Interestingly, in the NAc, Vgf protein is induced following chronic social defeat stress, while mRNA levels remain stable (Jiang et al., 2017). This may suggest that CSDS-induced Vgf expression may not necessarily be locally derived but be released by afferent innervation. Therefore, it is possible that NAc-projecting VTA DA neurons may be the source of Vgf protein induction in the NAc following CSDS. Therefore, it will be interesting to determine whether NAc-projecting neurons specifically express Vgf and mediate Vgf-induced plasticity in the NAc following CSDS. This may be achieved through circuit and cell-specific deletion of Vgf using Crispr-Cas9 genome editing (Senis et al., 2014).

4.10. Determine Cell-specificity of Morphine-regulated Genes Identified in Whole VTA Input.

We also find little overlap between morphine-regulated transcripts in whole VTA and DA-specific IP fractions. This suggests that there is a cumulative effect in the input fractions such that transcriptional modifications across multiple cell types mask DA-specific changes. It is likely that opioid-mediated inhibition of GABAergic VTA neurons

(via MOR GPCR activity) induces opposing molecular changes compared to molecular mediators of increased DA activity. While the majority of the experiments outlined in Chapter 3 focused on transcript alterations induced in VTA DA neurons, the molecular adaptations in other VTA cellular populations will be important to address. This can be achieved by using the same techniques outlined in Chapter 3, but with different Cre-driver lines for cell-specific L10a-GFP expression. For example, isolation of GABAergic mRNA can be achieved by crossing Rosa26-L10a-GFP mice with VGAT-Cre or GAD2-Cre mice. Likewise, the glutamatergic population may be isolated using VGLUT2-Cre mice. Although some caution will be needed in the interpretation of genomic expression of glutamatergic VGLUT2-fraction due to the presence of DA/glutamate co-releasing populations in the VTA.

Candidate genes identified in whole VTA can also be systematically validated first in whole VTA samples, and then in cell type-specific TRAP samples. One surprising finding from our studies was that the morphine-induced increase in SGK1 was only identified in the whole VTA input, not in the DA-specific fraction. There are two likely explanations for this discrepancy: 1) Sgk1 induction occurs in a non-dopaminergic cell type (e.g. GABA neurons) or 2) Sgk1 RNA is not being actively translated. SGK1 cellular specificity can be directly tested using combined IHC and *in-situ* hybridization of anti-Sgk1 probes in the VTA. Additionally, other Cre-driver lines can be used for TRAP analysis to assess Sgk1 expression in other cell types. We have completed preliminary studies using VGAT-Cre mice to detect changes in VTA GABA neurons, and surprisingly we do not observe a morphine-induced increase in SGK1. It is possible that morphine-induced SGK1 gene expression is physiologically distinct from the concurrent

increase in SGK1 kinase activity (Heller et al., 2015). There is evidence that while SGK1 gene induction is robust in the VTA following chronic opioids (2-fold increase), total SGK1 protein does not show a similar increase and remains stable (Heller et al., 2015). Thus, it will be important to first determine if SGK1 mRNA is being actively translated within the VTA. This can be achieved using a variation of the TRAP protocol with IP of all ribosomes (as opposed to cell-specific ribosomes). This would allow for confirmation that SGK1 is being induced and actively translated in the VTA. It is also possible that SGK1 is being actively translated in a minor cell population such that total SGK1 protein is not substantially changed in whole VTA. Therefore, if an appropriate cell type-specific Cre-driver line is available, morphine-induced expression of SGK1 can be directly validated similar to approaches used in Chapter 3.

4.11. Validation of Behavioral Relevance of Projection-specific Chronic Opioid-induced Plasticity.

Collectively, the dissertation research presented here identified both cell type-specific molecular adaptations and projection-specific plasticity in VTA DA neurons. An important next step would be to combine these findings in projection-specific validation to identify the behavioral significance of these changes. Firstly, the physiological and behavioral significance of opioid-induced adaptations in PFC-projecting neurons remains to be directly tested. I predict that because the VTA DA-PFC circuit is important in aversive processing, that these populations of VTA DA have reduced activity during chronic opioids and increased activity during opioid withdrawal. Similar techniques can be used to test this hypothesis as in previous studies that defined NAc projection-specific responses to drug reward (Lammel et al., 2008; Lammel et al., 2011; Margolis

et al., 2006; Mazei-Robison et al., 2011). For example, retrograde cell type-specific viral tracers (AAV5-DIO-eYFP) or combined TH immunohistochemistry and retrograde/anterograde tracers (Dill, fluorogold or retrobeads) can be combined with standard electrophysiological measurements to identify changes in activity directly following chronic morphine treatment or at different time points of withdrawal in PFC-projecting DA neurons. Use of optogenetic approaches to specifically manipulate activity of the VTA DA-PFC circuit may be a useful to elucidate the behavioral consequence of activating or inactivating PFC-projecting VTA DA neurons during morphine administration and reward paradigms (CPP, IVSA). Collectively, there are a multitude of directions that can be taken to determine the physiological and behavioral relevance of this understudied subpopulation of VTA DA neurons.

Additionally, projection-specific validation of chronic opioid-induced molecular adaptations identified in the RNAsequencing study would be a powerful tool to determine the physiological and behavioral significance of these changes. The development of addiction involves not only VTA reward processing but alterations in other upstream structures (NAc and PFC) which are critical for the progression to uncontrolled or compulsive drug use. Identification of the molecular mediators (in addition to DA itself), which are responsible for the transition to addiction are critical for the development of therapeutic intervention. Our identification of increased neuropeptide expression following chronic morphine may mediate synaptic and signaling changes in upstream structures. In order to determine the function of these neuropeptides following chronic opioid administration, one can use genomic and/or projection-specific knockout of a target gene in conjunction with measuring opioid-

induced reward behavior (such as CPA, IVSA, voluntary morphine drinking paradigm). Projection-specific knockout of specific genes can be obtained through Crispr-Cas9 mediated genome editing and can be a powerful tool to systematically confirm the behavioral significance of a specific gene. Additionally, other genetic mouse models for Cre-dependent expression or depletion of Nms and Vgf are readily available and previously validated (Jiang et al., 2017; Lee et al., 2015). For example, the necessity of Nms production in DA neurons for opioid-associated behavior can be determined by crossing floxed-Nms mice with DAT-Cre mice and assessing morphine reward using either drinking preference tasks, morphine self-administration, or CPP. A similar strategy can be utilized to determine the roles of Vgf and Gcg function in VTA DA neurons following chronic morphine treatment.

4.12. Conclusion

Results of the present study confirm diversity in VTA DA neurons and highlight the importance of identifying separate DA subpopulations to understand their specific roles in opioid dependence and addiction. This study filled a major knowledge gap in the field on both projection- and cell-specificity of chronic opioid plasticity. Specifically, we identified structural alterations in specific VTA DA projections that suggest chronic opioids may differentially alter circuit-specific DA activity and output. In order to better understand the molecular mediators of chronic opioid-induced VTA DA circuit function we utilized technological advances to specifically identify transcriptome changes in VTA DA neurons. Using TRAP and RNAsequencing we identified thousands of chronic opioid-regulated genes in the VTA. The results of this study pave a path for future in-depth validation of chronic opioid-induced adaptations using circuit and cell-type specific

applications. Chronic opioid-induced plasticity has not been well studied, primarily due to the complexity of the mesocorticolimbic system. Prior research has substantially focused on acute effects of opioids, which are fundamentally different than those of chronic opioids (Dacher & Nugent, 2011b; Mazei-Robison & Nestler, 2012; Ting & van der Kooy, 2012). The identification of novel molecular mediators and circuitry effects of chronic opioids is especially important given that long-term use of opioids dramatically increases the risk for opioid dependence and addiction. The United States is currently in the midst of an opioid epidemic where it is now estimated that an average of 115 people die a day from opioid-related overdose (CDC, 2017) and long-term use of prescription opioids increases the risk for both drug tolerance and accidental overdose. Therefore, the elucidation of novel chronic opioid-induced molecular adaptations is critical for the discovery of better pharmaceutical intervention for the treatment of opioid dependence.

REFERENCES

REFERENCES

- Al-Hasani, R., McCall, J. G., Shin, G., Gomez, A. M., Schmitz, G. P., Bernardi, J. M., . . . Bruchas, M. R. (2015). Distinct Subpopulations of Nucleus Accumbens Dynorphin Neurons Drive Aversion and Reward. *Neuron*, *87*(5), 1063-1077. doi:10.1016/j.neuron.2015.08.019
- Bassareo, V., De Luca, M. A., & Di Chiara, G. (2002). Differential Expression of Motivational Stimulus Properties by Dopamine in Nucleus Accumbens Shell versus Core and Prefrontal Cortex. *J Neurosci*, *22*(11), 4709-4719. doi:20026445
- Bassareo, V., & Di Chiara, G. (1999). Differential responsiveness of dopamine transmission to food-stimuli in nucleus accumbens shell/core compartments. *Neuroscience*, *89*(3), 637-641.
- Behnke, J., Cheedalla, A., Bhatt, V., Bhat, M., Teng, S., Palmieri, A., . . . Alder, J. (2017). Neuropeptide VGF Promotes Maturation of Hippocampal Dendrites That Is Reduced by Single Nucleotide Polymorphisms. *Int J Mol Sci*, *18*(3). doi:10.3390/ijms18030612
- Beier, K. T., Steinberg, E. E., DeLoach, K. E., Xie, S., Miyamichi, K., Schwarz, L., . . . Luo, L. (2015). Circuit Architecture of VTA Dopamine Neurons Revealed by Systematic Input-Output Mapping. *Cell*, *162*(3), 622-634. doi:10.1016/j.cell.2015.07.015
- Beitner-Johnson, D., & Nestler, E. J. (1993). Chronic morphine impairs axoplasmic transport in the rat mesolimbic dopamine system. *Neuroreport*, *5*(1), 57-60.
- Bozdagi, O., Rich, E., Tronel, S., Sadahiro, M., Patterson, K., Shapiro, M. L., . . . Salton, S. R. (2008). The neurotrophin-inducible gene *Vgf* regulates hippocampal function and behavior through a brain-derived neurotrophic factor-dependent mechanism. *J Neurosci*, *28*(39), 9857-9869. doi:10.1523/JNEUROSCI.3145-08.2008
- Carr, D. B., & Sesack, S. R. (2000a). GABA-containing neurons in the rat ventral tegmental area project to the prefrontal cortex. *Synapse*, *38*(2), 114-123. doi:10.1002/1098-2396(200011)38:2<114::AID-SYN2>3.0.CO;2-R
- Carr, D. B., & Sesack, S. R. (2000b). Projections from the rat prefrontal cortex to the ventral tegmental area: target specificity in the synaptic associations with mesoaccumbens and mesocortical neurons. *J Neurosci*, *20*(10), 3864-3873.
- CDC. (2017, July 18, 2017). Opioid Overdose: Overview of an epidemic. Retrieved from <https://www.cdc.gov/drugoverdose/data/index.html>

- Dacher, M., & Nugent, F. S. (2011a). Morphine-induced modulation of LTD at GABAergic synapses in the ventral tegmental area. *Neuropharmacology*, *61*(7), 1166-1171. doi:10.1016/j.neuropharm.2010.11.012
- Dacher, M., & Nugent, F. S. (2011b). Opiates and plasticity. *Neuropharmacology*, *61*(7), 1088-1096. doi:10.1016/j.neuropharm.2011.01.028
- Diana, M., Pistis, M., Muntoni, A., & Gessa, G. (1995). Profound decrease of mesolimbic dopaminergic neuronal activity in morphine withdrawn rats. *J Pharmacol Exp Ther*, *272*(2), 781-785.
- Ekstrand, M. I., Nectow, A. R., Knight, Z. A., Latcha, K. N., Pomeranz, L. E., & Friedman, J. M. (2014). Molecular profiling of neurons based on connectivity. *Cell*, *157*(5), 1230-1242. doi:10.1016/j.cell.2014.03.059
- Fields, H. L., & Margolis, E. B. (2015). Understanding opioid reward. *Trends Neurosci*, *38*(4), 217-225. doi:10.1016/j.tins.2015.01.002
- Fitzgerald, L. W., Ortiz, J., Hamedani, A. G., & Nestler, E. J. (1996). Drugs of abuse and stress increase the expression of GluR1 and NMDAR1 glutamate receptor subunits in the rat ventral tegmental area: common adaptations among cross-sensitizing agents. *J Neurosci*, *16*(1), 274-282.
- Floresco, S. B., West, A. R., Ash, B., Moore, H., & Grace, A. A. (2003). Afferent modulation of dopamine neuron firing differentially regulates tonic and phasic dopamine transmission. *Nat Neurosci*, *6*(9), 968-973. doi:10.1038/nn1103
- Ford, C. P., Mark, G. P., & Williams, J. T. (2006). Properties and opioid inhibition of mesolimbic dopamine neurons vary according to target location. *J Neurosci*, *26*(10), 2788-2797. doi:10.1523/JNEUROSCI.4331-05.2006
- Fu, A. K., & Ip, N. Y. (2017). Regulation of postsynaptic signaling in structural synaptic plasticity. *Curr Opin Neurobiol*, *45*, 148-155. doi:10.1016/j.conb.2017.05.016
- Fu, Y., Yuan, Y., Halliday, G., Rusznak, Z., Watson, C., & Paxinos, G. (2012). A cytoarchitectonic and chemoarchitectonic analysis of the dopamine cell groups in the substantia nigra, ventral tegmental area, and retrorubral field in the mouse. *Brain Struct Funct*, *217*(2), 591-612. doi:10.1007/s00429-011-0349-2
- Grace, A. A., & Bunney, B. S. (1984). The control of firing pattern in nigral dopamine neurons: single spike firing. *J Neurosci*, *4*(11), 2866-2876.
- Grace, A. A., Floresco, S. B., Goto, Y., & Lodge, D. J. (2007). Regulation of firing of dopaminergic neurons and control of goal-directed behaviors. *Trends Neurosci*, *30*(5), 220-227. doi:10.1016/j.tins.2007.03.003

- Grace, A. A., & Onn, S. P. (1989). Morphology and electrophysiological properties of immunocytochemically identified rat dopamine neurons recorded in vitro. *J Neurosci*, *9*(10), 3463-3481.
- Gysling, K., & Wang, R. Y. (1983). Morphine-induced activation of A10 dopamine neurons in the rat. *Brain Res*, *277*(1), 119-127.
- Heller, E. A., Kaska, S., Fallon, B., Ferguson, D., Kennedy, P. J., Neve, R. L., . . . Mazei-Robison, M. S. (2015). Morphine and cocaine increase serum- and glucocorticoid-inducible kinase 1 activity in the ventral tegmental area. *J Neurochem*, *132*(2), 243-253. doi:10.1111/jnc.12925
- Hikida, T., Morita, M., & Macpherson, T. (2016). Neural mechanisms of the nucleus accumbens circuit in reward and aversive learning. *Neurosci Res*, *108*, 1-5. doi:10.1016/j.neures.2016.01.004
- Ikemoto, S. (2007). Dopamine reward circuitry: two projection systems from the ventral midbrain to the nucleus accumbens-olfactory tubercle complex. *Brain Res Rev*, *56*(1), 27-78. doi:10.1016/j.brainresrev.2007.05.004
- Jiang, C., Lin, W. J., Sadahiro, M., Labonte, B., Menard, C., Pfau, M. L., . . . Salton, S. R. (2017). VGF function in depression and antidepressant efficacy. *Mol Psychiatry*. doi:10.1038/mp.2017.233
- Johnson, S. W., & North, R. A. (1992). Opioids excite dopamine neurons by hyperpolarization of local interneurons. *J Neurosci*, *12*(2), 483-488.
- Konietzny, A., Bar, J., & Mikhaylova, M. (2017). Dendritic Actin Cytoskeleton: Structure, Functions, and Regulations. *Front Cell Neurosci*, *11*, 147. doi:10.3389/fncel.2017.00147
- Koo, J. W., Mazei-Robison, M. S., Chaudhury, D., Juarez, B., LaPlant, Q., Ferguson, D., . . . Nestler, E. J. (2012). BDNF is a negative modulator of morphine action. *Science*, *338*(6103), 124-128. doi:10.1126/science.1222265
- Koo, J. W., Mazei-Robison, M. S., LaPlant, Q., Egervari, G., Braunscheidel, K. M., Adank, D. N., . . . Nestler, E. J. (2015). Epigenetic basis of opiate suppression of Bdnf gene expression in the ventral tegmental area. *Nat Neurosci*, *18*(3), 415-422. doi:10.1038/nn.3932
- Lammel, S., Hetzel, A., Hackel, O., Jones, I., Liss, B., & Roeper, J. (2008). Unique properties of mesoprefrontal neurons within a dual mesocorticolimbic dopamine system. *Neuron*, *57*(5), 760-773. doi:10.1016/j.neuron.2008.01.022
- Lammel, S., Ion, D. I., Roeper, J., & Malenka, R. C. (2011). Projection-specific modulation of dopamine neuron synapses by aversive and rewarding stimuli. *Neuron*, *70*(5), 855-862. doi:10.1016/j.neuron.2011.03.025

- Lane, D. A., Lessard, A. A., Chan, J., Colago, E. E., Zhou, Y., Schlussman, S. D., . . . Pickel, V. M. (2008). Region-specific changes in the subcellular distribution of AMPA receptor GluR1 subunit in the rat ventral tegmental area after acute or chronic morphine administration. *J Neurosci*, *28*(39), 9670-9681. doi:10.1523/JNEUROSCI.2151-08.2008
- Lee, I. T., Chang, A. S., Manandhar, M., Shan, Y., Fan, J., Izumo, M., . . . Yanagisawa, M. (2015). Neuromedin s-producing neurons act as essential pacemakers in the suprachiasmatic nucleus to couple clock neurons and dictate circadian rhythms. *Neuron*, *85*(5), 1086-1102. doi:10.1016/j.neuron.2015.02.006
- Lin, P., Wang, C., Xu, B., Gao, S., Guo, J., Zhao, X., . . . Zhou, W. (2014). The VGF-derived peptide TLQP62 produces antidepressant-like effects in mice via the BDNF/TrkB/CREB signaling pathway. *Pharmacol Biochem Behav*, *120*, 140-148. doi:10.1016/j.pbb.2014.03.003
- Lin, W. J., Jiang, C., Sadahiro, M., Bozdagi, O., Vulchanova, L., Alberini, C. M., & Salton, S. R. (2015). VGF and Its C-Terminal Peptide TLQP-62 Regulate Memory Formation in Hippocampus via a BDNF-TrkB-Dependent Mechanism. *J Neurosci*, *35*(28), 10343-10356. doi:10.1523/JNEUROSCI.0584-15.2015
- Liu, D., Tang, Q. Q., Yin, C., Song, Y., Liu, Y., Yang, J. X., . . . Cao, J. L. (2017). BDNF-mediated projection-specific regulation of depressive-like and nociceptive behaviors in mesolimbic reward circuitry. *Pain*. doi:10.1097/j.pain.0000000000001083
- Lu, Y., Wang, C., Xue, Z., Li, C., Zhang, J., Zhao, X., . . . Zhou, W. (2014). PI3K/AKT/mTOR signaling-mediated neuropeptide VGF in the hippocampus of mice is involved in the rapid onset antidepressant-like effects of GLYX-13. *Int J Neuropsychopharmacol*, *18*(5). doi:10.1093/ijnp/pyu110
- Lumafluor. (ND, 4/2015). LumaFluor Protocol. Retrieved from https://lumafluor.com/Protocol_Rev_8_05_.php
- Luscher, C., & Malenka, R. C. (2011). Drug-evoked synaptic plasticity in addiction: from molecular changes to circuit remodeling. *Neuron*, *69*(4), 650-663. doi:10.1016/j.neuron.2011.01.017
- Manchikanti, L. (2007). National drug control policy and prescription drug abuse: facts and fallacies. *Pain Physician*, *10*(3), 399-424.
- Margolis, E. B., Lock, H., Chefer, V. I., Shippenberg, T. S., Hjelmstad, G. O., & Fields, H. L. (2006). Kappa opioids selectively control dopaminergic neurons projecting to the prefrontal cortex. *Proc Natl Acad Sci U S A*, *103*(8), 2938-2942. doi:10.1073/pnas.0511159103

- Margolis, E. B., Toy, B., Himmels, P., Morales, M., & Fields, H. L. (2012). Identification of rat ventral tegmental area GABAergic neurons. *PLoS One*, *7*(7), e42365. doi:10.1371/journal.pone.0042365
- Mazei-Robison, M. S., Koo, J. W., Friedman, A. K., Lansink, C. S., Robison, A. J., Vinish, M., . . . Nestler, E. J. (2011). Role for mTOR signaling and neuronal activity in morphine-induced adaptations in ventral tegmental area dopamine neurons. *Neuron*, *72*(6), 977-990. doi:10.1016/j.neuron.2011.10.012
- Mazei-Robison, M. S., & Nestler, E. J. (2012). Opiate-induced molecular and cellular plasticity of ventral tegmental area and locus coeruleus catecholamine neurons. *Cold Spring Harb Perspect Med*, *2*(7), a012070. doi:10.1101/cshperspect.a012070
- McClung, C. A., Nestler, E. J., & Zachariou, V. (2005). Regulation of gene expression by chronic morphine and morphine withdrawal in the locus ceruleus and ventral tegmental area. *J Neurosci*, *25*(25), 6005-6015. doi:10.1523/JNEUROSCI.0062-05.2005
- Morales, M., & Root, D. H. (2014). Glutamate neurons within the midbrain dopamine regions. *Neuroscience*, *282*, 60-68. doi:10.1016/j.neuroscience.2014.05.032
- Nair-Roberts, R. G., Chatelain-Badie, S. D., Benson, E., White-Cooper, H., Bolam, J. P., & Ungless, M. A. (2008). Stereological estimates of dopaminergic, GABAergic and glutamatergic neurons in the ventral tegmental area, substantia nigra and retrorubral field in the rat. *Neuroscience*, *152*(4), 1024-1031. doi:10.1016/j.neuroscience.2008.01.046
- Namburi, P., Al-Hasani, R., Calhoon, G. G., Bruchas, M. R., & Tye, K. M. (2016). Architectural Representation of Valence in the Limbic System. *Neuropsychopharmacology*, *41*(7), 1697-1715. doi:10.1038/npp.2015.358
- Nugent, F. S., Penick, E. C., & Kauer, J. A. (2007). Opioids block long-term potentiation of inhibitory synapses. *Nature*, *446*(7139), 1086-1090. doi:10.1038/nature05726
- Phillipson, O. T. (1979). A Golgi study of the ventral tegmental area of Tsai and interfascicular nucleus in the rat. *J Comp Neurol*, *187*(1), 99-115. doi:10.1002/cne.901870107
- Robinson, T. E., Gorny, G., Savage, V. R., & Kolb, B. (2002). Widespread but regionally specific effects of experimenter- versus self-administered morphine on dendritic spines in the nucleus accumbens, hippocampus, and neocortex of adult rats. *Synapse*, *46*(4), 271-279. doi:10.1002/syn.10146
- Robinson, T. E., & Kolb, B. (1999a). Alterations in the morphology of dendrites and dendritic spines in the nucleus accumbens and prefrontal cortex following repeated treatment with amphetamine or cocaine. *Eur J Neurosci*, *11*(5), 1598-1604.

- Robinson, T. E., & Kolb, B. (1999b). Morphine alters the structure of neurons in the nucleus accumbens and neocortex of rats. *Synapse*, 33(2), 160-162. doi:10.1002/(SICI)1098-2396(199908)33:2<160::AID-SYN6>3.0.CO;2-S
- Robinson, T. E., & Kolb, B. (2004). Structural plasticity associated with exposure to drugs of abuse. *Neuropharmacology*, 47 Suppl 1, 33-46. doi:10.1016/j.neuropharm.2004.06.025
- Russo, S. J., Bolanos, C. A., Theobald, D. E., DeCarolis, N. A., Renthal, W., Kumar, A., . . . Nestler, E. J. (2007). IRS2-Akt pathway in midbrain dopamine neurons regulates behavioral and cellular responses to opiates. *Nat Neurosci*, 10(1), 93-99. doi:10.1038/nn1812
- Russo, S. J., Mazei-Robison, M. S., Ables, J. L., & Nestler, E. J. (2009). Neurotrophic factors and structural plasticity in addiction. *Neuropharmacology*, 56 Suppl 1, 73-82. doi:10.1016/j.neuropharm.2008.06.059
- Saal, D., Dong, Y., Bonci, A., & Malenka, R. C. (2003). Drugs of abuse and stress trigger a common synaptic adaptation in dopamine neurons. *Neuron*, 37(4), 577-582.
- Sarti, F., Borgland, S. L., Kharazia, V. N., & Bonci, A. (2007). Acute cocaine exposure alters spine density and long-term potentiation in the ventral tegmental area. *Eur J Neurosci*, 26(3), 749-756. doi:10.1111/j.1460-9568.2007.05689.x
- Senis, E., Fatouros, C., Grosse, S., Wiedtke, E., Niopek, D., Mueller, A. K., . . . Grimm, D. (2014). CRISPR/Cas9-mediated genome engineering: an adeno-associated viral (AAV) vector toolbox. *Biotechnol J*, 9(11), 1402-1412. doi:10.1002/biot.201400046
- Sesack, S. R., & Grace, A. A. (2010). Cortico-Basal Ganglia reward network: microcircuitry. *Neuropsychopharmacology*, 35(1), 27-47. doi:10.1038/npp.2009.93
- Swanson, L. W. (1982). The projections of the ventral tegmental area and adjacent regions: a combined fluorescent retrograde tracer and immunofluorescence study in the rat. *Brain Res Bull*, 9(1-6), 321-353.
- Takahata, R., & Moghaddam, B. (2000). Target-specific glutamatergic regulation of dopamine neurons in the ventral tegmental area. *J Neurochem*, 75(4), 1775-1778.
- Ting, A. K. R., & van der Kooy, D. (2012). The neurobiology of opiate motivation. *Cold Spring Harb Perspect Med*, 2(10). doi:10.1101/cshperspect.a012096
- Ungless, M. A., Whistler, J. L., Malenka, R. C., & Bonci, A. (2001). Single cocaine exposure in vivo induces long-term potentiation in dopamine neurons. *Nature*, 411(6837), 583-587. doi:10.1038/35079077

- Van Bockstaele, E. J., & Pickel, V. M. (1995). GABA-containing neurons in the ventral tegmental area project to the nucleus accumbens in rat brain. *Brain Res*, 682(1-2), 215-221.
- Vandecandelaere, A., Martin, S. R., & Engelborghs, Y. (1997). Response of microtubules to the addition of colchicine and tubulin-colchicine: evaluation of models for the interaction of drugs with microtubules. *Biochem J*, 323 (Pt 1), 189-196.
- Watakabe, A., Ohtsuka, M., Kinoshita, M., Takaji, M., Isa, K., Mizukami, H., . . . Yamamori, T. (2015). Comparative analyses of adeno-associated viral vector serotypes 1, 2, 5, 8 and 9 in marmoset, mouse and macaque cerebral cortex. *Neurosci Res*, 93, 144-157. doi:10.1016/j.neures.2014.09.002
- Wolf, D. H., Nestler, E. J., & Russell, D. S. (2007). Regulation of neuronal PLCgamma by chronic morphine. *Brain Res*, 1156, 9-20. doi:10.1016/j.brainres.2007.04.059
- Wolf, D. H., Numan, S., Nestler, E. J., & Russell, D. S. (1999). Regulation of phospholipase Cgamma in the mesolimbic dopamine system by chronic morphine administration. *J Neurochem*, 73(4), 1520-1528.
- Yang, H., de Jong, J. W., Tak, Y., Peck, J., Bateup, H. S., & Lammel, S. (2018). Nucleus Accumbens Subnuclei Regulate Motivated Behavior via Direct Inhibition and Disinhibition of VTA Dopamine Subpopulations. *Neuron*, 97(2), 434-449 e434. doi:10.1016/j.neuron.2017.12.022